

**Experimental Investigations on Tractor Tire Vibration Properties**

**Von der Fakultät Konstruktions-, Produktions- und Fahrzeugtechnik  
der Universität Stuttgart  
zur Erlangung der Würde eines Doktor-Ingenieurs (Dr.-Ing.)  
genehmigte Abhandlung**

**Vorgelegt von**

**Dipl.-Ing. Christian Brinkmann**

**aus Ankum**

Hauptberichter:	Prof. Dr.-Ing. S. Böttinger
Mitberichter:	Prof. Dr.-Ing. J. Wiedemann
Tag der mündlichen Prüfung:	05.10.2016

Institut für Agrartechnik  
Stuttgart 2016

## **Vorwort**

Die vorliegende Arbeit entstand während meiner Tätigkeit als wissenschaftlicher Mitarbeiter am Institut für Agrartechnik der Universität Hohenheim.

Mein besonderer Dank gilt Herrn Prof. Dr.-Ing. Dr. h.c. H.D. Kutzbach und Herrn Prof. Dr.-Ing. S. Böttinger, die diese Arbeit angeregt und betreut haben. Beide boten mir die Möglichkeit, das Thema selbstständig zu erarbeiten, hatten aber immer ein offenes Ohr für meine Fragen und haben diese Arbeit mit ihren Anregungen und konstruktiver Kritik bereichert. Herzlich danken möchte ich auch Herrn Prof. Dr.-Ing. J. Wiedemann für die Übernahme des Mitberichts.

Dem Industriepartner Goodyear Tires S.A. möchte ich für die Finanzierung des Projektes herzlich danken. Mein besonderer Dank gilt Herrn Albert Lerusse, der das Projekt initiiert hat und von dessen weitreichender Erfahrung im Bereich Reifenschwingungseigenschaften und wohlwollender Unterstützung ich profitieren durfte. Frau Dr. D. Maus und den Herren J. Schouten, J.-P. Hansenne und C. Thiry danke ich für die Hilfe bei der Durchführung der Modalanalysenversuche und die wertvolle fachliche Unterstützung.

All meinen Kolleginnen und Kollegen des Instituts danke ich für die angenehme Zusammenarbeit, die vielen intensiven Diskussionen und die freundliche Unterstützung. Bedanken möchte ich mich bei Herrn Dr. V. Schlotter für die Initiierung des Projekts und die Heranführung an das Thema. All meinen wissenschaftlichen Hilfskräften gilt mein Dank für die tatkräftige Unterstützung bei der Durchführung der Messungen sowie der Reparaturen und Umbauten an den Prüfeinrichtungen. Die Zeit am Institut werde ich in bester Erinnerung behalten.

Danken möchte ich auch meinen Eltern, die mir diesen Weg ermöglicht haben. Meiner Ehefrau Sandra und meinen Kindern danke ich für ihre Unterstützung, Rücksichtnahme und Geduld während der Erstellung dieser Arbeit.

**INDEX**

SYMBOLS .....	III
ABBREVIATIONS.....	IV
SUMMARY .....	V
ZUSAMMENFASSUNG.....	VIII
1 INTRODUCTION.....	1
2 STATE OF THE ART .....	4
2.1 Investigations of agricultural tires .....	4
2.2 Investigations of passenger car and truck tires .....	9
2.3 Modeling and simulation .....	15
2.3.1 Physical models .....	16
2.3.1.1 FEA models.....	16
2.3.1.2 Mechanical models of reduced complexity.....	17
2.3.1.3 Modal models.....	22
2.3.2 Empirical models.....	22
2.4 Summary and further approach.....	24
3 THE VIBRATION BEHAVIOUR OF TIRES .....	26
3.1 Vibration sources .....	26
3.2 Categorization of vibration mode shapes .....	28
3.2.1 Unloaded condition .....	28
3.2.2 Loaded condition.....	29
3.2.3 Cavity modes .....	30
3.3 Influencing parameters on tire vibration behaviour.....	31
3.3.1 Carcass construction .....	31
3.3.2 Tire construction .....	32
3.3.3 Tire size .....	33
3.3.4 Boundary conditions .....	34
3.3.5 Operating conditions .....	36
3.3.5.1 Tire load $F_z$ .....	36
3.3.5.2 Inflation pressure $p_i$ .....	37
3.3.5.3 Rolling speed $v_x$ .....	38
3.4 Experimental methods .....	40
4 EXPERIMENTAL FACILITIES AND SETUPS.....	46
4.1 Investigated tires .....	46
4.2 Modal analysis .....	48
4.2.1 Setup on single wheels .....	50
4.2.2 Setup on flat-belt test stand .....	53
4.3 Shaker device .....	55
4.3.1 Concept and technical data .....	55
4.3.2 Operating modes .....	57

---

4.4	Flat-belt tire test stand.....	60
4.4.1	Technical data.....	60
4.4.2	Sensors and data acquisition.....	61
4.4.3	Modal properties.....	66
4.4.4	Shaker tests.....	71
4.5	Research tractor.....	73
4.5.1	Technical data.....	73
4.5.2	Sensors and data acquisition.....	74
4.5.3	Shaker tests.....	78
4.5.4	Uniformity tests.....	81
4.5.5	Cleat tests.....	81
4.6	Analysis software “Farm Analysis”.....	83
4.6.1	Program structure.....	83
4.6.2	Analysis methods.....	85
5	RESULTS AND DISCUSSION.....	88
5.1	Experimental modal analysis of the single wheels.....	88
5.1.1	Unloaded condition.....	88
5.1.2	Loaded condition.....	90
5.1.3	Rim properties.....	92
5.1.4	Axle dynamics.....	96
5.2	Investigations on the flat-belt tire test stand.....	108
5.2.1	Modal analysis.....	108
5.2.1.1	Unloaded condition.....	109
5.2.1.2	Loaded condition.....	113
5.2.2	Shaker tests.....	119
5.2.2.1	Non-rolling condition.....	119
5.2.2.2	Rolling condition.....	128
5.3	Investigations on the research tractor.....	133
5.3.1	Shaker tests.....	133
5.3.1.1	Non-rolling condition.....	134
5.3.1.2	Rolling condition.....	139
5.3.2	Uniformity tests.....	143
5.3.3	Cleat tests.....	148
6	CONCLUSIONS AND OUTLOOK.....	155
7	REFERENCES.....	158
8	APPENDIX.....	172

**SYMBOLS**

$a$	$m/s^2$	acceleration
$b_{exc}$	mm	eccentric mass width
$c$	N/m	spring rate
$c_{air}$	m/s	sound velocity of air
$D$	%	damping
$d$	mm	diameter
$d_{exc}$	mm	eccentric mass diameter
$e_{sh}$	mm	shaker eccentricity
$F_{exc,lat}$	N	lateral excitation force
$F_{exc,rad}$	N	radial excitation force
$F_{exc,tan}$	N	tangential excitation force
$F_{sh}$	N	shaker excitation force
$F_z$	kN	vertical tire load
$F_z$	lbf	vertical tire load in pound-force (1 lbf $\triangleq$ 4,44822 N)
$f$	Hz	frequency
$f_{sh}$	Hz	shaker frequency
$g$	$m/s^2$	earth's gravity 9,81 $m/s^2$
$H$	$m/s^2/N$	frequency response function
$I_{xx,exc}$	$kgm^2$	eccentric mass moment of inertia around x
$I_{yy,exc}$	$kgm^2$	eccentric mass moment of inertia around y
$I_{zz,exc}$	$kgm^2$	eccentric mass moment of inertia around z
$m_{exc}$	kg	eccentric mass of shaker device
$p_i$	bar	tire inflation pressure
$Q$		resonance quality
$R_{oct,max}$	oct/min	maximum sweep rate
$r$	m	radius
$r_{dyn}$	m	dynamic rolling radius
$T_{sweep}$	min	sweep time
$V$	$m/s^2/N$	magnitude frequency response
$v$	km/h	rolling speed
$X$	N	complex input spectrum
$Y$	$m/s^2$	complex output spectrum
$\alpha$	$^\circ$	slip angle
$\rho$	$kg/m^3$	density
$\Phi$	$^\circ$	phase frequency response
$\varphi$	$^\circ$	phase shift
$\omega$	1/s	angular speed

**ABBREVIATIONS**

AS	Amplitude spectrum
CAE	Computer-aided engineering
DAQ	Data acquisition
ESD	Energy spectral density
F/A	Fore/Aft mode
FE	Finite element
FEA	Finite element analysis
FRF	Frequency Response Function
GTC*L	Goodyear Technical Center Luxemburg
KMD	Load cell
LF	Left front
LMB	Load pin
LR	Left rear
MA	Modal analysis
MDOF	Multi degree of freedom
NVH	Noise Vibration Harshness
PC	Personal computer
PS	Power spectrum (Auto power spectrum)
PSD	Power spectral density
RF	Right front
RR	Right rear
SDOF	Single degree of freedom
SIMO	Single Input Multiple Output
ST	Shaker test
TF	Transfer function

---

## SUMMARY

Vehicle vibrations have raised articulate awareness in agricultural industry during the last years. Especially, the legal basis with the EU directive 2002/44/EC and its implementation into national law with the corresponding ordinance have sensitized the manufacturers concerning the vibration behaviour of their vehicles accompanied with an increasing demand for ride comfort by the customers. Furthermore, vehicle components' stress due to vibration and shock is also significantly dependent on the tire's vibration characteristics. Only an optimized design and combination of the vehicle components can reduce vibrations and improve ride comfort and endurance strength.

In this thesis mechanical vibrations in the ride comfort frequency range between 10 Hz and 80 Hz are regarded. For the investigations a new mechanical shaker device has been developed and single frequency force excitations in the mentioned frequency range can be applied to a rolling tire. From excitation and response of the system it is possible to identify the vibration modes of the rolling tire. The shaker is designed to be applied both to a flat-belt test stand and a research tractor. Additionally, uniformity and cleat tests have been conducted with the research tractor in order to compare shaker, tire and impact excitations.

Sources for tire and vehicle vibrations can be driveway related (unevenness of the driveway and surface roughness), tire related (tire non-uniformities, tread pattern/lugs) and vehicle related (engine, transmission and other component vibrations). Generally, the unevenness of the driveway is the dominating source. For tractor tires running on usual road surface the radial runout and lugs have dominant influence on the wheel load fluctuations.

For the unloaded condition the tire shapes radial and lateral modes which transform for the loaded tire into vertical and longitudinal as well as lateral and steering modes. As influencing parameters on the tire vibration behaviour the tire size, boundary conditions and the operating conditions tire load, inflation pressure and rolling speed were regarded.

First investigation step was the experimental modal analysis of the free single wheel for the unloaded and loaded condition regarding also rim properties and axle dynamics. Secondly, on the flat-belt test stand the modal analysis was repeated for changed boundary conditions. With the shaker device the way of excitation was varied enabling the rolling of the tire during testing. Finally, the shaker tests were also carried out on the vehicle supplemented by real driveway excitations.

The results for the single wheel show that for this tire size within the frequency range 0 – 80 Hz up to 15 tire modes can occur. All of these can be determined precisely concerning eigenfrequency, modal damping and mode shape. The general influence of the inflation pressure on eigenfrequency and modal damping can be proven. From the analysis of the axle dynamics arises that the bigger the tire is the better is the clear identification of its modes. Besides the rigid body modes most 2<sup>nd</sup> order modes and further the Vertical and F/A modes show noticeable influence on the axle dynamics.

The modal analysis on the flat-belt test stand features an acceptable agreement with the results for the single wheel. Results of the shaker tests on this test rig show that most of the modes in the mentioned frequency range can be identified. Furthermore, the effects of excitation amplitude, tire load and inflation pressure variation on frequency and amplitude can be demonstrated qualitatively. One of the key aspects in this thesis to be examined was the speed influence. Results are showing a slight frequency decrease with the onset of rolling. The force amplitudes measured in the tread pattern increase at first with the onset of rolling and then decrease at speeds above 3 km/h significantly. 1<sup>st</sup> and 2<sup>nd</sup> Lateral, 1<sup>st</sup> Vertical as well as 1<sup>st</sup> and 2<sup>nd</sup> F/A modes still show noticeable amplitudes for the rolling tire.

The eigenfrequencies determined by shaker tests on the research tractor show a good agreement with the test rig. Concerning the wheel force and acceleration amplitudes with the onset of rolling also the slight frequency decrease can be observed. The amplitudes are decreasing by 35-50% and stay nearly on this level with increasing speed. Relevant amplitudes are exhibited by the 1<sup>st</sup> and 2<sup>nd</sup> Lateral, 1<sup>st</sup> F/A and 1<sup>st</sup> Vertical modes. Uniformity and cleat tests excite the tire in a



---

completely different way. Their frequency spectra show certain similarities. The above mentioned four tire modes are also for these operating conditions most relevant and can be identified. For the driver large vibration amplitudes are especially due to the bouncing and 1<sup>st</sup> Lateral mode. Above 12 Hz the isolation of the cabin and seat suspension is showing effect so that the driver's exposition caused by the higher order modes is not critical.

From these results it can be concluded that tractor tire modes have a noticeable influence on the vibration transfer into the vehicle. These vibrations first of all lead to increased stress for the vehicle components exposed to it. Secondly, lower frequency vibrations can be transferred to cabin and seat in large parts, especially if the cabin and seat suspension is not adjusted correctly.

## ZUSAMMENFASSUNG

In den vergangenen Jahren haben Fahrzeugschwingungen in der Landtechnikindustrie besondere Aufmerksamkeit erlangt. Insbesondere die gesetzlichen Rahmenbedingungen mit der EU Direktive 2002/44/EC und ihrer Umsetzung in nationales Recht verbunden mit steigenden Fahrkomfortanforderungen durch den Kunden haben die Hersteller in Bezug auf das Fahrzeugschwingungsverhalten sensibilisiert. Darüber hinaus sind Bauteilbeanspruchungen aufgrund von Vibrationen oder Stößen auch abhängig vom Schwingungsverhalten der Reifen. Nur durch eine optimierte Konstruktion und Kombination der Fahrzeugbauteile können Schwingungen reduziert und damit der Fahrkomfort und die Betriebsfestigkeit verbessert werden.

In Rahmen dieser Arbeit wird der für den Fahrkomfort relevante Frequenzbereich zwischen 10 und 80 Hz betrachtet. Für die Untersuchungen wurde ein neuer mechanischer Shaker entwickelt, mit dem eine monofrequente Kraftanregung im genannten Frequenzbereich auf den rollenden Reifen aufgebracht werden kann. Aus der Anregung und der Antwort des Systems können die Eigenschwingungsmoden des rollenden Reifens identifiziert werden. Der Shaker wurde so konzipiert, dass er sowohl auf einem Flachbandreifenprüfstand als auch einem Forschungstraktor betrieben werden kann. Zusätzlich wurden mit dem Traktor Rundlauf- und Schlagleistentests durchgeführt, um die Shaker-, Reifeneigen- und Fahrweganregungen vergleichen zu können.

Anregungsquellen für Reifen- und Fahrzeugschwingungen können verursacht werden durch den Fahrweg (Unebenheit, Oberflächenrauigkeit), den Reifen (Reifenunrundheiten, Profil/Stollen) und das Fahrzeug (Motor, Antriebsstrang und andere Komponentenschwingungen). Grundsätzlich sind Fahrbahnunebenheiten die dominierende Anregungsquelle. Bei Traktorreifen im normalen Straßenfahrbetrieb haben radiale Unrundheit und Profilstollen dominierenden Einfluss auf die Radlastschwankungen.

Im unbelasteten Zustand bildet der Reifen radiale und laterale Eigenformen aus, die sich im belasteten Zustand in vertikale und longitudinale sowie laterale und

sogenannte Steering Moden aufteilen. Als Einflussparameter auf das Reifenschwingungsverhalten wurden Reifengröße, Rand-/Einspannbedingungen und die Einsatzbedingen Radlast, Reifeninnendruck und Fahrgeschwindigkeit betrachtet und variiert.

Erster Untersuchungsschritt war die experimentelle Modalanalyse am freistehenden einzelnen Rad im unbelasteten und belasteten Zustand, bei der auch Felgeneigenschaften und Achsdynamik betrachtet wurden. Im zweiten Schritt wurde die Modalanalyse auf dem Flachbandprüfstand mit geänderten Randbedingungen wiederholt. Mit dem Shaker wurde dann die Anregungsart geändert, so dass auch am rollenden Reifen gemessen werden konnte. Schließlich wurden die Shakerversuche auch am Fahrzeug durchgeführt und ergänzt durch reale Fahrweganregungen.

Die Untersuchungsergebnisse am einzelnen Rad zeigen im Frequenzbereich 10 - 80 Hz bis zu 15 Eigenmoden, die hinsichtlich Eigenfrequenz, modaler Dämpfung und Eigenform allesamt mit hoher Genauigkeit bestimmt werden können. Der grundsätzliche Einfluss des Reifeninnendrucks auf Eigenfrequenz und modale Dämpfung kann nachgewiesen werden. Aus der Analyse der Achsdynamik kann die Schlussfolgerung gezogen werden, dass die Bestimmung der Eigenmoden eindeutiger wird je größer der Reifen ist. Neben den Starrkörpermoden zeigen die meisten Moden 2. Ordnung und die weiteren Vertikal- und F/A-Moden deutlichen Einfluss auf die Achsdynamik.

Die Modalanalyse am Flachbandprüfstand weist eine akzeptable Übereinstimmung mit den Ergebnissen am einzelnen Rad auf. Die Ergebnisse der Shaker-Tests auf dem Flachbandprüfstand zeigen, dass die meisten Moden identifiziert werden können. Darüber hinaus können die Auswirkungen von Änderungen der Anregungsamplitude, der Radlast und des Reifeninnendrucks auf Frequenz und Amplitude qualitativ nachgewiesen werden. Einer der zu untersuchenden Schlüsselaspekte dieser Arbeit war der Einfluss der Fahrgeschwindigkeit. Die Ergebnisse weisen eine leichte Verringerung der Eigenfrequenzen bei Rollbeginn auf. Die Kraftamplituden in der Reifenaufstandsfläche steigen zunächst bei Rollbeginn, fallen aber oberhalb von

3 km/h deutlich ab. 1. und 2. Lateral-, 1. Vertikal- sowie 1. und 2. F/A-Mode weisen auch für den rollenden Reifen noch deutliche Amplitudenüberhöhungen auf.

Eine gute Übereinstimmung mit den Ergebnissen am Flachbandprüfstand konnte auch für die Eigenfrequenzen erzielt werden, die mit Hilfe der Shaker-Versuche auf dem Forschungstraktor bestimmt wurden. Für Radkraft- und Beschleunigungsamplituden konnte mit Rollbeginn ebenfalls eine Verringerung der Eigenfrequenzen beobachtet werden. Die Amplitudenhöhe reduziert sich um 35-50% und verbleibt mit zunehmender Fahrgeschwindigkeit nahezu auf diesem Niveau. Relevante Amplituden zeigen die 1. und 2. Lateral-Mode sowie die 1. F/A- und 1. Vertikal-Mode. Die Anregung des Reifens bei Rundlauf- und Schlagleistentests unterscheidet sich elementar von der Shakeranregung. Dennoch weisen die Frequenzspektren bestimmte Ähnlichkeiten auf. Die o.g. vier Reifenmoden sind auch unter diese Anregungsbedingungen die relevantesten und können identifiziert werden. Für den Fahrer spürbare Vibrationen sind insbesondere auf Bouncing und 1. Lateral-Mode zurückzuführen. Oberhalb von 12 Hz zeigt die Isolierung durch Kabinen- und Sitzfederung Wirkung, so dass die durch Moden höherer Ordnung verursachte Exposition des Fahres nicht als kritisch zu bewerten ist.

Die Ergebnisse zeigen, dass die Eigenmoden von Traktorreifen einen deutlichen Einfluss auf die Schwingungsübertragung in das Fahrzeug haben. Diese Vibrationen führen in erster Linie zu einer erhöhten Belastung von Fahrzeugkomponenten. Darüber hinaus können niedrigfrequente Schwingungen zu großen Teilen in Kabine und Sitz übertragen werden, insbesondere wenn Kabinen- und Sitzfederung nicht korrekt abgestimmt sind.

## 1 INTRODUCTION

Vehicle vibrations of agricultural machinery have gained in importance enormously during the last years. Especially, the legal basis with the EU directive 2002/44/EC [1] and its implementation into national law with the corresponding ordinance [2] which is definitely mandatory from 2011 (agriculture and forestry with three more years transit time) has sensitized the manufacturers concerning the vibration behaviour of their vehicles accompanied with an increasing demand for ride comfort by the customers.

In several investigations and publications analysis, tuning and optimization of the tractor components (body/frame, drive train, suspended front axle, cabin and seat) on different tractors have been attended with the result that only an optimized combination can reduce vibrations and improve ride comfort and driving safety [3-5]. For passenger cars and trucks also the undercarriage has to be considered. The complex task is to isolate the driver and passengers from vibration without neglecting vehicle handling. The tires are the link between vehicle and driveway and therefore of special interest for the dynamic behaviour of vehicles. Tire-induced vibrations are one of the main sources of vibrations in vehicles [6]. Especially, for the high frequency range resonance peaks can be effectively reduced by the use of antiresonance. For agricultural and forestry tractors as well as mobile machinery being used for both transportation with driving velocities up to 80 km/h and field work various mutually contradictory demands arise. An evaluation of the vibration characteristics has to consider driving safety as well as ride comfort avoiding health hazards for the driver.

In [7] Pacejka distinguishes between low frequency and high frequency tire properties. In the high frequency range tires show several eigenfrequencies in vertical (radial), longitudinal (tangential) and lateral direction. For tractor tires this range starts above 10 Hz. The intensities of high frequency vibrations are lower than those in the low frequency range. But a light damping and matching local resonances of the vehicle components can lead to an amplification of mechanical vibrations and acoustical effects and thus to a decrease of ride comfort. Furthermore, Pacejka points out that high frequency vibration behaviour of rolling

tires had been dealt with only briefly in literature which is even more true for heavy tires.

In this thesis mechanical vibrations in the ride comfort frequency range up to 80 Hz are treated which is corresponding to the VDI Guideline 2257 "Human exposure to mechanical vibration – Whole body vibration" [8] and ISO 2631-1 [9; 10]. So the vertical (radial) and longitudinal (tangential) direction of tire vibration is of special interest. For the investigation of the broad frequency range for ride comfort issues a new mechanical shaker device has been developed in Hohenheim. With this device single frequency force excitations from about 3 Hz up to 80 Hz can be applied to a tire. From excitation and response of the system it is possible to identify the vibration modes of the tire. The shaker is designed to be applied to different testing facilities, available at Hohenheim: a Flat-belt Test Stand and a research tractor Fendt 509. Furthermore, uniformity and cleat tests have been conducted with the Fendt 509 in order to establish additional comparability between shaker, tire and impact excitation.

Besides the traditional methods of prototype testing powerful modelling tools enable to assess and design complete vehicle structures virtually at an early stage of the development process [11]. Tire manufacturers use very complex FEA-models of the tire to predict and check the characteristics during the design process [12]. For smaller tires like passenger car tires test rigs have been built which allow exciting tires at high frequencies to be able to validate the mentioned FEA-models for these frequency ranges. Modal characteristics of heavy tires could only be determined for the non-rolling condition e.g. by impact tests. The eigenfrequencies, mode shapes and modal damping are changing with the rolling speed of the tire which made it necessary to develop the mentioned investigation methods. Rubber characteristics and the behaviour of single tire components (e.g. carcass, belt) were not dealt with. The objective target of this research project is to examine the vibration behaviour of heavy tires in the frequency range from 10 up to 80 Hz for the non-rolling and rolling conditions on different testing facilities considering the corresponding environmental, boundary and operating conditions.

---

Moreover, the gained insight into the tire behaviour by these investigations can be applied to a corresponding tire model, which can display the vibration behaviour in the comfort range without being that complex as an FEA-model. With the analysed experimental investigations on the Hohenheim test rigs it should be possible to parameterize and validate this kind of model. By coupling such a tire model with an MBS-vehicle model it becomes possible to simulate driving manoeuvres of a complete vehicle.

Vehicle components' stress due to vibration and shock is significantly dependent on the tire's vibration characteristics since dynamics in the tire structure significantly contribute to the axle forces [13; 14]. Not only the level but also the spectral composition of forces is influenced by the tires. For this reason a preferably exact insight into the tire vibration behaviour can also contribute to an optimized design layout of vehicle components.

The examination of control tasks like anti-lock braking systems (ABS) require also tire models that can simulate high-frequency effects like low-frequency acoustics or brake chattering.

Furthermore, the driving surface is in direct contact with the tire and so extreme tire vibrations have big influence on stress, wear and economic life-time of the roads. Especially, for heavy vehicles like trucks, construction and agricultural machinery this is a common problem.

## 2 STATE OF THE ART

In the following chapter an overview of the investigations on the vibration behaviour of tires is given. Section 2.1 deals with agricultural tires in particular. As the market for passenger car and truck tires is much larger and the requirements concerning vehicle comfort have been much more distinct, number and extent of comfort relevant tire investigations are much larger than for agricultural tires. An overview is given in section 2.2. The review is limited to the interaction of tires on hard surface and the comfort relevant mechanical vibration behaviour which mainly is related to the vertical (radial) and longitudinal (tangential) directions. A detailed overview of investigations regarding vehicle handling can be found in [15]. Information about tire modelling is proceeded in section 2.3.

### 2.1 Investigations of agricultural tires

At the University of Hohenheim investigations on the vibration behaviour of agricultural tires have been carried out since 1978. The dynamic behaviour in the vertical direction has been analysed intensely on the Hohenheim flat-belt test stand [16-20]. Also the longitudinal forces were determined. The results represent an extensive database for vertical and longitudinal dynamics of agricultural tires from which a corresponding tire model was derived. For the description of the tire's spring and damping behaviour all parameters can be determined by drop tests. In this context the maximum frequency regarded was  $<10$  Hz. The combination of vibration and forces in all three directions were investigated on the Hohenheim Single-wheel tester by Armbruster, Barreilmeyer and Schlotter [21-23]. Schlotter analysed the influence of dynamic wheel loads on the horizontal forces [24; 25]. He carried out tests on passing different obstacles or exciting the measuring wheel of the Single-wheel tester by wheel load controller and the resulting vibration. Furthermore, he applied different tire models and calculated the transient force progression. Based on these works Ferhadbegovic developed the Hohenheim Tyre Model in MATLAB/Simulink as a dynamic so-called hybrid model for agricultural tires on rigid surface which uses both physical parameters (spring and damper coefficients) and empirically obtained data for the tire-ground characteristics [15]. In this context Schulze Zumkley examined an alternative



identification of tire parameters from road tests conducted with standard tractor equipped with new developed force measuring rims [26; 27]. Witzel extended the Hohenheim Tire Model in order to simulate passing obstacles [28-30].

Also the Institut für Landtechnik und Baumaschinen at the Technical University Berlin performed extensive investigations on agricultural tires. First examinations on the vibration behaviour of tractor tires were performed in 1975 by Sharon [31] and Owzar [32]. Sharon tested 23 different tractor tires for the vertical dynamic properties. First empiric equations allowed a numeric simulation. For technical reasons the influence of the driving velocity could not be considered yet. For this reason a tire test rig was designed where this influence could be examined [33; 34]. Kising compared three types of excitation (drop test, harmonic excitation, stochastic excitation) for the determination of the tire's dynamic properties and decided to perform stochastic excitations by a hydraulic pulser stimulating the lower frame of the flat-belt test stand with its belt and rolls. This root point excitation was limited in the maximum frequency of 10 Hz. Furthermore, Kising carried out investigations on the high-frequency lug-induced excitation of a radial and a diagonal tire by varying the driving speed from 0 – 50 km/h. Concerning the speed dependent resonances the half lug frequency is dominant. Lug-induced vibrations of diagonal tires are stronger than those of radial tires. Yeh examined the influence of the radial runout and unbalance on the dynamic behaviour of tractor tires [35]. The runout can cause heavy dynamic effects which have to be considered whereas unbalance only plays a minor role due to the low rotational speed. Siefkes designed an additional test rig for tractor tires [36]. He concentrated on tire dynamics in the contact area and the wear behaviour. In that context Siefkes calculated the first five eigenfrequencies of a standing tractor tire (18.4 R38 resp. 460/85 R38) by an FEA tire model and compared these results with the measuring results receiving an adequate accuracy. Furthermore, Siefkes compared the high frequent lug induced vertical axle accelerations of large agricultural tires [37]. Von Holst and Göhlich point out the influence of the noncircularity of tire and rim and emphasize that high-frequency dynamic effects are necessary to be considered in tractor simulation [38; 39]. For the simulation of the vertical dynamic behaviour of tractor tires von Holst compares an empirical and a physical tire model [40]. He describes different methods for the

determination of the vertical dynamic behaviour and the generation of input data for the parameterization of the tire models. Especially, for the physical tire model experiments on the mechanical vibration behaviour of the tire are necessary. A modal analysis for two different tractor tires was carried out for the in-plane direction. It could be shown that the lug-induced vibrations can excite the eigenmodes of the tire. The physical tire model used by von Holst is based on the work of Böhm [41]. Masenger investigated with a view to the rolling contact the dynamic behaviour of agricultural tires both on the road and soft soil [42]. Further investigations on the interaction between tractor tire and deformable soil [43] as well as the application of the corresponding tire model (section 2.2) for off-road vehicle simulation followed [44]. Böhm et al. performed further extensive research on tire dynamics which is specified in section 2.2.

In Braunschweig in the 1960s investigations on the dynamic loading of tractors were carried out and presented by Coenenberg [45]. Vehicle vibrations in a frequency range up to 75 Hz were measured and corresponding simplified frequency response systems were developed. In 1968 Wendeborn [46] investigated the ride comfort of tractors and in this context held the view based on several earlier publications that stiffness and damping could be determined on the non-rolling tire.

Hlawitschka [47] and Müller [48] also investigated vertical and longitudinal dynamic forces of agricultural tires in the 1970s in Dresden. A tractor model for the simulation of the forces acting on the front axle while passing obstacles was developed.

Laib from the University of Gödöllő examined the vibration excitation effect caused by deformable soil including the tire vibration behaviour [49].

In 1984 Stayner et al. from the Silsoe Research Institute examined the possibilities of tractor ride vibration simulation as a tool in the development process and divided it into the different parts [50]. They also emphasized the importance of a precise tire modelling and that the dynamic behaviour of rolling tractor tires needed further investigation for these purposes. Crolla and Horton from the

University of Leeds already regarded the factors which affect the dynamic behaviour of high speed tractors [51]. In cooperation with Stayner they proposed a tire model which was especially improved for the prediction of vibrations in longitudinal and lateral direction using a spring/damping combination in series [52]. The model was validated by comparison with extensive tractor tests passing a smooth track or a farm road for a frequency range up to 10 Hz. At the beginning of the 1990s examinations concerning the dynamic behaviour of tractor tires were carried out increasingly. Partially based on the results of Kising, Lines performed two similar experiments to investigate the differences of the transfer behaviour between rolling and non-rolling tire. On a hydraulic test stand a tractor was driven and vertically excited. In a second test setup a tractor was driven over a standard rough track. For both tests the transfer function was measured between the vertical input acceleration (second differential of ground elevation under the tire) and the acceleration on the cab floor under the driver's seat in six directions. The characteristics of rolling tires were found to be significantly different from those of non-rolling tires. Tire stiffness decreases at the onset of rolling and slowly increases in rolling speed. In the frequency range up to 12 Hz amplitude non-linearities appeared to be negligible for rolling tires. It appeared that at frequencies above half the lug passing frequency, tractor vibration is mainly correlated with excitation by radial runout tire lugs [53; 54].

Based on results of Crolla, Stayner and Lines, Deltenre and Destain investigated the vibration transfer behaviour of a tractor via model applying a vertical sine excitation to one wheel and simulating a sinusoidal track [55]. The influence of vehicle and tire parameters were shown limited to a maximum frequency of 10 Hz.

With a similar tractor model, but additional laboratory measurements and test drives Niskanen showed the effects of weight distribution, wheelbase and tire stiffness on the tractor vibration behaviour on smooth roads [56]. The source of excitation was the eccentricity of the tire.

At the Harper Adams University the vertical spring and damping behaviour of tractor tires was investigated with another Single-wheel tester. Keen passes a steel plate bumpy track laid on flat tarmac surface to generate a square wave input

to the wheel and a compacted sandy loam soil in a ground level soil tank to cut a sine wave into the surface. Thus, the influence of root point excitation by a cleat track or a sinusoidal flexible track has been considered for the calculation of spring and damping parameters [57]. A significant increasing of the damping on flexible subsoil was shown. The interaction of driving forces at the determination of the vertical damping parameters and the influence of a wheel suspension represent a substantial extension of the previous investigations [58]. Furthermore, an overview of investigations concerning vertical and lateral dynamic properties of tractor tires is recapitulated [25].

Ahmed and Goupillon from Franche-Compte University and Cemagref, France [59] presented a tractor model in DADS consisting of three suspended structures (tractor chassis, cabin and seat/driver unit). The tire was modelled as a suspended rigid ring. The vertical dynamic tire parameters (stiffness and damping) were calculated from the eigenfrequency, mass and decay rate which can be derived from the measured vertical acceleration signals of the wheel hub passing a standard ISO-5008 track (smooth track). Longitudinal and lateral stiffness were determined statically on the non-rolling tire and corrected by comparison between simulation and test.

At the University of Leuven Clijmans et al. analysed the effect of tire pressure (stiffness) and mass addition on the dynamic behaviour (resonance frequencies) of a lawn mower by experimental modal analysis [60]. The adapted modal models show good agreement with the measured vibrations. Furthermore, they carried out an experimental modal analysis of a tractor in order to derive a structural dynamic model that contains the eigenfrequencies, modal dampings and mode shapes of the machine [61]. The model can be used to examine the effects of possible design changes which inevitably involve local modifications in stiffness and mass/inertia. For vibration tests on heavy wheeled vehicles Anthonis, Kennes et al. designed a mobile shaker device which can excite the vehicle selectively in a range between 0.5 and 21 Hz [5; 62]. Additionally, Hostens et al. designed a six-degrees-of-freedom test rig for the investigation of machinery vibrations [63].

## 2.2 Investigations of passenger car and truck tires

At the 1. Institut für Mechanik of the Technical University Berlin extensive investigations on tire characteristics have been carried out since the 1960s dealing especially with the dynamic behaviour. Böhm pointed out early that a transient non-linear examination of the tire is inevitable for an exact modelling and introduced first non-linear tire calculations [41; 64; 65]. Based on these theoretical works Böhm presented a number of complex physical models. In 1985 he developed a 2D rigid ring model as a transient dynamic model which considers the fundamental mode behaviour of the belt up to 100 Hz for passenger car tires [66]. Oertel integrated the lug dynamics into the calculation of the contact forces [67]. Finally, the 2D rigid ring model was enhanced to a discretized elastic ring model and extended to a 3D model [68; 69]. In this context Zhang investigated the high-frequency transfer behaviour of chassis systems [70] and Kmoch developed testing methods for the evaluation of the dynamic tire properties [71]. Zachow presented a 3D-membrane shell model applied to a tractor tire on rigid surface and on soft soil [72]. Important results of the SFB 181 research project dealing with high-frequency wheel rolling contact will be referred to in chapter 3 [73]. The commercialized tire models RMOD-K and LMS CD-Tire have been established based on the work of Böhm.

In [7] Pacejka distinguishes for the tire in-plane dynamics between high and low frequency properties which is defined below the lowest natural frequency of the tire. For passenger car and truck tires he estimates this range up to about 20 Hz in the in-plane direction. For lateral vibration this limit has to be reduced. Further extensive investigations have been performed by Zegelaar [74; 75]. He examined the in-plane dynamics of passenger car tires. Developing a more detailed flexible and a compact rigid ring model he showed the validity for the latter model up to 80 Hz for the longitudinal and 100 Hz for the vertical direction. In this context he pointed out that the flexible modes may also have considerable amplitudes and need to be included into a corresponding high-frequency tire model depending on the regarded frequency range. He also presented a chronological survey of literature on experimental and theoretical analysis of tire in-plane vibrations. In the following Maurice extended and verified the SWIFT model for the lateral direction

and regarded combined slip conditions [76]. Schmeitz, finally, added and verified the possibility to calculate the tire's enveloping properties for arbitrary obstacles and road surfaces [77].

At the University of Leuven, Belgium, Kindt et al. investigated tire/road noise and the influence on vehicle structure borne noise. For this purpose experimental modal analysis [78] and special cleat tests on a new test rig were carried out for radial tires [79]. A three-dimensional flexible ring tire model was developed in parallel valid up to 300 Hz [80]. By a further test setup the tire's dynamic transfer behaviour was determined at its operational excitation levels [81].

Yu and Aboutorabi from Kumho [82] describe a combined tire, wheel and suspension FEA model for the non-rolling, inflated and loaded tire in vertical direction. For the vehicle bouncing mode the chassis vibration is high, but the spindle amplitude is low. The spindle vibration amplitude is high for the wheel hopping mode and the first radial mode where the latter is dominant for the transmission of vibration to the vehicle. Also the 2<sup>nd</sup> radial mode shows vibrations at the spindle. For higher resonance frequencies top and bottom of the tire are vibrating out-of phase leading to low vibrations of the spindle. So the tire vibrates in response to the road roughness, but only little forces are transmitted to the vehicle. In between the resonance frequencies the tire is rigid and road roughness is transmitted to the spindle. Consequently, the higher the modal density is the better the ride comfort of the tire might be.

Bruni et al. from Politecnico di Milano describe experimental tests on the parameter identification of a tire model for the study of in-plane dynamics in a frequency range of 0-130 Hz [83]. The tire model used is Pacejka's "rigid ring model". For passenger car tires this model is sufficient since all eigenfrequencies in this range can be simulated with a rigid ring.

Belluzzo et al. from Pirelli Pneumatici and Politecnico di Milano developed a mathematical tire model for predicting the dynamic vertical forces induced by road irregularities in a frequency range of 0-250 Hz [84]. The model was established for the optimization of the tires in the development process and can be parameterized

by virtual tests with 3D finite element tire models. First comparisons with indoor and outdoor tests showed good accuracy.

Extensive investigations on the modal behaviour and the vibration transmission of automotive tires have been carried out by Soedel et al. from Purdue University, West Lafayette, Indiana, U.S.A. in cooperation with the Firestone Tire and Rubber Company, Akron, Ohio, U.S.A. Soedel et al. present an analytical method which allows to calculate eigenfrequencies and mode shapes of the tire in contact to the ground from the corresponding experimental or theoretical results of the same tire not in contact to the ground [85-87].

In [88] Ushijima and Takayama from Bridgestone identify the dynamic characteristics of a loaded non-rolling tire via modal analysis. Then a passenger car suspension system including the tire is simulated and verified. For the rolling tire the non-rolling modal parameters are corrected by a factor estimated from measurements under rolling condition. The verification with cleat tests shows a good agreement.

Mousseau from Ford Motor Company formulated a simplified in-plane FE based tire model for durability road load simulations [14]. He came to the result that on the dynamic in-plane forces acting on the axle the first vibration modes have significant influence (1<sup>st</sup> F/A and 1<sup>st</sup> Vertical). Kao presents in [89] a three-dimensional dynamic tire model called BAT (bushing-analogy tire) model. In this model the tire is divided into a rigid wheel body (masses/inertia of rim, bead and half of the sidewall), connecting spring/damper elements representing the sidewall and a tread body (masses/inertia of tread, belt and half of the sidewall). Thus, not only rough terrain driving and severe manoeuvres can be realized but also the dynamic behaviour of the tire for the first modes can be modelled [90].

Scavuzzo et al. from Goodyear Tire & Rubber Company studied measured modes of tires for different vehicles. In [91] they describe how these modes influence vehicle ride quality and the parameters controlling these modes. In [92] they specially studied the effects of the spindle and patch boundary conditions. Liu also from Goodyear Tire & Rubber Company investigated the global dynamic response

of a rolling passenger car tire via finite element transient dynamics simulation [93]. Independent from the driving velocity two characteristic frequencies for the first vertical and fore/aft mode could be determined clearly.

Dorfi from Hankook Tire investigated the tire in-plane force transmission for rolling over cleats [94] and due to tire non-uniformities [95]. In this context he explains tire vibration phenomena and the influence of tire mass and stiffness on modal frequencies by applying different tire models. A comparison of experimental cleat test data with FTire simulation data shows very good correlation between reality and model. Furthermore, Dorfi et al. published two extensive SAE papers treating the vibration modes of radial tires. In [96] measurement, prediction and categorization of modes under different boundary conditions are described for a P235/75R17 radial tire. The second paper [97] deals with the influence of the rolling and non-rolling condition.

In Hannover Barz and Donges designed and established a new tire test rig for the determination of car tires' non uniformity influence in a frequency range of 0-300 Hz [98]. The results show that especially at higher velocities radial force variation and tangential force variation are not in inevitable dependency e.g. due to the 1<sup>st</sup> tire's belt eigenfrequency in the direction of circumference. Consequently, they point out the necessity of measuring the tires in the full speed range and regarding all six degrees of freedom in which the wheel can oscillate.

Lion from Munich investigated and modelled the relatively low frequency and high amplitude dependency of elastomer components exemplified for the vertical dynamic behaviour of a passenger car tire [99]. With increasing excitation amplitude the peak maxima are reduced and shifted towards lower frequency values which is explained with the strain softening of the elastomer. This effect is named "Payne effect" and arises in particle filled rubbers.

Said from Stuttgart describes in [100] the modifications of a drum tire test stand in order to reduce the measurement error in the comfort relevant frequency range (0-150 Hz) on the one hand and to enlarge the dynamic force measuring range, especially at the test rigs eigenfrequency on the other hand.



Allison and Sharp report on a research project on longitudinal vibrations of vehicles. In this context a special designed test rig is introduced which allows forcing to be applied by an electrodynamic shaker to the hub in vertical and longitudinal direction. The mathematical model of the tire is a rigid ring model and valid in the frequency range up to about 100 Hz for passenger car tires [101].

Leysens and Gnoerich give an overview on the tire-road noise generation and the interaction with the system vehicle [102]. The transmissibility of the tire determines the vibration spectrum of the input into the hub. The lower structural modes and the cavity resonance have the main influence on the force transfer behaviour below 300 Hz and are defined by the tire dimension, structure and inflation pressure. These parameters are fixed after the tire is optimized for handling. Thus, handling and vibration/noise performance have to be optimized simultaneously.

Dihua and Chengjian from Tsinghua University, Beijing, used experimental modal tire parameters to calculate the static vertical tire stiffness and the distribution of vertical and shear forces [103]. Furthermore, the tire enveloping properties were investigated.

Duvenir et al. from Michelin Tyre Company present the simulation of different NVH tests in ADAMS [104]. The tire modal model is derived from non-linear FE analysis by the so-called "Craig-Bampton" dynamic substructuring method [105] and is valid for a frequency range between 0 and 200 Hz. Translating the tire model into a flexible body in ADAMS leads to an easy coupling with other NVH-related modules and the simulation of full vehicles in ADAMS.

Ropers describes in [106] the investigations of tire vibrations at passing an obstacle. He points out that regarding the tire alone without consideration of the interaction with the undercarriage is not useful for comfort purposes. Different examples show that the vibrations at the wheel hub are strongly due to these interactions and the further boundary conditions. Modelling the tire in a frequency range up to 50 Hz is possible via rigid ring models. For higher frequencies the tire's belt bending modes have to be considered. For the investigated passenger

car tire it could be determined that tire vibrations with more than 140 Hz are nearly independent from carriage parameters.

In cooperation with Instron Structural Testing Systems (IST) OPEL has realized a “deterioration” test rig for complete vehicles [107]. The driven wheels are running on flat belts which can be excited vertically by hydraulic cylinders in a frequency range up to 50 Hz.

## 2.3 Modeling and simulation

For the strong influence of the tires on vehicle dynamics exact tire models are required [108-110] representing and predicting tire properties. Over the past 50 years a large number of different tire models have been developed and published. Depending on the field of application and the requirements and due to their approach the complexity, accuracy, calculating time and number of parameters are different starting at simple mathematical models up to detailed dynamic FEA models. This important differentiation between physical and empirical tire models is reflected in the structure of this chapter.

With growing complexity, the tire forces cannot only be calculated for the quasi-static and low-frequency range ( $< 10$  Hz) but also for high-frequency excitation based on the modal behaviour of the tire structure which allows ride comfort, bumpy road and operating load simulation. Thus, the describable frequency range is another distinctive feature. Furthermore, also recordable wave length of the road irregularities and the description of the ground contact are differentiating factors.

An overview on different important existing tire models used for passenger car development and requirements for different application areas in development are given by Bösch et al. [111] and Einsle [112]. Lugner compared the results of different tire models simulating defined test runs on a test rig and ascertained partially significant variations from each other [113]. As mentioned above, a division into handling and comfort models can be made due to the interesting frequency range. For tire handling models Ferhadbegović gives a detailed overview in his PhD thesis [15]. Thus, in the following the overview is limited to those tire models which are able to reproduce ride comfort vibration properties.

In this context it is necessary to mention that for ride comfort simulation not only the tire model but also the further vehicle model with the affecting sub-models have to satisfy the comfort frequency range up to 80 Hz and more which was already established by Zhang for passenger car models up to a frequency range of 150 Hz [70]. Böhm concluded that commonly used MBS vehicle models which cover frequencies up to approximately 20 Hz drop out as well as the very detailed

FEA models. The vehicle represented as a discrete mass-point-system is proposed [114]. Also Gipser refers to a reasonable balance between tire and vehicle model complexity [115].

### **2.3.1 Physical models**

Physical or mechanical models describe the processes occurring inside the tire by discretisation into mass elements and connecting them by spring/damper systems. The accuracy is depending on several factors particularly step size and level of discretization. Among a large number of special purpose mechanical tire models of reduced complexity this category can roughly be subdivided into spokes models, rigid ring models and flexible ring models. A completely different approach is the base of the so-called modal models which will be explained at the end of this section.

#### **2.3.1.1 FEA models**

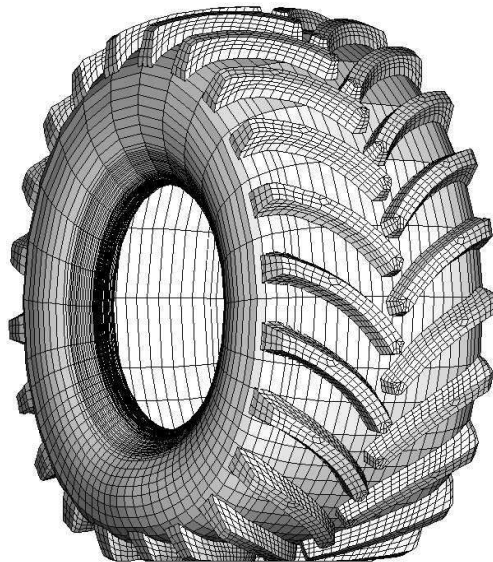
The most accurate tire models are 3D FEA models which also give a detailed insight into the tire's structure and, of course, belong to the flexible ring models. This is one reason why FE analysis has developed to the most important CAE tool during the tire development process [115]. Standard calculations are footprint analysis under static, steady-state rolling and certain transient conditions as well as stress and strength in carcass and belt, modal analysis and prediction of steady-state traction and cornering forces. Advanced applications are:

- rolling resistance and optimization,
- tire enveloping properties on short wavelength obstacles
- tire inflating process and tire-rim fitting
- traction on water, snow and soft soil
- estimation of friction energy dissipation, thermal maps and chemical evolutions
- tread wear simulation
- impact and misuse analysis
- coupled acoustic-structural analysis including excitation in the tread on different surfaces
- tire manufacturing (polymer synthesis)

Future challenges are:

- further integration of FEA procedure into the CAE process chain
- improvement of the material models for the different components
- geometrical refinements
- improvement of friction models
- development and improvement of different ground models
- damage simulation
- simulation of the mixing/forming/building process

A comprehensive collection of papers dealing with FEA for tires is attached in [115]. Fodor et al. from TAURUS Agrotyre and University of Miskolc, Hungary publish a finite element package specially developed for agricultural tires (**Figure 1**) due to their different tasks and properties compared with passenger car or truck tires and supporting a hierarchical design process [116].

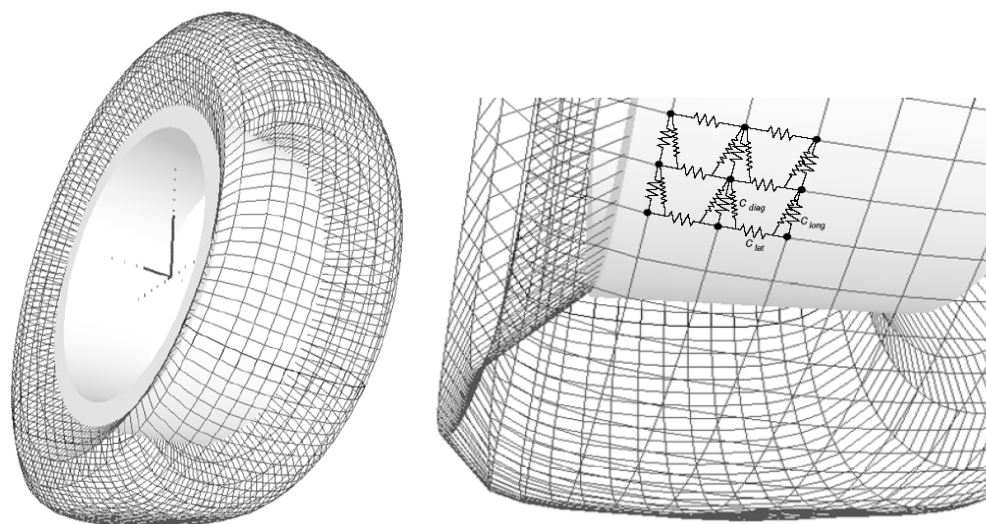


**Figure 1:** FEA model of a tractor tire [116]

### 2.3.1.2 Mechanical models of reduced complexity

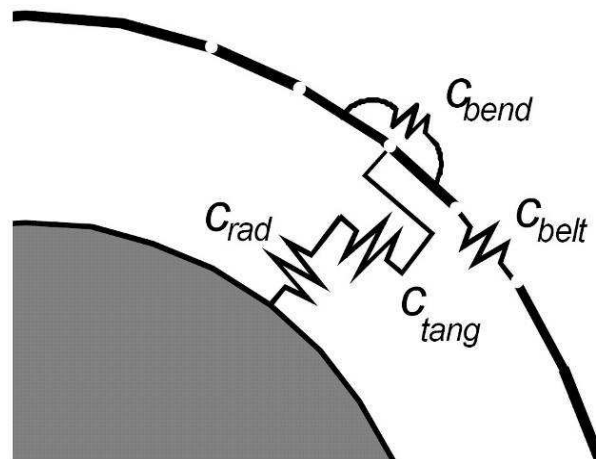
Concerning their complexity so-called flexible ring tire models can be classified below the FE models. Most known representatives of this category are FETire and

FTire from Gipser, RMOD-K 30/31 and LMS CDTire 30/40 respectively which have the same roots going back to Böhm [69] and the model of Mousseau et al. [14]. These so-called structural mechanical models work with a slightly coarser mesh. Their general functionality is similar to that of the above mentioned FEA models whereas computing time is considerably shortened.



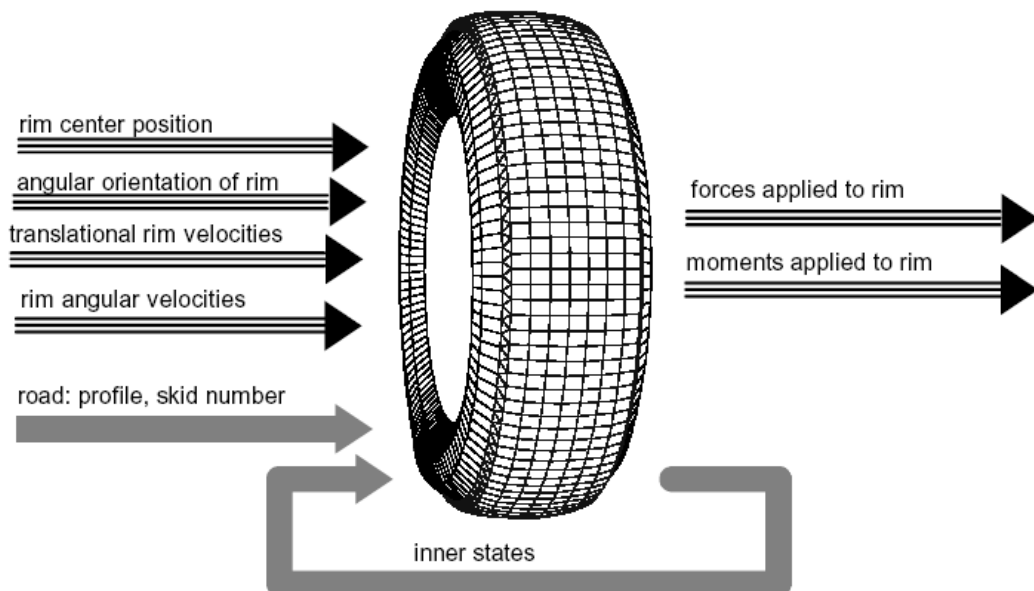
**Figure 2:** FETire: Mesh of structure model [115]

FETire is a coarse-mesh finite element tire model and belongs to the FTire family using the same program interface like FTire and RTire. With a structure model consisting of 1000 to 5000 lumped mass elements its real-time factor is about 300 at present. FETire is an advancement and redesign of DNS-Tire which was also developed by Gipser [117; 118]. Today it is mainly used for assistance in the parameterization of FTire, theoretical investigations on tire response to non-standard excitations and studies about the influence of tire design characteristics to handling and ride comfort properties. With the special version FETire/modal linearization and modal analysis of the unloaded tire can be carried out. By mesh refinement around the contact patch FETire/static can calculate non-linear static load-cases like high sharp-edged obstacles for the loaded but standing tire [115].



**Figure 3:** Two-dimensional belt discretisation, simplified [118].

As FTire seems to be the best compromise between range of application, calculating time and accuracy it is the most widely-used model of the FTire family. As many other mechanical models the kernel consists of two different parts. The description of the tire's stiffness, damping and inertia properties is summarized in the so-called structure model. Tread/road contact, computation of contact pressure distribution and friction forces belong to the tread model.



**Figure 4:** FTire input and output parameters [118]

The structure model consists of 80 to 200 lumped-mass elements connected via spatialized spring/damper elements. Concerning vibration the model is valid up to 150 Hz for in-plane and out-of-plane direction. Also vibration excitation by tire

imperfections, traction, handling and rolling resistance studies on uneven roads can be realized. Extensions like thermal and wear model, tire misuse, assessment of suspension control systems and sudden pressure loss have been integrated meanwhile. The real-time factor is specified to be 5 to 20. The required input parameters of FTire are shown in Figure 4. Contrary to most empirical or semi-empirical models the slip is not used as input parameter as it is interpreted as a result of the longitudinal force in the tread pattern [115; 118-123].

A similar approach to FTire is used by the also commercialized RMOD-K and its successor LMS Comfort and Durability Tire (CDTire). Applications of this model family range from comfort to stress/strength studies up to the simulation of handling properties. As mentioned above the roots of RMOD-K are going back to Böhm, Oertel and Fandre [69; 124-126]. Since 1996 it has been commercially available which permitted a broad distribution to the automobile manufacturers. Finally, LMS took over the model, renamed it as CDTire and has been the official supplier and distributor since 2002 for the most common MBS programs DADS, MSC.ADAMS and SIMPACK.

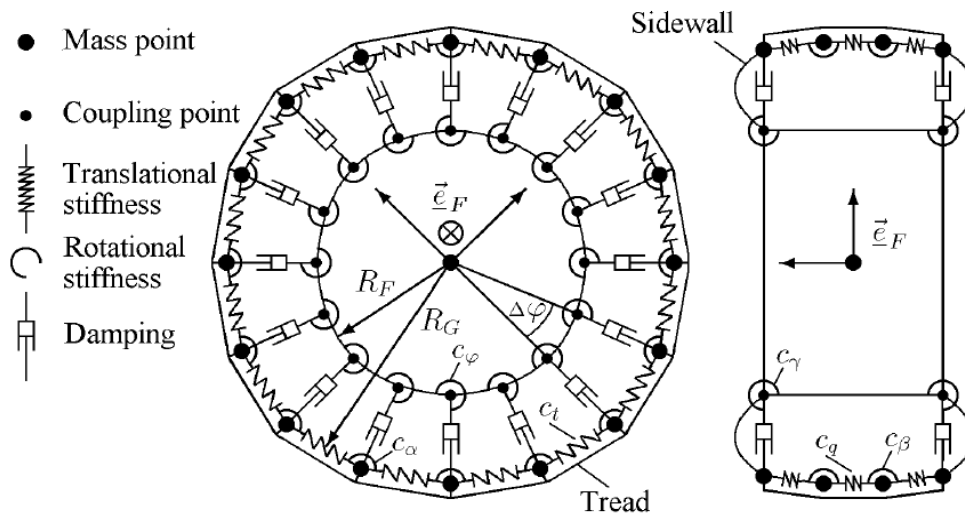
CDTire and RMOD-K respectively are subdivided into three parts:

- LMS CDTire 20 equals RMOD-K 20 (rigid ring model)
- LMS CDTire 30 equals RMOD-K 31
- LMS CDTire 40 equals RMOD-K 7.0

Contrary to CDTire 20 which belongs to the rigid ring models in CDTire 30 the belt is flexible. Thus, short-wave excitations in the tire's midplane can be considered. As shown in Figure 5 CDTire 40 is a further extension which discretizes not only in the midplane but in standard four parallel planes. By the increasing degrees of freedom the computing time is growing accordingly.

Limitations of CDTire are given in [127]. So only the inflated tire can be described. Furthermore, motorcycle and aircraft tires are not possible as well as off-road tires because of the height of their profile/lugs.





**Figure 5:** Structure model of CDTire 40 [128]

The model parameters of FTire and RMOD-K and their determination are quite similar which led to a good consistency of the calculation results between both model approaches [123]. Further applications of RMOD-K are presented in [128; 129].

Representatives of the rigid ring tire models are RTire (low-end member of the FTire model family), RMOD-K 20 and CD Tire 20. The steel belt as the heaviest vibrating part of the tire is modelled as one rigid body. Accordingly, only the rigid body modes of the tire can be reflected. Regarding passenger car tires these models cover a frequency range up to 100 Hz which make them suitable for ride comfort purposes. For the investigated heavy tires in this project the first flexible body modes occur far below 50 Hz and so restrict the application range considerably.

If the structural tire vibrations are of no interest and the corresponding limitation of the application is acceptable the so-called spokes models can be applied. Short wavelength unevennesses can be resolved with this approach.

### 2.3.1.3 Modal models

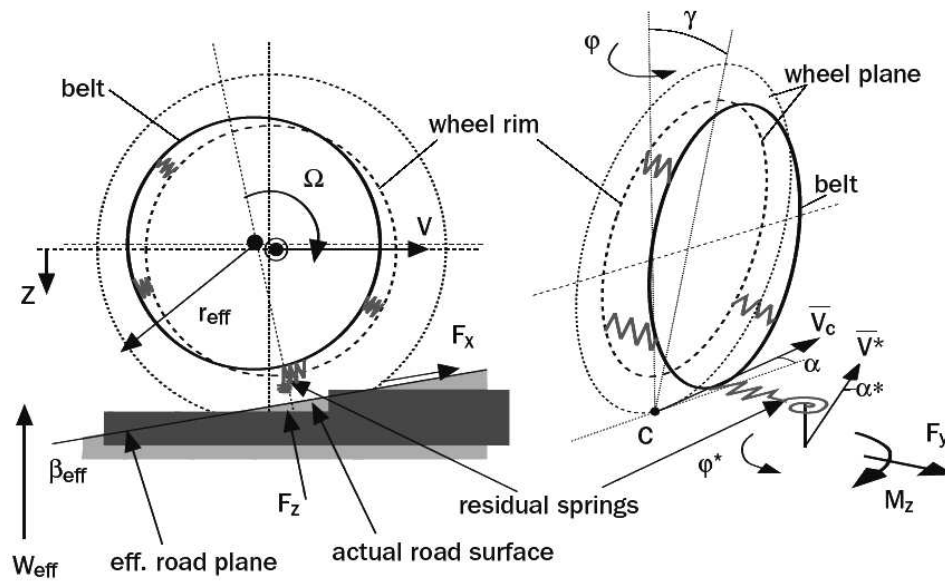
Modal models follow a quite different approach compared to the mechanical models described above. These models represent the tire structure as a flexible body within the MBS program. The contact model corresponds to the above mentioned models. In order to provide the modal data for such a flexible model a corresponding detailed FE model is necessary. The eigenfrequencies and related mode shapes can be reproduced quite exact since they are defined by a linear combination of the first mode shapes of the unloaded tire which might be a disadvantage for large deflections of the tire when rolling over high obstacles. Examples of this type can be found in [104; 130].

### 2.3.2 Empirical models

Empirical or phenomenological models are based on tire characteristic maps which have to be determined by extensive measurements on special tire test rigs. Their numerous parameters do usually not have a physical meaning and have a limited area of validity concerning the operational conditions. Main advantages are a high degree of accuracy and short computing time.

The most famous representative of this category is Magic Formula of which countless different versions and adoptions are in use. The extension of Magic Formula covering also transient conditions, short wavelength unevenness and the frequency range up to 100 Hz (for passenger car tires) is MF-Swift (Short Wavelength Intermediate Frequency Tire Model) [131; 132]. Figure 6 shows the general setup with a rigid ring and several spring elements. Further improvement of the reactions on short wavelength irregularities is achieved by a special non-linear road filter. Since the horizontal forces are still calculated by Magic Formula MF-Swift is assigned to the semi-empirical models. The main applications are:

- Strength/stress studies
- Tire shimmy behaviour
- Evaluation of driver assistance systems
- Cornering on uneven road



**Figure 6:** Basic setup of MF-Swift [132].

A further purely empirical method is the experimental determination of transfer functions between tread and axle in vertical direction which can directly be implemented into an MBS model as a force transmission element [133; 134]. Concerning the operating conditions this model, of course, is very limited and only vertical vibration can be described. Furthermore, this modelling approach requires a sufficient accuracy concerning frequencies and amplitudes. Nevertheless, for studies on special excitation cases and an analysis of the transfer path this method may be helpful. Dorfi proposed different approaches for the tire in-plane force generation due to either non-uniformities or cleat impacts [94; 95].

Summarizing the application of the described tire models on heavy and especially off-road tires in this project it has to be stated that from the commercially available models only FTire is feasible. Swift and CDTire (RMOD-K) had to be excluded due to their described limitations.

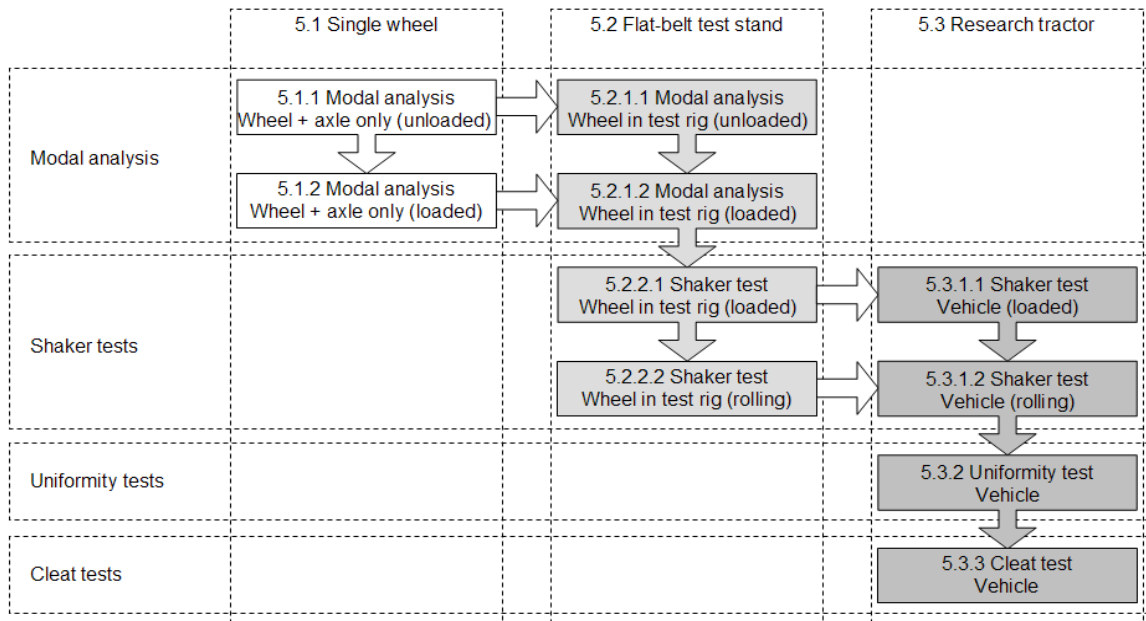
## 2.4 Summary and further approach

Comfort relevant vibrations of passenger car and truck tires were and are the objective of many research projects. Corresponding tire testing facilities do exist since relevancy and turnover are higher in this market segment. Furthermore, smaller tires can be modelled satisfactorily in the frequency range relevant for ride comfort up to 80 or even 100 Hz by so-called rigid ring tire models as the flexible tire modes usually occur above this range.

Investigations on agricultural and other heavy tires have mainly been carried out concerning handling or only for the standing tire. Only a few test rigs are existing which are dedicated to high-frequency vibration testing. Tire models capable for comfort have only roughly and rarely been parameterized for this sort of tires. A systematic validation is still outstanding. Furthermore, agricultural tires generally have lower resonance frequencies. Consequently, the mentioned frequency range up to 80 Hz contains more and also flexible tire vibration modes.

For this reason the experimental investigation of tractor tire vibrations by different testing methods is treated in this thesis. Main objective is to determine the tire vibration modes with respect to different boundary and operating conditions.

Figure 7 shows the derived schematic approach to the comparative tire vibration examinations. At first, by the method of the experimental modal analysis the front and rear wheel's eigenfrequencies, modal dampings and mode shapes are determined for different boundary conditions of the contact patch and the spindle. Another modal analysis was carried out on the rear tire mounted on the flat-belt test stand for the unloaded and loaded condition to check a possible influence of the rig. These results are compared with those of the shaker tests with the non-rolling tire on the flat-belt test stand. Hereafter, the influence of rotational speed is investigated. In parallel the described shaker tests were also carried out with the research tractor which enables a comparison between test rig and vehicle. By the uniformity tests the influence of the modal tire behaviour under operating conditions is examined. Additionally, the results of cleat tests are used to check the influence of this more complex excitation against the preceding findings.



**Figure 7:** Schematic approach to comparative tire vibration investigations

### 3 THE VIBRATION BEHAVIOUR OF TIRES

Concerning vehicle vibration several authors defined different classifications by frequency range. In [70] Zhang proposes the following division:

- Handling performance and vehicle stability 0 to 5 Hz
- Ride comfort and vibrations 5 to 50 Hz
- Acoustic properties over 40 Hz

Mitschke, however, differentiates between tangible (< 20 Hz) and audible (> 100 Hz) vibrations which can also be expressed by vibration and noise. The transition range between 20 and 100 Hz is characterized by the term “harshness” [135]. The commonly used abbreviation “NVH” (Noise, Vibration and Harshness) is resulting from this classification.

In [15] Ferhadbegović presents the Hohenheim Tire Model and its validation for tractor tires in the frequency range up to 10 Hz which is relevant for driving dynamics. For tractor tires starting at about 10 Hz the first tire modes occur. These modes are supposed to have an influence on the vibration transfer behaviour and consequently on the axle dynamics. According to the VDI Guideline 2257 [8] for impairment of the sense of well-being, performance and health and the ISO 2631-1 [9; 10] the upper frequency is defined with 80 Hz. This limit was also adopted by Bösch [111] and Schmeitz [77]. Consequently, for the following conducted investigations a frequency range between 10 and 80 Hz has been selected.

#### 3.1 Vibration sources

Vehicle vibrations can be excited by different sources at different frequency domains:

- Unevenness of the driveway and surface roughness (driveway related)
- Tire non-uniformities (geometry, stiffness and mass), tread pattern/lugs (tire related)
- Transient slip conditions between tire and driveway
- Engine, transmission and other component vibrations (vehicle related)

In the frequency range up to 30 Hz the unevenness of the driveway is the most intensive source of excitation for a passenger car as a vibrating system. The driveway is exciting vertical motions by the unevenness on the one hand, and it is stressed by the generated wheel load variations on the other hand. Generally, the driveway excitation consists of various amplitudes and wave lengths of non regular distances and thus is stochastic [136]. For tractor tires Schlotter, however, showed the dominant influence of radial runout and lugs on the wheel load fluctuations compared to the stochastic excitation by a usual road surface [23].

Regarding the pneumatic tire in the high-frequency range both the structural mechanics of the tire itself and the contact mechanics to the ground have to be considered and are intrinsically tied to each other [73]. Accordingly, global (structural dynamic) and local (limited to the contact area) deformations can be distinguished. Global deformations (static deformations and mode shapes) arise from variable contact forces which apply in one imaginary contact point. Local deformations are limited to the contact area and their effects can be treated quasi statically except the lug influence. Concerning the interaction between contact mechanics, tire and suspension dynamics, generally, the tire's dynamic action on the axle, on the ground and on the ambient air have to be distinguished. For passenger car tires Böhm pointed out that by the rolling contact the radial rigid body modes are excited most at frequencies up to 100 Hz. The harmonics (flexible modes) have influence on force distribution on the road, on the rim and on the air in the wheelhouse, but hardly on the vertical and horizontal axle dynamics. In fact, the flexible modes of the belt may affect the stick/slip conditions of the lugs in the tread and, thus, may lead to a loss of driving stability. Cleat tests on a roller drum showed effects of the tire dynamics on the wheel axle up to approximately 150 Hz [114].

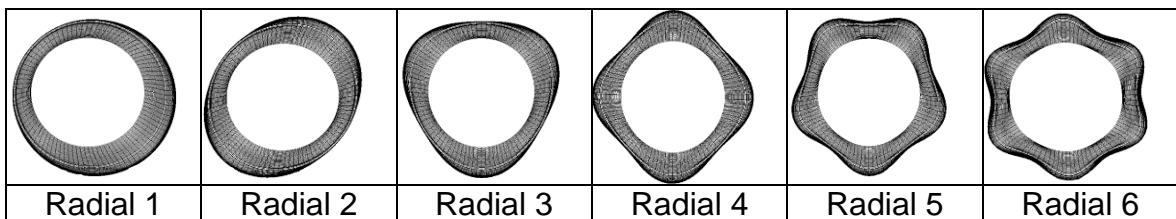
### 3.2 Categorization of vibration mode shapes

The naming convention used to identify the tire modes varies considerably in literature. According to [137] in the following the naming convention used throughout this thesis is explained.

#### 3.2.1 Unloaded condition

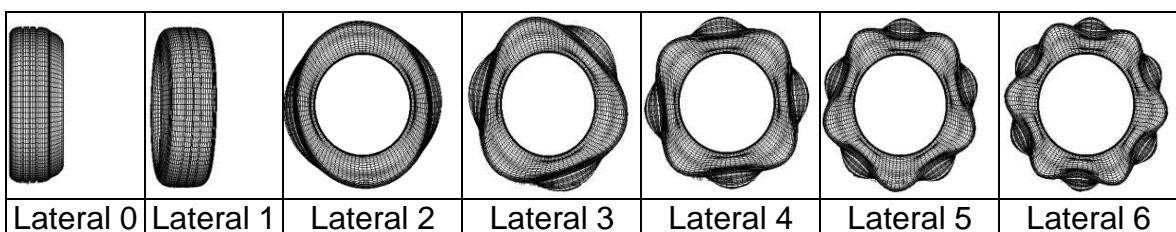
For the unloaded condition (free patch) **Table 1** shows the radial or in-plane mode shapes. As Radial 0 mode shape which is not shown because of its exceptional position the rotation around the axle against the rim is introduced (also often called “torsion” mode) although in some references also the so-called “breathing” mode is referred to as Radial 0 mode [85]. The Radial 1 mode is the translational displacement of the rigid belt. The following higher modes manifest a deformation of the belt where the number of nodes and antinodes is corresponding to the mode number.

**Table 1:** Radial mode shapes of an unloaded tire (free patch)



The lateral or out-of-plane modes exhibit the same coherence concerning the numbering. The rigid body modes usually have a lower eigenfrequency due to the lower stiffness of the sidewall in lateral direction [138]. The Lateral 0 mode is the pure lateral translation of the rigid belt, Lateral 1 represents a pure rotation around the in-plane axes.

**Table 2:** Lateral mode shapes of an unloaded tire (free patch)

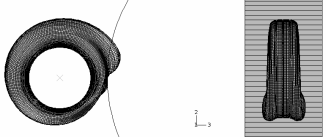
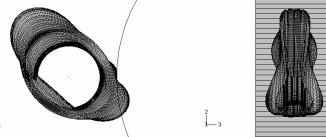
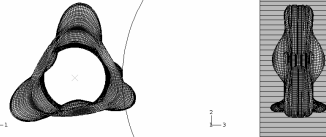
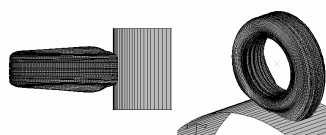
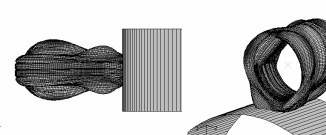
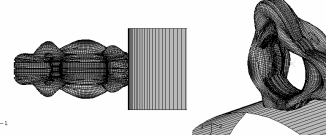
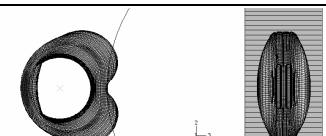
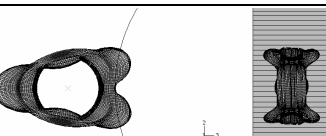
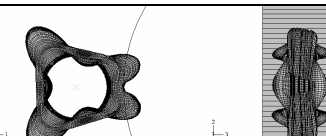
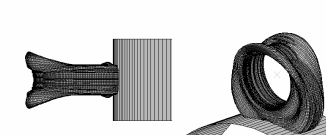
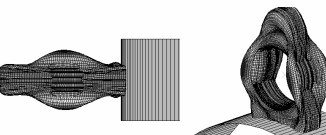
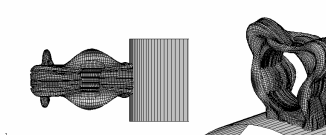

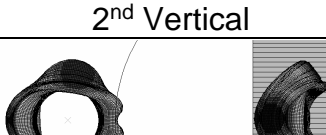
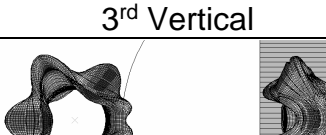
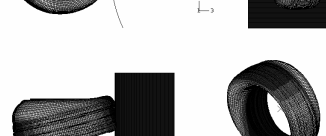
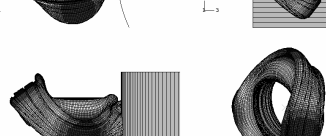
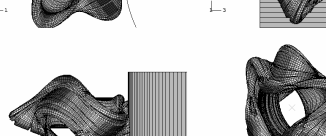




### 3.2.2 Loaded condition

As explained below in 3.3.4 the axle's (spindle) constraint conditions directly affect the modes of the loaded tire. Table 3 contains the mode shapes of a loaded tire (fixed patch) and pinned or fixed spindle for the first three harmonics.

**Table 3:** Mode shapes of a loaded tire [137]

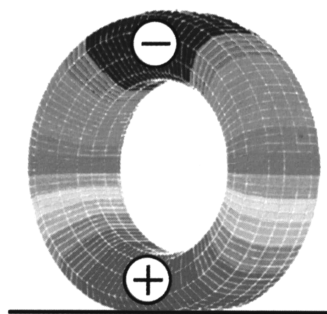
	Rigid body mode	1 <sup>st</sup> flexible mode	2 <sup>nd</sup> flexible mode
In-plane / radial modes	 1 <sup>st</sup> F/A	 2 <sup>nd</sup> F/A	 3 <sup>rd</sup> F/A
	 1 <sup>st</sup> Vertical	 2 <sup>nd</sup> Vertical	 3 <sup>rd</sup> Vertical
	 1 <sup>st</sup> Lateral	 2 <sup>nd</sup> Lateral	 3 <sup>rd</sup> Lateral
	 1 <sup>st</sup> Steering	 2 <sup>nd</sup> Steering	 3 <sup>rd</sup> Steering
	 1 <sup>st</sup> Lateral	 2 <sup>nd</sup> Lateral	 3 <sup>rd</sup> Lateral
	 1 <sup>st</sup> Steering	 2 <sup>nd</sup> Steering	 3 <sup>rd</sup> Steering

According to Wheeler et al. [96] the four loaded modes' categories are related back to the unloaded tire modes. Consequently, the radial modes transform into vertical and F/A (longitudinal) modes (in-plane modes) and the lateral modes transform into lateral and steering modes (out-of-plane modes). Further explanations are given in 3.3.5.

For a free spindle the so-called "hop" or bouncing modes [92] additionally occur in vertical, lateral and F/A direction. In some references these modes are also integrated into the tire's mode shapes. Since these modes are no modes of the mechanical tire structure itself ("hoop" mode) but in fact the consequence of the tire with included mass acting as a 3D one-mass-oscillator they are not included in the given naming convention in this thesis. Consequently, they are identified as vertical, lateral and F/A bouncing modes.

### 3.2.3 Cavity modes

A strong excitation of the vehicle can be induced by the vibrating air column inside the tire which is called air cavity resonance. Its frequency mainly depends on the size/length of the air volume. For car tires this frequency can be excited by rolling on rough roads which can be perceived clearly by passengers [12]. Coincidence with the first mode of the rim should be avoided.



**Figure 8:** Vibrating air column inside a tire [12]

The air cavity resonance frequency can roughly be calculated by

$$f_{cav} \approx \frac{c_{air}}{2 \cdot \pi \cdot r_{mid}} \quad (1)$$

where  $c_{air}$  is the sound velocity of air in m/s and  $r_{mid}$  is the mid-sidewall radius in m [139]. Regarding the sound velocity there is only a temperature dependency but in

fact no influence of the inflation pressure. The approximately calculated air cavity resonance frequency of the selected rear wheel (4.1) is about 83 Hz and of the front wheel (4.1) about 118 Hz. Von Holst measured approx. 93 Hz on a 18.9 R34 tire [40]. According to equation (1) about 91 Hz is the result which confirms the validity of this equation. Since the frequencies are all above the regarded range between 10 and 80 Hz the cavity modes are not further regarded in this thesis.

### 3.3 Influencing parameters on tire vibration behaviour

Since the tire vibration modes are supposed to have influence on ride comfort it is important to understand the affecting parameters which are discussed in the following sections.

#### 3.3.1 Carcass construction

Numerous comparative investigations concerning the vibration behaviour of bias-ply and radial passenger car tires have been published. In [140] Potts presents the effects of tire structure and design on the tire's vibration behaviour. Generally, it can be stated that radial tires show lower eigenfrequencies than bias-ply tires. This effect is also confirmed for truck, earthmover and farm tires by Scavuzzo et al. [91]. In Table 4 the frequencies between two farm tires of the same size are compared. It shows up to 70% higher eigenfrequencies for the bias-ply tire. For earthmover tires the difference is even higher (up to 90%). Since in this thesis the focus is set on radial tires this parameter is no further part of the experimental investigations.

**Table 4:** Comparison of resonant frequencies for bias and radial farm tires [91]

Mode shape	frequency, Hz		difference, %
	Radial 20.8 R38	Bias 20.8-38	
1st F/A	14	20	+42
2nd F/A	36	57	+58
3rd F/A	44	70	+59
1st Vertical	30	51	+70
2nd Vertical	40	64	+60
1st Lateral	15	17	+13
2nd Lateral	23	37	+61
3rd Lateral	41	52	+27

### 3.3.2 Tire construction

Within the family of radial tires a large number of design parameters can be changed. Scavuzzo et al. [91] compare an all season passenger car tire (P205/70R14) and a corresponding high performance tire (P225/60VR15). The varied parameters are tire geometry (width, cross section, rim diameter) and consequentially tire stiffness, tire mass, rim mass and inertia. According to Scavuzzo et al. the lateral bouncing, the 1<sup>st</sup> lateral and the F/A bouncing modes are mainly influenced by the rim mass and inertia which leads to lower eigenfrequencies for the high performance tire. 3<sup>rd</sup> lateral and 1<sup>st</sup> F/A mode are affected by the design characteristics improving the handling performance which leads to higher eigenfrequencies for the high performance tire. Vertical and steering modes all show slightly higher frequencies for the high performance tire due to the increased stiffness and the larger rim.

**Table 5:** Comparison of resonant frequencies between an all season tire and a high performance tire [91]

Mode shape	frequency, Hz		difference, %
	P205/70R14	P225/60VR15	
F/A bounc	6	5	-17
1st F/A	46	58	+26
2nd F/A	90	94	+ 4
Vertical bounc	19	20	+ 6
1st Vertical	84	88	+ 5
Lateral bounc	10	8	- 20
1st Lateral	35	33	- 6
2nd Lateral	57	58	+ 2
3rd Lateral	74	101	+36
1st Steering	20	21	+ 5
2nd Steering	80	83	+ 4

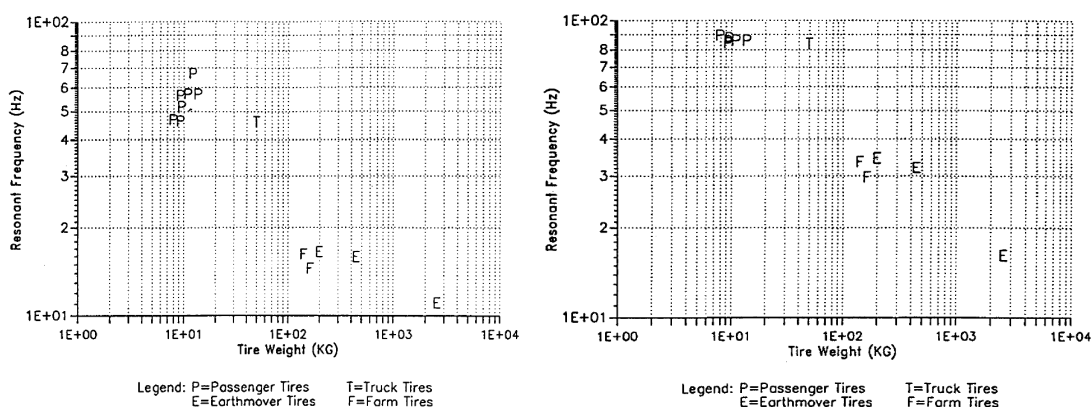
Furthermore, the effects of changes in sidewall construction and tread compound were examined for a P185/75R14 tire. The values show that the variation of construction parameters can significantly shift the tire's resonant frequencies which enables a ride optimization of a tire for the dynamic characteristics of a certain vehicle. For this thesis the tire construction parameters were not followed up further during the experimental investigations.

**Table 6:** Comparison of resonant frequencies for P185/75R14 tires of similar construction [91]

Mode shape	frequency, Hz		difference, %
	P185/75R14 Standard Design	P185/75R14 Experimental Design	
F/A bounc	5	5	0
1st F/A	59	50	-15
2nd F/A	113	108	- 4
Vertical bounc	20	19	- 5
1st Vertical	102	94	- 8
Lateral bounc	9.6	8.9	- 7
1st Lateral	31	28	-10
2nd Lateral	57	50	-12
3rd Lateral	85	78	- 8
1st Steering	21	17	-19
2nd Steering	76	71	- 7

### 3.3.3 Tire size

Within a tire family the above mentioned carcass construction and tire construction parameters usually are the same. With the tire size including diameter, width and weight there is a further important parameter affecting tire vibration modes. Again Scavuzzo et al. [91] present a comprehensive overview for radial tires. Figure 9 shows the data of seven passenger car, one truck, two farm and three earthmover tires for the 1<sup>st</sup> F/A and 1<sup>st</sup> Vertical mode.



**Figure 9:** 1<sup>st</sup> F/A (left) and 1<sup>st</sup> Vertical (right) modes frequencies as a function of weight for different sized tires [91]

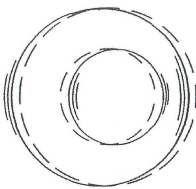
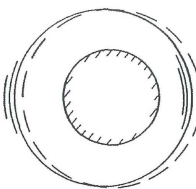
The tires were each tested at their typical load and inflation. In this case the tire weight is the measure of the tire size. As expected the eigenfrequencies are lower

for large tires. Mentionable is the large gap in frequency between passenger car and farm tires which confirms the thesis that for farm tires many more resonant frequencies are located in the ride comfort frequency range up to 80 Hz to be considered for an evaluation. In this thesis with a 520/70 R38 and a 480/70 R24 farm tire two different sizes are compared.

### 3.3.4 Boundary conditions

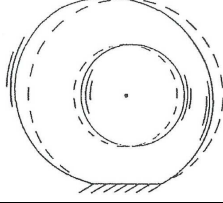
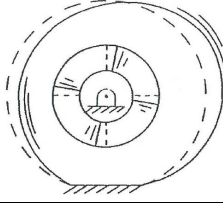
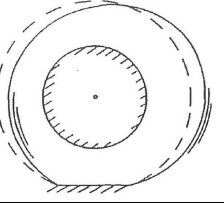
Richards et al. [92] and Mousseau [14] documented that the boundary conditions of spindle and patch affect the tire vibration modes generally, but extremely the lower order modes. For the spindle three different boundary conditions were examined in [92] via FE-model and modal test: free (wheel can translate and rotate), pinned (wheel can only rotate) and fixed (wheel bolted down rigidly). The patch can either be free (unloaded condition) or fixed (loaded). Table 7 shows the comparison for an unloaded tire. For this condition the free (suspended from bungee cords) and fixed spindle is regarded. Large differences can be determined for the rigid-body modes. For the higher-frequency modes wheel motion is smaller.

**Table 7:** Tire modes for an unloaded P205/70 R15 ( $p_i = 2.4$  bar) [92]

Mode shape	frequency, Hz	
	Free Wheel	Fixed Wheel
		
Radial 0	100	62
Radial 1	96	76
Radial 2	98	98
Lateral 0	53	42
Lateral 1	88	45
Lateral 2	82	82

The most significant result is that of the Radial 0 mode with an increase from 62 Hz for the fixed wheel up to 100 Hz for the free wheel. In case of the free wheel the former contact point to the ground in mind can be replaced by a mass equal to that of the wheel with the result that the natural frequency has to be multiplied by 1.41. Since the factor is obviously higher here it can be concluded that the inertia of the rim is less than that of the tire.

**Table 8:** Tire modes for a loaded P205/70 R15 ( $p_i = 2.4$  bar) [92]

Mode shape	frequency, Hz		
	Free Wheel	Pinned Wheel	Fixed Wheel
			
1st F/A	46	32	65
2nd F/A	104	100	94
Vertical bounc	17	---	---
1st Vertical	89	80	80
1st Lateral	31	43	43
2nd Lateral	58	73	73
3rd Lateral	79	---	---
1st Steering	15	48	48
2nd Steering	84	---	---

For the loaded tire (fixed patch) Table 8 shows the comparison for the three different spindle (wheel) conditions. The “free wheel” configuration corresponds to the setup of the experimental modal analysis of the single wheels shown in 4.2.1 and 5.1.2. Generally, it can be stated that the largest differences occur for the first modes of each type. The 1<sup>st</sup> F/A mode was measured at 32 Hz for the pinned wheel. For this condition rim mass and inertia have big influence and can shift the eigenfrequency distinctly. According to 3.2.2 only for the free wheel the vertical bouncing mode can be identified, for pinned and fixed wheel the 1<sup>st</sup> vertical tire mode at 80 Hz is the lowest. Regarding the 1<sup>st</sup> lateral and 1<sup>st</sup> steering mode at the free wheel the rim is free to oscillate whereas for the two other conditions only the tire can oscillate which results in remarkably lower eigenfrequencies for the free wheel.

Since different testing methods and facilities have been used in the context of this thesis the influence of the boundary conditions will have to be considered during analysis.

### 3.3.5 Operating conditions

The tire vibration modes are further affected by the operating conditions. Therefore, previous results on the influence of tire load, inflation pressure and rolling speed are explained.

#### 3.3.5.1 Tire load $F_z$

For trucks, construction machinery and especially tractors the tire load can vary dramatically due to their application. According to Scavuzzo et al. (Table 9) for a car tire load reduction of about 20% has nearly no effect on the eigenfrequencies of the higher order modes. The change of the 1<sup>st</sup> steering mode frequency is due to the shorter footprint resulting from the lower load. The reductions in the bouncing modes are attributed to changes in the characteristics of the modal test rig with free spindle.

**Table 9:** Effect of tire load for a P205/70 R14 with free spindle [91]

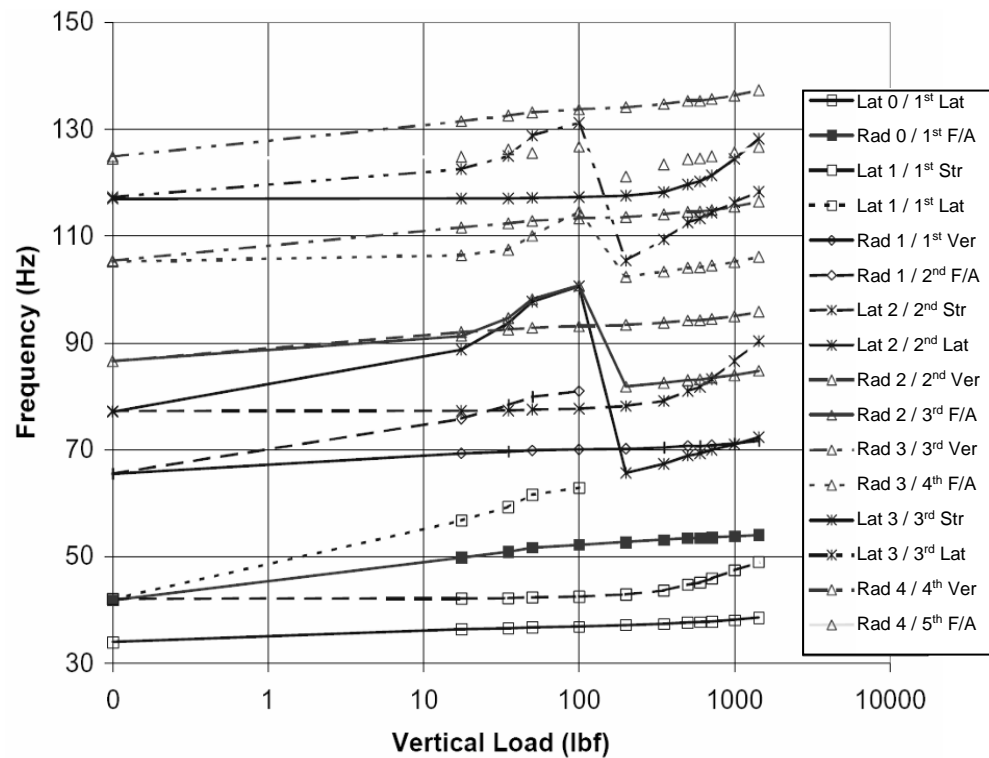
Mode shape	frequency, Hz		difference, %
	Reference $F_z = 4890 \text{ N}$ $p_i = 2.07 \text{ bar}$ $v_x = 0 \text{ km/h}$	Decreased load $F_z = 3900 \text{ N}$ $p_i = 2.07 \text{ bar}$ $v_x = 0 \text{ km/h}$	
F/A bounc	5.5	4.8	- 13
1st F/A	46	46	0
2nd F/A	90	94	+ 4
Vertical bounc	19	18	- 5
1st Vertical	84	84	0
Lateral bounc	9.6	8.3	- 14
1st Lateral	35	33	- 6
2nd Lateral	57	57	0
3rd Lateral	74	74	0
1st Steering	20	18	- 10
2nd Steering	80	80	0

Wheeler et al. investigated the effect of load on the modes of a slightly bigger car tire than Scavuzzo with fixed spindle in [96]. Figure 10 shows the eigenfrequencies plotted over vertical load in a wider range starting at 0 lbf (unloaded) up to 1400 lbf (6227 N).

As already mentioned in 3.2.2 Wheeler et al. point out that the radial modes of the unloaded tire split into vertical and longitudinal (F/A) modes and the lateral modes



transform into lateral and steering modes. All modes slightly increase in frequency with growing load. In the usual range of vehicle application (700-1400 lbf  $\approx$  3114-6228 N) the eigenfrequencies of the F/A and vertical modes only change little whereas the steering modes increase about 10% over this range.



**Figure 10:** Effect of vertical tire load for a P235/70 R17 with fixed spindle [96]

### 3.3.5.2 Inflation pressure $p_i$

Increasing inflation pressure is expected to lead to higher eigenfrequencies. Table 10 shows that this assumption is not true for all modes. Most of the frequencies grow by 1 to 5% for an increase of inflation pressure of 0.33 bar. The first exception is the 1<sup>st</sup> steering mode frequency which decreases 5%. This can be explained with the shorter footprint at increased inflation which leads to a shorter lever arm for the resisting motion and consequently to a lower modal stiffness. The F/A and lateral bouncing modes also have lower frequencies due to the shorter footprint.

**Table 10:** Effect of inflation pressure for a P205/70 R14 [91]

Mode shape	frequency, Hz		difference, %
	<b>Reference</b> $F_z = 4890$ N $p_i = 2.07$ bar $v_x = 0$ km/h	<b>Increased pressure</b> $F_z = 4890$ N $p_i = 2.40$ bar $v_x = 0$ km/h	
F/A bounc	5.5	5.4	- 2
1st F/A	46	48	+4
2nd F/A	90	91	+1
Vertical bounc	19	20	+5
1st Vertical	84	86	+2
Lateral bounc	9.6	9.5	- 1
1st Lateral	35	36	+3
2nd Lateral	57	59	+4
3rd Lateral	74	76	+3
1st Steering	20	19	- 5
2nd Steering	80	83	+4

### 3.3.5.3 Rolling speed $v_x$

In previous investigations several authors demonstrated a noticeable drop of the tire eigenfrequencies at the onset of rolling [79; 91; 97]. Table 11 shows the effect of rolling on the eigenfrequencies of all modes up to 100 Hz for a P205/70 R14 tire determined by Scavuzzo et al.

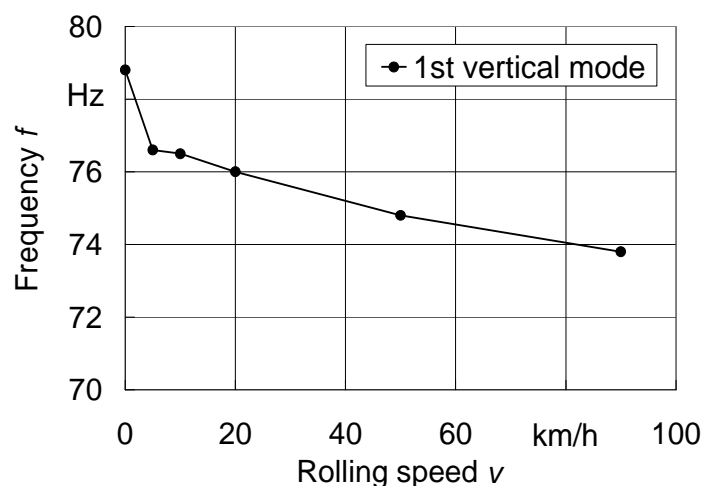
**Table 11:** Effect of rolling speed for a P205/70 R14 with free spindle [91]

Mode shape	frequency, Hz		difference, %
	<b>Reference</b> $F_z = 4890$ N $p_i = 2.07$ bar $v_x = 0$ km/h	<b>Rolling tire</b> $F_z = 4890$ N $p_i = 2.07$ bar $v_x = 8$ km/h	
1st F/A	46	42	-9
2nd F/A	90	88	-2
Vertical bounc	19	18	-5
1st Vertical	84	80	-5
Lateral bounc	9.6	9.4	-2
1st Lateral	35	33	-6
2nd Lateral	57	54	-5
3rd Lateral	74	70	-5
1st Steering	20	19	-5
2nd Steering	80	77	-4

The rolling speed of 8 km/h causes an approximately 5% decrease of most eigenfrequencies compared to the non-rolling condition. A further increase of rolling speed above 8 km/h causes little additional change in resonant frequency which confirms that mainly the rolling itself and not so much the speed is affecting the tire modal characteristic. Scavuzzo et al. constitute the frequency drop with the

rolling tire being able to relieve stresses created in the footprint during the modal cycle which results again in a lower modal stiffness [91].

Dorfi et al. in [97] also show the initial decrease of frequency due to the onset of rolling for the 1<sup>st</sup> vertical mode but furthermore demonstrate an additional 2 Hz drop in frequency within the speed range of 20 to 90 km/h (Figure 11). Regarding this mode in the speed range between 60 and 100 km/h for several tires of same size but different construction it is stated that the frequency drop due to the speed increase is smaller than the variation of frequencies due to tire construction. Furthermore, it is proven that simulations with tire models parameterized by modal properties of the unloaded, non-rolling tire can lead to significant overprediction of eigenfrequencies especially for tires with low cross section. Consequently, dynamic testing under realistic operating conditions is demanded to check the validity of models.



**Figure 11:** Effect of rolling speed on 1<sup>st</sup> vertical mode for a P235/75 R17 with free spindle [97]

Dorfi et al. attribute the change of tire mode frequencies to three physical phenomena [97]:

- Change in stiffness and damping properties of rubber due to cycling
- Doppler effect in wave propagation due to tire rotation
- Stiffening from centrifugal forces

### 3.4 Experimental methods

All tire models mentioned in 2.3 have one big challenge in common. Model data (model parameters) need to be supplied. Gipser specifies two possible approaches. Available detailed FE models can calculate these data from different virtual tests as far as they have been validated before. Otherwise, measurements on suitable test rigs are inevitable [115].

For the determination of the vibration behaviour the measuring object can be excited by three different methods [20; 33; 100]:

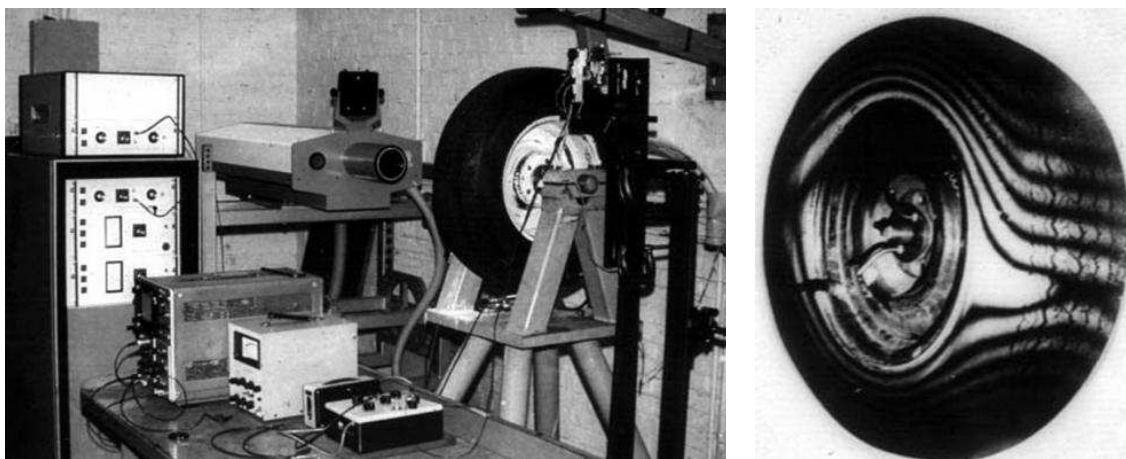
- impulsive/shock excitation
- harmonic excitation
- stochastic/broadband noise excitation

An impulsive excitation e.g. an impulse hammer excitation (experimental modal analysis) or passing a cleat is performed in single actions, whereas harmonic and stochastic excitation occurs during a dedicated period. Harmonic oscillations consist of defined sine oscillations. The phase shift between excitation and response characterizes the damping properties of the tire. According to Kung et al. [86] any periodic road waviness can be decomposed into a summation of harmonic waves, so that the harmonic excitation is a fundamental case in tire research. Stochastic excitation causes inordinate vibrations and displays e.g. passing a bumpy farm track close to reality.

In [74] Zegelaar gives a survey of literature on experimental analysis of tire in-plane vibrations structured in a similar way by the influencing parameters. The classic modal analysis, referred to in 4.2, is used most often but with the restriction that only non-rolling tires can be investigated. A further method is the excitation of the tire via the axle and measuring the reaction forces in the tread pattern. This is conducted by shaker tests referred to in 4.3. Tire non-uniformities act directly opposed and excite in the tread pattern while measuring the reaction at the axle. This is reflected in the uniformity tests and described in 4.5.4. As a further method the excitation of the tire by the driveway and measuring the force responses at the

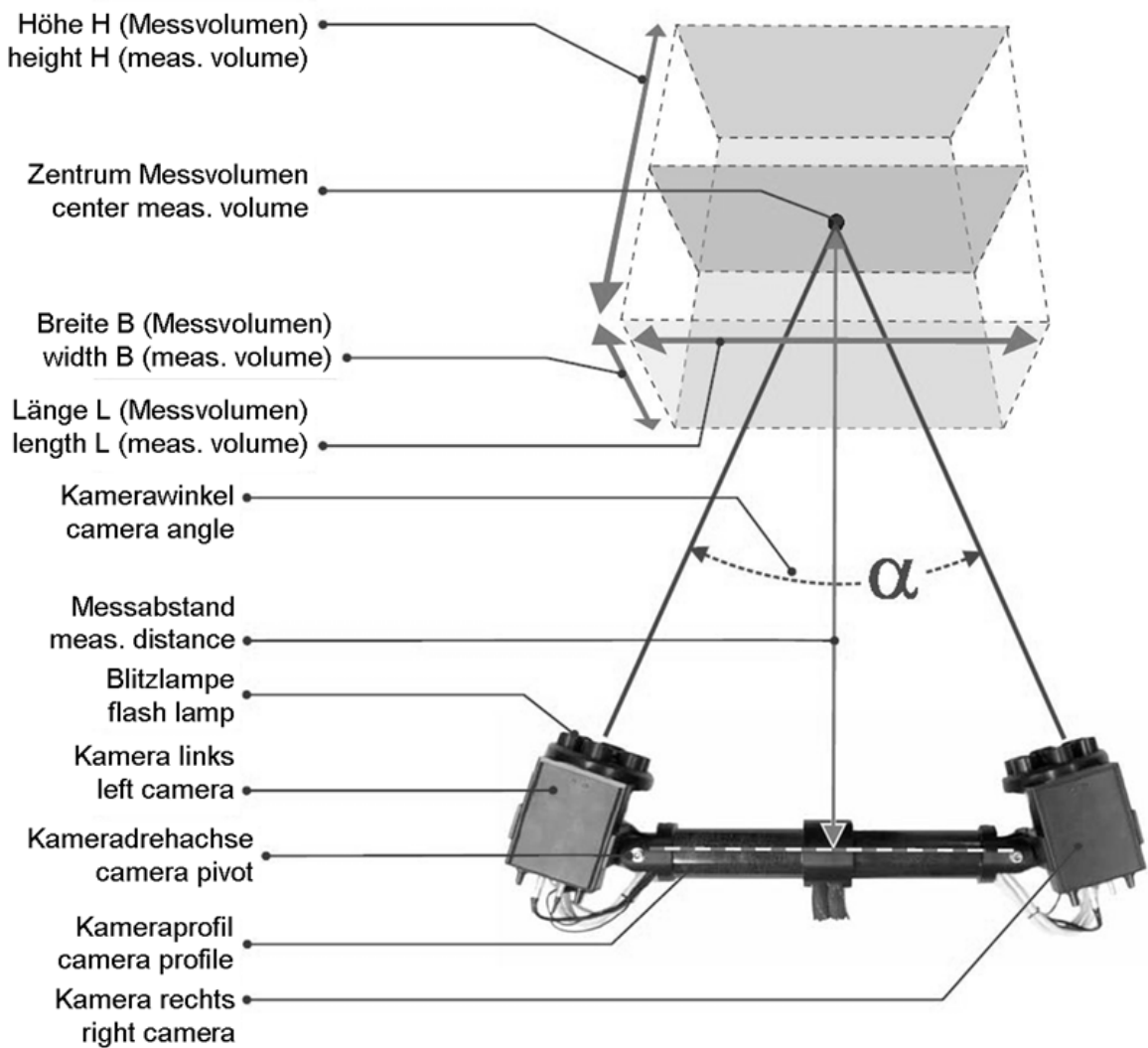
spindle is mentioned represented by the cleat tests (4.5.5). An extension is the recording of the excitation forces of/under a cleat.

With all three latter methods the tire's vibration transfer behaviour can be examined. The relevant eigenfrequencies can be detected but hardly the corresponding mode shapes. For their identification and visualisation holography has been used also for the rolling tire [140-142].



**Figure 12:** Experimental setup for pulsed laser holographic detection of shock wave propagation (left), Radial 0 mode of passenger car tire [140]

A further visualisation method is referred to in the following. In the context of this project the optical 3D measuring system PONTOS was tested for the visualization and identification of tire mode shapes. PONTOS uses the concept of the calibrated stereo camera setup (Fig. 13) for the determination of 3D coordinates and consequently 3D displacement and 3D deformation. For this purpose optical markers are applied to the surface of the object which do not have any disturbing effect during the test because of their small weight ( $<0.05$  g) and size. The number of markers is not limited and has no influence on the sampling rate. The PONTOS measuring head is positioned arbitrary on a tripod in front of the measuring object. The calculation of coordinates and displacement respectively object deformation is carried out via offline analysis. For the present application the PONTOS system was used with high-speed cameras and triggered LED light. Herewith typically recording rates up to 500 images/s at 1.3 Megapixel camera resolution can be achieved or higher rates at reduced camera resolution.



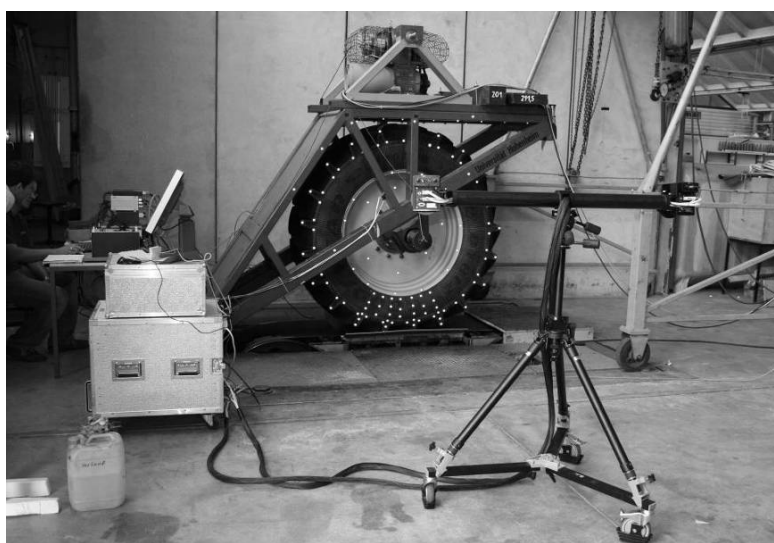
**Figure 13:** Measuring principle of the optical 3D measuring system PONTOS [143]

**Table 12:** Technical Data of the PONTOS system

System configurations	2M / 4M/ HS
Camera resolution (2M)	1600 x 1200 pixels
Camera resolution (4M)	2048 x 2048 pixels
Camera resolution (HS)	1280 x 1024 pixels
Frame rate	500 Hz at 1280 x 1024 pixels
	1000 Hz at 1280 x 512 pixels
Accuracy	0.01 to 0.05 mm
Number of measured markers	unlimited
Sensor dimensions	1300 mm x 200 mm x 140 mm

Short exposure times at high-speed recordings usually require expensive lighting systems. This problem was solved via the integrated lighting and the optical reflecting markers. Complex and dynamic motions and deflections are recorded as a spate of pictures and can be played back also as video. Additionally, the output of diagrams into reports respectively the export in standard data format is available.

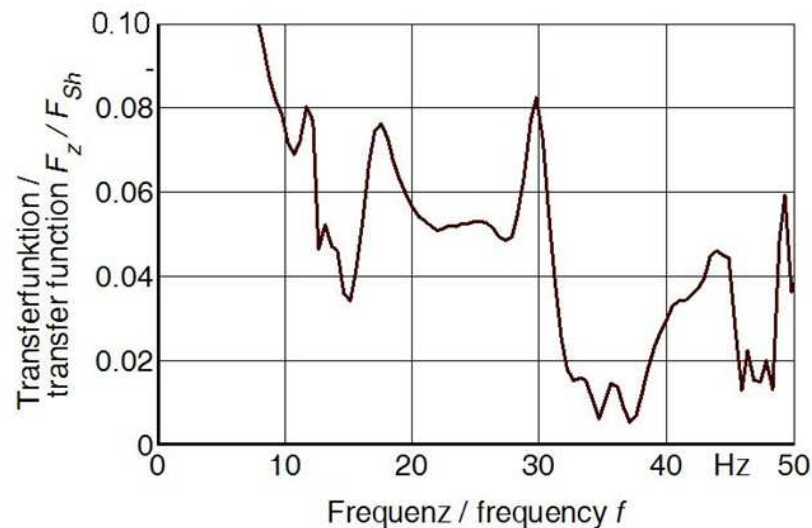
For the present application the optical measuring system PONTOS was used to investigate the dynamic deformation and vibration behaviour of a large-volume tractor tire at different operating conditions. For this purpose the system was set up in front of the Hohenheim flat-belt tire test stand and optical markers for the identification of the measuring points were applied to the tire and the test stand rocker (Figure 14). In parallel to the optical measuring system PONTOS all tests are also recorded with the conventional measuring system installed on the test rig, so that accelerations (3D), rotation speed (wheel and shaker), tire deflection and forces (vertical and longitudinal) are also available for further analysis.



**Figure 14:** Measuring setup of the PONTOS system on the flat track

Limited to a maximum sampling time of 1.6 s of the PONTOS system at a sampling rate of 500 Hz and a resolution of 1280 x 1024 pixel it is not possible to record a complete frequency sine sweep (4 min). Therefore, the sine sweep at first was recorded with the measuring system on the flat-belt test stand and analysed in a frequency range between 3 and 50 Hz at an eccentricity of the four shaker

masses (6.18 kg) of 5.72 mm. Fig. 3 shows the transfer function calculated from the ratio of vertical force in the tread and excitation force of the shaker. Obviously to notice are peaks at about 12.0 / 17.5 / 30.0 / 42.5 and 49.0 Hz. These peaks represent tire eigenfrequencies which each show a typical mode shape. The results of the experimental modal analysis (5.1.2) of the same tire and the eigenfrequencies determined here are matching quite well.

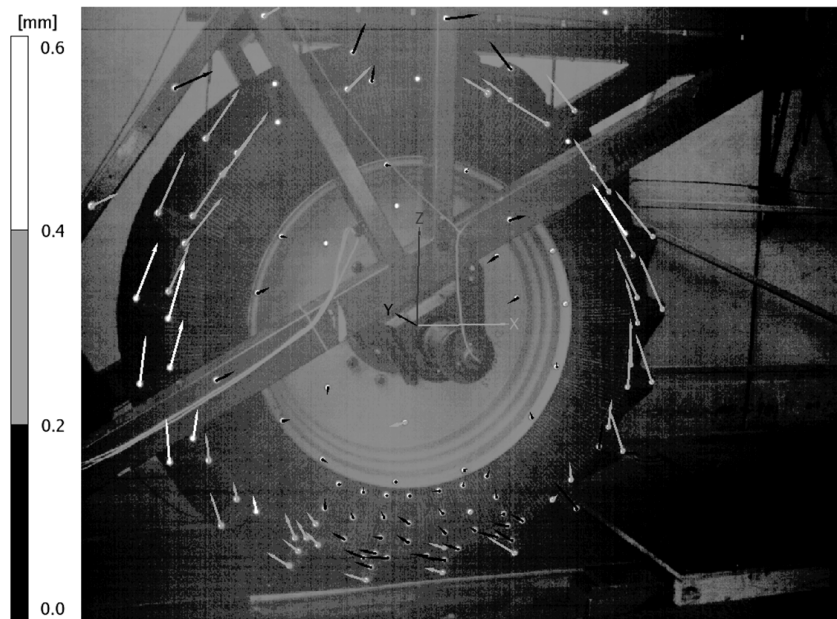


**Figure 15:** Transfer function between vertical force  $F_z$  in the tread pattern and shaker excitation force  $F_{Sh}$  ( $F_{z,stat} = 20$  kN,  $p_i = 1,2$  bar,  $v = 0$  km/h,  $f_{Sh} = 3 - 50$  Hz,  $e_{Sh} = 5,72$  mm)

With the measuring system PONTOS the belonging mode shapes should be acquired optically, depicted and compared with the mode shapes determined by the experimental modal analysis. For this purpose each of the eigenfrequencies are excited individually by the shaker. At constant shaker excitation frequency a recording with the optical measuring system is conducted meanwhile. In spite of constant single-frequency excitation the tire, however, not only vibrates with the excited mode shape, but also further mode shapes can be excited. For the rolling tire the excitation by radial runout and by the lugs have to be considered. Therefore, for visualization of each mode shape a band-pass filter has to be applied. Exemplary the first vertical mode shape at about 30 Hz is depicted in its top reversal point. The arrows show direction and magnitude of the displacement of each measuring point. All points of the rim were chosen as global transformation points, which means that direction and magnitude of the



displacements are referenced on the measuring points of the rim. It can also be noticed, that also the rim shows small deformations. On the one hand this effect can be attributed to the measuring inaccuracy, on the other hand to the vibration and deformation behaviour of the rim. A comparison with the first vertical mode determined by the modal analysis shows very good correlation. Also for the further eigenfrequencies up to 50 Hz the corresponding mode shapes determined by the modal analysis can be found.



**Figure 16:** 1<sup>st</sup> Vertical mode shape in the top reversal point at approx. 30 Hz ( $F_{z,stat} = 20$  kN,  $p_i = 1,2$  bar,  $v = 0$  km/h,  $e_{Sh} = 5,72$  mm)

The presented analysis results of the conducted measurements with the optical measuring system PONTOS show a good correlation with the results of the experimental modal analysis for the standing tire, which was carried out under comparable conditions. Thus, the general applicability of the measuring system for the investigation of tire vibration and deformation was proven. Important aspect and part of this thesis is the comparability of experimental tire vibration investigations concerning different methods on the one hand and different test rigs on the other hand. In order to determine tire parameters relevant for driving dynamics simulation Zamow carried out defined measurements with passenger car tires on different test rigs and ascertained partially significant variations [144]. For high frequency vibrations of tractor tires such comparative investigations are unknown to the author.

## 4 EXPERIMENTAL FACILITIES AND SETUPS

In the subsequent chapters the examined tires and all testing facilities used for the different investigation methods are described. Within this project several modifications had to be conducted since design and measuring equipment was originally not intended for high-frequency vibration investigations. Furthermore, the flat-belt test stand with the shaker and the tractor have been modelled via multibody simulation [145; 146].

### 4.1 Investigated tires

As it was one of the main objectives of this project to compare measurements on different facilities the tire size was selected with respect to the research tractor (4.5.1). Consequently, one front (Goodyear Optitrac 812 480/70 R24) and one rear tire (Goodyear Optitrac 812 520/70 R38) were investigated. The tires were selected as random samples from series production. The technical data of these tires are shown in Table 13.

**Table 13:** Data of investigated tires [147]

	<b>480/70 R24</b>	<b>520/70 R38</b>
Rim size	W15L x 24	W16L x 38
Width, mm	499	519
Outer diameter, mm	1315	1751
Rolling circumference, mm	3970	5258
Static rolling radius, mm	585	782
No. of lug pairs	18	21
Mass (rim incl.), kg	162	304
Load / speed index	138A8	150A8

The tire's self-excitation is one important and strong source. It consists of a low-frequency part generated by the tire runout and a high-frequency part excited by the lugs. These two excitation sources are directly dependent on the driving velocity, the rolling radius and the number of lugs/runouts which makes them to be

identified relatively easy. Table 14 and Table 15 show the excitation frequencies and harmonics for both tires due to the adjusted driving velocities. As defined before frequencies up to 80 Hz have been considered. The effect of the different harmonics was examined with the uniformity tests presented in 5.3.2.

**Table 14:** Self-excitation of a 480/70 R24 at different speeds

Speed <i>v</i> km/h	Rolling radius <i>r<sub>dyn</sub></i> mm	Runout frequency Hz		Lug frequency Hz					
		1st	2nd	1st	2nd	3rd	4th	5th	6th
3	632	0.21	0.42	3.78	7.56	11.34	15.11	18.89	22.67
5		0.35	0.70	6.30	12.59	18.89	25.19	31.49	37.78
8		0.56	1.12	10.08	20.15	30.23	40.30	50.38	60.45
11		0.77	1.54	13.85	27.71	41.56	55.42	69.27	
15		1.05	2.10	18.89	37.78	56.68	75.57		
25		1.75	3.50	31.49	62.97				
35		2.45	4.90	44.08					
50		3.50	7.00	62.97					

**Table 15:** Self-excitation of a 520/70 R38 at different speeds

Speed <i>v</i> km/h	Rolling radius <i>r<sub>dyn</sub></i> mm	Runout frequency Hz		Lug frequency Hz					
		1st	2nd	1st	2nd	3rd	4th	5th	6th
3	837	0.16	0.32	3.33	6.66	9.98	13.31	16.64	19.97
5		0.26	0.53	5.55	11.09	16.64	22.19	27.74	33.28
8		0.42	0.85	8.88	17.75	26.63	35.50	44.38	53.25
11		0.58	1.16	12.20	24.41	36.61	48.81	61.02	73.22
15		0.79	1.58	16.64	33.28	49.92	66.57		
25		1.32	2.64	27.74	55.47				
35		1.85	3.70	38.83	77.66				
50		2.64	5.28	55.47					

## 4.2 Modal analysis

The modal analysis determines eigenfrequencies, damping values and mode shapes of a vibratory system. From this information the resonance behaviour of a structure is to be concluded and a mathematical dynamic model can be formulated. It can be distinguished between the experimental and the analytical modal analysis. A necessary assumption is that the systems behave linearly which means that response and excitation are proportional. This implies the three principles:

- Superposition: Frequency Response Function (FRF) is not dependent on the type of excitation.
- Homogeneity: FRF is not dependent on the excitation level.
- Reciprocity: FRF is independent of which of the points is used for excitation or response.

The analytical modal analysis is carried out on a computer model of the component which can be a lumped mass system or an FE model. It is based on the geometry and material data and leads to a set of coupled differential equations. In a first step the eigenvalues with eigenfrequencies and damping are calculated. In a second step the eigenvectors and thus the mode shapes are determined. The model of the structure can also be decoupled which means that each mode is represented by a differential equation of a single degree of freedom (SDOF) model consisting of its modal mass, damping and stiffness.

The experimental modal analysis is applied on available structures where the measuring points are defined. At these points forces are induced and accelerations are recorded which can be correlated. The positions of the measuring points describe the structure. With the eigenvalues a mathematical model is generated which provides the expected vibration response amplitudes for defined excitation forces. The experimental modal analysis can be divided into two different methods:

- phase resonance method
- phase separation method

For the phase resonance method the structure is excited by a sine force signal. The frequency is shifted until the system is in resonance which can be identified by a 90° phase shift between excitation and response signal. For an improved quality of the mode shape several electro dynamic shakers are installed at the characteristic locations. They are controlled due to the expected mode shape. This method is often applied on complex structures like aeroplanes.

Much more common is the phase separation method mainly known by the impulse hammer tests which was also used in this project. The structure is excited broadband usually at one driving point. At all predefined measuring points and the driving point itself the response acceleration signal is recorded. This common technique is also called Single Input Multiple Output (SIMO). Between response spectra and excitation spectrum the so-called Frequency Response Functions (FRF)  $\underline{H}(f)$  can be calculated by dividing the complex output spectrum  $\underline{Y}(f)$  by the complex input spectrum  $\underline{X}(f)$ .

$$\underline{H}(f) = \frac{\underline{Y}(f)}{\underline{X}(f)} = \frac{Y_{real}(f) + iY_{imag}(f)}{X_{real}(f) + iX_{imag}(f)} = H_{real}(f) + iH_{imag}(f) \quad (2)$$

The magnitude frequency response  $V(f)$  and the phase frequency response  $\Phi(f)$  can be calculated from real and imaginary part of the FRF.

$$V(f) = |\underline{H}(f)| = \sqrt{H_{real}^2(f) + H_{imag}^2(f)} \quad (3)$$

$$\Phi(f) = \arctan\left(\frac{H_{imag}(f)}{H_{real}(f)}\right) \quad (4)$$

For the analysis of the transfer functions the FRF of the mechanical models is mathematically fitted to the measured FRF so that from these models the eigenfrequencies and modal dampings can be recalculated again. As models single-degree of freedom (SDOF) and multi-degree of freedom (MDOF) models are used. Amplitudes and phases are computed again. From the modal coordinates the mode shapes can be determined. By a parameter identification also the modal masses, stiffness and damping can be calculated and hence the experimental mathematical model is established by a set of independent differential equations [134; 148-150].

Separate information on the structural mechanics of the tire can be obtained by the experimental modal analysis for different boundary conditions of the spindle with or without ground contact presented in 5.1.1 and 5.1.2 as well as in 5.2.1.1 and 5.2.1.2.

For the comparison with tests described in the following the axle dynamics during the modal analysis were regarded more closely in 5.1.4. Wheeler et al. used the term global motion which means that large contiguous portions of the structure are moving in the same direction [96]. Consequently, eigenfrequencies and corresponding mode shapes of the loaded tires can be redetermined with some restrictions only from the two 3D accelerometer signals (Figure 18, Pos. 19/20) and the global motion can be estimated by regarding their amplitudes.

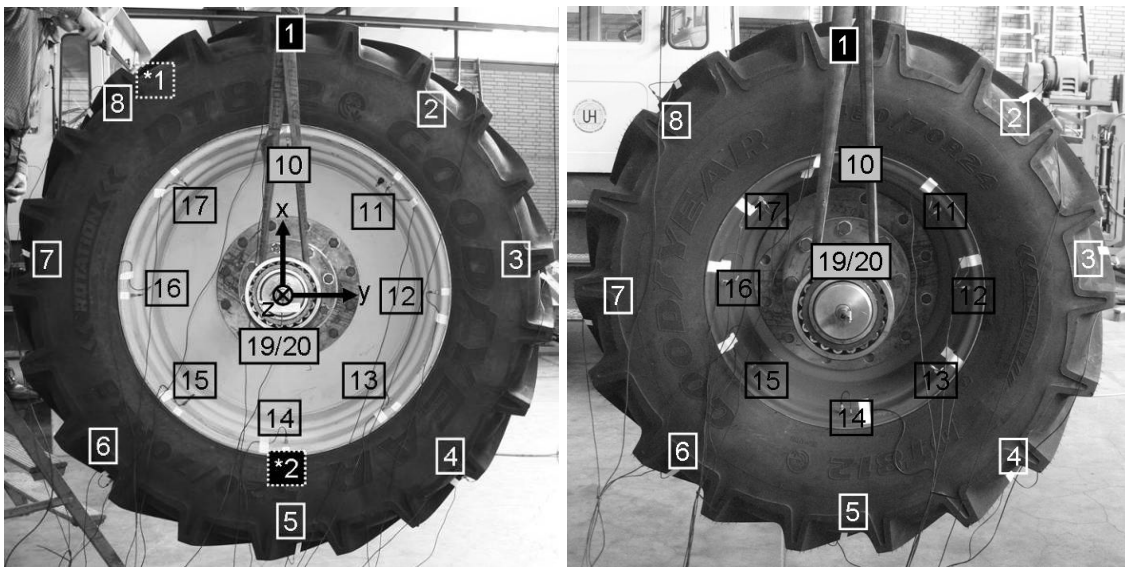
#### 4.2.1 Setup on single wheels

At first, an Experimental Modal Analysis was conducted on the non-rolling single tires under different boundary conditions. As mentioned in 4.1 one front and one rear wheel were tested. Additionally, the single rear rim was also examined. Main objective of these tests was the determination of the tires' modal characteristics without the influence of a testing facility.



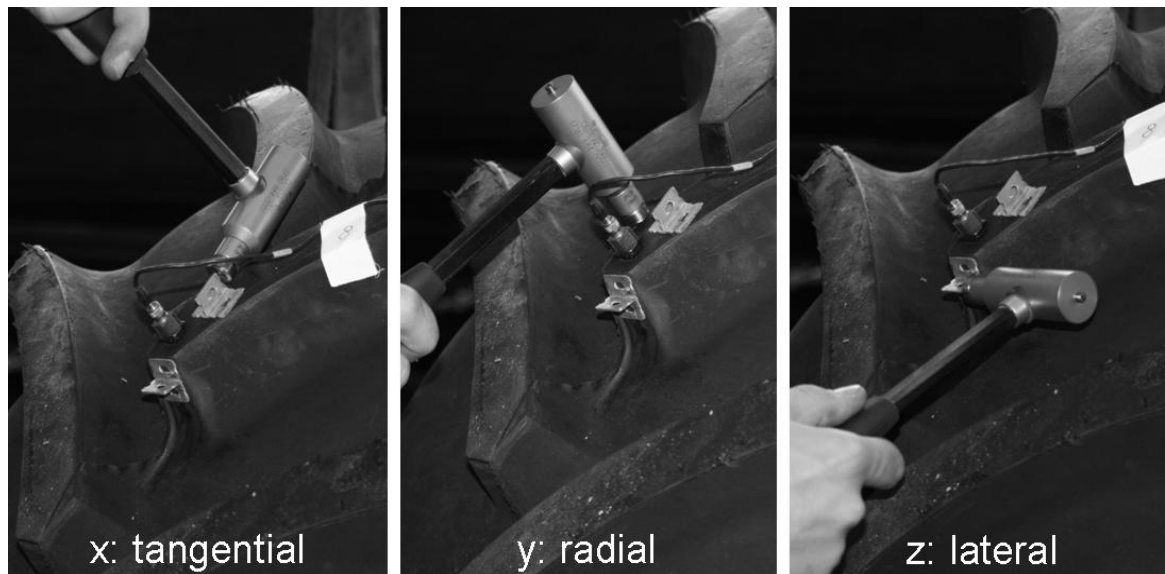
**Figure 17:** Measuring setup for Experimental Modal Analysis

As measuring system a Brüel & Kjaer PULSE platform was used consisting of a multichannel portable data acquisition unit (Type 3560D) connected to a PC with the PULSE LabShop (Version 11.2.0). Data analysis and post processing was carried out with the post-test analysis tool MEscope from Vibrant Technology. For the input a corresponding impulse hammer was used. 18 triaxial piezoelectric accelerometers (Type 4524B) were glued on tire, rim and axle in the following arrangement (Figure 18).



**Figure 18:** Arrangement of accelerometers (1-8, 10-17, 19-20) and excitation points (\*1 for tire excitation, \*2 for rim excitation) on rear (left) and front wheel (right)

Figure 19 shows the excitation point and operation for the three spatial directions. For a reproducible impact two steel brackets were glued on the corresponding lug directly besides the accelerometer. For each direction and parameter setup 10 repetitions were conducted.



**Figure 19:** Excitation of the tire

The unloaded wheel was examined at first. Figure 20 shows the single wheels / rim suspended by two long ropes. Besides the used “free wheel” spindle condition vertical and horizontal motion can be constrained as well as the rotation about the axle. Furthermore, it is possible to investigate the wheel in a real vehicle suspension. These spindle boundary conditions have influence on the rigid body modes of the tire [74]. Especially, the Radial 0 mode which is also often denoted as circumferential mode is strongly dependent on the spindle rotational constraint.



**Figure 20:** Suspended wheels and single rim



For the loaded condition the wheel was set down onto the ground after removing accelerometer No. 5 which was positioned in the center of the tread. The resulting tire load consisted of the weight of the tire and the rim plus the flat-belt test rig's axle (190 kg) and 6 extra steel plates (252 kg). Thus, the tire load of the front wheel was 6 kN and that of the rear wheel 7.5 kN. The wheels with the attached weights were balanced to such extent that they stood up straight without being touched additionally. Figure 21 shows the loaded wheel assembly. Test results of these setups are presented in 5.1.



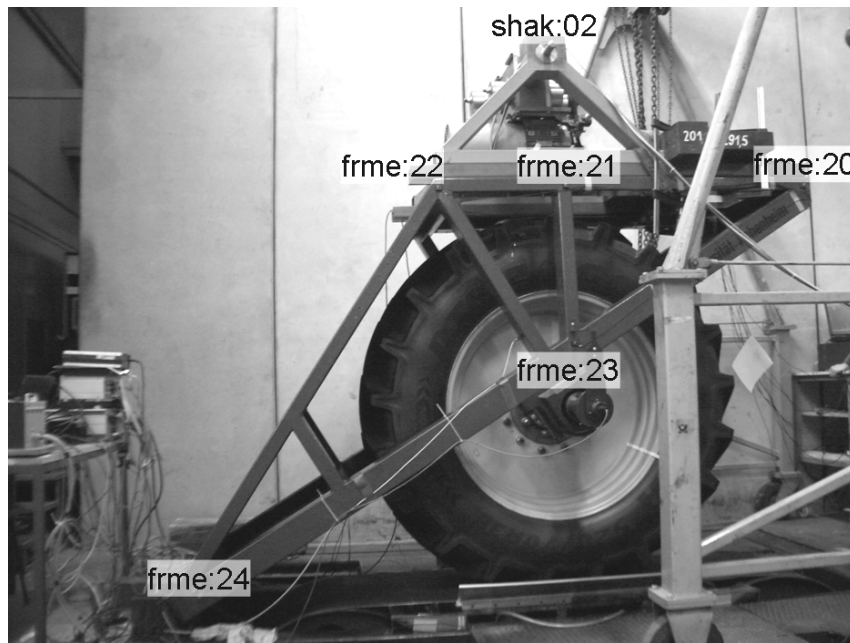
**Figure 21:** Loaded wheel assembly

#### 4.2.2 Setup on flat-belt test stand

As a next step a modal analysis was conducted for the rear tire mounted on the flat-belt test stand both under unloaded and loaded condition (free and fixed patch). According to 3.3.4 this configuration is ideally neither the free nor the pinned wheel since only the longitudinal translation of the axle is blocked. For a pinned wheel configuration the rocker would have to be fixed rigidly to the ground.

Main objective was to determine the influence of the test rig in order to establish comparability. Therefore, the rig was equipped with 12 triaxial accelerometers. The

arrangement of the sensors on the rig's right hand side is illustrated in Figure 22. Symmetric about the center plane the left hand side arrangement is identical. Additionally, for comparison with the modal analysis of the single wheel (4.2.1) the tire was equipped with 8 accelerometers and investigated in the same way.



**Figure 22:** Installed accelerometers (right hand side)

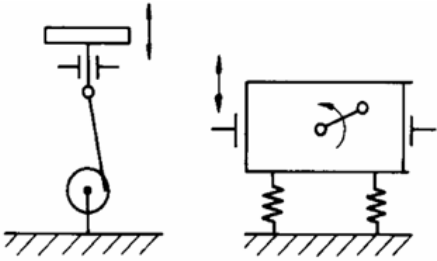
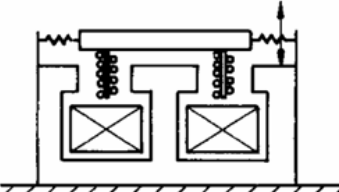

For data acquisition the system DIFA Scadas III (LMS) was used. Excitation was realized again with a corresponding impulse hammer. The frequency response of the rocker was recorded for two rocker positions: the rocker attached to a coil spring without touching the ground (suspended) and the wheel standing on the track supporting the rocker. In order to detect the influence of additional masses on the rocker's modal behaviour three different ballasting setups were tested. The results are presented in 5.2.1. Parallel to these modal tests the different running modes (drop test, radial runout test and shaker test) were recorded to be able to compare.

## 4.3 Shaker device

### 4.3.1 Concept and technical data

For vibration and modal testing shaker devices are used to excite a component. Table 16 shows the different principles of excitation. Accordingly, different methods can be realized. Mechanical shaker devices base on rotating unbalanced or eccentric masses and consequently only allow a harmonic excitation. With hydraulic and electric shaker devices any type of excitation as mentioned above can be realized whereas the electric method allows the highest frequencies. The shaker tests presented in this thesis have been carried out with a mechanical shaker device described more detailed in the following.

**Table 16:** Active principle of shaker devices [150]

mechanical	electric	hydraulic
 <p data-bbox="311 1272 678 1375">Eccentric excited shaker      Unbalance shaker</p>	 <p data-bbox="786 1290 1018 1357">Electro dynamic shaker</p>	 <p data-bbox="1193 1290 1332 1357">Hydraulic shaker</p>

Main function of the shaker is the introduction of defined oscillations into the rocker of the flat-belt test stand or into the frame of the tractor. Therefore, the different concepts of excitation were compared and evaluated by the following criteria:

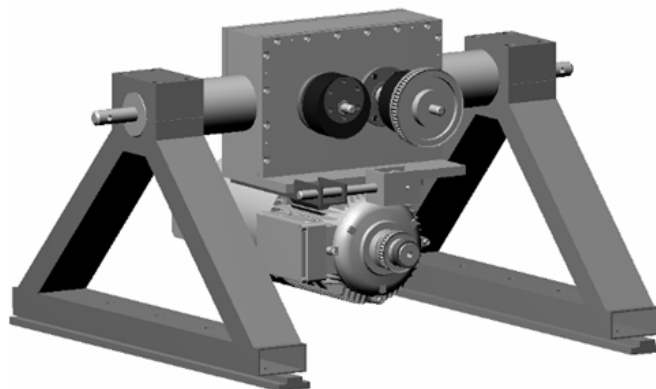
- Different possibilities of excitation (harmonic, stochastic, impact)
- Handling
- Application on different test rigs
- Different directions of excitation
- Mounting
- Control complexity

- Complexity of manufacturing / purchase
- Costs

Result of this evaluation was the decision for a mechanical shaker concept by inertial excitation. Main advantage is the availability for use in on-site testing, e.g. on mobile test rigs or vehicles, but also reduced complexity and costs.

The shaker consists of two shafts each with two eccentric masses mounted. By a spur gear unit the shafts counter rotate with the same rotational speed. The centrifugal forces generate the resulting unidirectional sinusoidal force. The sinusoidal excitation generated by inertial shakers is virtually undistorted, which is another advantage over the other types of shakers when used in sine-dwell and sine-sweep tests [152]. Allison et al. applied in an analogous manner both sinusoidal and random forcing by an electromagnetic shaker to a tire vibration test rig [101]. Since the random forcing resulted in a very poor signal to noise ratio, the sinusoidal excitation was preferred.

As the shaker should be able to run at different frequencies and amplitudes the eccentricity of the masses is continuously variable. An electric motor (5.5 kW) is flanged to the gear box and used to drive the device by a toothed drive belt. The design of the device suspension enables the adjustment of the inclination.



**Figure 23:** 3D-CAD-model of shaker device

The unbalanced masses  $m_{exc}$  each weigh 6.18 kg and the eccentricity can be varied from 0 to 33 mm which equates to an angle of twist between 0 and 180°.

The double-pole electric motor has a maximum rotational speed of 3000 rpm. With a gear transmission ratio of 1:2, which also can be inverted, the maximum excitation frequency is theoretically either 25 Hz or 100 Hz. The minimum frequency of 2 Hz is limited by flutter at lower speeds [153-156].

The shaker device is controlled via frequency converter which is installed in a mobile control cabinet. Two operating methods can be selected. The frequency converter can either be controlled manually via operating interface on the front side of the cabinet or externally via PC.

### 4.3.2 Operating modes

As mentioned above the concept of the shaker device follows the principle of rotating unbalanced masses. According to the equation of motion for a rotating unbalanced mass the following equation shows that both the eccentricity of the masses  $e_{Sh}$  and the rotational speed  $f_{Sh}$  (shaker frequency) have direct influence on the shaker excitation force amplitude  $\hat{F}_{Sh}$ .  $n_{m,exc}$  is the number of the unbalanced masses ( $n_{m,exc} = 4$ ).

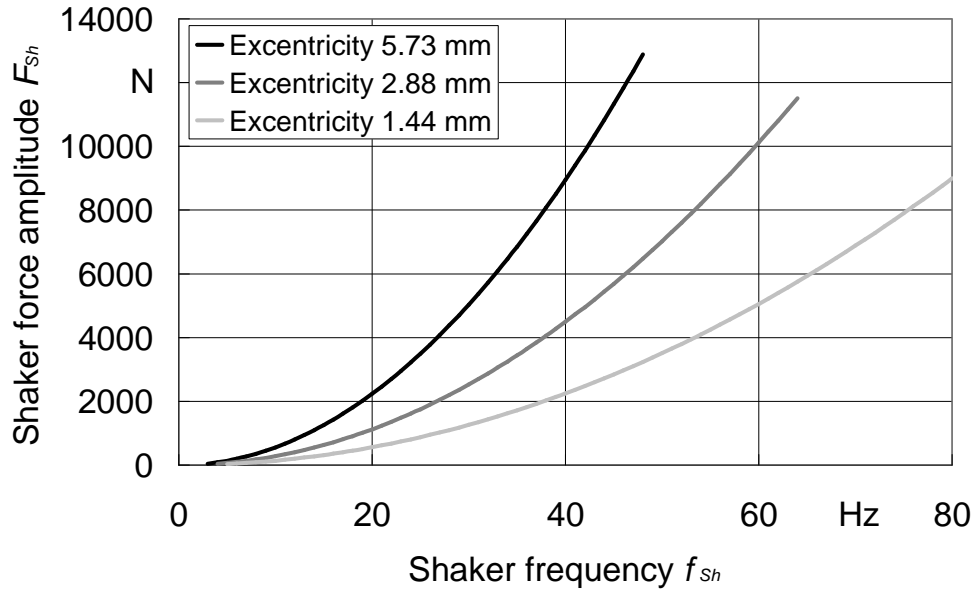
$$\hat{F}_{Sh} = n_{m,exc} \cdot m_{exc} \cdot e_{Sh} \cdot (2 \cdot \pi \cdot f_{Sh})^2 \quad (5)$$

Consequently, shaker frequency and excitation force amplitude cannot be set independently during a sine sweep test which was selected to pass partly or even completely through the comfort-relevant frequency range within one test run. For the investigation of the amplitude influence three different excentricities were set (Figure 24). The limiting factor is the maximum bending stress of the shaker shafts which was calculated to stand an excitation force of 12000 N.

**Table 17:** Parameter settings

	Excentricity $e_{Sh}$ , mm	Start freq. $f_{Sh,start}$ , Hz	End freq. $f_{Sh,end}$ , Hz
Setting 1	5.73	3	48
Setting 2	2.88	4	64
Setting 3	1.44	5	80

Figure 24 shows the shaker force amplitude as a function of the shaker frequency. Considering the limitation at 12000 N the maximum frequency of each sweep becomes visible.



**Figure 24:** Shaker excitation force versus shaker frequency for three different eccentricity settings ( $m_{exc} = 24.72$  kg)

The sweep rate of the sine sweep test needs to be sufficiently slow so that resonances can engage their complete amplitudes. For the calculation of the maximum sweep rate  $R_{oct,max}$  the results of the modal analysis were used. The following equation [151] shows the relationship

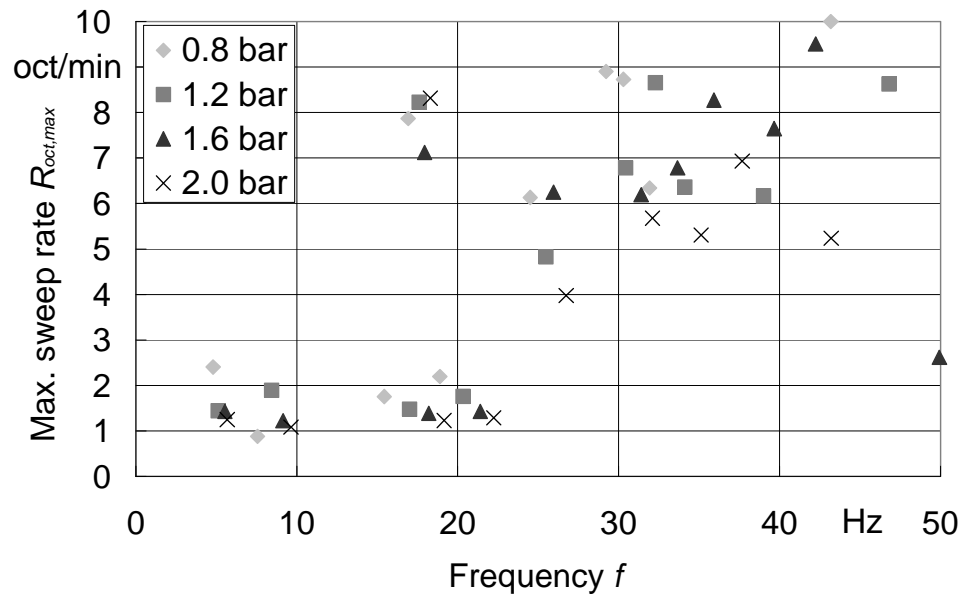
$$R_{oct,max} \leq \frac{f_{res}}{Q^2 \cdot \ln(2)} \cdot 60 \left[ \frac{\text{oct}}{\text{min}} \right] \quad (6)$$

where  $f_{res}$  is the resonance frequency and  $Q$  the resonance quality factor calculated from the damping ratio  $D$  by:

$$Q = \frac{1}{2 \cdot D} \quad (7)$$

In the following figure the calculated maximum sweep rates of the 520/70 R38 tire for all resonance frequencies up to 50 Hz at the four different inflation pressures are plotted against frequency. It can be stated that the sweep rate is increasing with growing frequency. This means the lower resonances are decisive for the maximum sweep rate. Comparing front and rear tire it becomes evident that the

rear tire is the critical one since it shows lower damping values at lower frequencies.



**Figure 25:** Maximum sweep rate for resonances of 520/70 R38 tire at different inflation pressure

All sweep rates are located above 1 oct/min except one which is slightly below and belongs to a lateral mode. This is why it was decided to select 1 oct/min as sweep rate.

In order to have constant cycle times for resonances of the same quality an exponential frequency sweep was selected which is also the standard for vibration control programs, here often named as logarithmic sweep. The frequency change versus the time is according to the equation [151]

$$f(t) = f_{start} \cdot 2^{R_{oct} \cdot \frac{1}{60} t} \quad (8)$$

With the following equation the sweep time can be calculated [151].

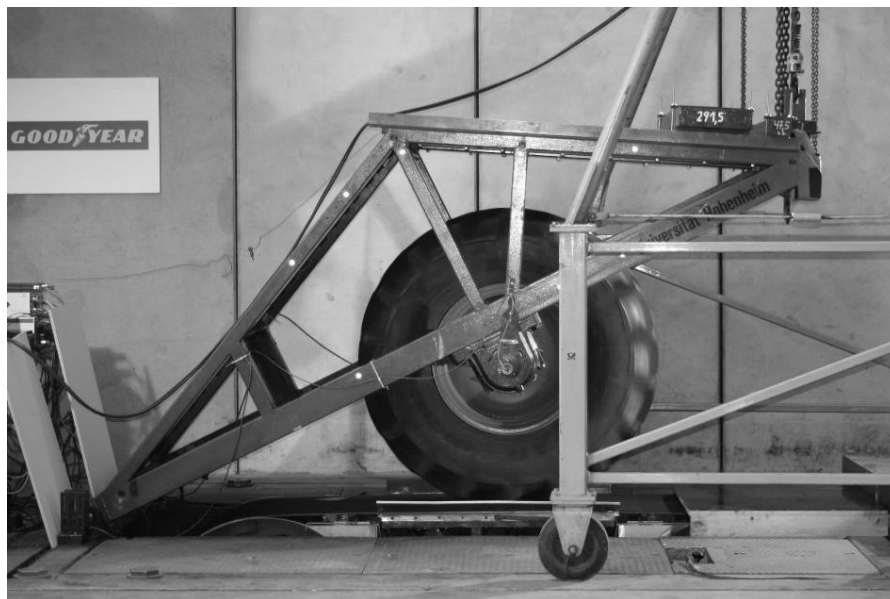
$$T_{sweep} = \frac{1}{R_{oct}} \cdot \frac{1}{\log(2)} \cdot \log\left(\frac{f_{Sh,end}}{f_{Sh,start}}\right) \quad (9)$$

According to the parameter settings in Table 17 this leads to a sweep time of exactly 4 minutes. With these equations in the data acquisition software DASyLab the so-called generator module was programmed so that the shaker device was controlled correspondingly.

## 4.4 Flat-belt tire test stand

### 4.4.1 Technical data

Design and functionality of the Hohenheim flat-belt tire test stand have been presented in numerous publications [18-20]. So in this chapter the focus is on the vibration behaviour of the test rig which plays a decisive role for the investigations of the comfort relevant vibration behaviour of the tires. In order to eliminate influences of the test rig it is important that the first eigenfrequency of the rig is above the defined measuring range. Originally, the Hohenheim flat-belt test stand was not designed for measuring high-frequency tire characteristics. Requirement was to measure in the range of driving dynamics (0 - 5 Hz) which includes the bouncing frequency of small, hard tires (max. 5 Hz). Langenbeck [18] roughly estimated the lowest eigenfrequency of the test rig in longitudinal direction to be 11 Hz. Ferhadbegović developed an MBS model of the test rig [15].



**Figure 26:** Hohenheim flat-belt tire test stand

In the context of this project the vibration behaviour of heavy tires in the comfort relevant range up to 80 Hz had to be investigated. Eigenfrequencies of this order and their influence cannot be neglected anymore.



#### 4.4.2 Sensors and data acquisition

As already mentioned the test rig and its measurement instrumentation have been presented in several publications. So in the following only the new installed sensors and equipment are specified. Their technical data are listed in Table 18.

**Table 18:** Technical data of the Entran accelerometers [157]

Manufacturer	Entran
Type	EGCS-D0-5
Measuring range	$\pm 5$ g
Frequency range (nom./min)	0 - 150 Hz / 80 Hz
Non-linearity	$\pm 1\%$
Supply voltage	+15 V
Operating / compensated temperature	-40 - 120 °C / 20 - 80 °C

For amplification and conditioning of the accelerometer signals a new 12-channel amplifier box was developed and built to add six further accelerometers.

Furthermore, a new angular sensor for the determination of shaker speed and position was installed. Technical data on the new angular sensor can be found in Table 19.

**Table 19:** Angular sensor of the shaker shaft [158]

Manufacturer	Novotechnik
Type	RSC2200
Measuring range	0-360°
Supply voltage	+5 V
Vibration properties	5 - 2000 Hz / $A_{\max}=0,75$ mm / $a_{\max}=20$ g
Operating temperature range	-40 - +85°C

In Table 20 all sensors installed on the flat-belt test stand are listed with their specifications. Their locations at the test rig are shown in Figure 27.

**Table 20:** List of all sensors

No. of sensor	sensor	Abbrev.	range	max. deviation	Measured quantity
1	Load cell 5t	KMD1	0 – 23,3 kN	$\leq 0,025\%$	Vertical force
2,3	Load cell 2t	KMD2/3	0 – 13,5 kN	$\leq 0,025\%$	Vertical force
4,5	Load pin 10t	LMB l/r	0 – 20 kN	$\pm 0,5\%$	Long. force
6	Slide resistor	Wegpoti	0 – 450 mm	$\pm 0,05\%$	Dist. between wheel center and ground
7	Angular sensor wheel	Angle Wheel	0-360°	$\pm 0,035\%$	Angle of wheel
8	Angular sensor shaker	Angle Shaker	0-360°	$\pm 0,1\%$	Angle of shaker shafts
9, 10, 11, 12, 13, 14	Accelerometer	Lon/Ver/Lat Acc L/R	$\pm 5$ g		Acceleration of rocker
15, 16	Rot. pulse encoder	Counter Wheel /Drum	5000 increments per rotation	$0,0036\%/360^\circ$	Rot. speed of wheel and drum

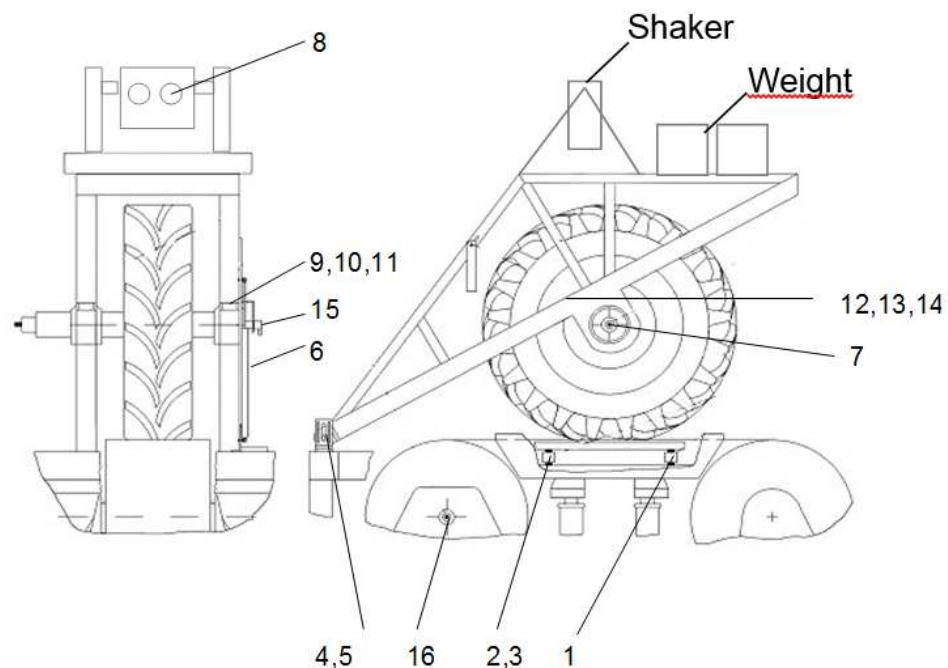
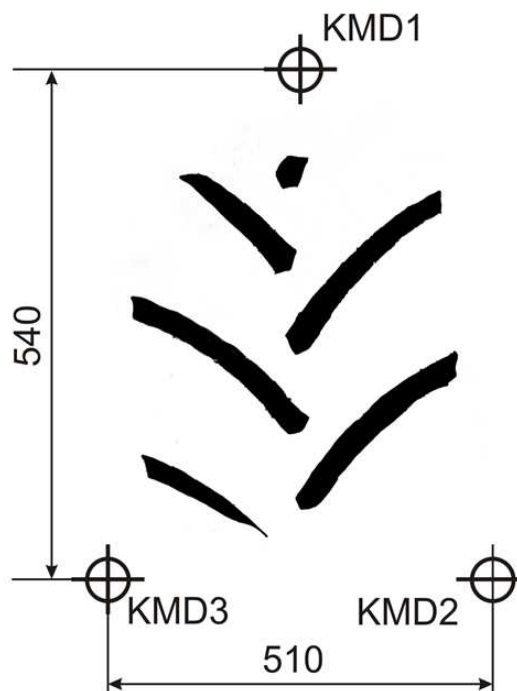
**Figure 27:** Sensor positions at the test rig (Numbers refer to Table 20)

Figure 28 shows the triangular arrangement of the three load cells in the tread pattern from the top view. These three sensors are of special importance concerning the investigation of tire mode shapes on the flat-belt test stand. Since

mode shapes have characteristic spatial propagation the single or combined force signals allow the identification of different shapes.



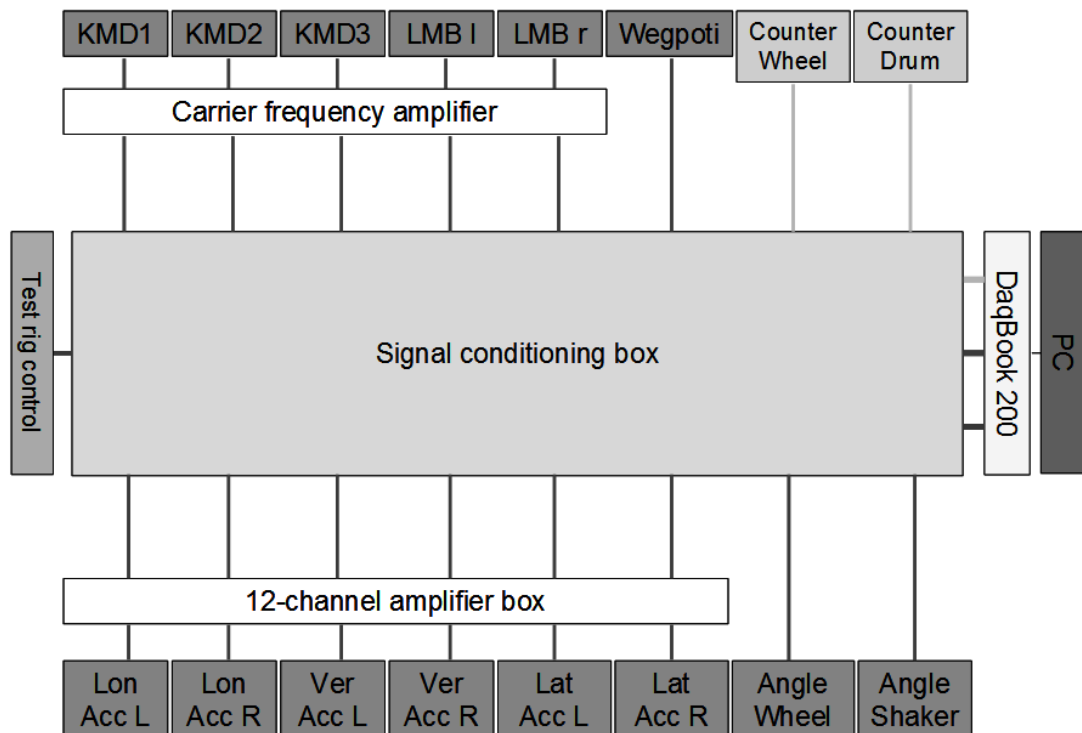
**Figure 28:** Top view of triangular arrangement of load cells in the tread pattern

As a junction for all available signals and a power supply for the sensors a new signal conditioning box was developed and built. An integrated accumulator allows a quick start-up and operation on vehicles or other locations where a power supply is not easily available. The signal conditioning box is linked to an IOtech DaqBook/200 which provides data conversion and communications link between the data source of transducers and signal conditioners and the data processor of the PC. All hardware components are specified in Table 21. The complete DAQ hardware configuration is shown in Figure 29 and Figure 30.

In addition to the hardware also the data acquisition (DAQ) software was exchanged. The software DASyLab® was introduced on the flat-belt test stand also in order to be compatible with other testing facilities at the Institute of Agricultural Engineering. A detailed description of the DASyLab® worksheet with all its settings can be found in [159].

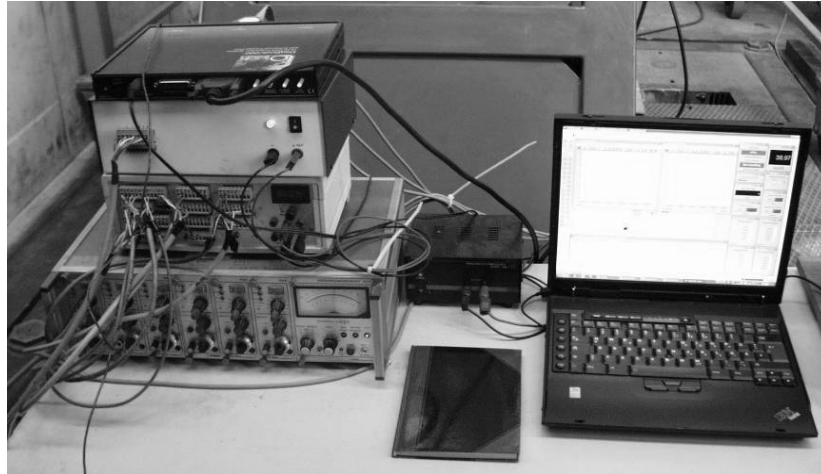
**Table 21:** Hardware components

Device	Manufacturer	Technical data
PC	IBM Tinkpad A31	Intel Pentium 4 1.8 GHz 768 MB RAM, 40 GB hard drive, 2x USB, 1x Seriell, 1x Parallel
Measuring board	IOtech DaqBook/200	16 analog input channels 24 digital input/output channels 5 counter channels 2 analog output channels Power supply 12 V
Carrier frequency amplifier	Elan VD 6	Carrier frequency 5 kHz ( $\pm 5\%$ ) Synchronization voltage $7,5V_{\text{eff}}$ Synchronization range $\pm 100$ Hz Output range $\pm 10$ V
Signal conditioning box	Self-made	Strip terminal for all input channels of the DaqBook/200 Power supply for +5 V, +10 V, +12 V, $\pm 15$ V, 0 - 12 V adjustable, Power supply 12 V
12-channel amplifier box	Self-made	Strip terminal for 12 accelerometers, amplification and offset adjustment separately for each channel Output range $\pm 5$ V Power supply 15 V



**Figure 29:** Data acquisition wiring scheme

The belt speed can be controlled now not only via operator panel but also via PC. In this case in DASyLab® the speed is selected and transferred via Parallel Port to the DAQBook where it is converted into an analog signal which is the input signal for the belt-speed control. Speed and direction of the shaker can also be controlled manually or by PC.



**Figure 30:** Signal conditioning and data acquisition hardware

### 4.4.3 Modal properties

The modal properties of the complete test rig with the installed tire also were investigated. Since only the behaviour of the complete test rig acting as one system was of interest a separate modal analysis of single rig components was abandoned. Furthermore, the benefit of a component-by-component analysis was assessed not to justify the immense effort.

Thus, for the interpretation of the following tests with rolling tire always the interaction between rig and tire has to be considered. When the tire is excited for instance the vibrations can be transferred over the rim into the test rig. If these oscillations match exactly with an eigenfrequency of the rocker the amplitude increases which leads to a corruption of the results.

Since the modal properties of the rig had to be extracted the modal analysis was performed with three different setups which differ by the load applied to the rocker. The first setup is only the rocker which leads to a vertical tire load of 10 kN named "unloaded" in the following. For the second setup the shaker was attached to the rocker ("loaded with shaker") which means a tire load of 14 kN. For the third and last setup additional weights (Figure 27) were mounted so that 20 kN were achieved for the tire load ("shaker+load"). These three configurations were each measured for both tire loading conditions "suspended/unloaded" and "loaded onto flattrack". As the further tire parameters were retained unchanged the tire's modal properties itself can be expected to be the same.

All detectable modes are listed and shortly described in Table 22. The peaks of the transfer function at 6 - 9 Hz (Mode No. 1), at 29 - 37 Hz (Mode No. 3) and for the two shaker configurations at 49 - 55 Hz (Mode No. 4) are obviously mass dependent. At about 14 Hz (Mode No. 2a) only a very small decrease of the frequency can be noticed due to the mass increase. The loading condition of the tire (suspended vs. loaded onto flattrack) has influence on the rig modes' frequencies and dampings but not on the characteristic shapes.

**Table 22:** Frequencies and dampings of the test rig's modes

Mode No.	suspended						Description
	unloaded		loaded with shaker		shaker+load		
	Freq. [Hz]	Damp. [%]	Freq. [Hz]	Damp. [%]	Freq. [Hz]	Damp. [%]	
1	8.20	3.87	7.99	4.38	6.42	2.74	1st lateral
2a	14.16	1.21	14.14	1.25	13.92	3.60	1st torsion around main brace bearings fix
	16.15	1.75	15.80	1.66			lateral
2b			20.09	2.24	18.44	2.08	1st torsion around main brace bearings fix
3	33.97	2.13	32.98	2.20	29.37	2.45	2nd lateral
4			55.28	0.69	49.14	0.95	torsion around x+shaker with opp phase
	58.26	0.60	57.04	1.12			
5			65.82	1.53	60.19	1.93	torsion around x+shaker with opp phase
6					65.56	1.95	2nd torsion around main brace
					73.87	1.16	lateral + torsion

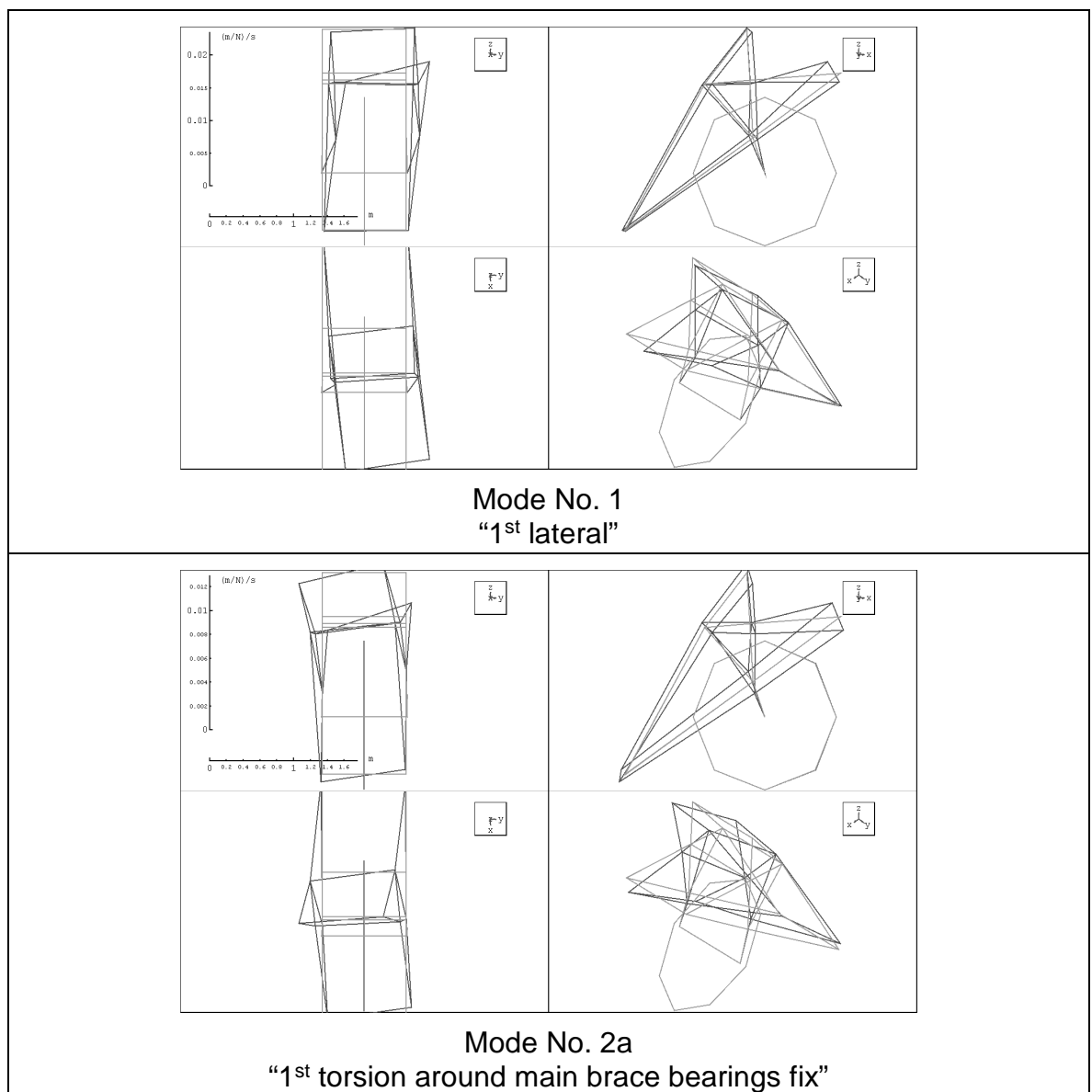
Mode No.	loaded onto flattrack						Description
	unloaded		loaded with shaker		shaker+load		
	Freq. [Hz]	Damp. [%]	Freq. [Hz]	Damp. [%]	Freq. [Hz]	Damp. [%]	
1	9.17	9.23	8.06	9.35	6.14	8.39	1st lateral
2a	14.55	1.17	14.60	1.41	14.03	3.46	1st torsion around main brace bearings fix
	16.80	1.87			15.00	3.13	lateral
2b	25.03	5.44	17.38	2.19	17.55	1.88	1st torsion around main brace bearings fix
3	36.85	1.12	36.42	1.26	32.82	1.15	2nd lateral
4			55.06	0.91	48.83	1.55	torsion around x+shaker with opp phase
	61.80	1.99	56.44	0.91			
5					59.85	2.15	torsion around x+shaker with opp phase
6	65.96	1.23			64.89	1.25	2nd torsion around main brace
	73.61	0.49			72.89	1.29	lateral + torsion

As expected from the design of the rig most of the mode shapes have a mainly lateral character. The described dependency on the mass applied to the rocker indicates an eigenfrequency of the test rig. On closer examination mode No. 1 and 3 mainly occur for the y-direction. Regarding the corresponding mode shapes (Table 23) confirms this assumption so that these shapes can be interpreted as lateral mode shapes of the rocker (1st lateral at 6.42 / 6.14 Hz and 2nd lateral at 29.37 / 32.82 Hz). Modes No. 2a and 2b are symmetric torsion modes of the rocker. Only a small decrease of the frequency can be noticed due to the mass increase.

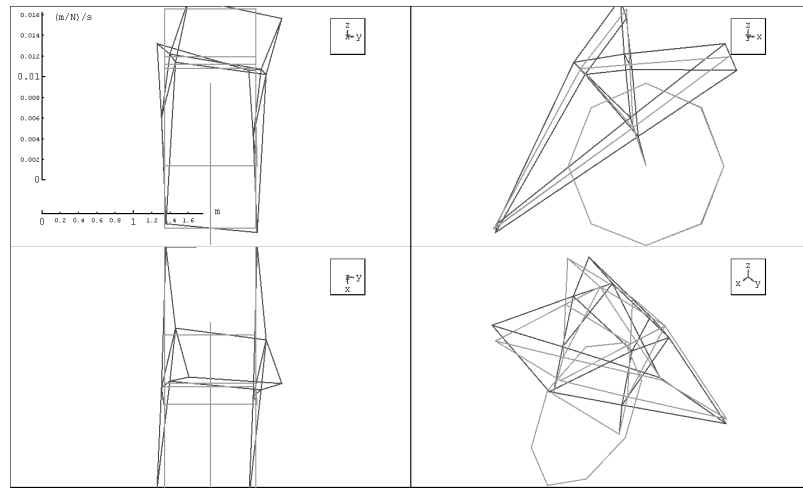
At about 48 Hz another peak of the FRF of the rocker can be found. Regarding the different directions a distinctive maximum in lateral direction and smaller amplitude in vertical direction were determined. Furthermore, it strikes that this peak only occurred as long as the shaker was assembled to the rocker. Regarding the corresponding mode shape it can be seen clearly that the shaker moves in lateral direction which has a direct effect on the rocker. The following Table 23 shows the shapes of the clearly detectable modes which are mentioned in Table 22. As already stated all modes show a lateral character. This means for the determination of the tire modes that especially the lateral tire modes have to be

regarded very carefully in order to distinguish between rig and tire mode e.g. at around 14 Hz (Mode No. 2a) where the suspended tire shows the Lateral 0 and the loaded tire the 1st Lateral mode. Thus, it has to be examined whether these are really eigenfrequencies of the tire or excited by the rocker. The supposed tire modes will be examined very exactly in the next chapter especially compared to the modal analysis mentioned before.

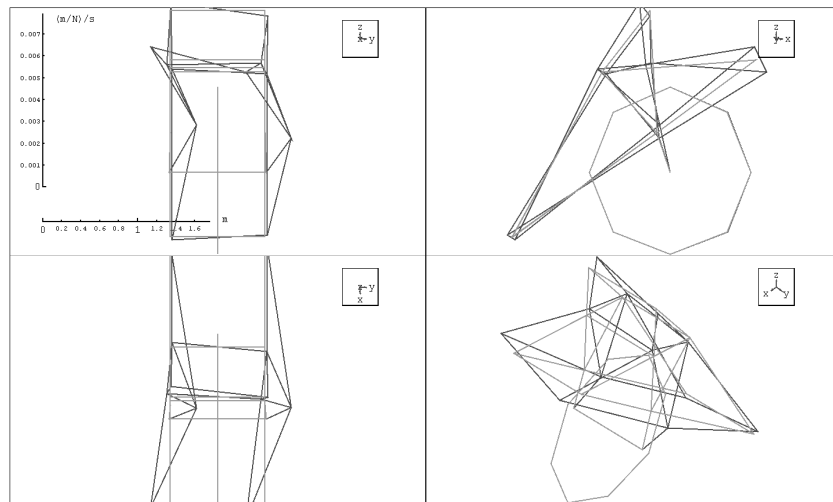
**Table 23:** Mode shapes of the rocker with mounted shaker and 450 kg additional load for both suspended and loaded condition



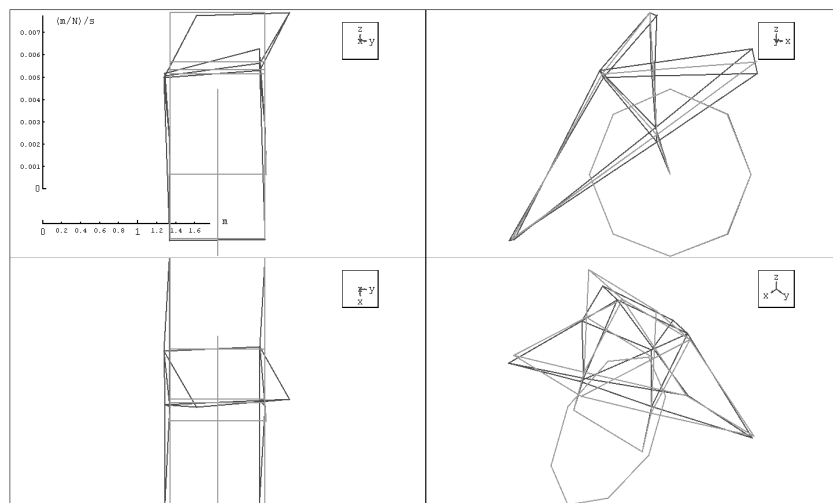




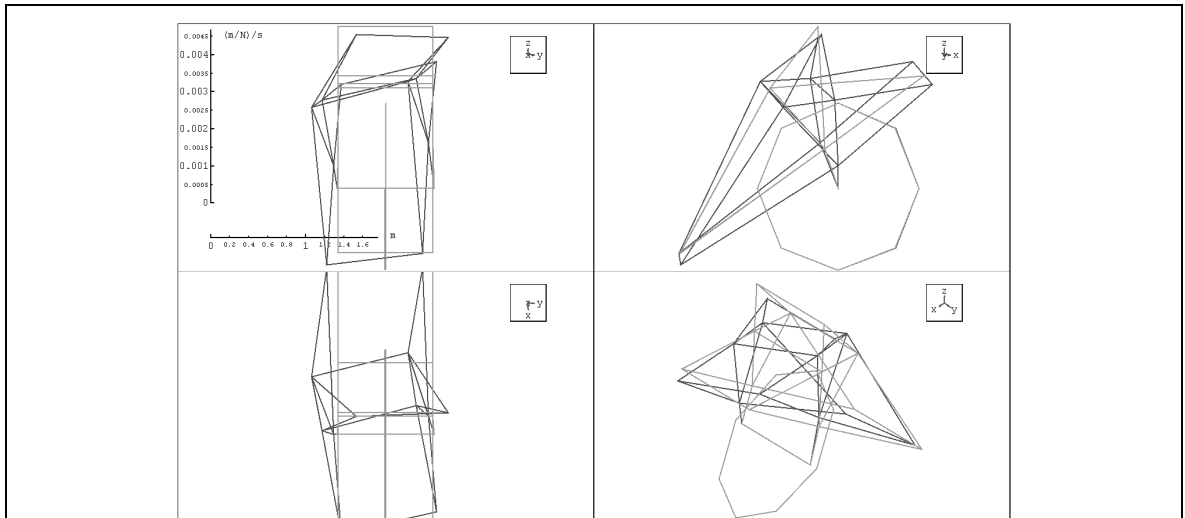
**Mode No. 2b**  
 "1<sup>st</sup> torsion around main brace bearings fix"



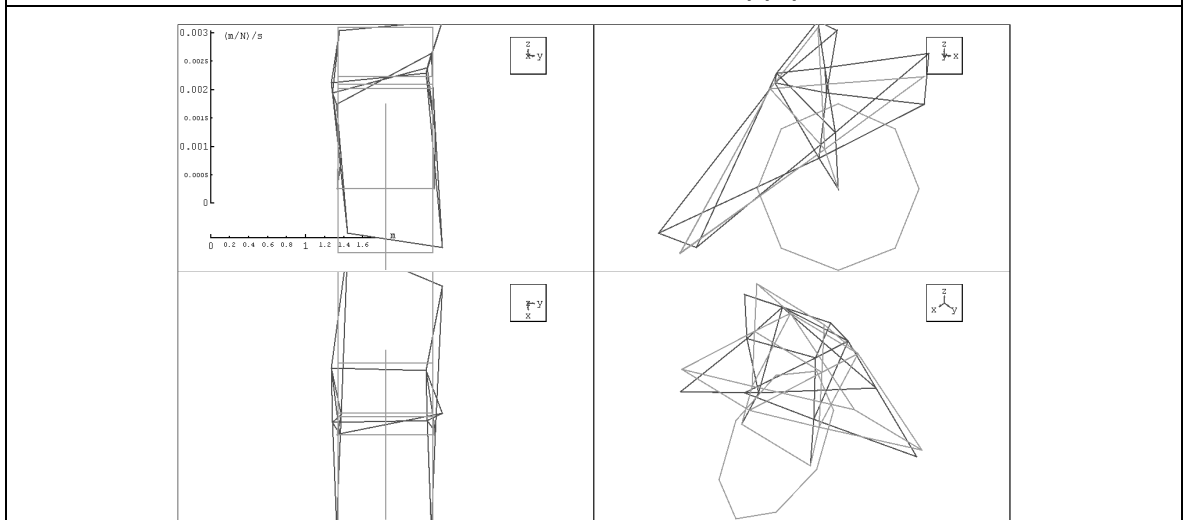
**Mode No. 3**  
 "2<sup>nd</sup> lateral"



**Mode No. 4**  
 "torsion around x+shaker with opp phase"

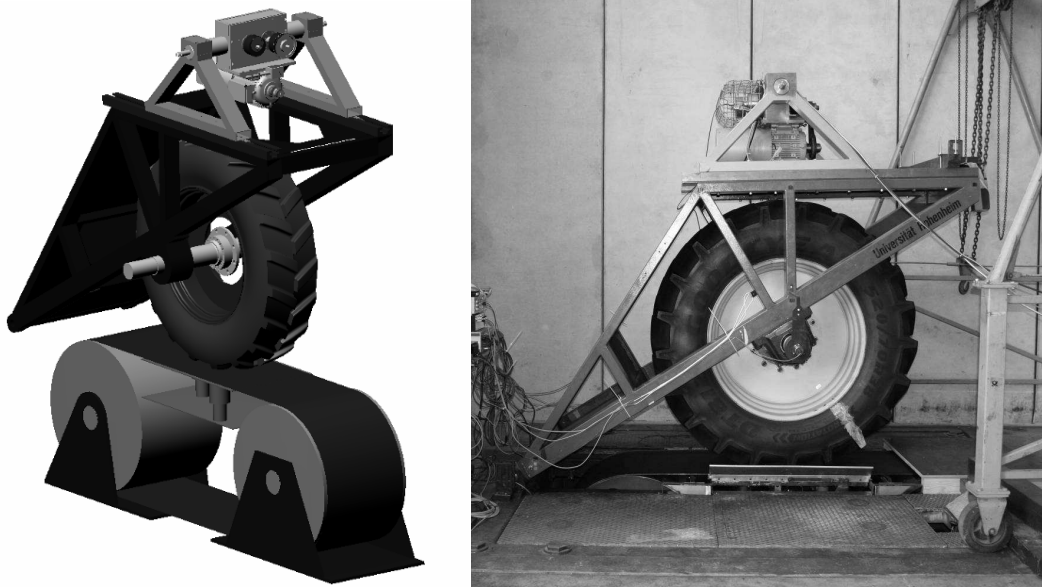


Mode No. 5  
 "torsion around x+shaker with opp phase"



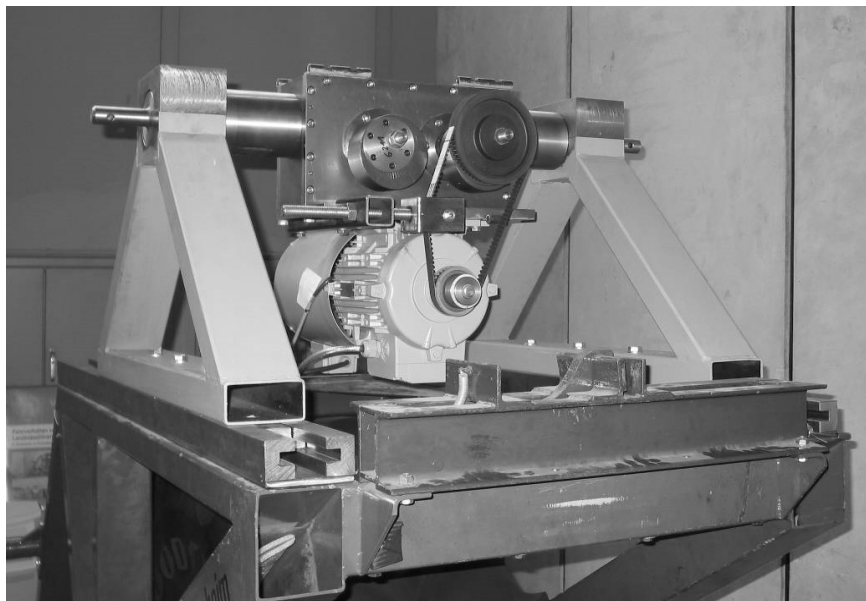
Mode No. 6  
 "2<sup>nd</sup> torsion around main brace"

#### 4.4.4 Shaker tests



**Figure 31:** Flat-belt test stand with assembled shaker device in CAD and real

The complete shaker device (Figure 31) is assembled on the rocker of the test rig by a rail system and can be fixed with a clamping mechanism (Figure 32). This allows an infinitely variable longitudinal position of the shaker device on the rocker. Within this project, however, all tests were run in the position directly above the wheel axle (Figure 31 right).



**Figure 32:** Rail system and clamping mechanism on test rig

For the shaker tests 5 parameters remain that can be varied and were investigated:

- shaker excentricity  $e_{sh}$  [mm]
- tire load  $F_z$  [kN]
- inflation pressure  $p_i$  [bar]
- driving speed  $v$  [km/h]
- shaker frequency  $f_{sh}$  [Hz]

Tire load, inflation pressure and driving speed have been selected due to the tractor specifications and best practice settings. The tractor specifications are described in 4.5.1. In the following Table 24 the investigated set of parameters on the flat-belt test stand are listed.

**Table 24:** Variation of test parameters for shaker tests on the flat-belt test stand

Shaker exctr. $e_{sh}$ , mm	Tire load $F_z$ , kN	Infl. pressure $p_i$ , bar	Driving speed $v$ , km/h	Shaker freq. $f_{sh}$ , Hz
5.73	14	0.8	0	3 – 48
			3	
1.44	17	1.2	5	
			8	
			11	
1.44	20	1.6	15	5 – 80
			25	
			35	
			50	

## 4.5 Research tractor

### 4.5.1 Technical data



**Figure 33:** Instrumented Fendt Favorit 509 C with view inside the cabin

An instrumented Fendt Favorit 509 C at the Institute of Agricultural Engineering is used for driving dynamics and ride comfort investigations. The tractor was equipped at the Institute of Agricultural Machinery at the Technical University of Munich. Several research projects have been performed with the tractor and the force measuring rims were designed and manufactured there [145; 160; 161]. Böhler developed an MBS model of the tractor [145], modified for the adaption to the Hohenheim Tire Model by Ferhadbegović [15].

**Table 25:** Selected technical data of the research tractor

Type	Fendt Favorit 509 C
Engine	4-cylinder, turbo charger
Power	70 kW (95 PS)
Wheelbase	2330 mm
Maximum speed	50 km/h
Front tires	480/70 R24
Rear tires	520/70 R38
Front axle suspension	hydropneumatic (level controlled, lockable)

The tractor offers six gears with 4-level power shift, four-wheel drive and differential gear automatic, compressed air brake, load sensing hydraulic system, front/rear power lift, front-end loader and front/rear p.t.o. shaft.

Since the wheel / tire load is one operating parameter supposed to influence the vibration behaviour of the tire in the following table the weights / loads are listed including the maximum allowed values in order to estimate the operating range.

**Table 26:** Tractor weight, axle and wheel loads

Actual weight (measuring equipm. incl.)	61470 N (max. 90000 N)
Front axle load	26920 N (max. 42000 N)
Rear axle load	34550 N (max. 66000 N)
Left front wheel load	12950 N (max. 21000 N)
Right front wheel load	13970 N (max. 21000 N)
Left rear wheel load	17020 N (max. 33000 N)
Right rear wheel load	17530 N (max. 33000 N)

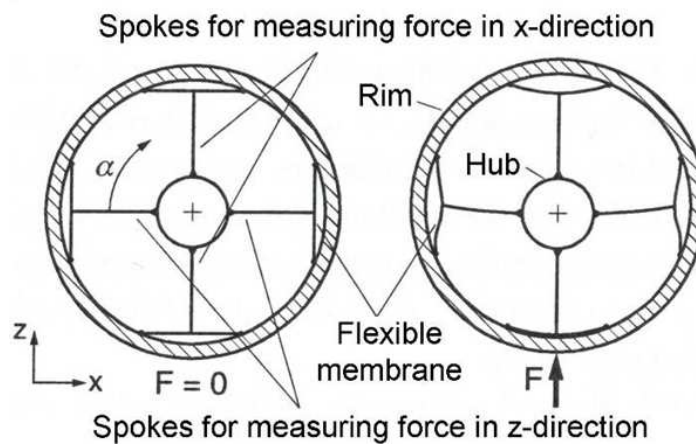
For the front axle the unsymmetric weight distribution between left and right is due to the measuring rim which is only installed on the right side and weighing additional 100 kg. For the rear axle the measuring equipment installed mainly on the right hand side inside the cabin causes the weight difference of approx. 50 kg.

#### 4.5.2 Sensors and data acquisition

For the determination of the wheel forces the tractor is instrumented with two measuring rims on the rear axle and one measuring rim on the front axle (right hand). The functional principle of the rims is shown in Figure 34.

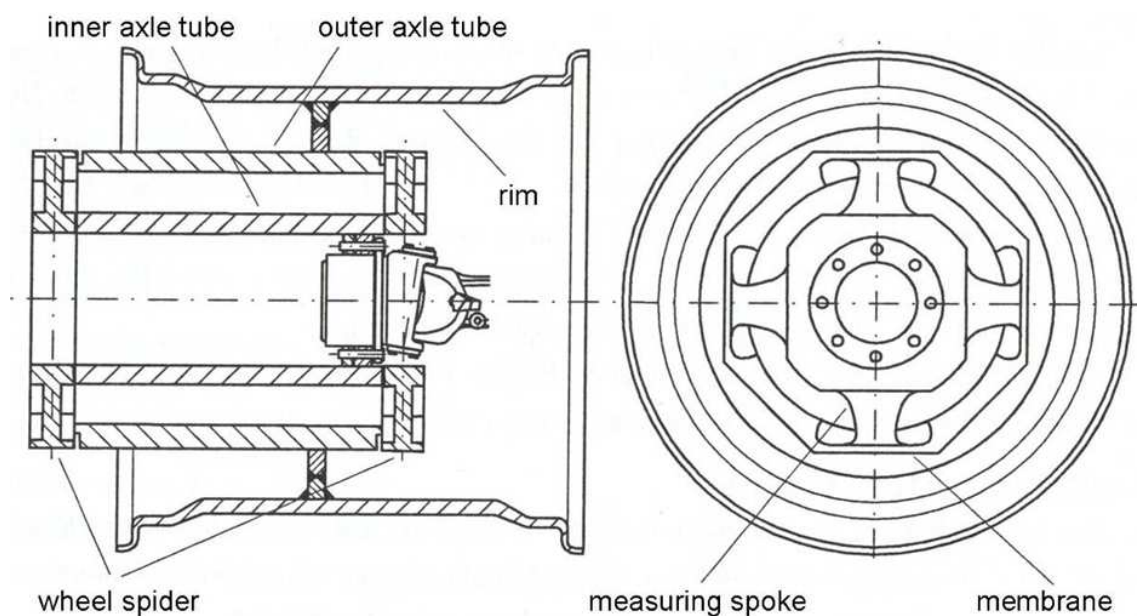
The spokes are connected to the hub inside rigidly and to membranes outside which are weak in radial direction. Consequently, the spokes can only show biaxial bending which is measured via calibrated strain gages for each direction. Lateral forces are calculated from the deflections of all spokes in y-direction neglecting the

angular position of the wheel. For the determination of vertical and longitudinal forces the actual angle of each spoke needs to be considered.



**Figure 34:** Functional principle of the measuring rims [160]

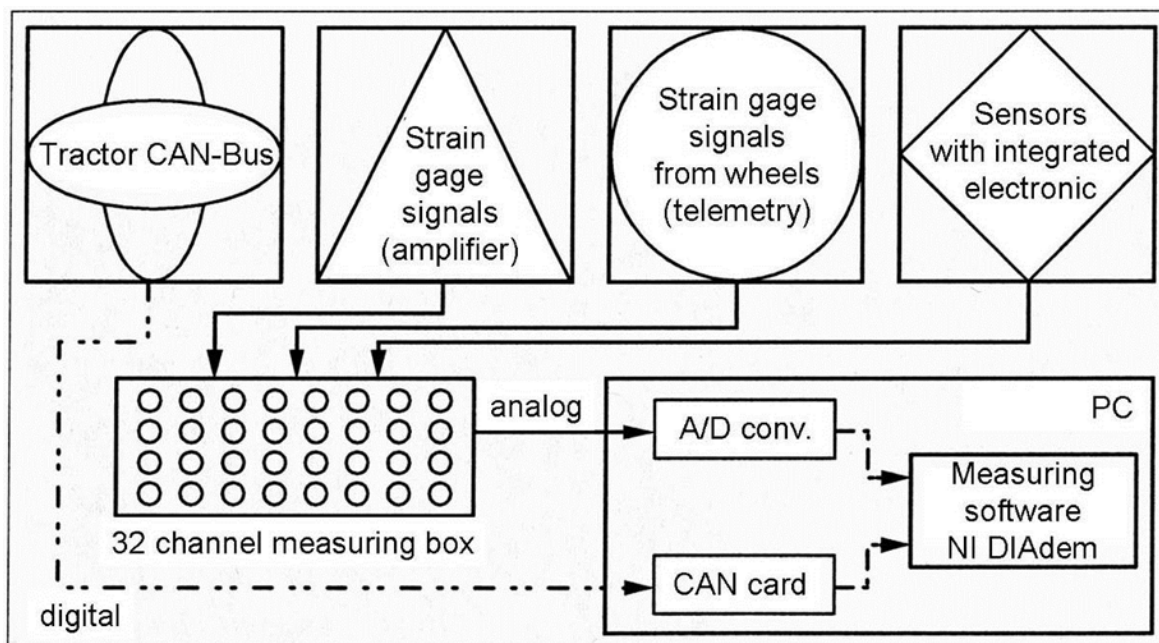
The front rim is working with the same principle but its design differs from the rear rims. For mounting and dismounting the wheel or the tire it is important to know the assembly (Figure 35).



**Figure 35:** Front measuring rim [160]

The basic structure of the measuring system is shown in Figure 36. The signals are collected in a 32-channel measuring box. The further processing for the analog

channels is performed by a 32-channel PCI card (Goldammer Multi III) and for the digital signals by a CAN card (Softing) inside a portable PC. The software used for data acquisition is NI DIAdem (National Instruments).



**Figure 36:** Data acquisition system on research tractor [160]

Table 39 contains the sensors which were installed and connected with the existing DAQ system as required for each test series. After recording the signals in the DAQ software DIAdem a so-called Auto-Sequence is started which calculates the following channels (Table 27).

Together with the CAN-Bus signals (Table 28) all channels are stored in one ASCII data file. For analysing these tests a MATLAB subroutine was integrated into the program "Farm analysis" which converts the DIAdem files into the standard file format. Subsequently, also the analysis program "Farm analysis" can be used described in 4.6.



**Table 27:** Calculated signals

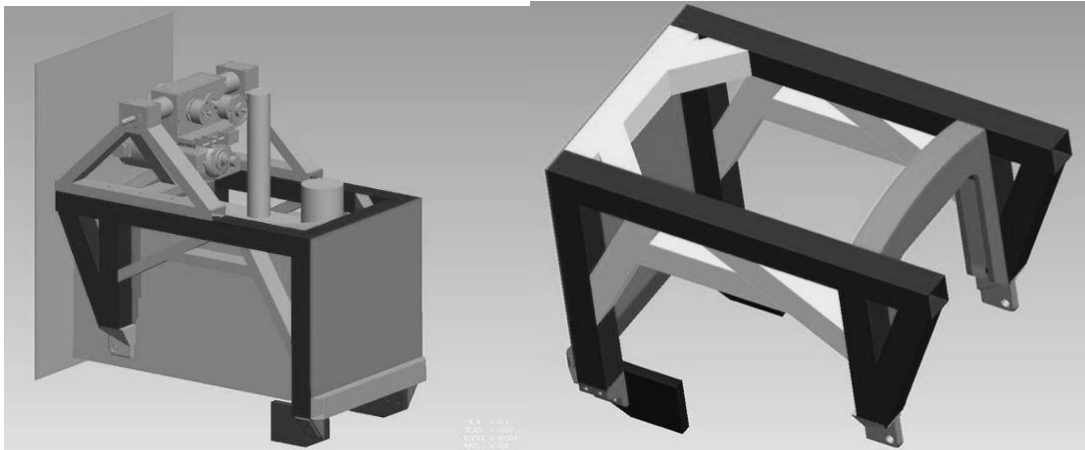
Channel No.	Data source	Abbrev.	range	max. deviation	Measured quantity
33	Calculated	F_HR_Li_V	0 - 100 kN	100 N	Vertical force of left rear wheel
34	Calculated	F_HR_Li_H	0 - 100 kN	100 N	Longitud. force of left rear wheel
35	Calculated	F_HR_Re_V	0 - 100 kN	100 N	Vertical force of right rear wheel
36	Calculated	F_HR_Re_H	0 - 100 kN	100 N	Longitud. force of right rear wheel
37	Calculated	F_HA_V	0 - 200 kN	200 N	Vertical force of rear axle
38	Calculated	F_HA_H	0 - 200 kN	200 N	Longitud. force of rear axle
39	Calculated	F_VR_Re_H	0 - 100 kN	100 N	Longitud. force of right front wheel
40	Calculated	F_VR_Re_V	0 - 100 kN	100 N	Vertical force of right front wheel
41	Calculated	M_VR_Re	0 - 120 kNm	120 Nm	Drive torque of right front wheel
42	Calculated	Shaker_freq	0 - 100 Hz		Shaker frequency
43	Calculated	Shaker_force	0 - 12 kN		Shaker force

**Table 28:** Tractor CAN-Bus signals

Channel No.	Data source	Abbrev.	range	max. deviation	Measured quantity
1, 3, 5, 7, 9	Tractor CAN-Bus	Zeit			Time CAN-channels
2	Tractor CAN-Bus	Drehzahl			Engine speed
4	Tractor CAN-Bus	Geschw_theo			Wheel speed
6	Tractor CAN-Bus	Geschw_wahr	0 - 360°	±0,035%	Radar speed
8	Tractor CAN-Bus	LS	1 - 4		Selected gear
10	Tractor CAN-Bus	V/R			Driving direction (forward/rearward)

### 4.5.3 Shaker tests

For assembling the shaker with the Fendt tractor a support frame was designed. The main challenge was to achieve a sufficient stiffness as the console had to be designed around the engine and its peripheral devices. Therefore, several design loops followed by FEA modal calculations had to be carried out in order to shift the first eigenfrequencies above the investigated frequency range [162].



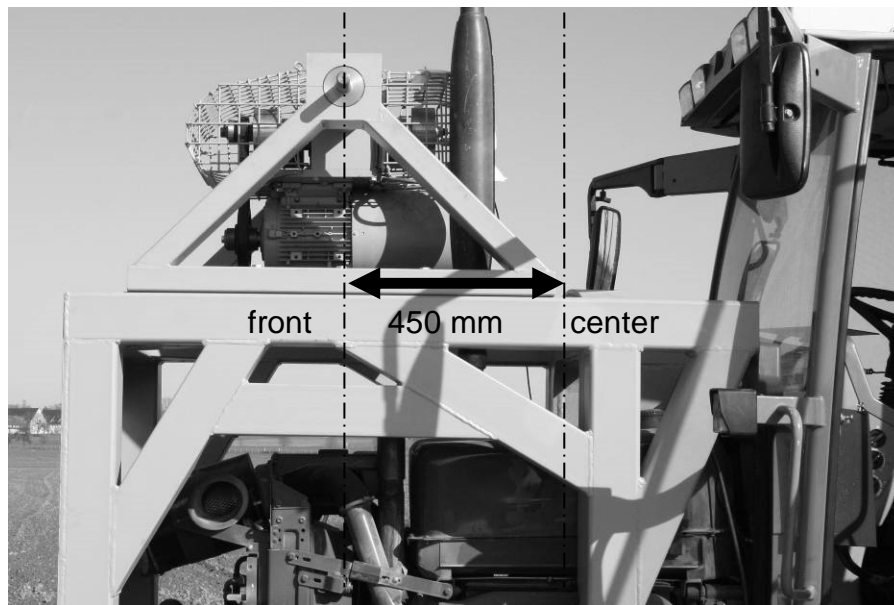
**Figure 37:** Shaker adapter frame for the research tractor

Figure 37 shows the final version for the adapter with assembled shaker. Figure 38 shows the support frame with shaker in its position on the tractor.



**Figure 38:** Shaker installed on Fendt Favorit 509

For the power supply of the shaker on the tractor an electric generator was used. Frequency converter and control box as well as the electric generator were placed on a small two-axle-trailer so that there was no vibration influence on the tractor [162].



**Figure 39:** Shaker position on tractor

The mass of the support frame including auxiliary equipment is 490 kg. The center of gravity is located directly above the center of the front axle. The shaker device was tested in two positions (Figure 39). The first position (“front”) is again with the center of gravity directly above the center of the front axle so that the following weights apply to the tractor (Table 29).

**Table 29:** Tractor weight, axle and wheel loads with assembled shaker device in “front” position

Actual weight (measuring equipm. incl.)	70470 N (max. 90000 N)
Front axle load	35920 N (max. 42000 N)
Rear axle load	34550 N (max. 66000 N)
Left front wheel load	17450 N
Right front wheel load	18470 N
Left rear wheel load	17020 N
Right rear wheel load	17530 N

For the “center” position the shaker device is shifted 450 mm towards the cabin. The changed axle loads can be found in Table 30.

**Table 30:** Tractor weight, axle and wheel loads with assembled shaker device in “center” position

Actual weight (measuring equipm. incl.)	70470 N (max. 90000 N)
Front axle load	35130 N (max. 42000 N)
Rear axle load	35340 N (max. 66000 N)
Left front wheel load	17060 N
Right front wheel load	18080 N
Left rear wheel load	17410 N
Right rear wheel load	17920 N

The following table shows the set of parameters that were varied during the test program.

**Table 31:** Variation of test parameters for shaker tests with Fendt Favorit 509 (480/70 R24, 520/70 R38)

Shaker position	Shaker exctr. $e_{sh}$ , mm	Infl. pressure $p_i$ , bar	Driving speed $v$ , km/h	Shaker freq. $f_{sh}$ , Hz
front	5.72	0.8	0	3 – 48
			3	
center	2.88	1.2	5	4 – 64
			8	
			11	
	1.44	1.6	15	5 – 80

Since the shaker device is restricting the driver’s view on the road, for safety reasons the driving speed had to be limited to 15 km/h.

#### 4.5.4 Uniformity tests

For the examination of the operating mode vibration behaviour uniformity tests are conducted in order to analyse the effect of the self-excitation by the tire. The test can be carried out quasi-static over the complete speed range on a flat driveway. Therefore, the instrumented tractor was driven at a defined speed sweep. Practically, this means the tractor was quickly accelerated to its max. speed of 50 km/h and after the start of the measurement decelerated very slowly, so that resonances could engage their complete amplitude during that time.

#### 4.5.5 Cleat tests

Cleat tests are a common method for the evaluation of vibration properties of tires. On the one hand cleat tests can be used for the determination of the so-called swallow-behaviour of tires. On the other hand, by passing a cleat a wideband excitation of the tire is generated comparable to the excitation with a modal hammer.

Zegelaar emphasizes that the excitation of the tire by short wavelength road unevenness (e.g. cleats) is very complex [74]. Two effects can be held on: the tire partially or completely envelopes the obstacles and it acts as a geometric filter. This leads to the result that the response at the axle is much smoother than the shape of the obstacles. Zegelaar also recommends a single cleat experiment for the validation of the frequency of the vertical mode of vibration.

Kindt illustrated in [79] the influence of rolling speed, inflation pressure and excitation amplitude on a passenger car tire's resonance frequencies. Concerning the rolling speed the analysis revealed a significant drop of the resonant frequencies at the onset of rolling. As the rolling speed increases further, the tire shows a stiffening effect. Furthermore, an excitation amplitude dependency of the structural response for road impact excitations was shown due to the Payne effect (2.2, page 12).

Böhm carried out cleat tests on a roller drum test rig with passenger car tires. The frequency spectra show the rigid body modes of the tire but hardly flexible modes which is interpreted that the contact patch is reacting quasi statically [163].

Gough investigated tires rolling over short wavelength obstacles and indicated three responses: variations in vertical and longitudinal force as well as in rotational velocity [164].

Very important is the selection of an appropriate cleat size. On the one hand, the impulse should be as narrow as possible, on the other hand at least one lug pair permanently must have contact with the surface of the cleat to realize a reproducible contact area on two lugs (Figure 40). Schlotter [23], Hechenblaikner [4] and Holst [40] also tested tractor tires with quite different cleat sizes.



**Figure 40:** Tread pattern of a tractor tire passing two different cleat width

So after several preliminary tests with heights between 40 and 120 mm three different heights (38, 58 and 78 mm) and a length of 58 mm were chosen for the further tests.



**Figure 41:** Wooden cleats, height: 78/58/38 mm, width: 58 mm

The following table shows the set of parameters that were varied during the test program.

**Table 32:** Variation of test parameters for cleat tests with Fendt Favorit 509

Cleat height $h_c$ , mm	Inflation pressure $p_i$ , bar	Driving speed $v$ , km/h
38	0.8	5
58	1.2	10
78	1.6	20
		30
		40
		50

Several sensor channels on the DAQ system were changed for the cleat tests and can be found in Table 40.

#### 4.6 Analysis software “Farm Analysis”

The ASCII data files can be processed with a MATLAB analysis program. Therefore, the frame of an existing analysis program was modified and enhanced in order to use a standardized interface.

##### 4.6.1 Program structure

The program structure can be regarded in Figure 42.

4 M-Files			
Farm_analysis	Loaddasy_farm_analysis	Processing_Call-back	Plot_processing_setup
- Main menu	- Reading data file - Importing data into MATLAB	- Control of setup window  - Determination of additional information	- Calculation of signal analysis  - Graphical representation of results

**Figure 42:** Program structure “Farm Analysis”

Three additional programs enable to convert data files recorded with Hohenheim tire test facilities: the flat-belt test stand (“match FBP files”), the single wheel tester [23] (“match ERM files”) and the research tractor (“match Diadem files”) into the standard format. Furthermore, all additional channels which are calculated from the measuring channels are attached to the data file. These subroutines have been integrated as the first three buttons (dark grey) into the “Farm analysis” main menu and pose the first step of the data analysis (Figure 43 left). After this matching several files can be loaded and processed in the plot processing setup window.



**Figure 43:** Main menu (left) and plot processing setup window (right)

Regarding this window the user starts selecting the data files in the upper left corner and continues the setup of the analysis clockwise by selecting the channels, defining block size/overlap and further analysis settings until the “plot” button starts the defined analysis.

A detailed description of the program and modifications is given in the project thesis of Reibert [165]. Besides smoothing the time signals by a moving average it is possible to average a set of tests in the frequency domain. A frequency-based



weighting according to the VDI guideline 2057 (human vibration sensation) is also implemented for the subjective/objective comfort evaluation [166-168].

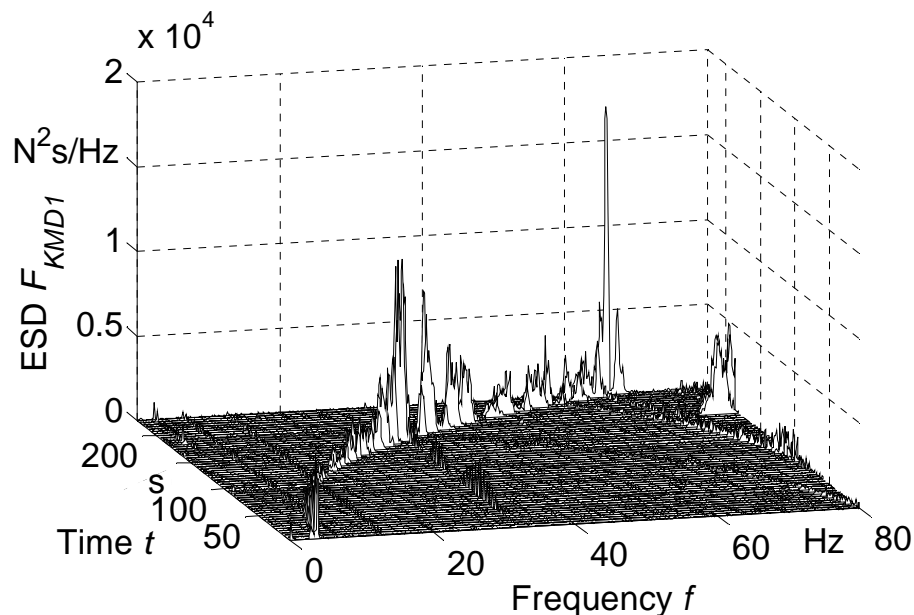
#### 4.6.2 Analysis methods

The following analysis methods can be distinguished:

- 2D-plot: Plotting two arbitrary channels against each other
- Time plot: Checking the signal in the time domain
  
- Amplitude spectrum (AS) → deterministic signals
- Power spectrum (PS) → deterministic signals
- Power spectral density (PSD) → noisy signals
- Energy spectral density (ESD) → transient signals
  
- Transfer function (TF)

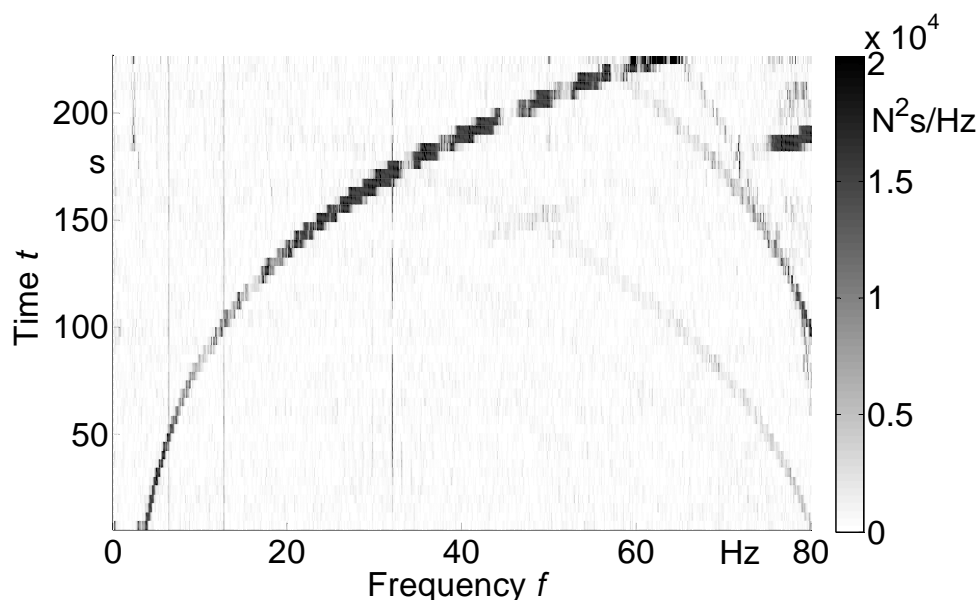
For the interpretation of the shaker tests the performed shaker sweep can be regarded as quasi-stationary. For the analysis, however, the problem arises that the window size has to be sufficiently small in order to detect one special mode excited at a certain frequency. A small window size on the other hand leads to a limited frequency resolution. As a useful supplementary analysis instrument the energy spectral density (ESD) can be applied. Since in this case the energy content of the signal is displayed against the frequency, the time signal is treated as a transient signal with the advantage that mode peaks do not disappear with increasing block size, but remain nearly constant. The analysis of a transient signal means consequently, that no window function (rectangular window) is to be used.

A complete overview of the spectral representation is given by the Waterfall diagram (Figure 44). In this representation the frequency spectra of all single blocks are plotted one after another against the time so that additionally the time information of the complete test is kept.



**Figure 44:** Energy spectral density waterfall diagram of force  $F_{KMD1}$

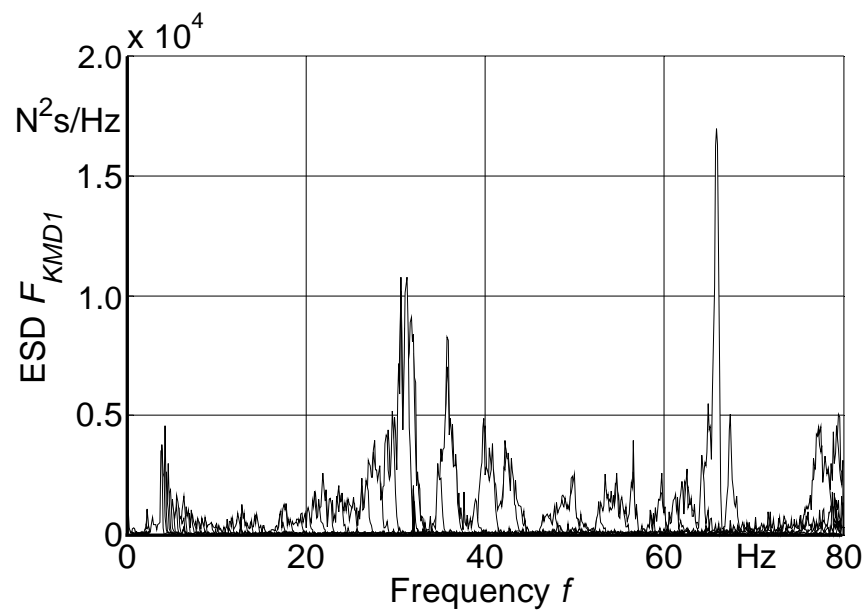
Based on the waterfall diagram two views are helpful for a detailed analysis. The first derived representation is the top view (x-y-plane) of the waterfall diagram called spectrogram (Figure 45).



**Figure 45:** Energy spectral density spectrogram of force  $F_{KMD1}$

From this representation especially steady state and transient effects can be analysed and separated from each other.

Since all kinds of excitation can be decomposed into a summation of harmonic waves, a superposition is allowed. With the conducted “peak hold” analysis the effect of the shaker excitation on the tire is superposed covering the complete recording time of a shaker test and thus the corresponding frequency range. This representation corresponds to the view from the front (x-z-plane) on the waterfall diagram (Figure 44).



**Figure 46:** Energy spectral density peak hold of force  $F_{KMD1}$

## 5 RESULTS AND DISCUSSION

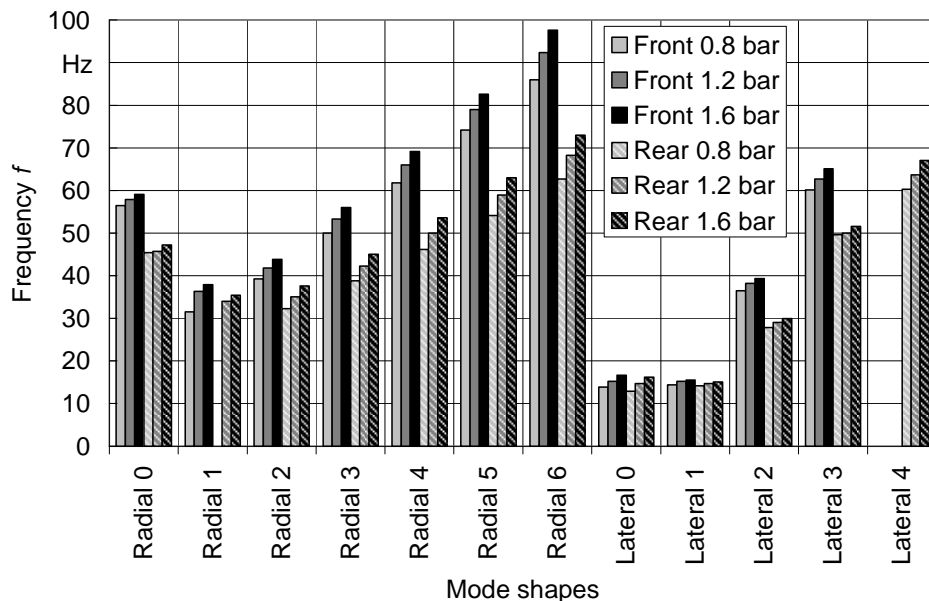
In the following the measuring data acquired by the different investigation methods and analysis results are presented. As already mentioned before the tire vibration modes are strongly dependent on the boundary and operating conditions [96].

### 5.1 Experimental modal analysis of the single wheels

The tire's modal behaviour is highly dependent on the boundary conditions of contact patch and spindle [74; 90]. This is why the experimental modal analysis was carried out for two boundary conditions: a free (unloaded) tire suspended on a low-frequency hanger assembly and a tire loaded on the ground (cf. section 4.2.1).

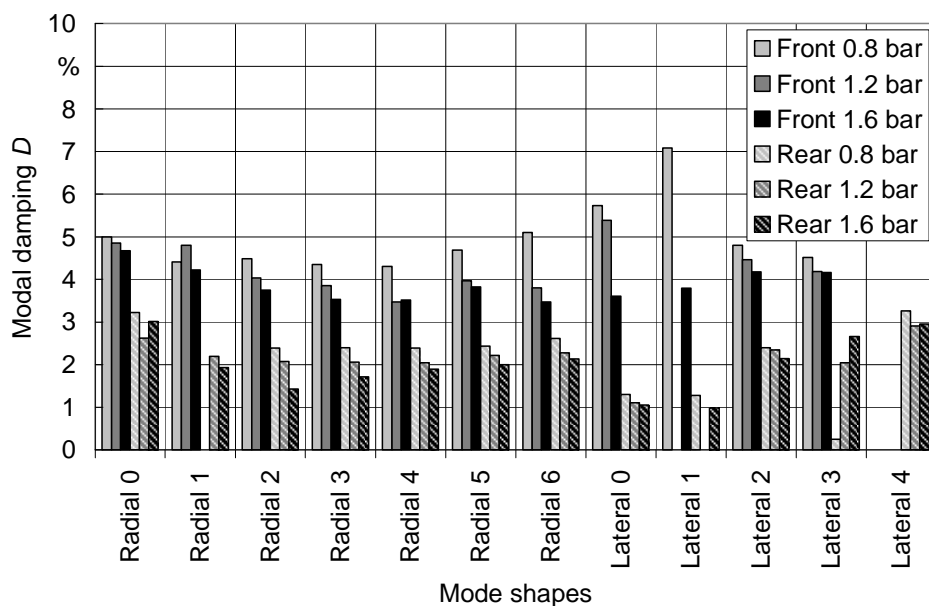
#### 5.1.1 Unloaded condition

The following diagrams show the identified mode shapes with the corresponding eigenfrequencies (Figure 47) and modal damping (Figure 48). The nomenclature of mode shapes can be found in section 3.2. Regarding the eigenfrequencies it is conspicuous that the front tire values of the so-called flexible modes exceed those of the rear tire considerably. With higher mode shapes the difference is increasing. For the rigid body mode frequencies (Radial/Lateral 0/1) the difference is hard to determine except for the Radial 0 mode which has to be regarded separately anyway due to the strong constraint dependency. As expected the frequencies are increasing with growing inflation pressure. Regarding the range from 0.8 to 1.6 bar the frequency shift can be more than 10 Hz. Both lateral rigid body modes show by far the lowest eigenfrequencies and are located in a very small frequency band whereas the Lateral 1 mode shows as the only one nearly no difference due to inflation pressure variation.



**Figure 47:** Mode shapes with eigenfrequencies of an unloaded Goodyear Optitrac 480/70 R24 (Front) and 520/70 R38 (Rear)

Since the modal damping is the parameter most difficult to determine the observed variability is quite high. Some conclusions can be drawn, nevertheless. Firstly, the damping values of the rear tire are considerably smaller than those of the front one. Most values of the front tire vary around 3 – 5 %, those of the rear tire mainly range around 1.5 – 2.5 %.

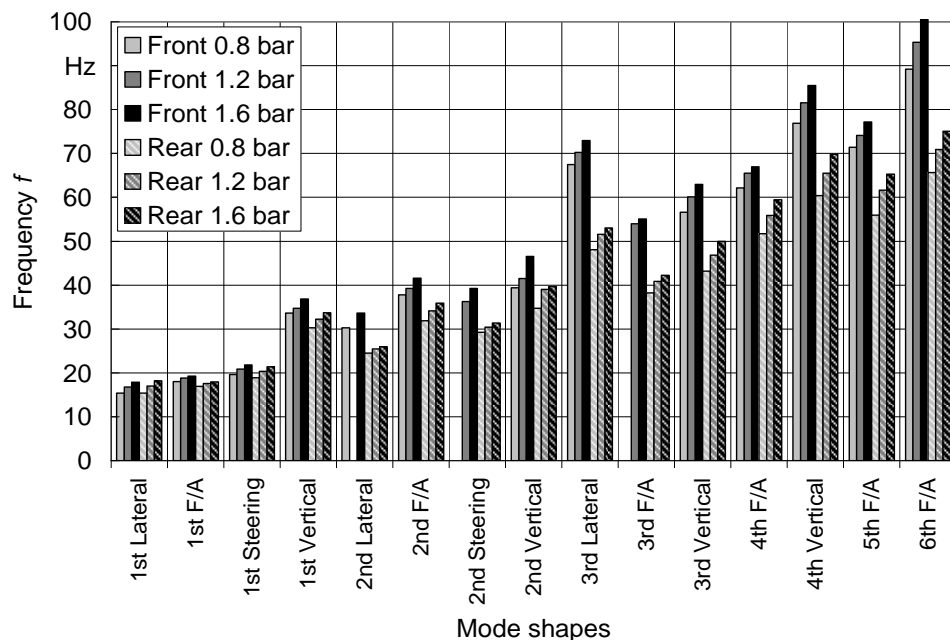


**Figure 48:** Mode shapes with modal damping of an unloaded Goodyear Optitrac 480/70 R24 (Front) and 520/70 R38 (Rear)

Two interesting exceptions have to be stated. Compared to the other modes both lateral rigid body modes show a significant decrease of damping for the rear tire whereas the values for the front one are rather increasing. Generally, an increasing inflation pressure leads to a decreasing damping. All values can be found in Table 41 and Table 42.

### 5.1.2 Loaded condition

The tire's contact to the ground leads to the loss of symmetry of the structure and complicates the mathematical expression as the tangential (circumferential) mode components cannot longer be expressed by harmonic functions. The nomenclature of the mode shapes for a loaded tire can be found in Table 3. The following figures do not consider frequency and damping of the vertical and lateral bouncing modes which correspond to eigenfrequency and damping of the tire idealized as a one-mass-oscillator for the two directions. They are directly dependent on the mass connected to the tire and consequently not treated as tire vibration modes.

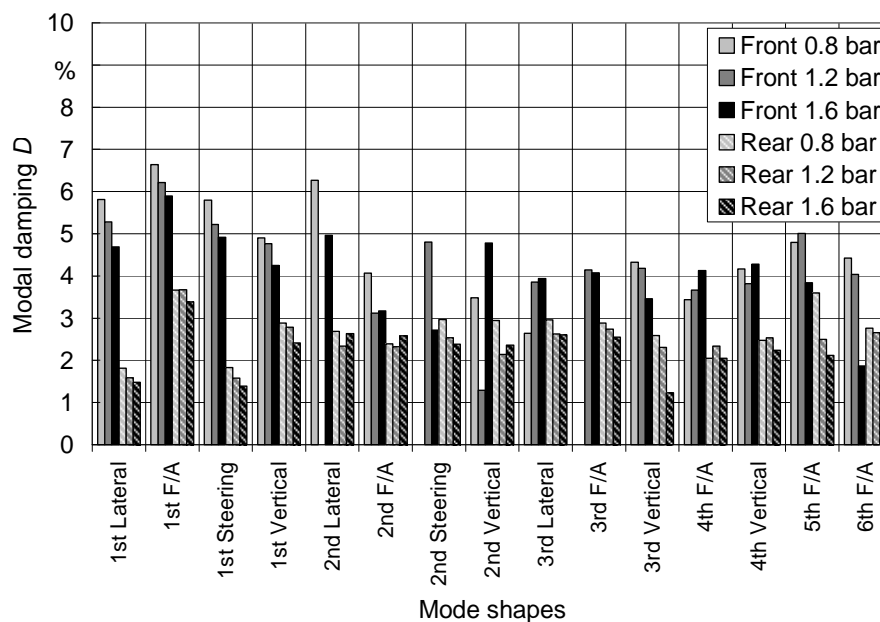


**Figure 49:** Mode shapes with eigenfrequencies of a loaded Goodyear Optitrac 480/70 R24 (Front,  $F_z = 6.0$  kN) and 520/70 R38 (Rear  $F_z = 7.5$  kN)

The 4<sup>th</sup>, 5<sup>th</sup> and 6<sup>th</sup> modes are difficult to determine but could be identified by this modal analysis. Contrary to passenger car tires up to 15 tire modes can be found in the comfort relevant frequency range between 10 and 80 Hz.

Similar to the unloaded condition the eigenfrequencies of the rigid body modes (1<sup>st</sup> Lateral, 1<sup>st</sup> F/A, 1<sup>st</sup> Steering and 1<sup>st</sup> Vertical) only differ a little comparing front and rear tire. For the flexible modes the eigenfrequencies of the front tire are considerably higher than those of the rear one. Again growing inflation pressure leads to an increase of eigenfrequency. These frequency results are generally according to the results of Scavuzzo et al. [91] who measured many different sized tires including also a 20.8 R38 (520/85 R38) on a vibration test rig.

Regarding the damping the values of the rear tire are considerably smaller than those of the front one especially for the rigid body modes. The influence of growing inflation pressure leading to a lower damping can be confirmed. All values can be found again in the Appendix in Table 43 and Table 44.

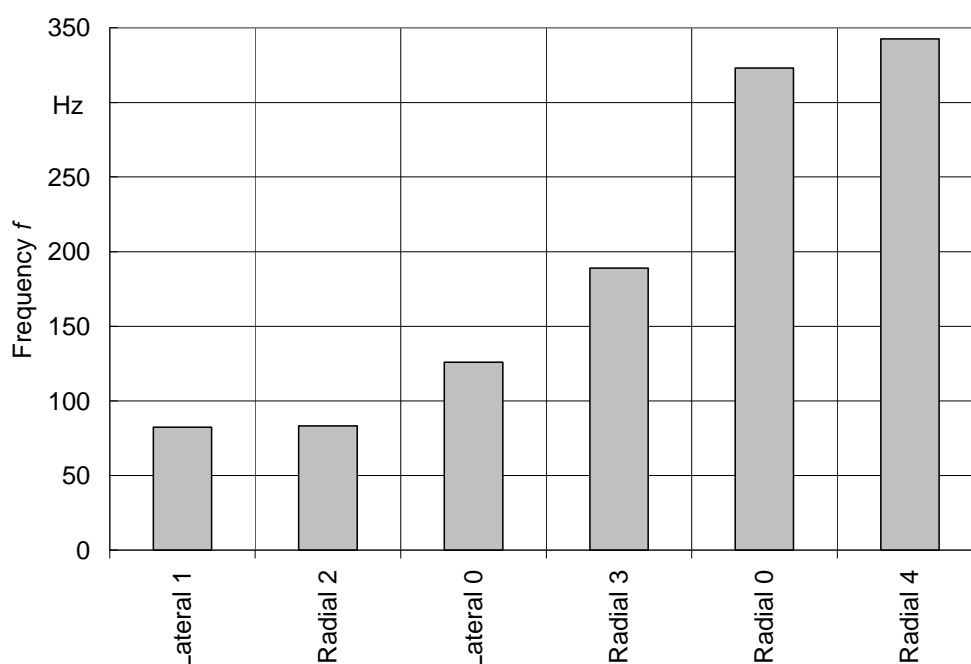


**Figure 50:** Mode shapes with modal dampings of a loaded Goodyear Optitrac 480/70 R24 (Front,  $F_z = 6.0$  kN) and 520/70 R38 (Rear  $F_z = 7.5$  kN)

### 5.1.3 Rim properties

Another important objective of this modal analysis was to investigate the modal behaviour of the rim. In order to determine the modes of the discrete rim another modal analysis was carried out for the rear rim / axle assembly without tire mounted (Figure 20, right). The following two figures show the eigenfrequencies and modal dampings of the detected rim modes. Additionally, the values can be checked in Table 45.

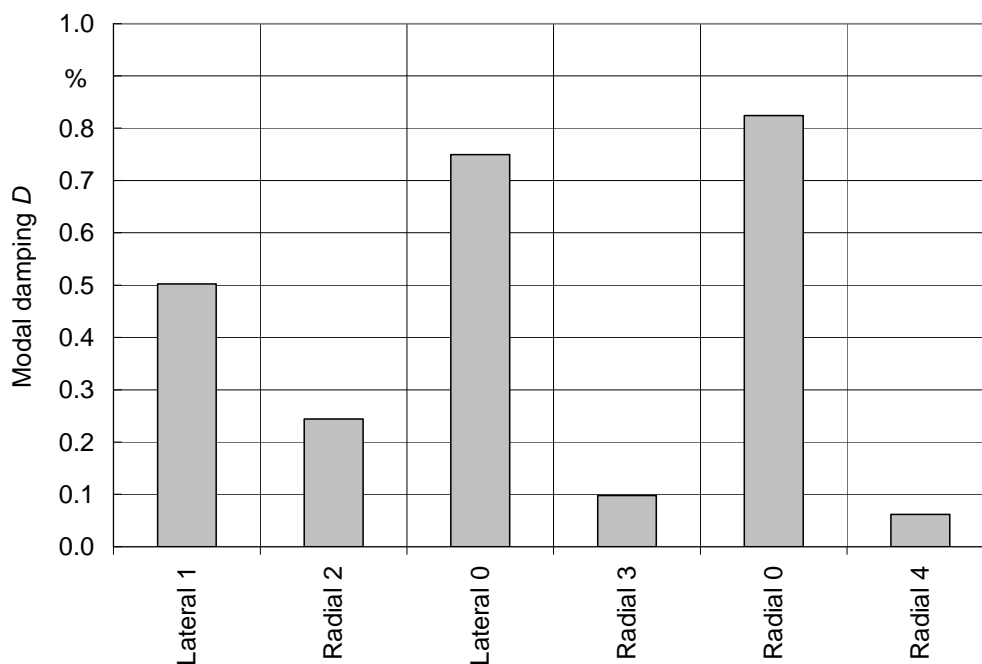
The lowest eigenfrequency which could be detected for this W16Lx38 rim is the Lateral 1 mode at about 82 Hz. Very close-by at about 83 Hz the Radial 2 mode appeared. The next mode is the translational lateral rigid body mode (Lateral 0) at 126 Hz. The Radial 3 mode follows at about 189 Hz. Not before 323 Hz the radial displacement of the axle against the rim acting as a rigid body occurs (Radial 0) whereas the Radial 4 mode at about 342 Hz is the highest observed mode.



**Figure 51:** Mode shapes with eigenfrequencies of the rear rim (W16L x 38)

As expected, the damping values generally show considerably lower amounts compared to the tire modes due to the different material properties of steel and rubber. Noticeable are the higher damping values for the lateral modes compared to the radial ones.

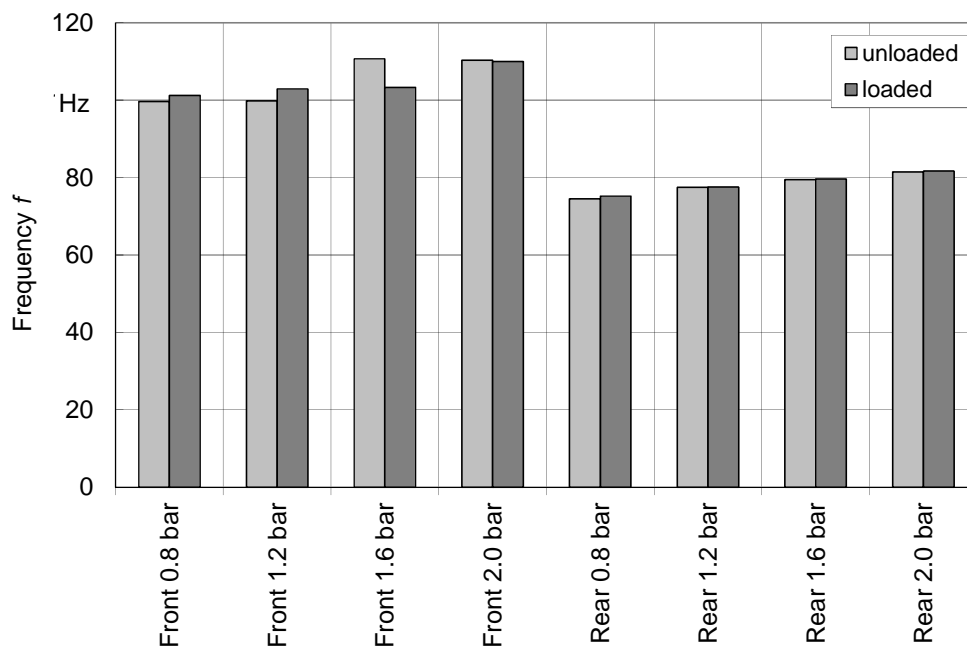




**Figure 52:** Mode shapes with modal dampings of the rear rim (W16L x 38)

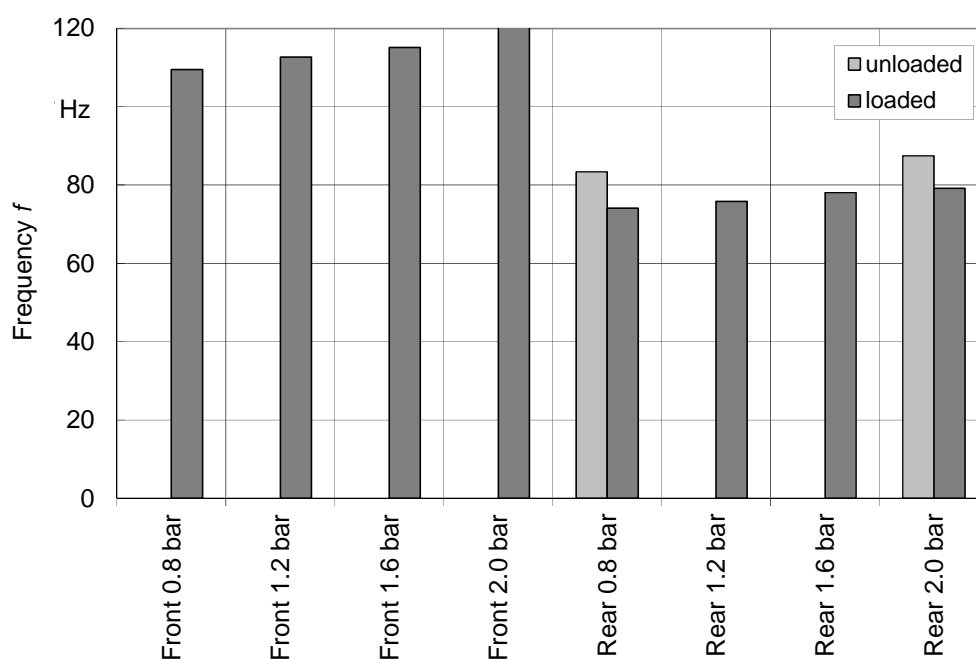
Based on the single rim modal analysis both the assembled front and rear rim with tire were examined. The following diagrams show eigenfrequencies and modal dampings of the rim's Radial 2 (Figure 53) and Lateral 1 (Figure 54) modes for both wheel/axle setups unloaded and loaded at different inflation pressure. The assembly was excited at the tire's driving point \*1 (Figure 18).

For both tires and loading conditions it can be retained an increase of eigenfrequency with growing inflation pressure. Regarding the rear tire at first it can be stated that the order of magnitude for both modes corresponds to the above mentioned results of the single rim considering additional pre-stressing and mass of the tire.



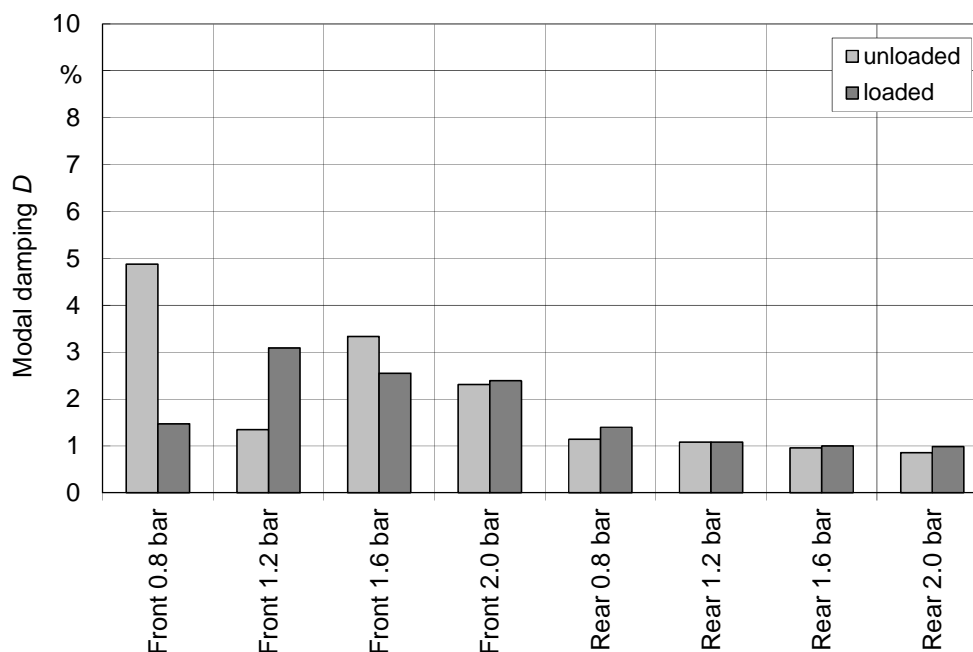
**Figure 53:** Eigenfrequencies for the Radial 2 mode of the rim (front: W15Lx24; rear: W16Lx38) with mounted tire, excitation of tire

For the Radial 2 mode there is nearly no influence of the loading condition whereas for the Lateral 1 mode loading the tire seems to lead to a noticeable decrease of the rim eigenfrequency. The support of the loaded tire by the ground is leading to an additional damping effect on the lateral movement of the rim.



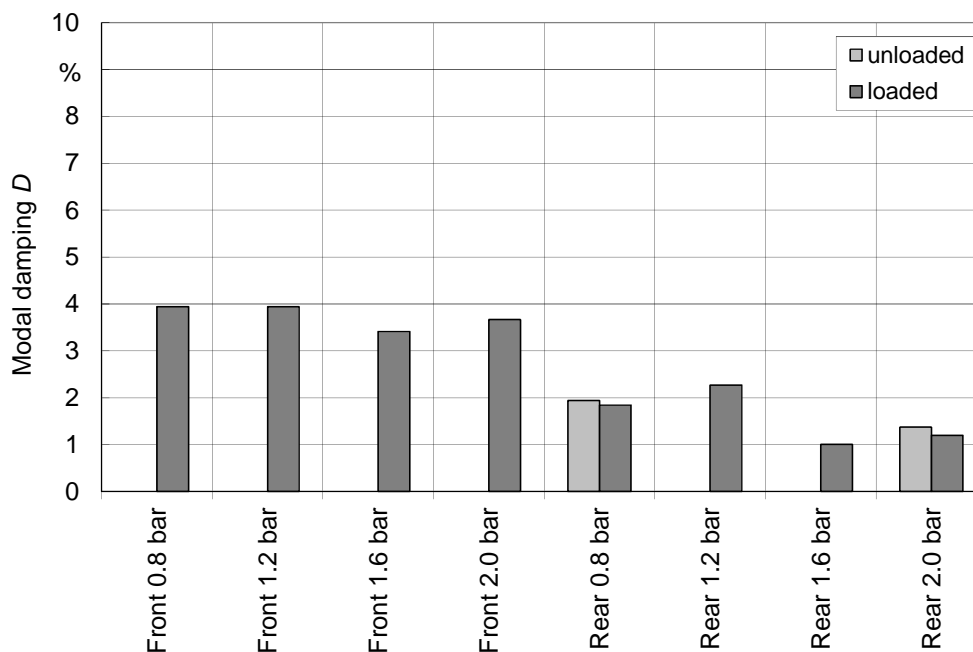
**Figure 54:** Eigenfrequencies for the Lateral 1 mode of the rim (front: W15Lx24; rear: W16Lx38) with mounted tire, excitation of tire

Furthermore, for the smaller front rim the Lateral 1 mode always shows higher frequency values compared to the Radial 2 mode contrary to the rear rim. For the unloaded condition none of the front tire's Lateral 1 modes could be identified within the investigated frequency range. The rear tire's Lateral 1 mode at 1.2 and 1.6 bar inflation pressure were not identified clearly because of the interference with other tire modes.



**Figure 55:** Modal dampings for the Radial 2 mode of the rim (front: W15Lx24; rear: W16Lx38) with mounted tire, excitation of tire

For the Radial 2 mode the variation of the damping values is quite strong, but it can be stated that the damping is decreasing with increasing inflation pressure (Figure 55). Furthermore, the front rim's damping for this mode seems to be higher than that of the rear rim. No clear estimation can be made on the influence of the loading condition which also applies for the Lateral 1 mode. As mentioned above higher damping values were determined for the lateral mode compared to the radial one. In spite of the strong variation a slight decrease of damping with increasing inflation pressure can be held again.

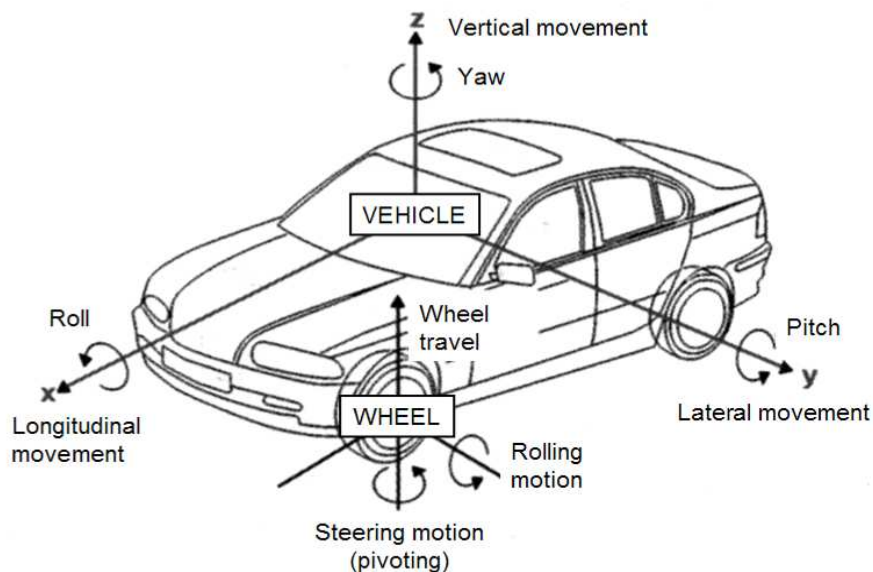


**Figure 56:** Modal dampings for the Lateral 1 mode of the rim (front: W15Lx24; rear: W16Lx38) with mounted tire, excitation of tire

#### 5.1.4 Axle dynamics

Regarding the investigations on the flat-belt test stand and on the tractor especially for the rolling condition it is necessary to detect eigenfrequencies and corresponding mode shapes without a set of accelerometers around the tire's circumference. For the determination of vehicle ride comfort the axle dynamics are of great interest. Wheeler et al. used the term "global motion" which means that large contiguous portions of the tire structure are moving in the same direction [96]. Thus, in this chapter the eigenfrequencies and corresponding mode shapes of the loaded tires introduced in 5.1.2 are redetermined as far as possible only from the two 3D accelerometer signals (sensors No. 19 and 20 in Figure 18) and the global motion can be estimated by regarding their amplitudes. The frequency range is limited to 100 Hz.

Regarding the axle dynamics requires a non-rotating coordinate system affixed to the vehicle. The standard system is shown in Figure 57 [12]. For the further interpretation this system will be used. Table 33 shows the transformation convention.



**Figure 57:** Vehicle coordinate system according to ISO 8855 [12]

**Table 33:** Direction definition

Measuring coordinate system	ISO 8855 vehicle coordinate system	Axle (sensors No. 19+20) Figure 18	Excitation point (point/sensor No. 8) Figure 18
x	z	vertical	tangential
y	x	longitudinal	radial
z	y	lateral	lateral

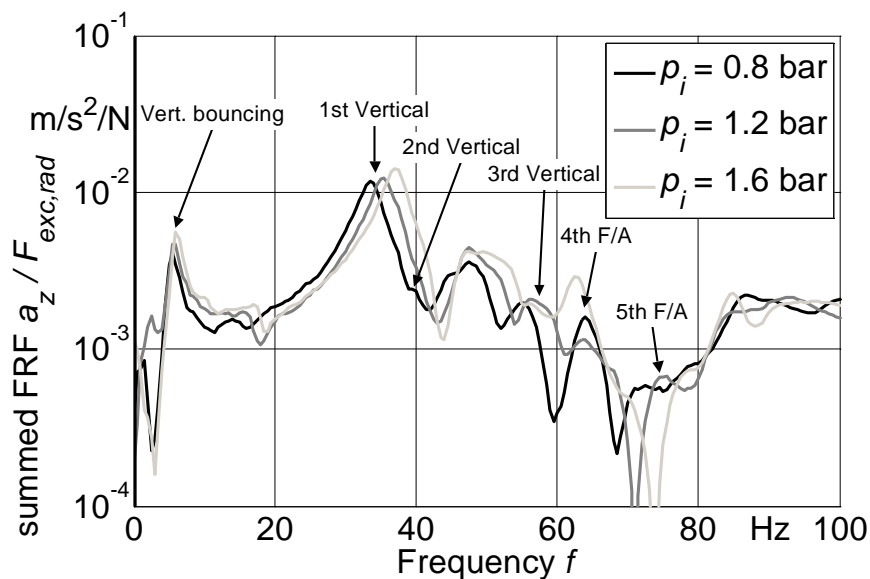
As mentioned above, in the frequency range up to 100 Hz there are numerous tire modes several of which are situated very close to each other. Besides the three different directions for a precise extraction of the single mode shapes the phase dependency of the appropriate channels on both sides of the axle can be used. For some modes there is even redundancy with a further signal. Table 34 shows the allocation of the channels to the tire mode shapes. Generally, by adding the FFT spectra of the two corresponding channels the in-phase relation is emphasized. Subtraction leads to an amplification of the out-of-phase oscillations. For the three directions this results in three in-phase and two out-of-phase spectra since the lateral accelerometers are placed on the same line.

The results of the modal analysis for the loaded tires (Table 43 and Table 44) have been used to confirm frequency and shape of the identified modes.

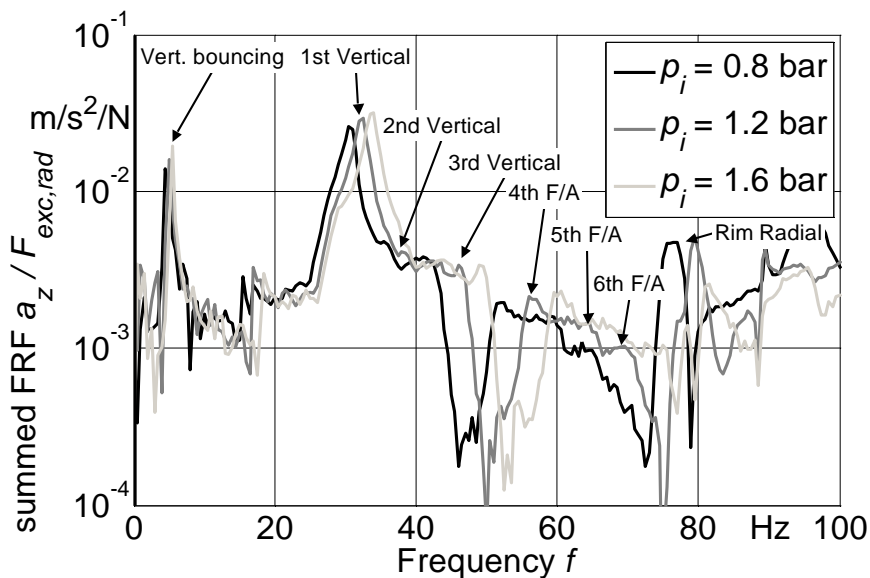
**Table 34:** Identification of mode shapes

<b>Mode shape</b>	<b>1<sup>st</sup> acc. direction</b>	<b>2<sup>nd</sup> acc. direction</b>	<b>Exc. direction</b>
Vert. Bouncing	z in-phase	---	radial
Lat. Bouncing	y in-phase	z out-of-phase	lateral
1 <sup>st</sup> Lateral	y in-phase	z out-of-phase	lateral
1 <sup>st</sup> F/A	x in-phase	---	tangential
1 <sup>st</sup> Steering	x out-of-phase	---	lateral
1 <sup>st</sup> Vertical	z in-phase	---	radial
2 <sup>nd</sup> Lateral	y in-phase	x/z out-of-phase	lateral
2 <sup>nd</sup> F/A	x in-phase	---	tangential
2 <sup>nd</sup> Steering	x out-of-phase	---	lateral
2 <sup>nd</sup> Vertical	z in-phase	---	radial
3 <sup>rd</sup> Lateral	y in-phase		lateral
3 <sup>rd</sup> F/A	x in-phase		tangential
3 <sup>rd</sup> Vertical	z in-phase		radial
4 <sup>th</sup> F/A	x in-phase		tangential
4 <sup>th</sup> Vertical	z in-phase		radial
5 <sup>th</sup> F/A	x in-phase		tangential
6 <sup>th</sup> F/A	x in-phase		tangential

The following 10 figures show the mentioned five spectra for the front and the rear tire. Figure 58 and Figure 59 show the summed FRF's for the two axle z-directions. Thus, the translational vertical movement (z in-phase) of the axle is emphasized which occurs mainly with the vertical modes. As expected the vertical bouncing and the 1<sup>st</sup> vertical mode can be identified clearly. The latter shows the highest amplitude regarding this signal. With growing inflation pressure frequency and also amplitude are increasing. The 2<sup>nd</sup> vertical mode of the front tire is hard to determine from the recorded axles' vertical acceleration signals.



**Figure 58:** Summed FRF's of front tire axle's vertical accelerations related on radial excitation force

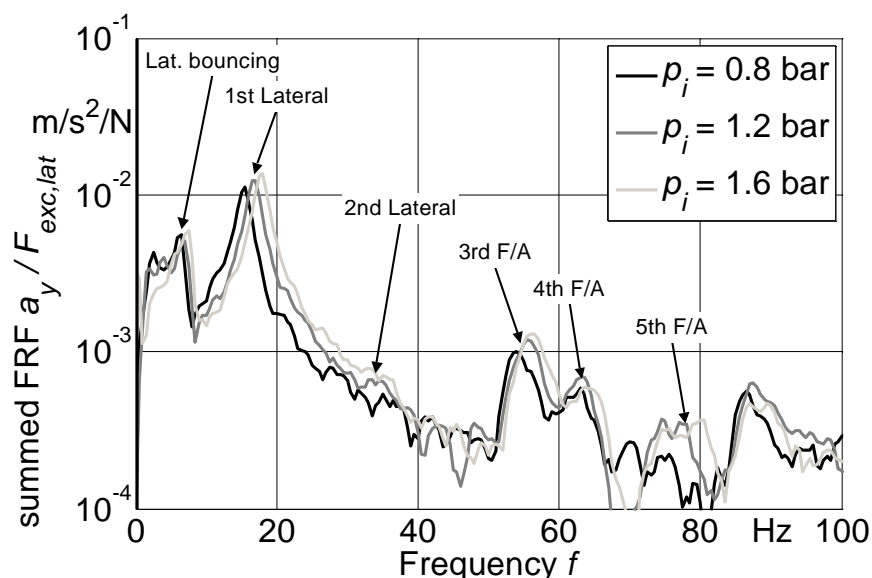


**Figure 59:** Summed FRF's of rear tire axle's vertical accelerations related on radial excitation force

For the rear tire, however, the corresponding peaks are visible even though with much lower amplitude. The 3<sup>rd</sup> vertical mode for both front and rear tire can be determined. Again the sharpness of the peak is better for the rear tire where the amplitude is similar to that of the 2<sup>nd</sup> vertical mode. This effect is due to the

comparably lower damping of the rear tire already mentioned in 5.1.2. Remarkably, the 4<sup>th</sup> F/A mode can be clearly identified. Regarding the magnitudes there is another considerable mode round 80 Hz. According to the prior investigations on the rim characteristics this mode can be identified as the Radial 2 mode of the rim. As the frequency range is limited to 100 Hz this mode cannot be detected for the front tire.

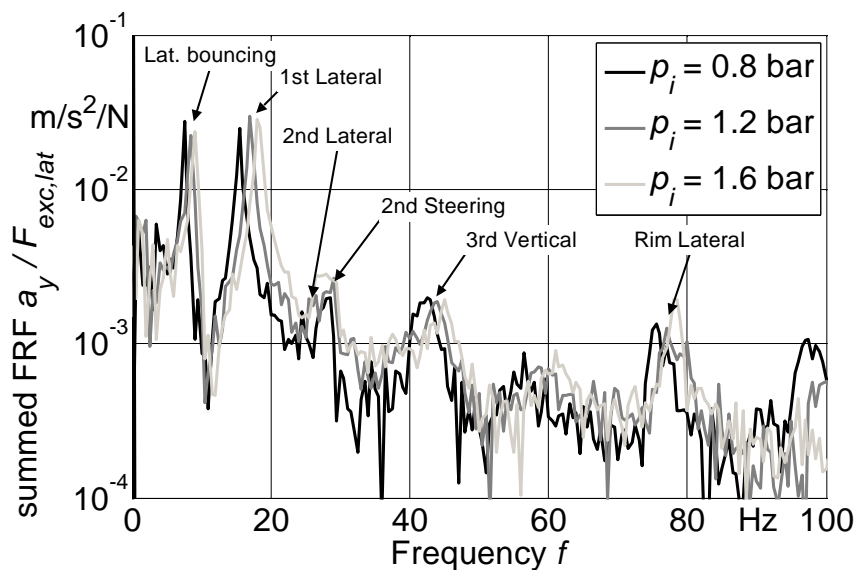
Figure 60 and Figure 61 show the summed FRF's for the lateral direction due to lateral excitation. Referring to Table 34 the lateral modes should be detectable by this illustration. Indeed, the lateral bouncing mode and especially the 1<sup>st</sup> lateral mode can be read very clearly. For the latter mode the frequency shift and growing amplitude with increasing inflation pressure becomes very apparent.



**Figure 60:** Summed FRF's of front tire axle's lateral accelerations related on lateral excitation force

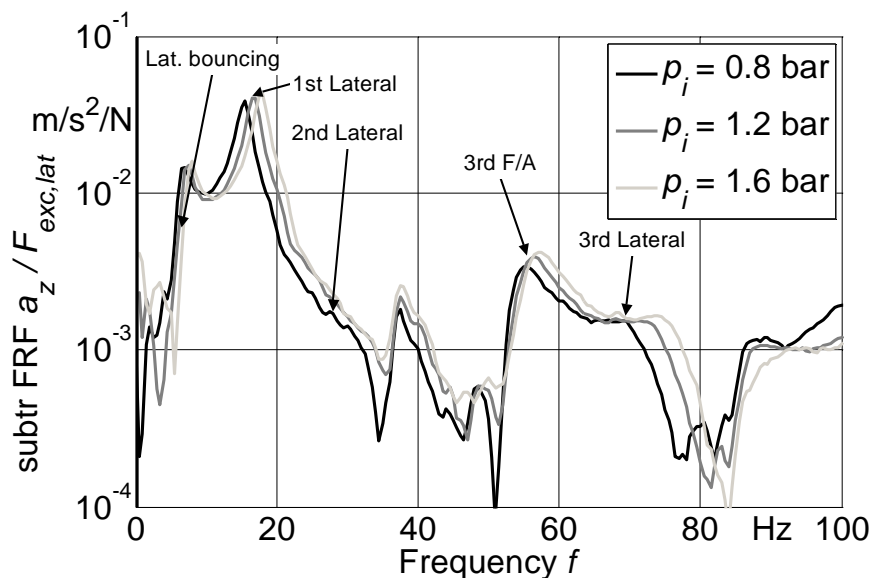
The lateral acceleration signals of the rear wheel axle in Figure 61 covertly show peaks of the 2<sup>nd</sup> lateral mode. Directly below 80 Hz four clear peaks with high magnitude appear. They can be allocated to the rim's Lateral 1 mode which was identified before quite close below the Radial 2 mode for this rim.





**Figure 61:** Summed FRF's of rear tire axle's lateral accelerations related on lateral excitation force

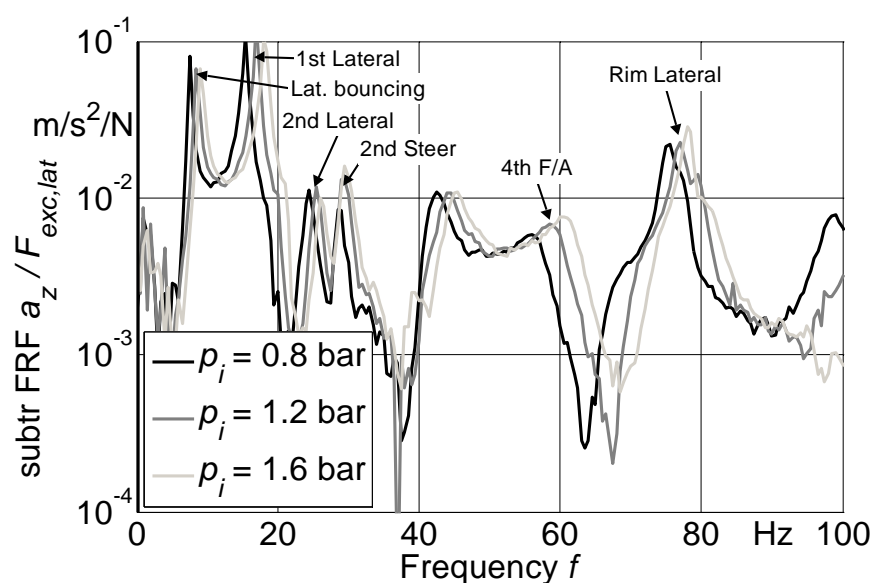
Regarding the front tire the 3<sup>rd</sup>, 4<sup>th</sup> and 5<sup>th</sup> F/A modes can be identified surprisingly. The 2<sup>nd</sup> lateral mode is not, the 3<sup>rd</sup> lateral is hardly visible. These modes can be determined rudimentary via the out-of-phase signals of the vertical accelerations (Figure 62).



**Figure 62:** Subtracted FRF's of front tire axle's vertical accelerations related on lateral excitation force

As a further signal for the determination of the lateral modes the vertical out-of-phase accelerations can be considered. Lateral bouncing and 1<sup>st</sup> lateral mode can be read at least with the same quality as mentioned above for both tires. Regarding the front tire in Figure 62 the 3<sup>rd</sup> lateral mode frequencies can be estimated between 67 and 75 Hz. The 3<sup>rd</sup> F/A is even more sharp between 53 and 58 Hz. The peaks at about 38 Hz could not be assigned since the 2<sup>nd</sup> lateral mode has been determined before at about 30 up to 35 Hz. Possibly this is the 2<sup>nd</sup> Steering mode.

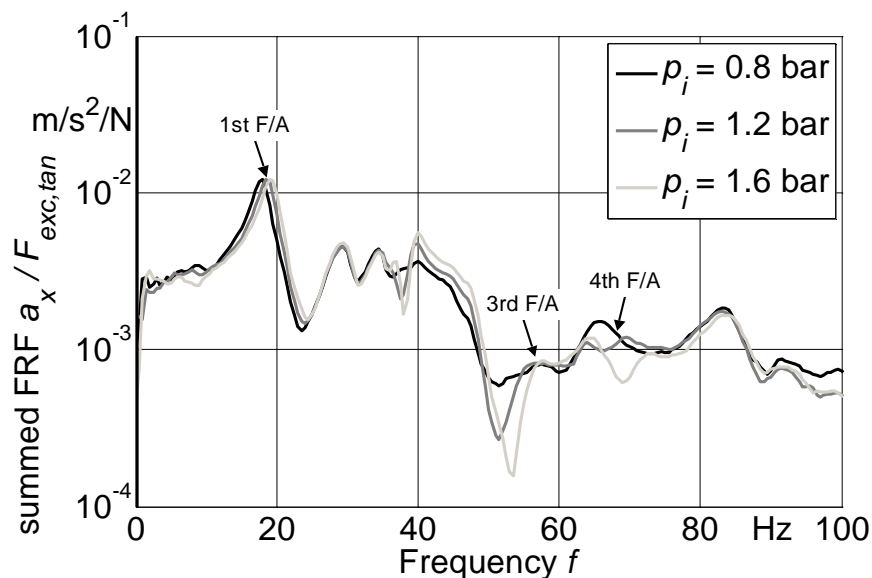
The rear tire's FRF's illustrated in Figure 63 allow the determination of the 2<sup>nd</sup> lateral mode separated from the 2<sup>nd</sup> steering mode. The 4<sup>th</sup> F/A mode and the rim's Lateral 1 mode also can be read. In this diagram the peaks between 42 and 47 Hz can not be assigned to any of the tire modes.



**Figure 63:** Subtracted FRF's of rear tire axle's vertical accelerations related on lateral excitation force

For the F/A modes the axle's longitudinal in-phase accelerations are expected to show characteristic peaks at the corresponding frequencies. The following two figures show these FRF's for the front and the rear tire. For both tires very exact to determine is the 1<sup>st</sup> F/A mode. Compared with the other rigid body modes (1<sup>st</sup> vertical, 1<sup>st</sup> lateral and 1<sup>st</sup> steering) the frequency increase due to growing inflation pressure is quite small. This fact can be attributed to the side wall stiffness that is

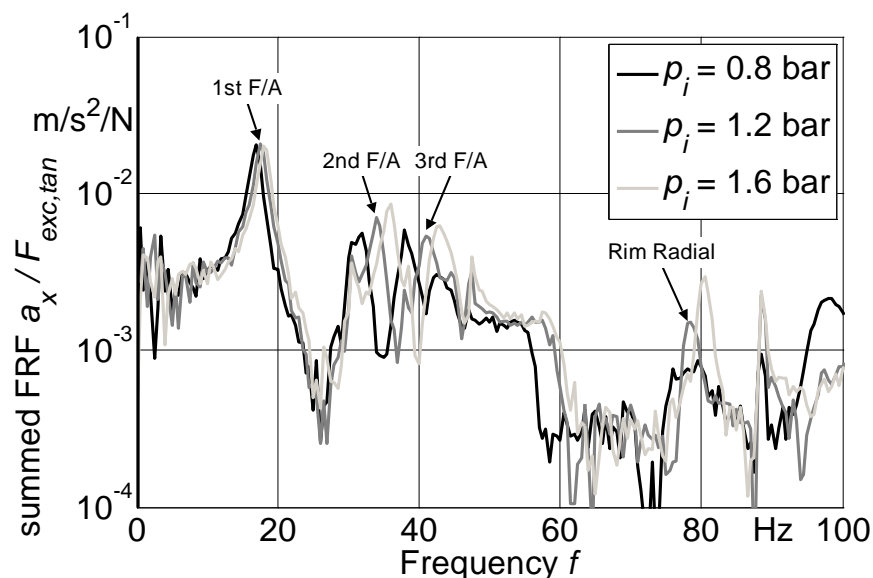
playing a more important role here whereas the other modes are dominated by the inflation pressure generated stiffness.



**Figure 64:** Summed FRF's of front tire axle's longitudinal accelerations related on tangential excitation force

Regarding the front tire the 3<sup>rd</sup> and 4<sup>th</sup> F/A modes only roughly can be estimated at 53 up to 57 Hz and at 62 up to 68 Hz. The 2<sup>nd</sup> F/A mode which was identified between 38 and 44 Hz is not extractable and the four peaks between 30 and 40 Hz cannot be assigned to any other tire modes.

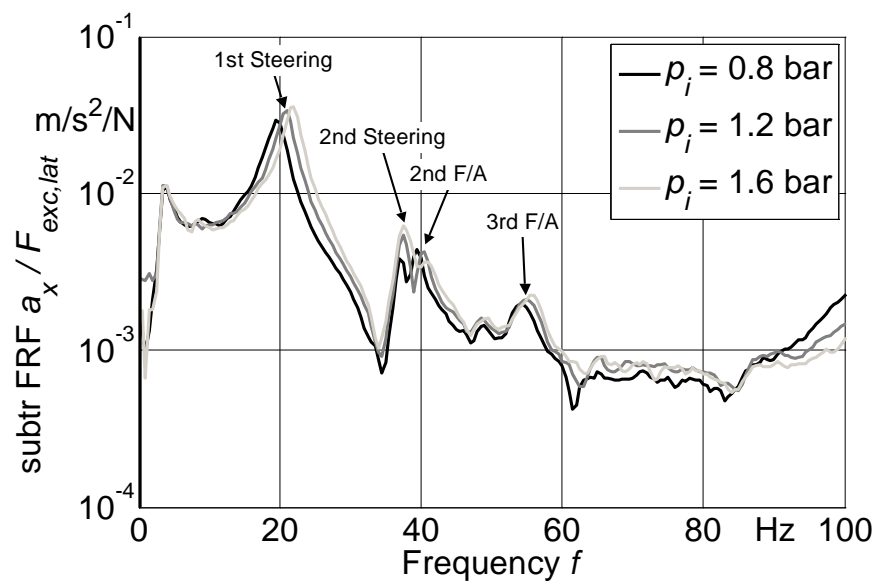
The rear tire signal however shows the 2<sup>nd</sup> and 3<sup>rd</sup> F/A mode quite sharply and with the mentioned frequency shift due to rising inflation pressure. The 4<sup>th</sup> F/A mode seems to have no influence on the axle dynamics. Again the rim's Radial 2 mode shows its influence on the axle dynamics at around 80 Hz.



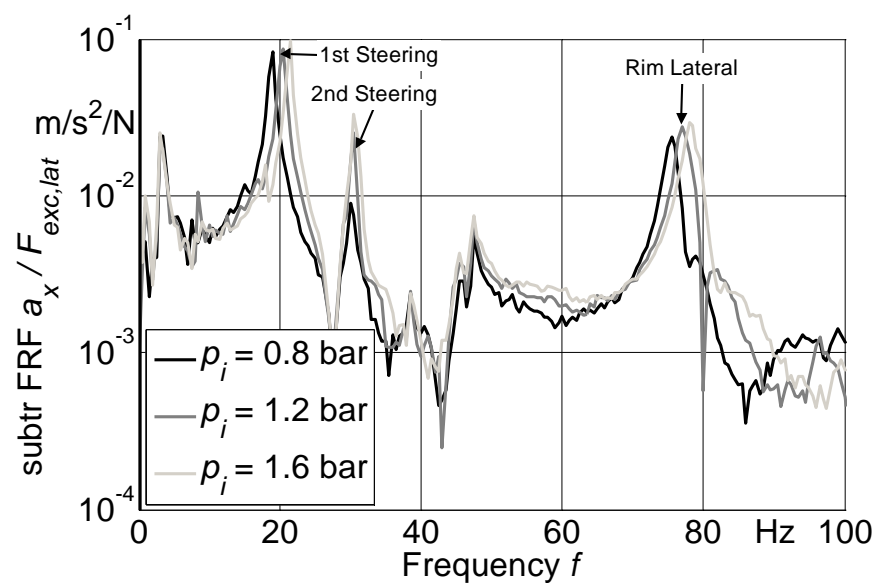
**Figure 65:** Summed FRF's of rear tire axle's longitudinal accelerations related on tangential excitation force

The last set of modes are the steering modes of which only two were identified during the previous investigations. Figure 66 and Figure 67 show the out-of-phase signal FRF for the front and the rear tire. The 1<sup>st</sup> steering mode becomes very apparent associated with the typical frequency shift and increase of amplitude due to growing inflation pressure. The 2<sup>nd</sup> steering mode is not that clearly to determine because of the interference with the 2<sup>nd</sup> F/A mode. Visible is again the 3<sup>rd</sup> F/A mode between 53 and 57 Hz which is the last peak within the investigated frequency range at the same time.

Regarding the rear tire the 1<sup>st</sup> and 2<sup>nd</sup> steering modes are very clearly to read. Between 35 and 50 Hz three more peak areas can be seen which cannot be allocated exactly. Very sharp and with enormous amplitude the Lateral 1 mode of the rim appears shortly below 80 Hz and reconfirms again the influence of the rim's rigid body modes on the axle dynamic behaviour.



**Figure 66:** Subtracted FRF's of front tire axle's longitudinal accelerations related on lateral excitation force



**Figure 67:** Subtracted FRF's of rear tire axle's longitudinal accelerations related on lateral excitation force

The following two tables summarize the analysis of the axle dynamics for the two tires due to the quality and usability of the signals.

**Table 35:** Identification of the front tire's mode shapes

Mode shape	1 <sup>st</sup> acc. direction	2 <sup>nd</sup> acc. direction	Exc. direction
Vert. Bouncing	z in-phase	---	radial
Lat. Bouncing	y in-phase	z out-of-phase	lateral
1 <sup>st</sup> Lateral	y in-phase	z out-of-phase	lateral
1 <sup>st</sup> F/A	x in-phase	---	tangential
1 <sup>st</sup> Steering	x out-of-phase	---	lateral
1 <sup>st</sup> Vertical	z in-phase	---	radial
2 <sup>nd</sup> Lateral	y in-phase	z out-of-phase	lateral
2 <sup>nd</sup> F/A	x in-phase	---	tangential
2 <sup>nd</sup> Steering	x out-of-phase	---	lateral
2 <sup>nd</sup> Vertical	z in-phase	---	radial
3 <sup>rd</sup> Lateral	y in-phase	z out-of-phase	lateral
3 <sup>rd</sup> F/A	x in-phase	y in-phase	tangential/lat
3 <sup>rd</sup> Vertical	z in-phase		radial
4 <sup>th</sup> F/A	x in-phase	y in-phase	tangential/lat
4 <sup>th</sup> Vertical	z in-phase	y in-phase	radial/lat
5 <sup>th</sup> F/A	x in-phase	y in-phase	tangential
6 <sup>th</sup> F/A	x in-phase		tangential

█ : Clearly identified modes      █ : Assessable modes

According to Böhm [69] for passenger car tires up to 100 Hz only the rigid body modes appear for the measured vertical and horizontal axle accelerations but not the higher order modes (flexible modes). This assumption is based on a tire with an ideal mass, damping and stiffness distribution. In this case only the rigid body displacements have influence.

The results confirm that the rigid body modes have a clear influence on the axle dynamics. Furthermore, for the two tractor tires also a number of flexible modes are visible at least. This means that there is a tolerance concerning the mass, damping and stiffness distribution. Since for the bigger tire visibility and identification are more accurate than for the smaller tire, it can be concluded that a wider tolerance range is and has to be accepted due to tire manufacturing technology.

**Table 36:** Identification of the rear tire's mode shapes

Mode shape	1 <sup>st</sup> acc. direction	2 <sup>nd</sup> acc. direction	Exc. direction
Vert. Bouncing	z in-phase	---	radial
Lat. Bouncing	y in-phase	z out-of-phase	lateral
1 <sup>st</sup> Lateral	y in-phase	z out-of-phase	lateral
1 <sup>st</sup> F/A	x in-phase	---	tangential
1 <sup>st</sup> Steering	x out-of-phase	---	lateral
1 <sup>st</sup> Vertical	z in-phase	---	radial
2 <sup>nd</sup> Lateral	y in-phase	z out-of-phase	lateral
2 <sup>nd</sup> F/A	x in-phase	---	tangential
2 <sup>nd</sup> Steering	x out-of-phase	z out-of-phase	lateral
2 <sup>nd</sup> Vertical	z in-phase	---	radial
3 <sup>rd</sup> Lateral	y in-phase		lateral
3 <sup>rd</sup> F/A	x in-phase		tangential
3 <sup>rd</sup> Vertical	z in-phase		radial
4 <sup>th</sup> F/A	x in-phase	z in-phase	tangential/rad
4 <sup>th</sup> Vertical	z in-phase		radial
5 <sup>th</sup> F/A	x in-phase		tangential
6 <sup>th</sup> F/A	x in-phase		tangential

█ : Clearly identified modes

█ : Assessable modes

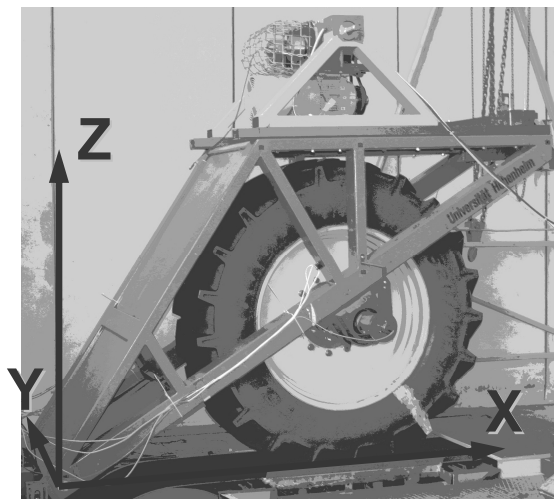
## 5.2 Investigations on the flat-belt tire test stand

With the experimental modal analysis of the wheel and its axle the tire's modal data for different boundary conditions could be determined without the influence of a test rig. In the next step a modal analysis was also carried out for the rear tire mounted on the flat-belt test stand to compare the results and detect possible influences of the rig. In the following, two subchapters the possible determination of the tire's modal properties via shaker tests and uniformity tests is investigated.

### 5.2.1 Modal analysis

In the following, the results of the experimental modal analysis on the flat-belt test stand are presented. For the tire it is distinguished again between unloaded and loaded condition.

For the further analysis the coordinate system shown in Figure 68 is agreed. Processes in the “x-z direction” are called “in-plane”. The “y-direction” is also described as “out-of-plane”.



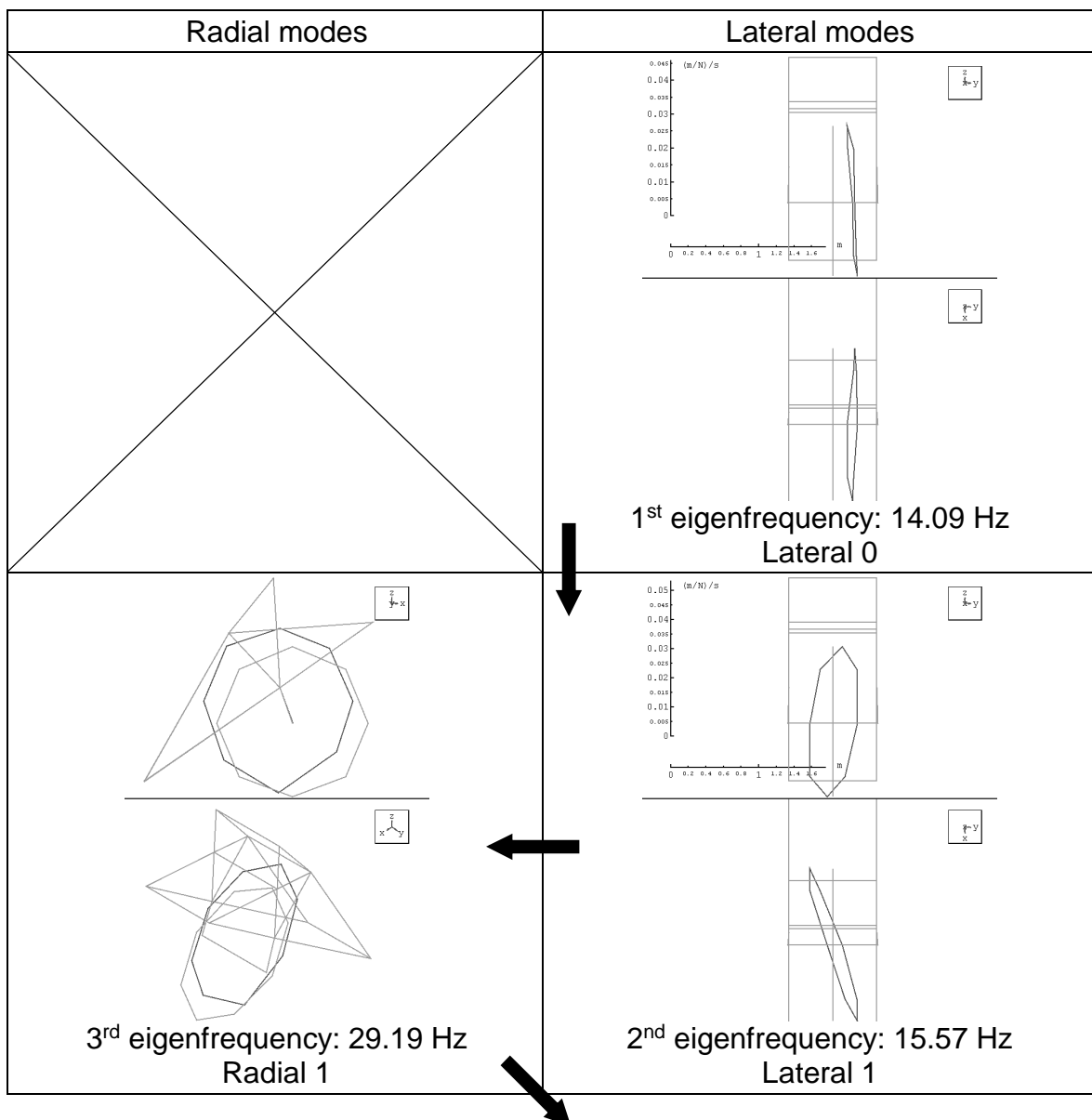
**Figure 68:** Coordinate system of the flat track

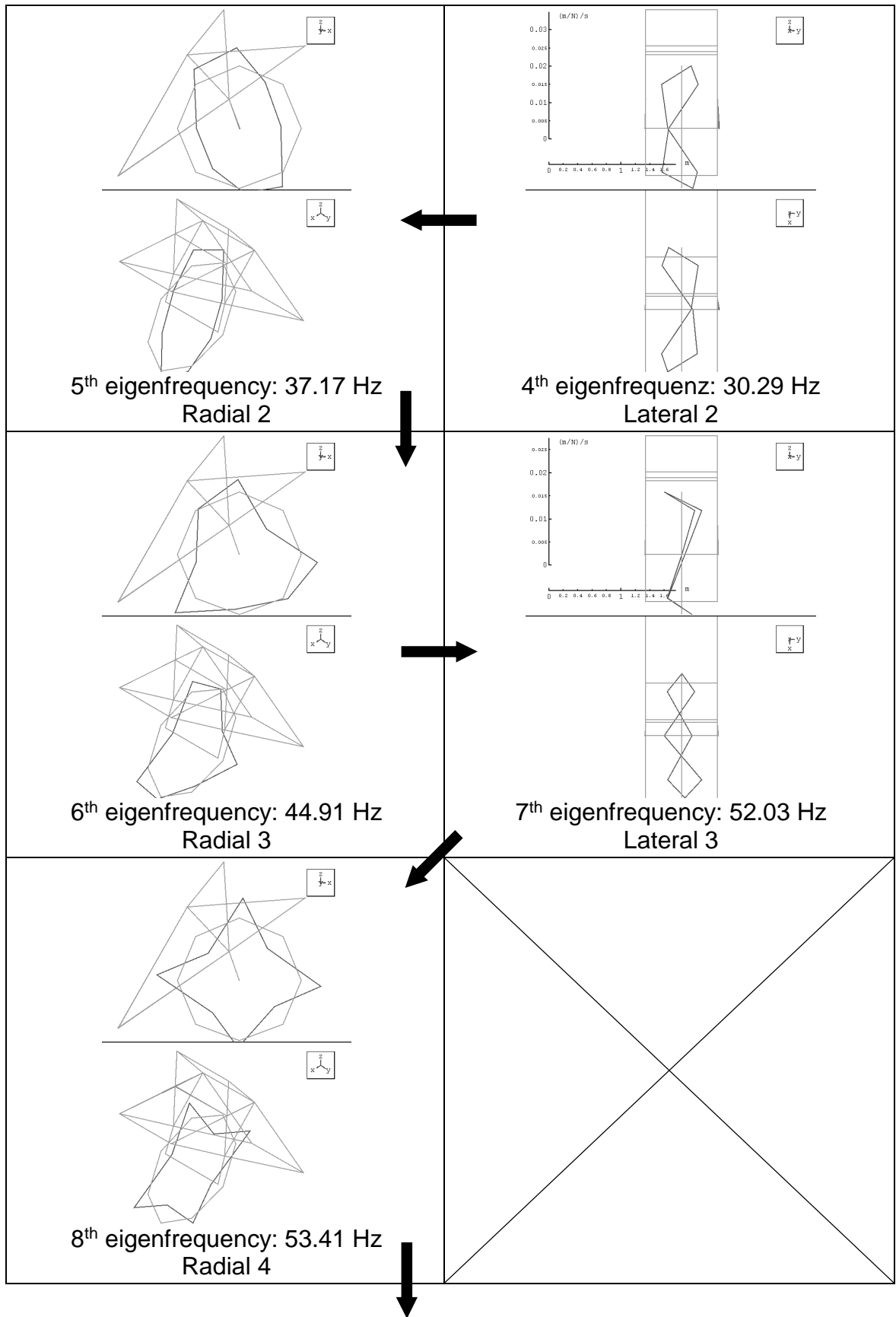


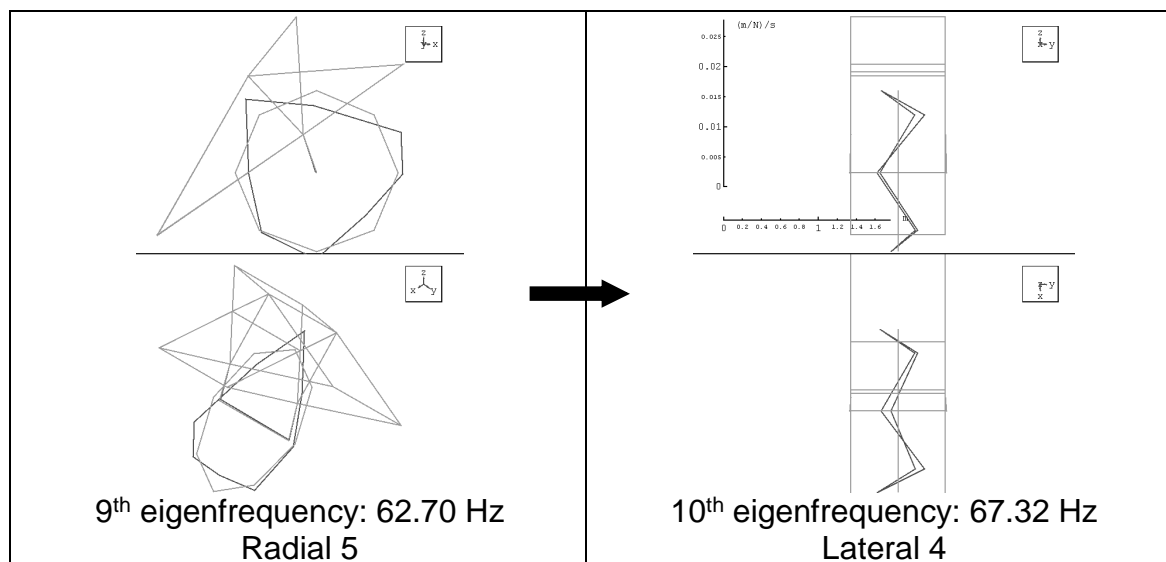
### 5.2.1.1 Unloaded condition

As already investigated in 5.1.1 also for this restraint condition of the tire the corresponding mode shapes could be detected (Table 37). For this purpose 8 accelerometers had been distributed among the circumference of the tire and enabled a precise determination of the tire modes.

**Table 37:** Tire mode shapes of an unloaded Goodyear Optitrac 520/70 R38 (Rear) mounted in the test rig ( $v = 0$  km/h,  $F_z = 0$  kN,  $p_i = 1.5$  bar)







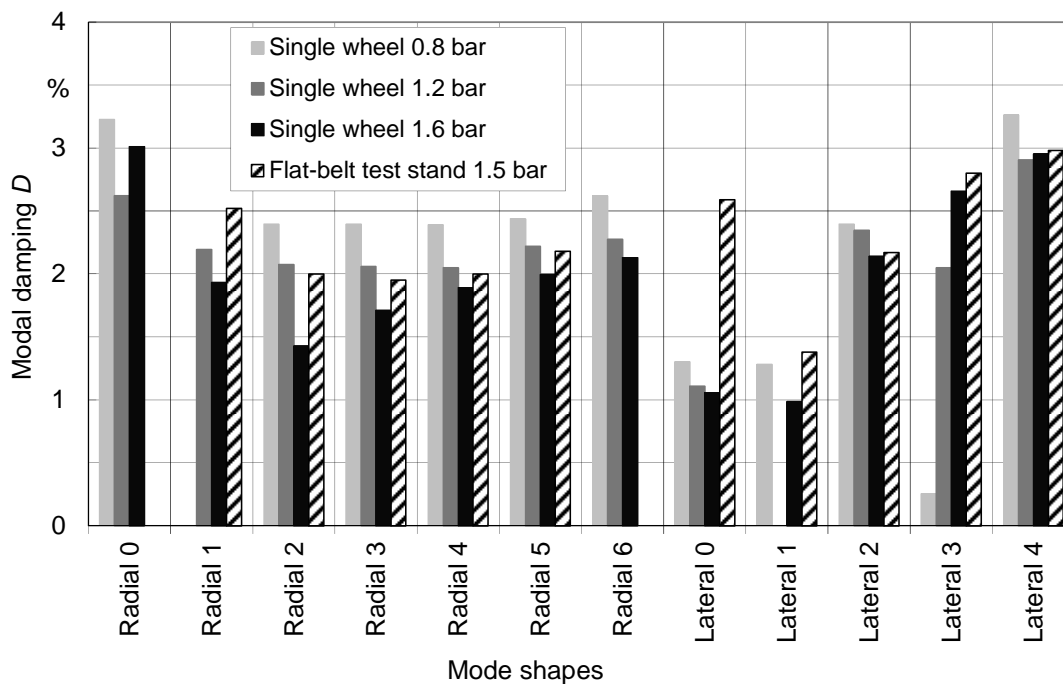
The tire's radial modes show no interferences with the rig modes determined above. Regarding the lateral modes there is interference for the Lateral 0 mode which coincides with mode No. 2a of the rig. The Lateral 2 mode (30.29 Hz) is also situated near rig mode No. 3 (29.37 Hz) but for this case the mass dependency is separating rig and tire mode. The Lateral 3 and 4 modes, however, can be distinguished quite well from the nearer rig modes.

In the following, the comparison with the above mentioned modal analysis results of the single wheel is drawn. Figure 69 shows the unloaded rear tire's eigenfrequencies for five different inflation pressures of which 1.5 bar was adjusted for the rig analysis.



**Figure 69:** Eigenfrequencies of an unloaded Goodyear Optitrac 520/70 R38 (Rear) mounted in the test rig ( $p_i = 1.5$  bar) compared with results of modal analysis of the single wheel (5.1.1) ( $p_i = 0.8 / 1.2 / 1.6$  bar)

The Radial 0 mode could not be detected for the rear tire installed into the flat-belt test stand. The radial modes 2 up to 5 fit quite exact into the gap between 1.2 and 1.6 bar. For the lateral modes 2 up to 4 this is similar whereas the frequencies of the 1.5 bar setup seem to be a little higher than for the 1.6 bar setup. This phenomenon can probably be explained by using two different measuring systems and by the interval of one and a half years between the two measurements which may lead to a first deterioration of the tire. Much more noticeable is the frequency deviation for the further whole-body modes (Radial 1 and Lateral 0) which can even more be observed for the damping values (Figure 70). Since these modes strongly affect the axle dynamics and thus the vibration transmission towards the test rig this deviation has to be due to the influence of the two different restraint conditions. This conclusion corresponds to the findings of Zegelaar who stated that the spindle boundary conditions affect the rigid body modes of the tire [75].



**Figure 70:** Modal dampings of an unloaded Goodyear Optitrac 520/70 R38 (Rear) mounted in the test rig ( $p_i = 1.5$  bar) compared with results of modal analysis of the single wheel (5.1.1) ( $p_i = 0.8 / 1.2 / 1.6$  bar)

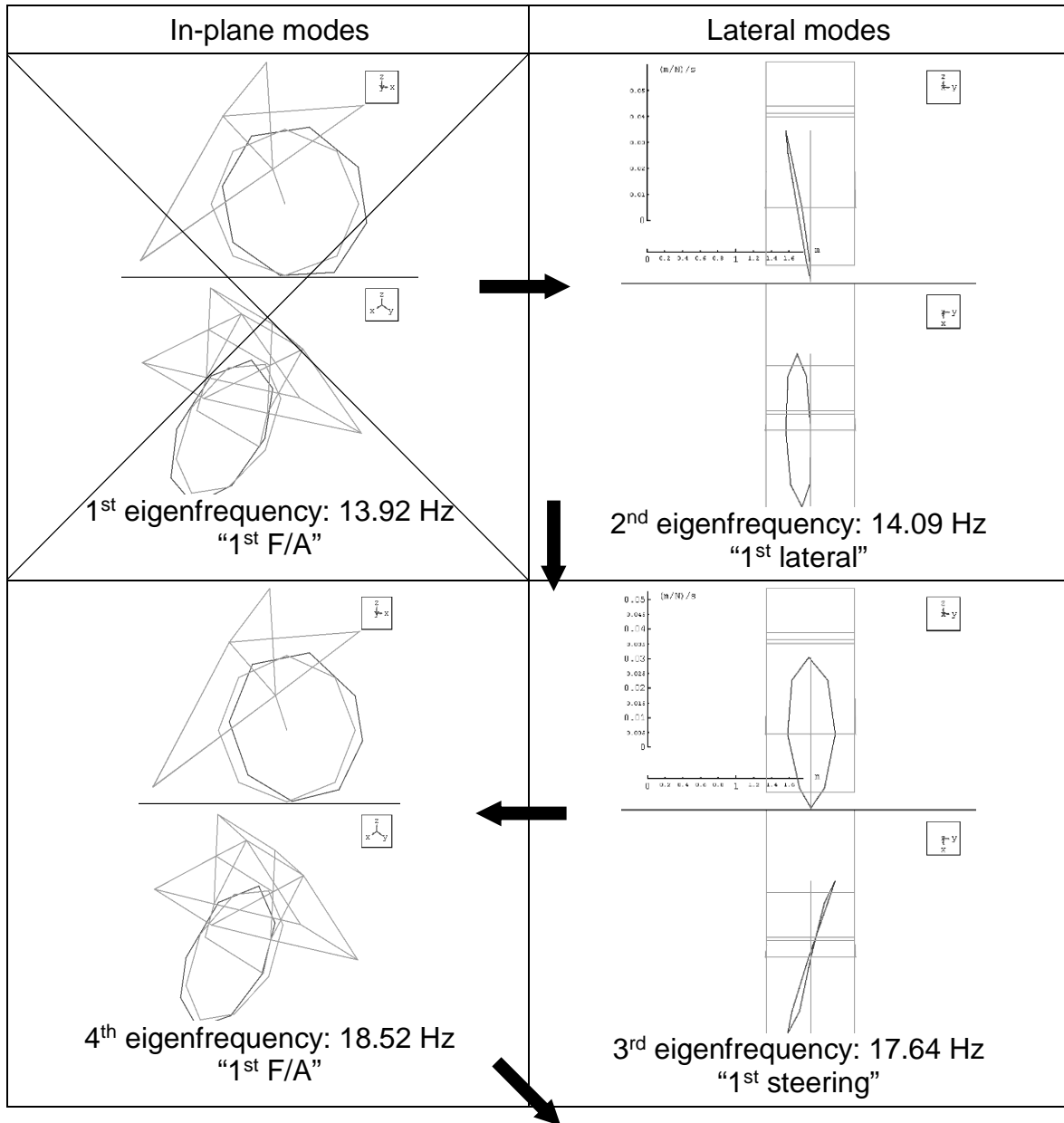
As already mentioned before the modal damping values scatter over a much wider range than the frequencies. Nevertheless, for the flexible body modes a quite good correlation can be determined again whereas the rigid body modes show the above mentioned stronger deviation.

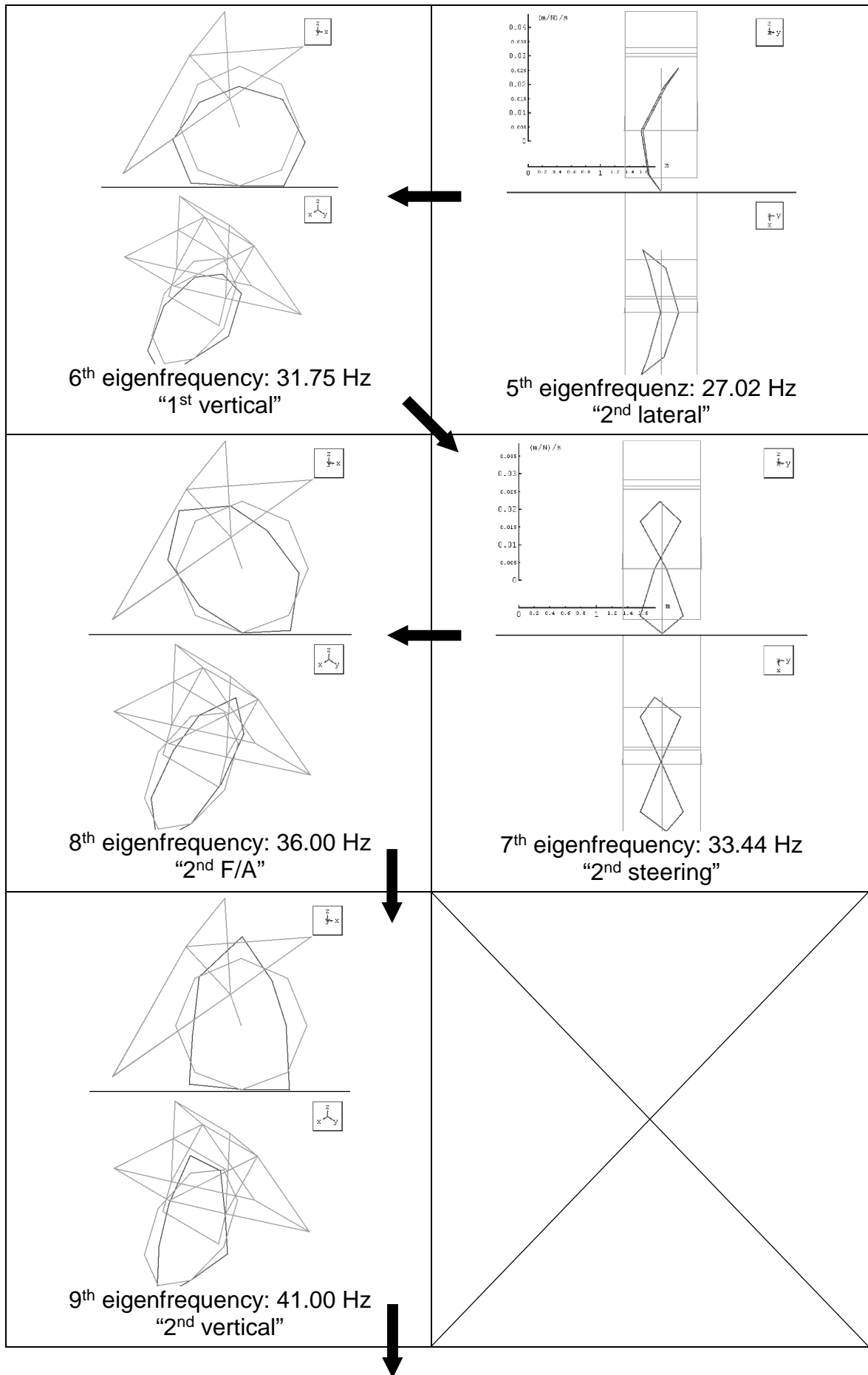
### 5.2.1.2 Loaded condition

For the loaded condition the rocker-wheel assembly with mounted shaker device and additional weight was positioned onto the flat belt so that the tire was ballasted with 20 kN. Table 38 shows the determined mode shape order with eigenfrequency divided into the two main directions (in-plane and lateral modes). It can be detected that the tire has two critical frequencies in the range about the rocker's mode No. 2a: at 13.92 Hz (1<sup>st</sup> F/A) and at 14.09 Hz (1<sup>st</sup> lateral). Thus, for the following shaker tests this frequency range has to be examined carefully whether this is the mode of the test rig alone or additionally a superposed excitation by the tire. The frequency and also the direction always have to match with a corresponding mode shape. Though the rig's modes No. 2b and 3 are near

the tire's 1<sup>st</sup> steering mode and between the 1<sup>st</sup> vertical and 2<sup>nd</sup> steering mode but differ on the direction of the mode shapes which makes a separation easier.

**Table 38** : Tire mode shapes of a loaded Goodyear Optitrac 520/70 R38 (Rear) mounted in the test rig ( $v = 0$  km/h,  $F_z = 20$  kN,  $p_i = 1.5$  bar)





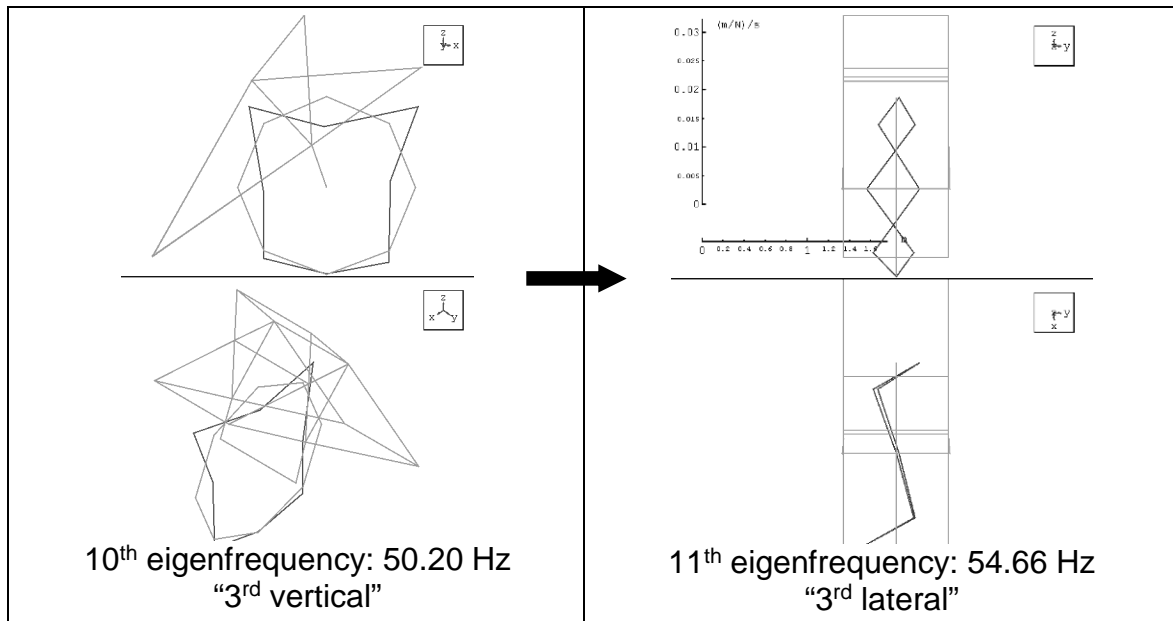
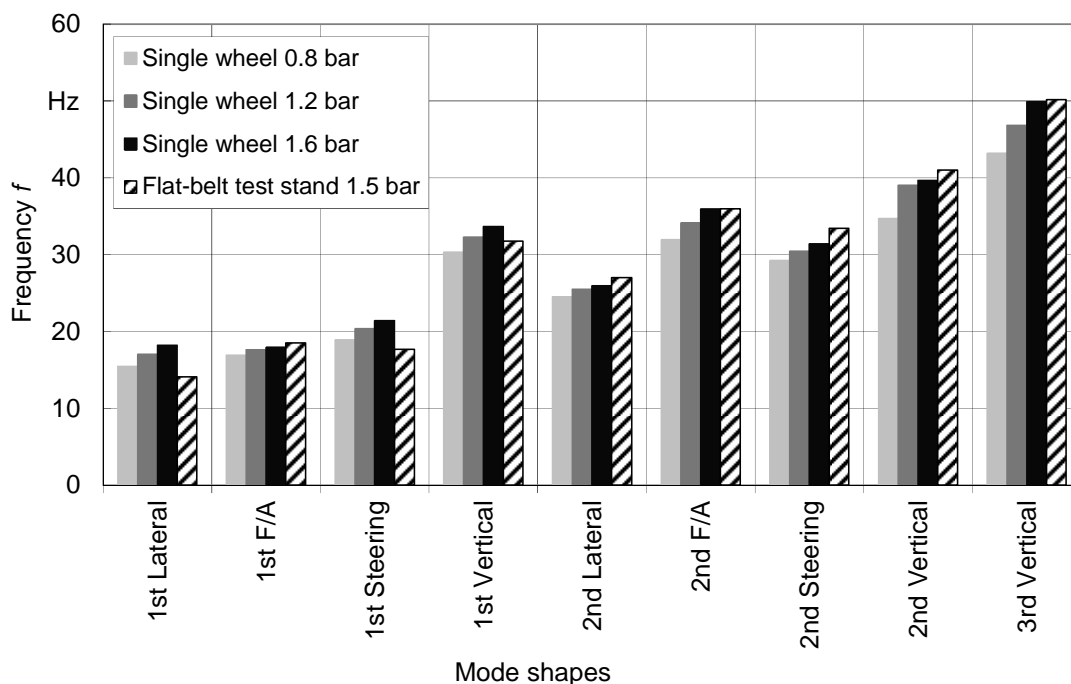


Figure 71 and Figure 72 show again the comparison with the modal analysis of the single wheel described in 5.1.2. Except for three of the rigid body modes all mode shapes of this test rig analysis show higher eigenfrequencies than those of the modal analysis of the single wheel. Considering the higher vertical load of 20 kN instead of 7.5 kN this is corresponding to the results of Wheeler et al. [96] who stated slightly increasing frequencies with growing load for all modes especially for the steering modes. The opposite characteristic of the rigid body modes in this case can again be explained with the different restraint conditions. Also the order of the modes sorted by frequency is corresponding closely to the results of Wheeler et al. [96].

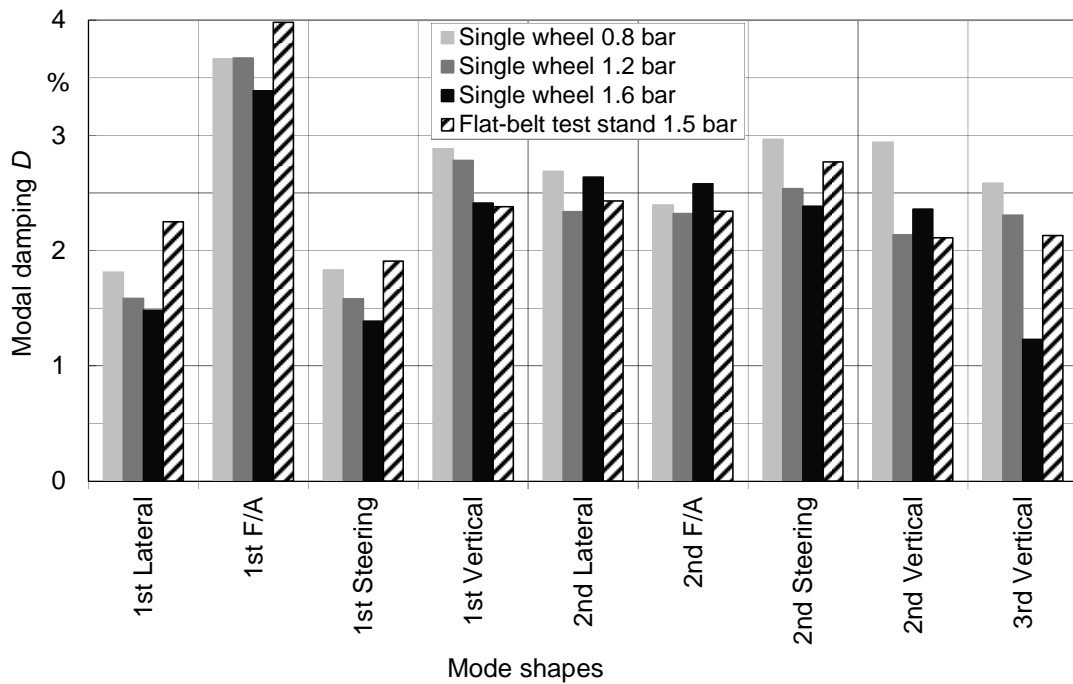




**Figure 71:** Mode shapes with eigenfrequencies of a loaded Goodyear Optitrac 520/70 R38 (Rear) mounted in the test rig ( $p_i = 1.5$  bar,  $F_z = 20$  kN) compared with results of modal analysis of the single wheel (5.1.2) ( $p_i = 0.8 / 1.2 / 1.6$  bar,  $F_z = 7.5$  kN)

Figure 72 shows the modal dampings of the determined tire mode shapes. Regarding the first three rigid body modes and the 2<sup>nd</sup> steering mode an increase of the damping compared to the single wheel can be found for the modal analysis on the test rig which can be explained with the larger contact zone in the tread pattern due to the higher vertical load. For the further modes the damping values are in line with the single wheel modal analysis considering the above mentioned broad distribution.

Shortly summarized it can be stated that the modal tire behaviour determined by modal analysis on the Hohenheim flat-belt tire test stand is comparable with the modal analysis of the single wheel (cf. chapter 5.1) if the different boundary conditions (vertical load and restraint conditions of the spindle) are considered. For more detailed investigations on the restraint conditions of the spindle the single wheel analysis is recommended whereas for a variation of the patch restraint conditions and of the wheel load the flat-belt test stand is preferable.



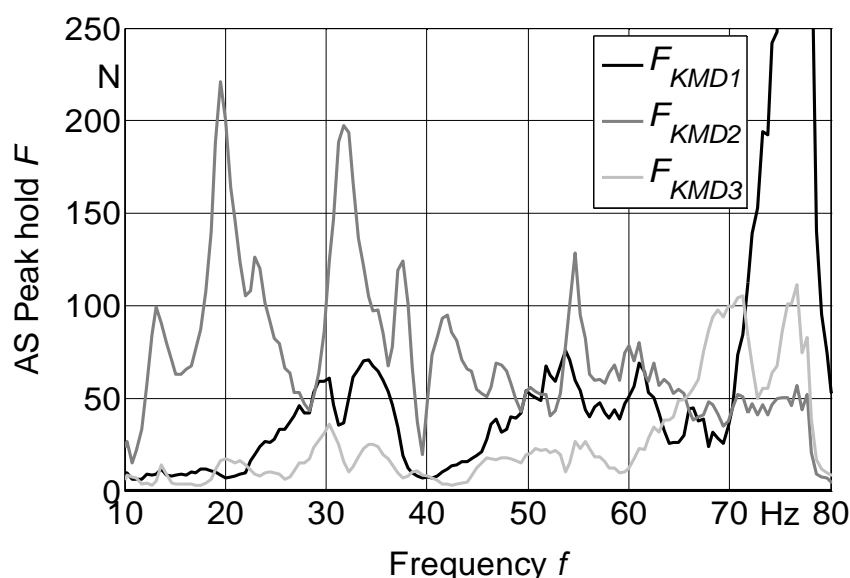
**Figure 72:** Mode shapes with modal dampings of a loaded Goodyear Optitrac 520/70 R38 (Rear) mounted in the test rig ( $p_i = 1.5$  bar,  $F_z = 20$  kN) compared with results of analysis of the single wheel (5.1.2) ( $p_i = 0.8 / 1.2 / 1.6$  bar,  $F_z = 7.5$  kN)

## 5.2.2 Shaker tests

In the next step the shaker tests were carried out on the flat-belt test stand for the loaded, but non-rolling tire so that the results of the modal analysis and the shaker tests become comparable.

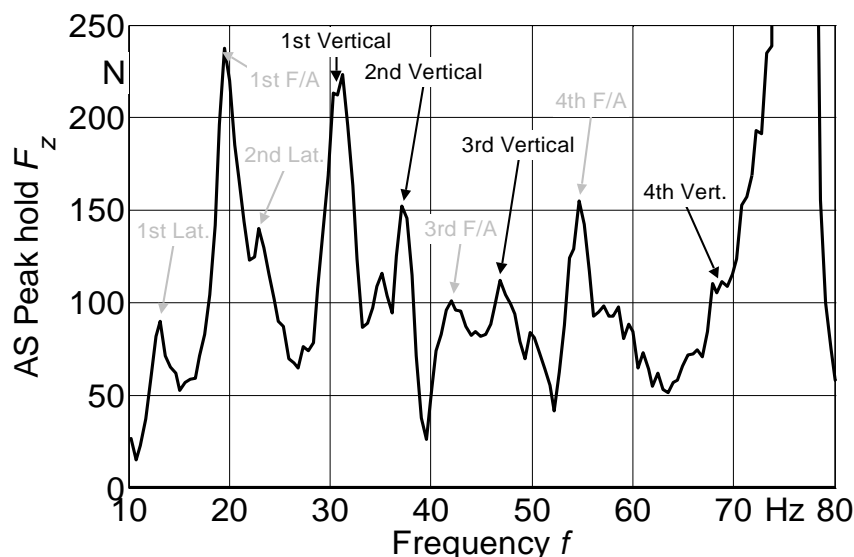
### 5.2.2.1 Non-rolling condition

With a view to the results of 5.1.4 all available signals were evaluated with respect to the information content of the tire vibration behaviour. Table 20 and Figure 27 show specification and location of all sensors installed on the flat-belt test stand. After the acceleration signals have been found to be hard to interpret the focus was set on the force signals especially on the three load cells. Figure 73 exemplifies the amplitude spectra of the three single load cell signals.



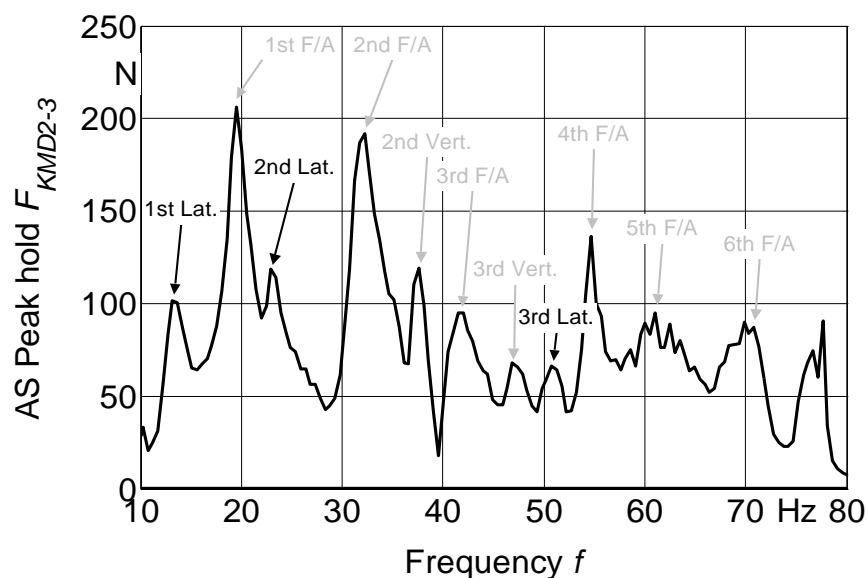
**Figure 73:** Amplitude spectrum peak hold (4.6.2) of the three single load cell signals for Goodyear Optitrac 520/70 R38 (Rear) ( $e_{sh} = 1.44$  mm,  $F_z = 14$  kN,  $p_i = 1.2$  bar,  $v = 0$  km/h,  $f_{sh} = 5$ -80 Hz); Rectangular window, block size 2048

For the further interpretation the three force channels are combined in such a way that the tire modes can be derived from the characteristic peaks of each signal. The sum of all three load cells (KMD total) is actually the tire load which peaks should indicate particularly the vertical tire modes (Figure 74).



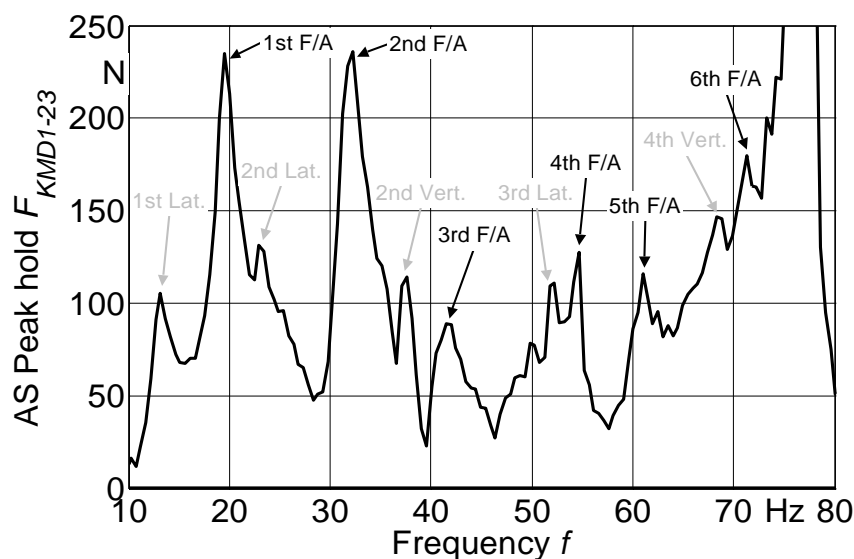
**Figure 74:** Amplitude spectrum peak hold of vertical load  $F_z$  (KMD total) for Goodyear Optitrac 520/70 R38 (Rear) ( $e_{Sh} = 1.44$  mm,  $F_z = 14$  kN,  $p_i = 1.2$  bar,  $v = 0$  km/h,  $f_{Sh} = 5$ -80 Hz); Rectangular window, block size 2048

The difference of load cell No. 2 and 3 (KMD 2-3) should amplify the effect of the lateral mode shapes (Figure 75).



**Figure 75:** Amplitude spectrum peak hold of differential force signal  $F_{KMD\ 2-3}$  for Goodyear Optitrac 520/70 R38 (Rear) ( $e_{Sh} = 1.44$  mm,  $F_z = 14$  kN,  $p_i = 1.2$  bar,  $v = 0$  km/h,  $f_{Sh} = 5$ -80 Hz); Rectangular window, block size 2048

The difference between load cell No. 1 and the sum of load cells No. 2 and 3 (KMD 1-23) should emphasize the F/A modes (Figure 76).

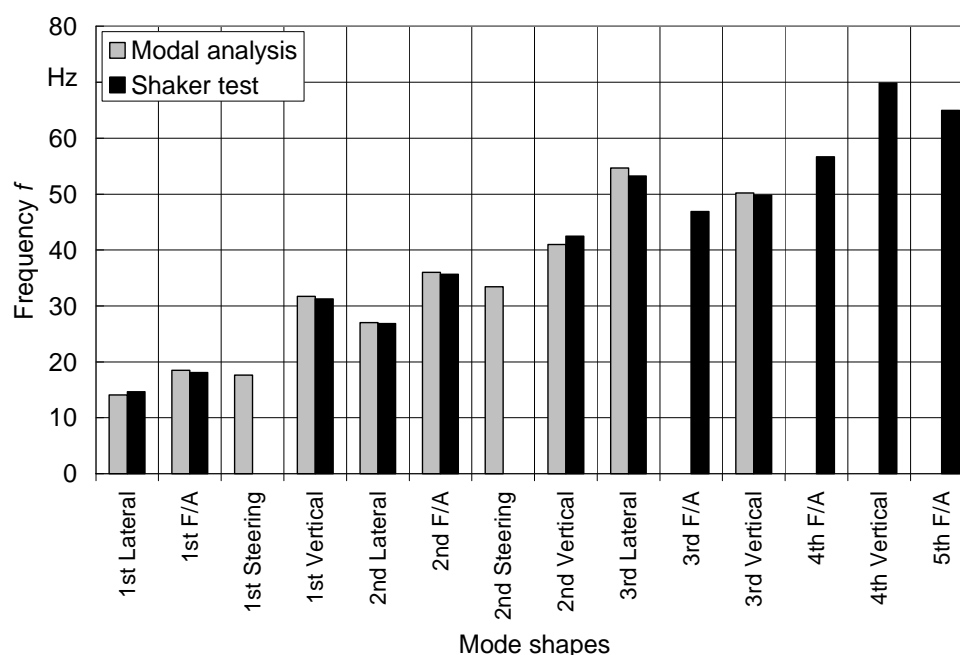


**Figure 76:** Amplitude spectrum peak hold of differential force signal  $F_{KMD\ 1-23}$  for Goodyear Optitrac 520/70 R38 (Rear) ( $e_{Sh} = 1.44$  mm,  $F_z = 14$  kN,  $p_i = 1.2$  bar,  $v = 0$  km/h,  $f_{Sh} = 5-80$  Hz); Rectangular window, block size 2048

As expected the signal of the vertical load  $F_z$  contains the most meaningful information on the vertical tire modes since in this case all three load cells are stressed in-phase due to the in-plane symmetry of the vertical mode shapes in the tread pattern leading to amplification. Consequently, the signal of  $F_{KMD\ 1-23}$  is expected to show especially the frequency peaks of the F/A modes as load cell No. 1 is placed longitudinally before the tire's contact point, but laterally in the middle of the tire plane. Due to their arrangement the two other single load cells additionally contain the information on the lateral modes. With the sum of these two signals and the difference to load cell No. 1 the F/A modes can be confirmed. The steering modes could not be detected clearly from the available signals. Since these modes either perform a rotation or a deformation about the vertical axis, the vibrating tire mass is not a translatory but a rotatory inertia. The resulting torques are supported by the rocker and cannot be recorded with the existing sensor equipment.

Generally, it can be concluded that for the rigid body modes and the first flexible vertical, F/A and lateral modes the eigenfrequencies can be identified more clearly than for the higher order modes. Regarding the formation of the mode shapes (Table 3) and considering the increasing number of knodes can explain this fact as well as the results of Böhm [69] and Wheeler et al. [96]. Concerning the force amplitudes of the non-rolling tire the 1<sup>st</sup> and 2<sup>nd</sup> Lateral, 1<sup>st</sup>, 2<sup>nd</sup>, 3<sup>rd</sup> and 4<sup>th</sup> F/A and 1<sup>st</sup>, 2<sup>nd</sup> and 3<sup>rd</sup> Vertical modes show the biggest impact.

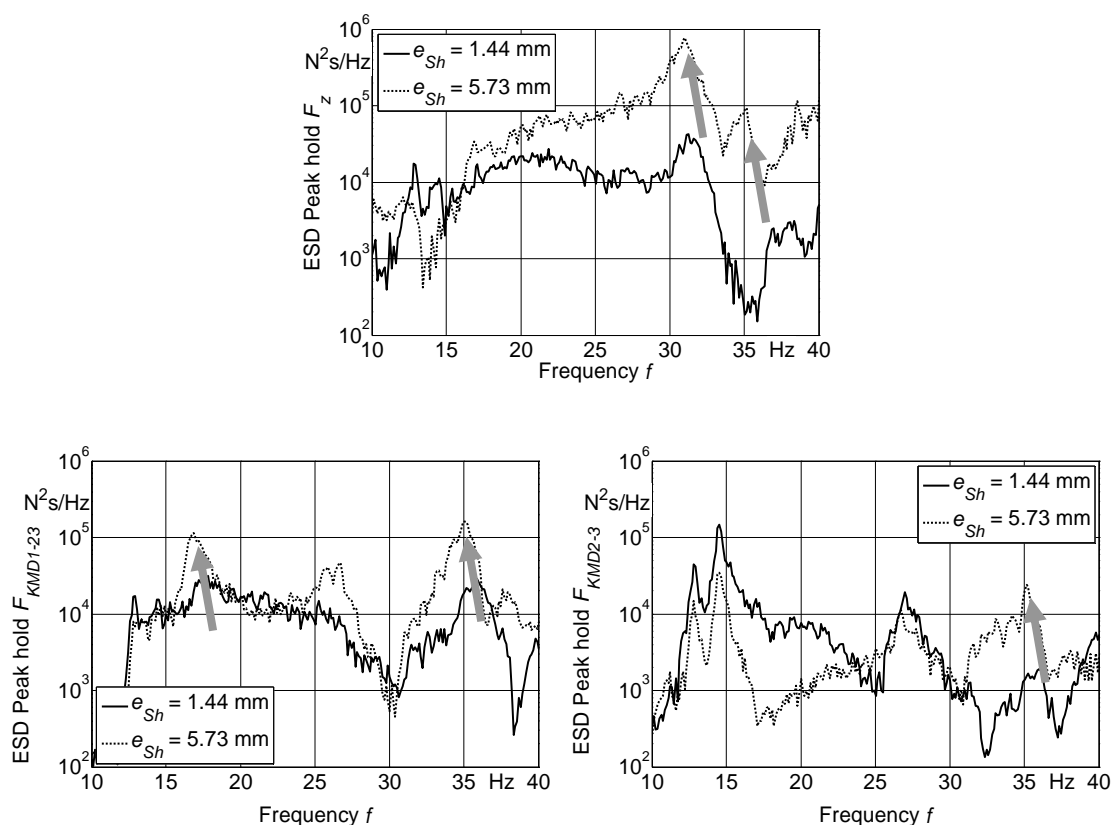
In Figure 77 and Table 46 the eigenfrequencies determined via modal analysis and via shaker excitation both performed on the flat belt test stand are compared. The results show a quite close agreement tending to slightly higher frequencies at the modal analysis. This effect can be explained by the lower excitation amplitude caused by the small impulse hammer for the modal analysis. On the following pages the influence of the shaker excitation amplitude is examined with similar results.



**Figure 77:** Mode shapes with eigenfrequencies of a loaded Goodyear Optitrac 520/70 R38 (Rear) mounted in the test rig determined from modal analysis ( $F_z = 20$  kN,  $p_i = 1.5$  bar,  $v = 0$  km/h) and shaker test ( $e_{Sh} = 1.44$  mm,  $F_z = 20$  kN,  $p_i = 1.5$  bar,  $v = 0$  km/h,  $f_{Sh} = 5$ -80 Hz)

## Shaker amplitude influence

After these first results of the shaker test have been reconfirmed by comparison with the modal analysis the influence of the further parameters mentioned in 3.3.5 is investigated. Already in the preliminary tests the influence of the shaker excitation amplitude was examined on the 520/70 R38 tire. As shown in 4.3.1 the excentricity of the shaker masses therefore can be adjusted.



**Figure 78:** Influence of the shaker amplitude  $e_{Sh}$  on the ESD peak hold of vertical load  $F_z$  (load cells total) and the two combined load cell signals for Goodyear Optitrac 520/70 R38 (Rear) ( $F_z = 20$  kN,  $p_i = 1.5$  bar,  $v = 0$  km/h,  $f_{Sh} = 5$ -40 Hz); Rectangular window, block size 8192

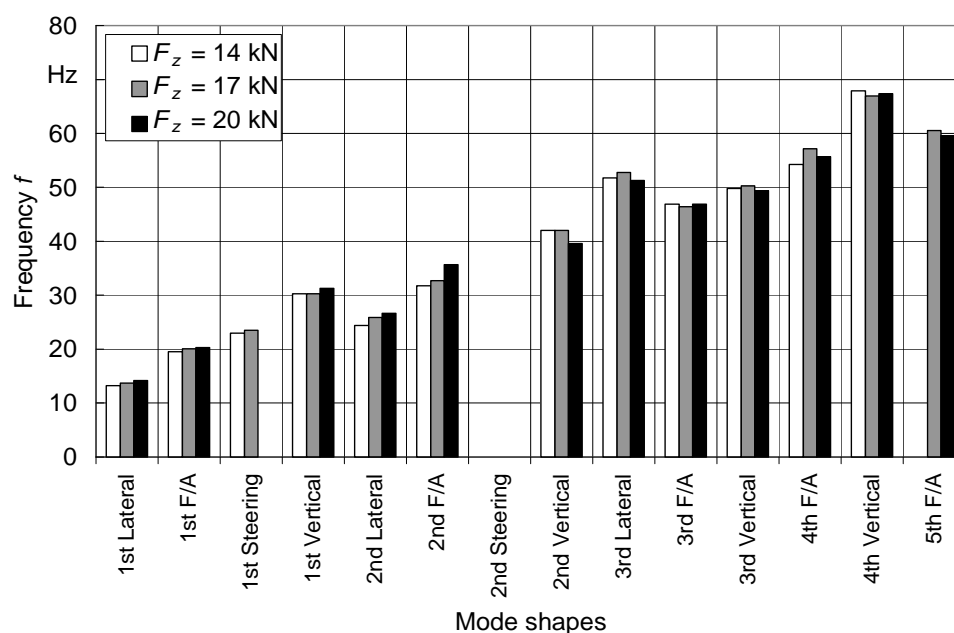
Figure 78 shows the difference between the highest and the lowest shaker excentricity by the energy spectral density (ESD) of the vertical force signals. The ESD was used for the identification due to the better frequency resolution which was already referred to in 4.6.2. Generally, all modes in the frequency range up to 40 Hz can be determined for both settings. But it becomes obvious that for the higher shaker amplitude there is a slight decrease of the higher modes'

eigenfrequencies which is in agreement e.g. with the results of Lion [99] and Kindt [79]. This effect can be explained with the strain softening of the elastomer at higher amplitudes.

In the following the effects of varying tire's operating conditions are examined. For the non-rolling tire these are tire load and inflation pressure.

### Tire load influence

Figure 79 shows the influence of the tire load for the selected rear tire regarding three different tire loads (14, 17 and 20 kN).

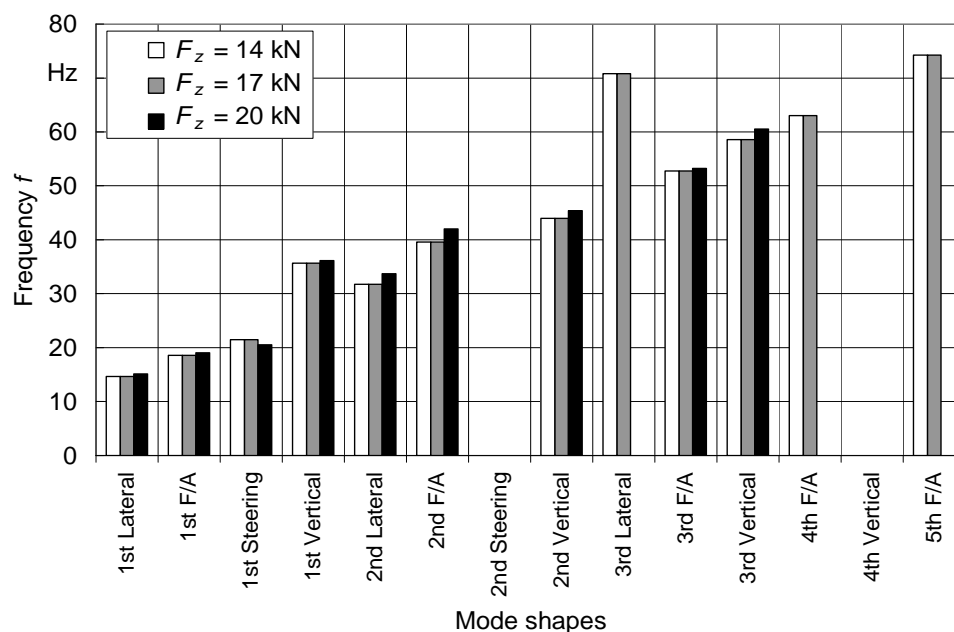


**Figure 79:** Influence of tire load  $F_z$  on the eigenfrequencies of Goodyear Optitrac 520/70 R38 (Rear) determined from shaker test ( $e_{Sh} = 1.44$  mm,  $p_i = 1.2$  bar,  $v = 0$  km/h,  $f_{Sh} = 5-80$  Hz) compared with modal analysis

In conformity with Scavuzzo et al. [91] there is no clear effect of the tire load regarding the higher order tire modes. Only for the lower order modes the results of Wheeler et al. [96] can partly be confirmed who stated slightly increasing frequencies with growing load for all modes especially for the steering modes. As mentioned above the steering modes could not be identified with this setup. An exception is the 1<sup>st</sup> steering mode which could at least be identified clearly at 14 and 17 kN tire load. From the lower order modes especially F/A and lateral modes show a frequency increase between 3% and 12% with growing tire load.



For the selected tractor front tire Figure 80 shows the effect of the tire load on the modal frequencies. Regarding the tractor specifications the selected front tire loads represent nearly the full application range.

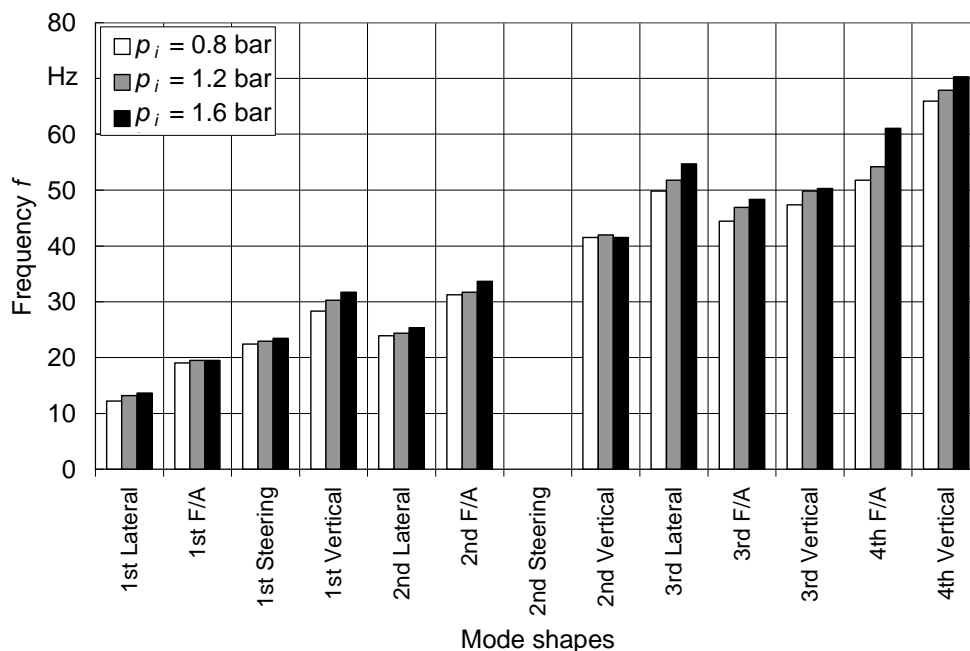


**Figure 80:** Influence of tire load  $F_z$  on the eigenfrequencies of Goodyear Optitrac 480/70 R24 (Front) determined from shaker test ( $e_{Sh} = 1.44$  mm,  $p_i = 1.2$  bar,  $v = 0$  km/h,  $f_{Sh} = 5$ -80 Hz)

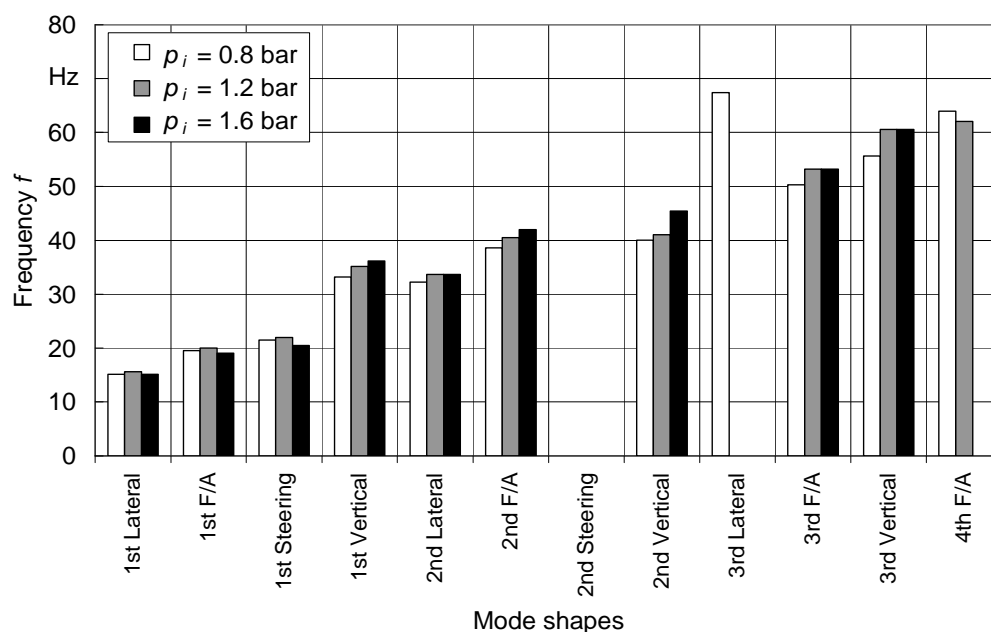
Unlike the bigger rear tire here the lower order modes do not show a consistent frequency increase due to growing tire loads either. The variation is below +/- 7%. Furthermore, several of the higher order mode frequencies could not be determined clearly. So for the front tire conformity with the results of Scavuzzo et al. [91] is only indicated.

### Inflation pressure influence

In a next step the influence of the inflation pressure was examined. The selected pressure values are best practice values according to the recommendations of the tire manufacturer. Figure 81 and Figure 82 show the eigenfrequencies at three different inflation pressures for the rear and the front tire.

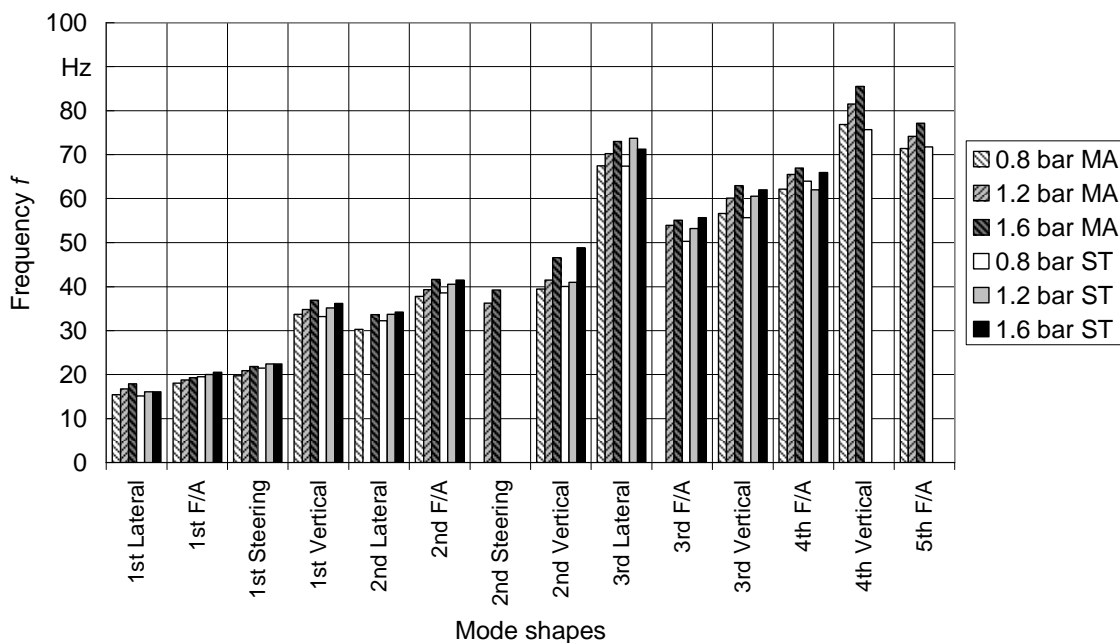


**Figure 81:** Influence of inflation pressure  $p_i$  on the eigenfrequencies of Goodyear Optitrac 520/70 R38 (Rear) determined from shaker test ( $e_{Sh} = 1.44$  mm,  $F_z = 14$  kN,  $v = 0$  km/h,  $f_{Sh} = 5-80$  Hz)



**Figure 82:** Influence of inflation pressure  $p_i$  on the eigenfrequencies of Goodyear Optitrac 480/70 R24 (Front) determined from shaker test ( $e_{Sh} = 1.44$  mm,  $F_z = 14$  kN,  $v = 0$  km/h,  $f_{Sh} = 5-80$  Hz)

Similar to the results of the modal analysis an increase of the eigenfrequency due to growing inflation pressure can be noticed. Regarding the amplitudes a general effect is that the amplitudes slightly grow with increasing inflation pressure.

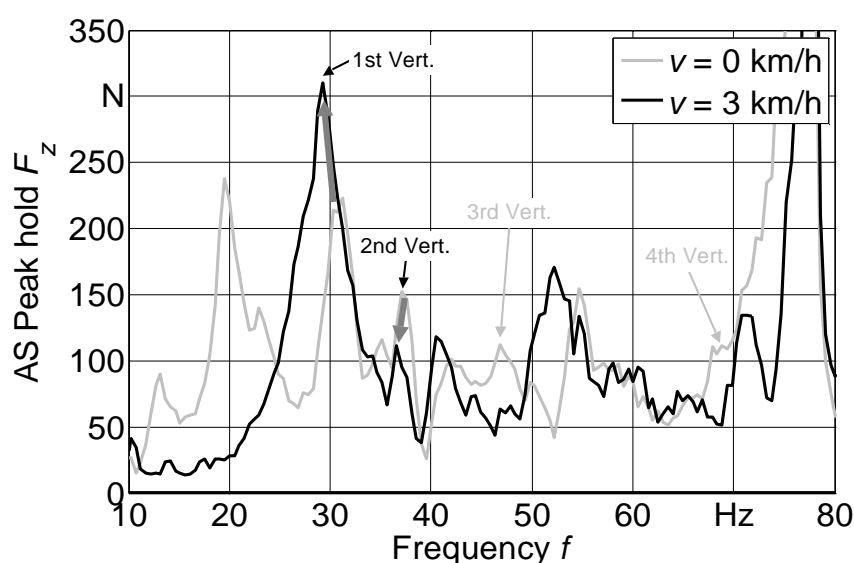


**Figure 83:** Mode shapes with eigenfrequencies of a loaded Goodyear Optitrac 480/70 R24 (Front) determined from modal analysis (MA) on single wheel ( $F_z = 6.0$  kN,  $v = 0$  km/h) and shaker test (ST) on flat-belt test stand ( $e_{Sh} = 1.44$  mm,  $F_z = 14$  kN,  $v = 0$  km/h,  $f_{Sh} = 5-80$  Hz)

Figure 83 shows the comparison of eigenfrequencies between modal analysis on the single wheel and shaker test for the front tire (480/70 R24). There is a tendency of slightly higher eigenfrequencies for the lower order modes of the shaker test. Considering the higher wheel load during the shaker test this corresponds to the above mentioned results.

### 5.2.2.2 Rolling condition

In a next step and as a major subject of the examinations described in this thesis the influence of rolling and rolling speed was analysed. The following three figures show the amplitude spectra of the three tread force signals as mentioned in the chapters above. At first, the vibration behaviour between the standing tire (0 km/h) and the slowly rolling tire (3 km/h) is compared. In the rolling condition the tire is not excited anymore only by the shaker, but also by itself. As mentioned in Table 15 at 3 km/h both radial runout and the first three lug frequencies are below the regarded range of 10 Hz.

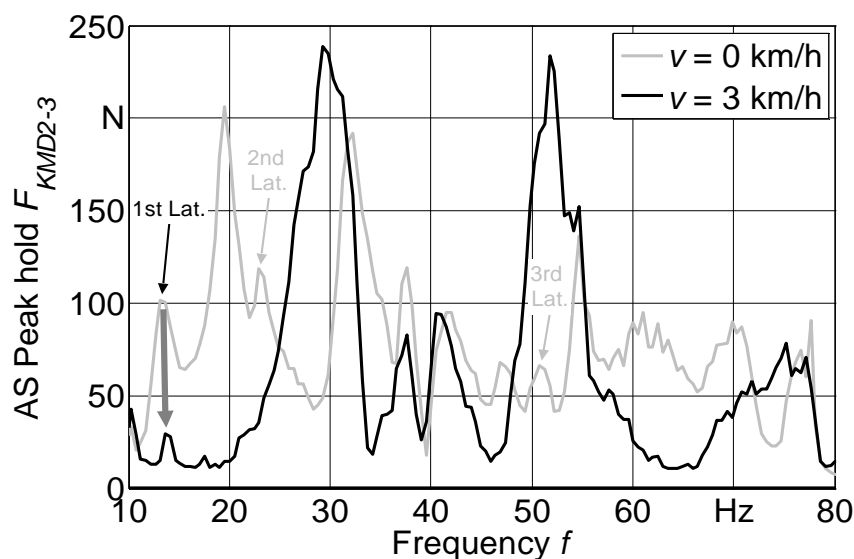


**Figure 84:** Amplitude spectrum peak hold of vertical load  $F_z$  (KMD total) for Goodyear Optitrac 520/70 R38 (Rear) at  $v=0$  and 3 km/h ( $e_{Sh} = 1.44$  mm,  $F_z = 14$  kN,  $p_i = 1.2$  bar,  $f_{Sh} = 5-80$  Hz); Rectangular window, block size 2048

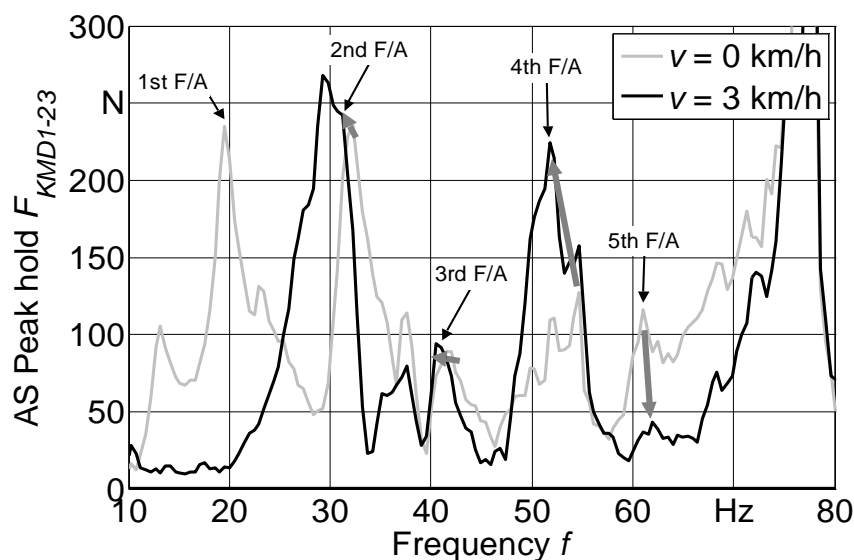
Regarding the vertical modes (Figure 84) it becomes obvious that with the onset of rolling the 1<sup>st</sup> Vertical mode frequency slightly decreases by 1-2 Hz affiliated with a strongly growing amplitude by 35%. For the 2<sup>nd</sup> Vertical mode the frequency also slightly decreases whereas the amplitude is reduced from 150 N to 110 N. For the 3<sup>rd</sup> and 4<sup>th</sup> Vertical modes no clear amplitude peaks could be identified at 3 km/h.

The lateral modes emphasized in Figure 85 show a very striking change due to the onset of rolling. The amplitude peaks of the 1<sup>st</sup> and 2<sup>nd</sup> Lateral modes nearly

completely disappear. In the frequency range between 12 and 21 Hz the amplitude range is on a very low level below 25 N. So the 1<sup>st</sup> F/A mode can neither be identified clearly anymore (Figure 86).



**Figure 85:** Amplitude spectrum peak hold of differential force signal  $F_{KMD\ 2-3}$  for Goodyear Optitrac 520/70 R38 (Rear) at  $v=0$  and 3 km/h ( $e_{Sh} = 1.44$  mm,  $F_z = 14$  kN,  $p_i = 1.2$  bar,  $f_{Sh} = 5-80$  Hz); Rectangular window, block size 2048

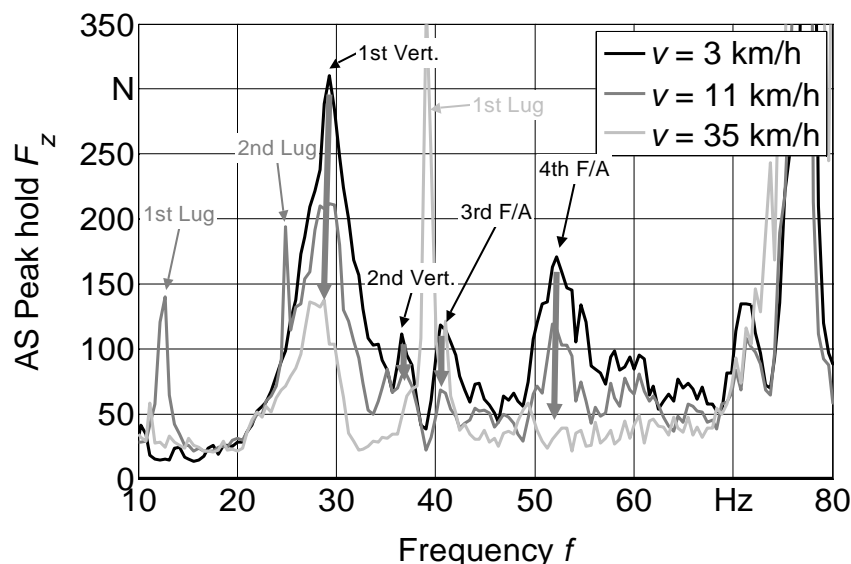


**Figure 86:** Amplitude spectrum peak hold of differential force signal  $F_{KMD\ 1-23}$  for Goodyear Optitrac 520/70 R38 (Rear) at  $v=0$  and 3 km/h ( $e_{Sh} = 1.44$  mm,  $F_z = 14$  kN,  $p_i = 1.2$  bar,  $f_{Sh} = 5-80$  Hz); Rectangular window, block size 2048

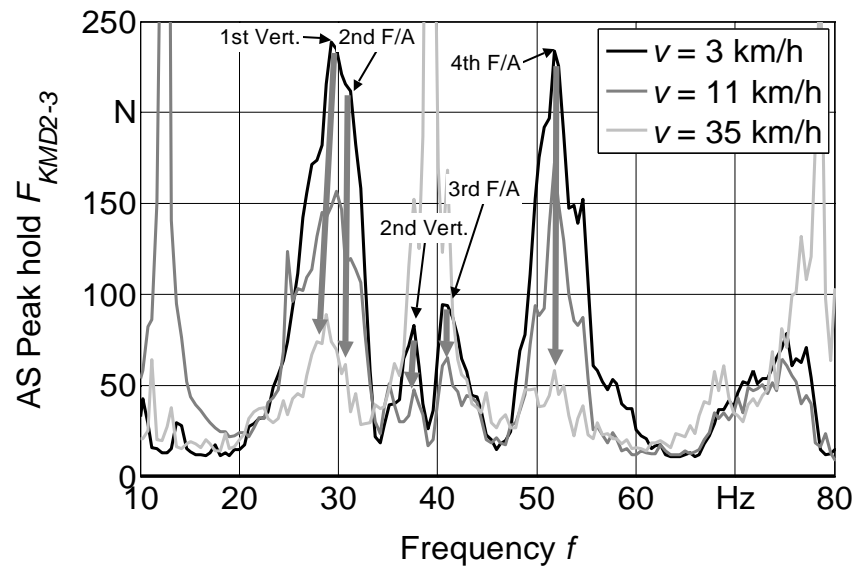
The 3<sup>rd</sup> Lateral mode disappears below the high amplitude of the adjacent 4<sup>th</sup> F/A mode. Regarding the 2<sup>nd</sup> and 3<sup>rd</sup> F/A modes a slight frequency decrease at nearly constant amplitude can be assessed. Besides the already mentioned 1<sup>st</sup> Vertical mode the 4<sup>th</sup> F/A mode shows a similar variation concerning the onset of rolling by a slight decrease of frequency and an even stronger increase of amplitude (+75%). In contrast the 5<sup>th</sup> F/A mode shows a slightly increasing frequency and a strongly decreasing amplitude.

### Speed influence

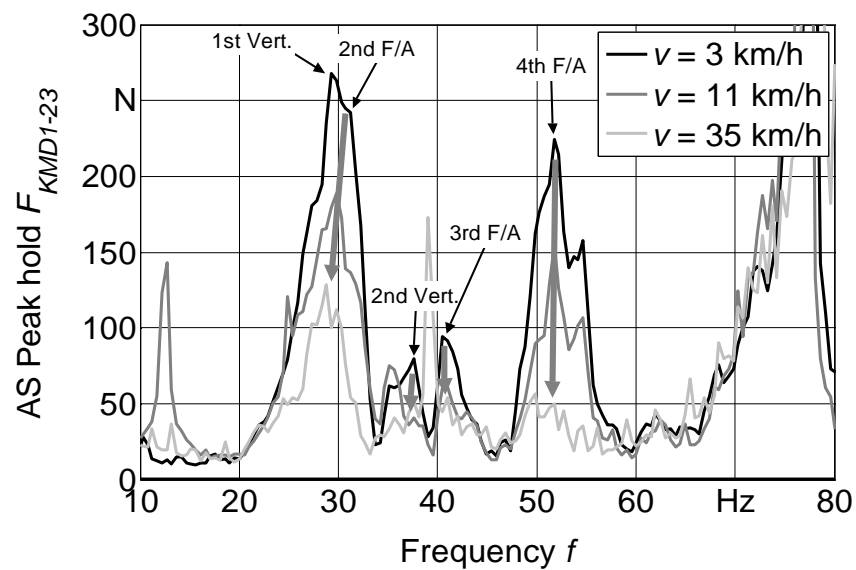
For higher speeds the lug excitation and its harmonics are inside the regarded frequency range. For an analysis of the speed influence two criteria had an influence on the selected speed steps. On the one hand the speeds should not be multiples of each other in order to detect and exclude peaks evoked by self-excitation. On the other hand at least the 1<sup>st</sup> and 2<sup>nd</sup> harmonics were tried to be placed in a frequency range where no or only single modes were located.



**Figure 87:** Amplitude spectrum peak hold of vertical load  $F_z$  (KMD total) for Goodyear Optitrac 520/70 R38 (Rear) at  $v = 3, 11$  and  $35$  km/h ( $e_{Sh} = 1.44$  mm,  $F_z = 14$  kN,  $p_i = 1.2$  bar,  $f_{Sh} = 5-80$  Hz); Rectangular window, block size 2048



**Figure 88:** Amplitude spectrum peak hold of differential force signal  $F_{KMD\ 2-3}$  for Goodyear Optitrac 520/70 R38 (Rear) at  $v = 3, 11$  and  $35$  km/h ( $e_{Sh} = 1.44$  mm,  $F_z = 14$  kN,  $p_i = 1.2$  bar,  $f_{Sh} = 5-80$  Hz); Rectangular window, block size 2048



**Figure 89:** Amplitude spectrum peak hold of differential force signal  $F_{KMD\ 1-23}$  for Goodyear Optitrac 520/70 R38 (Rear) at  $v = 3, 11$  and  $35$  km/h ( $e_{Sh} = 1.44$  mm,  $F_z = 14$  kN,  $p_i = 1.2$  bar,  $f_{Sh} = 5-80$  Hz); Rectangular window, block size 2048

Regarding all three diagrams it becomes obvious that the 1<sup>st</sup> Lateral, the Vertical and the F/A modes show noticeable amplitudes for the rolling tire. The eigenfrequencies for all of these tire modes show either a slight decrease or stay constant. Additionally, all amplitudes are decreasing clearly with increasing speed. For the 1<sup>st</sup> Lateral mode at 11 km/h the 1<sup>st</sup> lug frequency is matching the mode's eigenfrequency. This is leading to a strong exaggeration of the amplitude for the lateral dominated signal  $F_{2-3}$  (Figure 88). In the further frequency range up to 25 Hz the amplitude peaks are reduced so that they cannot even be identified as tire modes anymore. For the vibration transfer behaviour on the vehicle this effect can be looked upon favourably since unhealthy vibrations the driver is exposed to are reduced.



### **5.3 Investigations on the research tractor**

According to Scavuzzo et al. [91] the tire resonances can contribute to the vibrations felt by the driver. For tractor tires this relationship was investigated on a specially equipped tractor. The accelerations of seat and cabin are drawn on for evaluation. To improve ride comfort on tractors, cabin and seat suspension systems should be designed to isolate the axle vibrations from the driver.

Important for the further analysis and interpretation is the fact that the investigated set of tires on the tractor though was identical in construction and charge, but not one and the same. Due to inevitable tolerances this can lead to slight differences between eigenfrequencies and amplitudes of the investigated tire sets.

As a first step of the tractor test program the shaker tests have been carried out and analyzed. With this defined excitation in non-rolling condition the vibration behaviour of the tires on the tractor is compared with that on the flat-belt test rig. Secondly, uniformity and cleat tests are analysed. These tests are representative for the usual types of excitation: self-excitation and excitation by the drive way.

#### **5.3.1 Shaker tests**

The examination of the tire vibration behaviour and its effect on vehicle and driver is the main objective of this thesis. Since the driver on a standard tractor is sitting nearly exactly on top of the rear axle, further results are shown for the rear tire which is the direct transfer path to the driver including cabine and seat suspension.

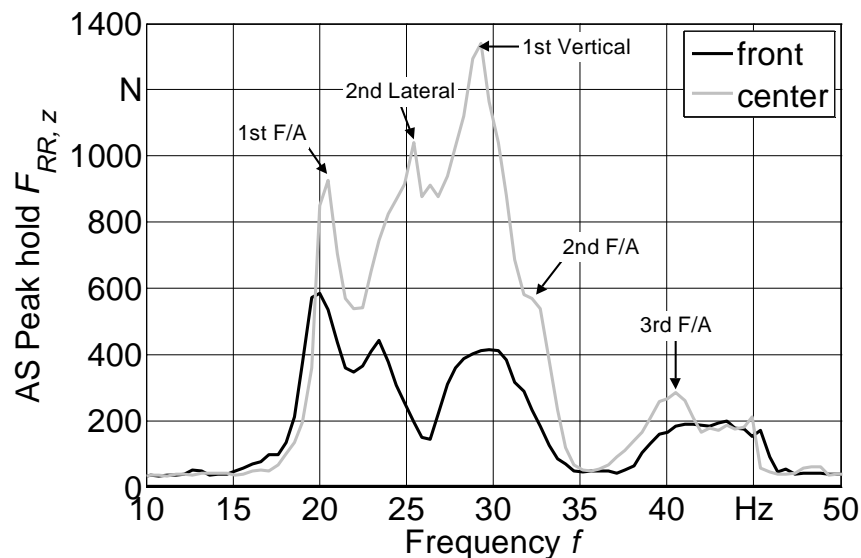
Furthermore, it has to be ascertained that above 55 Hz the acceleration and force signals obviously become unclean due to resonances of tractor subassemblies. For this reason in the following diagrams the frequency range between 10 and 50 Hz is regarded.

### 5.3.1.1 Non-rolling condition

As a first parameter the shaker position was checked. As explained in 4.5.3 the two positions “front” and “center” can be realized.

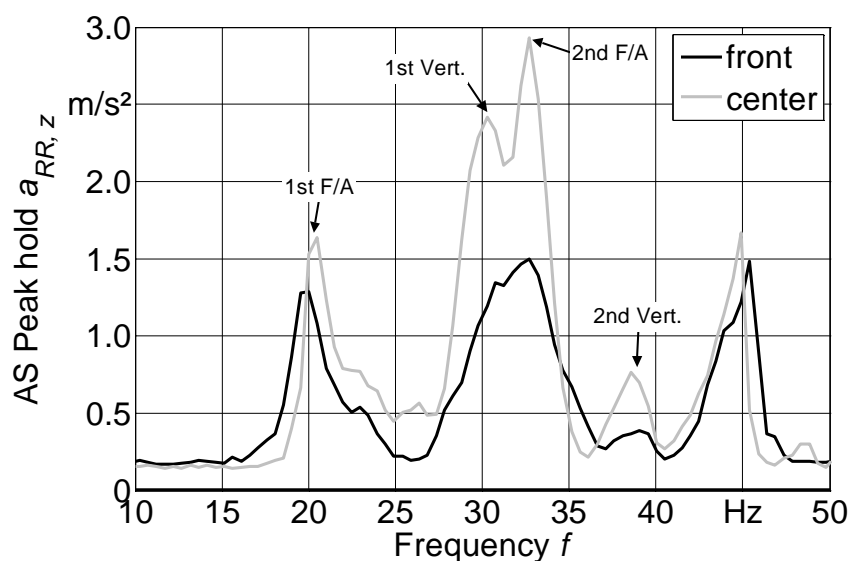
#### Shaker position influence

Due to the position and the direction of excitation the effect on the front axle is expected to be higher than for the rear axle. Ideally, in the front position when the shaker is exactly above the front axle the excitation of the rear axle should be reduced demonstrably. This effect was generally proven by the results of first shaker tests on the tractor concerning the shaker position exemplified by the vertical (z-) force and acceleration of the right rear wheel in Figure 90 and Figure 91.



**Figure 90:** Amplitude spectrum peak hold of the right rear wheel's vertical force signal  $F_{RR,z}$  for shaker positions front and center (Goodyear Optitrac 520/70 R38,  $e_{Sh} = 5.73$  mm,  $F_z = 17.2/17.6$  kN,  $p_i = 1.2$  bar,  $v = 0$  km/h,  $f_{Sh} = 3-48$  Hz); Rectangular window, block size 512

Further two interesting effects need to be mentioned in this context. On the one hand the “strong” modes with high amplitude like 1<sup>st</sup> F/A or 1<sup>st</sup> Vertical are obviously also excited by small excitation amplitudes (position “front”) even though on a corresponding lower level. On the other hand the sharpness of the amplitude peaks decreases. Some peaks even disappear completely and thus cannot be identified as a tire mode anymore (2<sup>nd</sup> and 3<sup>rd</sup> F/A in force signal).



**Figure 91:** Amplitude spectrum peak hold of the right rear wheel's vertical acceleration signal  $a_{RR,z}$  for shaker positions front and center (Goodyear Optitrac 520/70 R38,  $e_{Sh} = 5.73$  mm,  $F_z = 17.2/17.6$  kN,  $p_i = 1.2$  bar,  $v = 0$  km/h,  $f_{Sh} = 3-48$  Hz); Rectangular window, block size 512

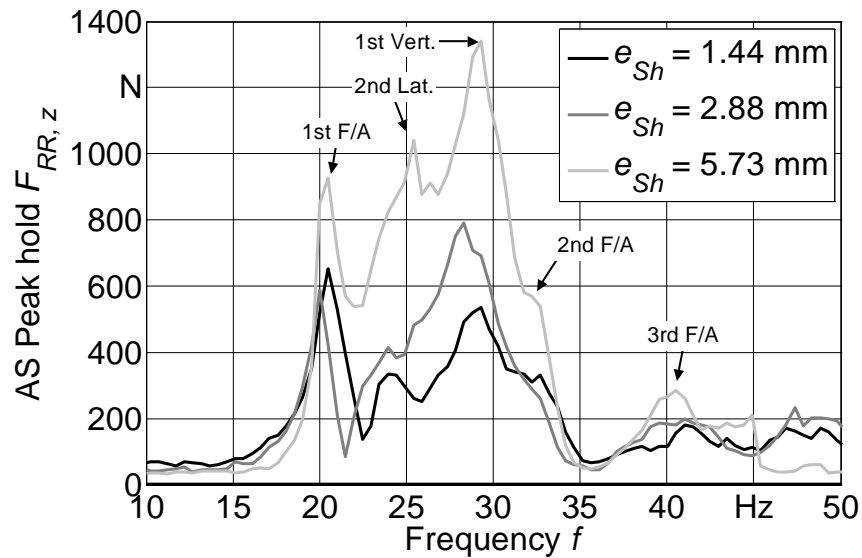
Since the shaker's center position is obviously leading to clearer results for the identification of the rear tire modes, all further examinations on the tractor have been carried out with this setting in the following.

### Shaker amplitude influence

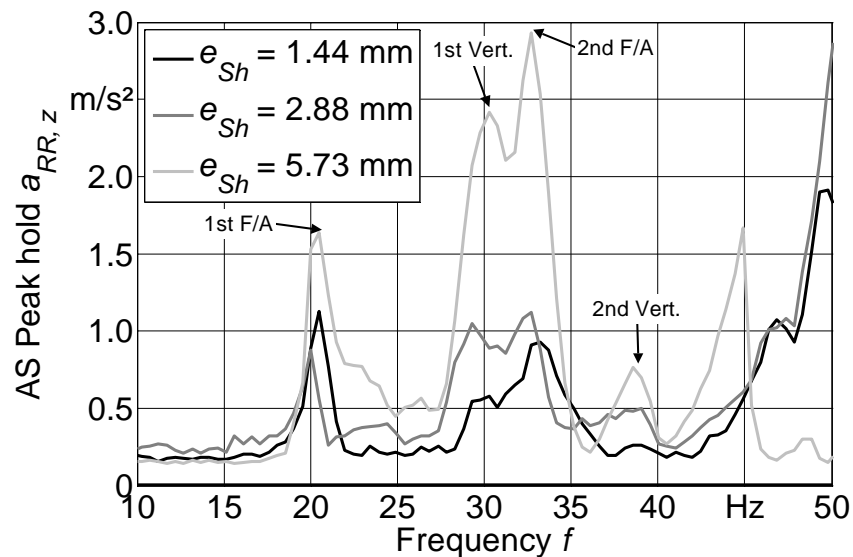
Similar to the excitation amplitude examinations on the flat-belt test stand the three pre-defined shaker amplitude settings were tested on the tractor again. All three settings can cover now the regarded frequency range up to 48 Hz.

Regarding force (Figure 92) and acceleration (Figure 93) of the right rear wheel for the vertical (z-) direction the 1<sup>st</sup> F/A and 1<sup>st</sup> Vertical modes can be identified clearly by both signals. The 2<sup>nd</sup> Lateral mode can be ascertained for the force, but not for the acceleration signal. Contrary to this the 2<sup>nd</sup> F/A mode shows a lower and less sharp peak for the force signal, but the maximum amplitude for the acceleration. Only in the acceleration signal the 2<sup>nd</sup> Vertical mode appears at the maximum shaker amplitude and nearly disappears when decreasing it. The 3<sup>rd</sup> F/A, however, only appears in the force signal, also with strongly decreasing amplitude at lower

shaker amplitude. Generally, the amplitude increase due to the shaker excitation amplitude increase can be identified over the whole frequency range.

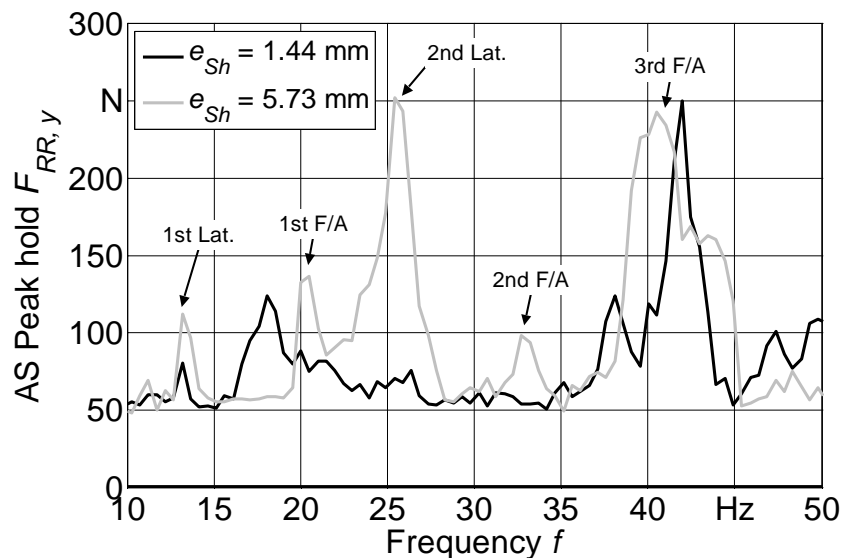


**Figure 92:** Amplitude spectrum peak hold of the right rear wheel's vertical force signal  $F_{RR,z}$  for different shaker amplitudes (Goodyear Optitrac 520/70 R38, shaker position center,  $F_z = 17.6$  kN,  $p_i = 1.2$  bar,  $v = 0$  km/h); Rectangular window, block size 512

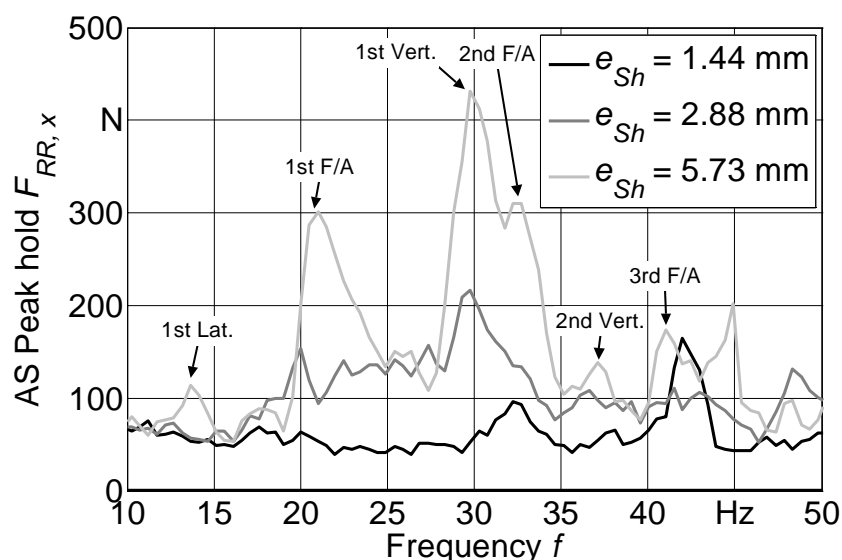


**Figure 93:** Amplitude spectrum peak hold of the right rear wheel's vertical acceleration signal  $a_{RR,z}$  for different shaker amplitudes (Goodyear Optitrac 520/70 R38, shaker position center,  $F_z = 17.6$  kN,  $p_i = 1.2$  bar,  $v = 0$  km/h); Rectangular window, block size 512

Figure 94 and Figure 95 show the amplitude spectra for the right rear wheel's lateral and longitudinal forces. As expected from the lateral force signal the 1<sup>st</sup> and 2<sup>nd</sup> Lateral modes can be identified clearly. But also 1<sup>st</sup>, 2<sup>nd</sup> and 3<sup>rd</sup> F/A mode frequencies can be determined at maximum shaker amplitude.



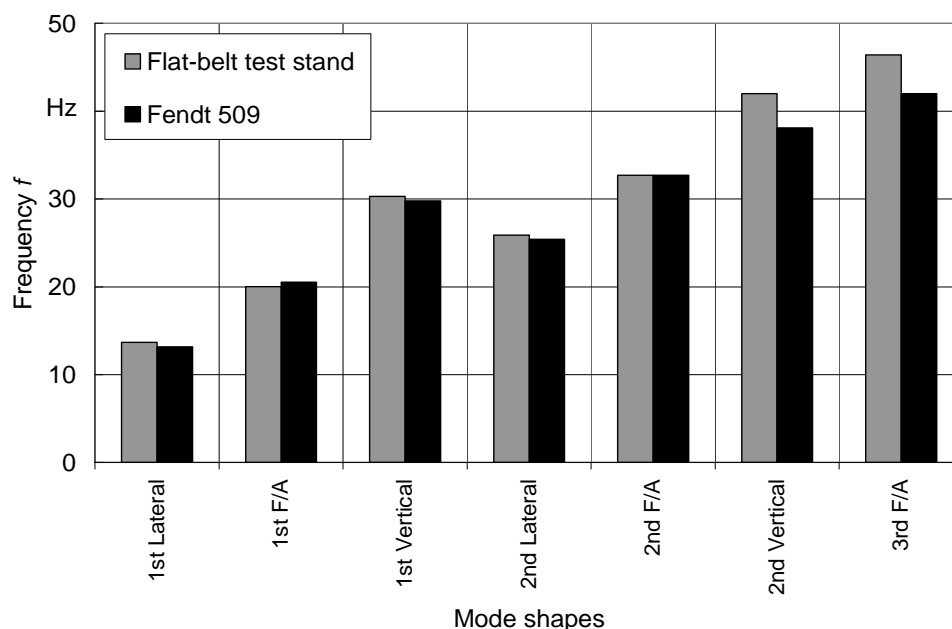
**Figure 94:** Amplitude spectrum peak hold of the right rear wheel's lateral force signal  $F_{RR,y}$  for different shaker amplitudes (Goodyear Optitrac 520/70 R38, shaker position center,  $F_z = 17.6$  kN,  $p_i = 1.2$  bar,  $v = 0$  km/h); Rectangular window, block size 512



**Figure 95:** Amplitude spectrum peak hold of the right rear wheel's longitudinal force signal  $F_{RR,x}$  for different shaker amplitudes (Goodyear Optitrac 520/70 R38, shaker position center,  $F_z = 17.6$  kN,  $p_i = 1.2$  bar,  $v = 0$  km/h); Rectangular window, block size 512

In the x- or longitudinal direction the first two F/A modes appear conspicuously besides the 1<sup>st</sup> Vertical mode. Again the best determination is possible at maximum shaker excitation amplitude.

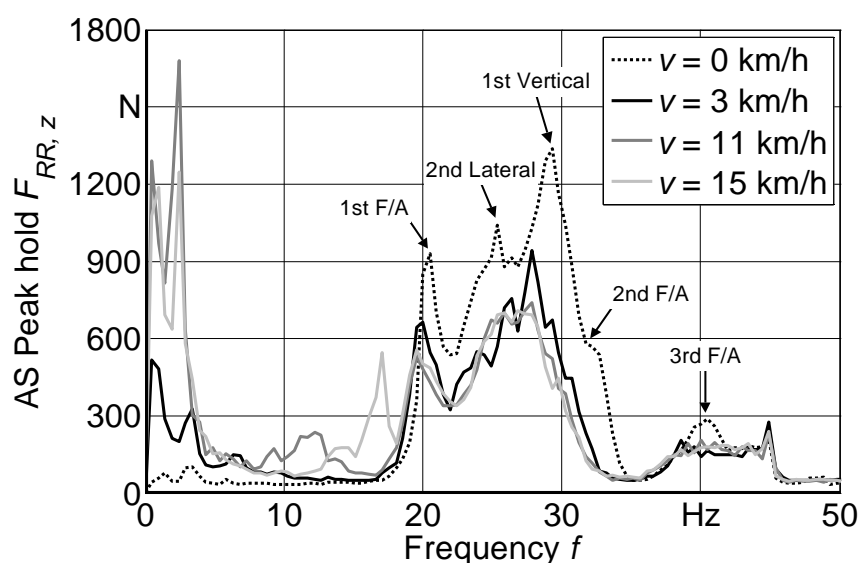
The comparison with the shaker test results on the flat-belt test stand is summarized in the following figure. Tire load, inflation pressure and speed certainly agree for both measurements. Regarding the mode shapes located within the 0 up to 50 Hz range due to the mentioned restrictions on the tractor a good agreement can be retained. Only the 2<sup>nd</sup> Vertical and 3<sup>rd</sup> F/A mode frequencies deviate from each other more than 1 Hz. Accordingly, the general ability of the tractor test setup could be proven for the above mentioned frequency range.



**Figure 96:** Mode shapes with eigenfrequencies of a loaded Goodyear Optitrac 520/70 R38 (Rear) from shaker tests on the flat-belt test stand and on the tractor ( $e_{Sh} = 1.44/5,73$  mm,  $F_z = 17,0/17,2$  kN,  $p_i = 1.2$  bar,  $v = 0$  km/h,  $f_{Sh} = 5-48$  Hz)

### 5.3.1.2 Rolling condition

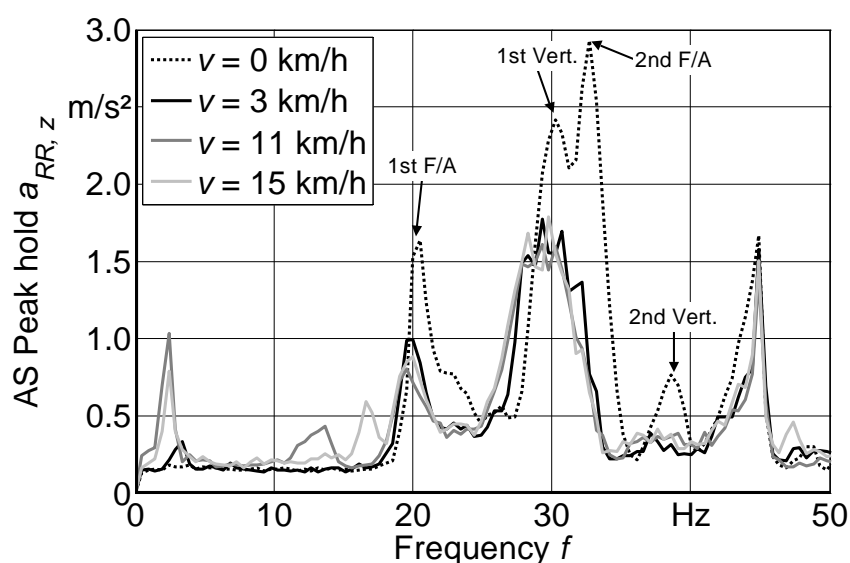
In the shaker tests with the non-rolling tire described above the frequency range below 10 Hz was not regarded since the shaker excitation energy is quite small in this range. As soon as the tire is rolling there are further sources of excitation by the lugs, the radial runout and the driveway where this low-frequency range is relevant for. This is why the following diagrams are expanded by the range between 0 and 10 Hz.



**Figure 97:** Amplitude spectrum peak hold of the right rear wheel's vertical force signal  $F_{RR,z}$  for different speeds (Goodyear Optitrac 520/70 R38, shaker position center,  $e_{Sh} = 5.73$  mm,  $F_z = 17.6$  kN,  $p_i = 1.2$  bar,  $f_{Sh} = 3-48$  Hz); Rectangular window, block size 512

Starting again with the vertical direction force (Figure 97) and acceleration (Figure 98) spectra show a similar shape. Exceptions are the 2<sup>nd</sup> Lateral and 2<sup>nd</sup> F/A modes. First regarding the 3 km/h an amplitude drop above 20 Hz can be recognized. Furthermore, the vehicle bouncing and pitching modes below 5 Hz are slightly excited by the 1<sup>st</sup> lug frequency at 3.3 Hz. The higher order frequencies obviously do not play a role, since the 0-km/h-curve and the 3-km/h-curve nearly equal each other up to 20 Hz. For 11 and 15 km/h the corresponding 1<sup>st</sup> order lug frequencies can be identified at 12.2 and 16.6 Hz. This means that for the selected speeds there is only little influence by the tire's self-excitation above 20 Hz. Since the driveway was a smooth road also the external excitation is neglectable.

Consequently, the curves above 20 Hz can be compared directly due to the same and only defined excitation by the shaker. In fact, all curves show the same shape and coincide quite well. Consequently, the onset of rolling shows the biggest impact on the variation of the mode's frequencies and amplitude peaks. For the 1<sup>st</sup> and 2<sup>nd</sup> F/A and Vertical modes frequencies are reduced by 1-2 Hz and amplitudes are decreasing by 35-50%. The 2<sup>nd</sup> Vertical and 3<sup>rd</sup> F/A mode peaks nearly completely disappear and are hard to determine for the rolling tire.

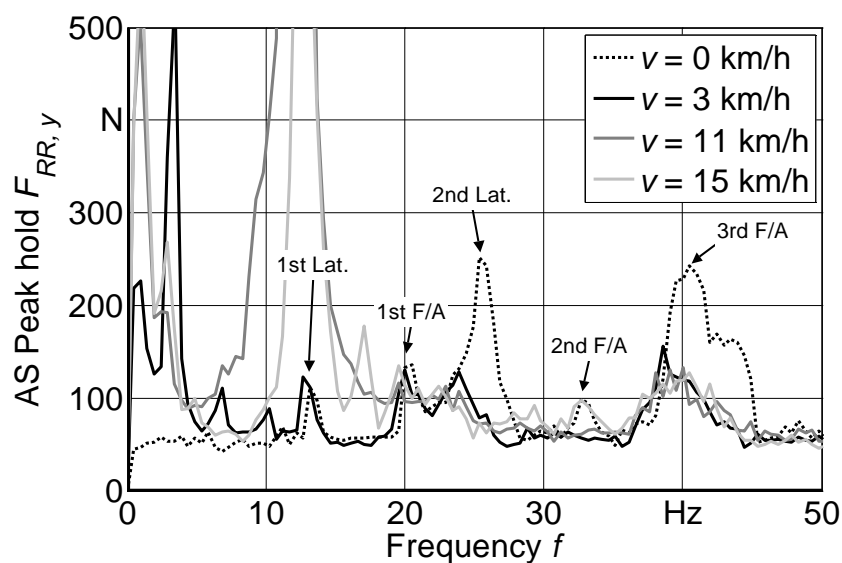


**Figure 98:** Amplitude spectrum peak hold of the right rear wheel's vertical acceleration signal  $a_{RR,z}$  for different speeds (Goodyear Optitrac 520/70 R38, shaker position center,  $e_{Sh} = 5.73$  mm,  $F_z = 17.6$  kN,  $\rho_i = 1.2$  bar,  $f_{Sh} = 3-48$  Hz); Rectangular window, block size 512

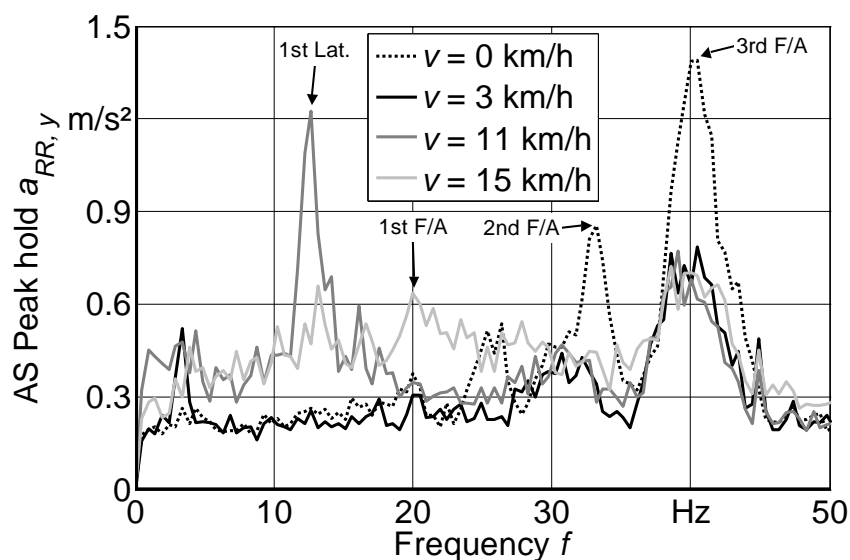
In lateral direction in both signals the 1<sup>st</sup> and 2<sup>nd</sup> Lateral modes can be ascertained as expected. Additionally, the 1<sup>st</sup>, 2<sup>nd</sup> and 3<sup>rd</sup> F/A become apparent. Regarding the curve for 3 km/h the same effects as mentioned above can be determined which are a slightly reduced frequency and a considerable decrease of amplitude. At 11 km/h the first order lug frequency of 12.2 Hz nearly exactly matches the 1<sup>st</sup> Lateral mode frequency. This is leading to an enormous increase of the force amplitude up to more than 2500 N (Figure 99) and still a considerable growth of the lateral acceleration amplitude up to more than 1.2 m/s<sup>2</sup> (Figure 100). At 15 km/h the force peak is reduced to 800 N and the acceleration peak is decreasing down to



0.65 m/s<sup>2</sup>. These results are demonstrating the general relevance of tire modes for the dynamic impact on the vehicle by tire self-excitation at certain speeds.

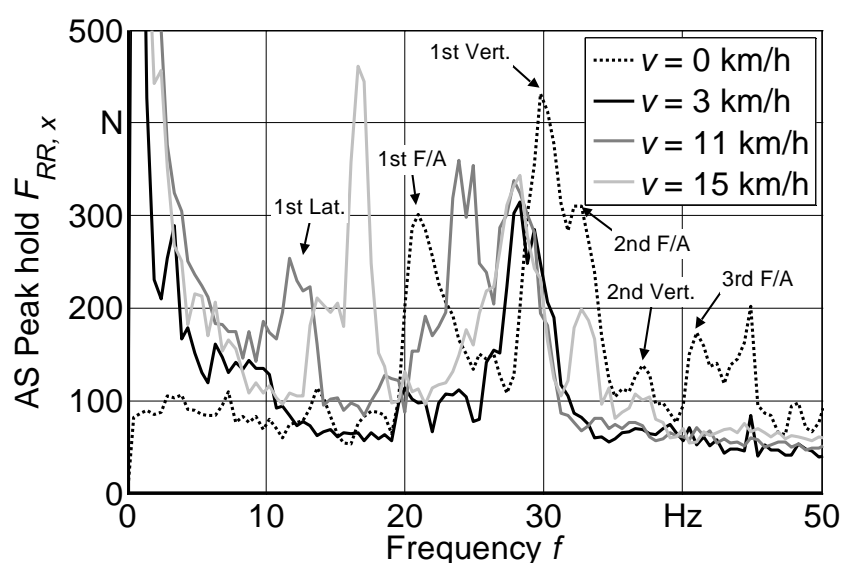


**Figure 99:** Amplitude spectrum peak hold of the right rear wheel's lateral force signal  $F_{RR,y}$  for different speeds (Goodyear Optitrac 520/70 R38, shaker position center,  $e_{Sh} = 5.73$  mm,  $F_z = 17.6$  kN,  $p_i = 1.2$  bar,  $f_{Sh} = 3-48$  Hz); Rectangular window, block size 512



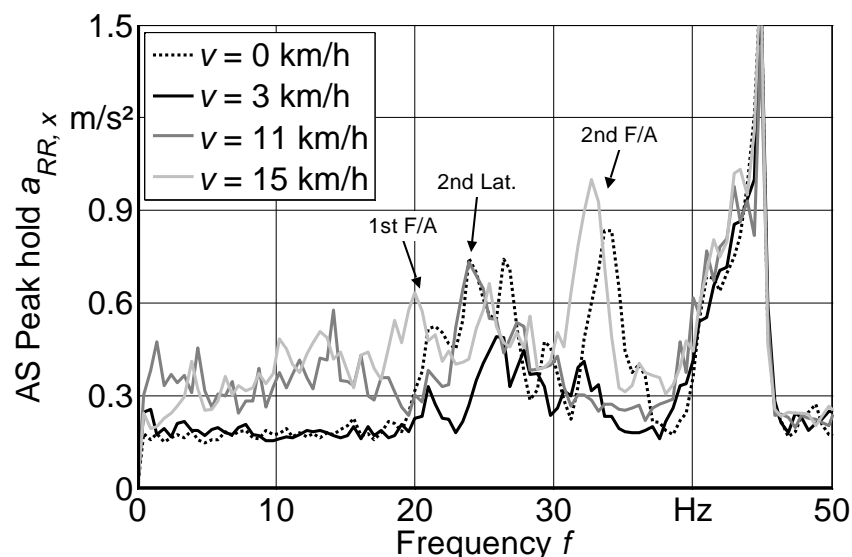
**Figure 100:** Amplitude spectrum peak hold of the right rear wheel's lateral acceleration signal  $a_{RR,y}$  for different speeds (Goodyear Optitrac 520/70 R38, shaker position center,  $e_{Sh} = 5.73$  mm,  $F_z = 17.6$  kN,  $p_i = 1.2$  bar,  $f_{Sh} = 3-48$  Hz); Rectangular window, block size 512

Regarding the longitudinal or driving direction of the vehicle the 1<sup>st</sup> and 2<sup>nd</sup> F/A mode can be identified precisely as expected. The 1<sup>st</sup> Vertical mode shows high amplitudes for the force signal, but for the acceleration signal these are neglectable. At 11 km/h the 1<sup>st</sup> and 2<sup>nd</sup> order lug frequencies fit the 1<sup>st</sup> and 2<sup>nd</sup> Lateral modes. Especially for the 2<sup>nd</sup> Lateral mode this leads to increasing amplitudes at around 24.5 Hz for both signals. At 15 km/h the impact caused by the 1<sup>st</sup> and 2<sup>nd</sup> order lug frequency (16.5 / 33 Hz) is even bigger. Especially the acceleration amplitude for 2<sup>nd</sup> F/A mode shows a considerable increase compared to the other speed settings.



**Figure 101:** Amplitude spectrum peak hold of the right rear wheel's longitudinal force signal  $F_{RR,x}$  for different speeds (Goodyear Optitrac 520/70 R38, shaker position center,  $e_{Sh} = 5.73$  mm,  $F_z = 17.6$  kN,  $p_i = 1.2$  bar,  $f_{Sh} = 3-48$  Hz); Rectangular window, block size 512

Generally noticeable for the x- and y-direction is that contrary to the z-direction the curves for 11 and 15 km/h are running on a higher level and less smooth than those for 3 km/h over the whole range. This effect can be explained by the increasing influence of road irregularities with growing speed. Even very small unevenness can cause big short-term impacts on the tire. An extreme case is a cleat which is investigated in 5.3.3.



**Figure 102:** Amplitude spectrum peak hold of the right rear wheel's longitudinal acceleration signal  $a_{RR,x}$  for different speeds (Goodyear Optitrac 520/70 R38, shaker position center,  $e_{Sh} = 5.73$  mm,  $F_z = 17.6$  kN,  $p_i = 1.2$  bar,  $f_{Sh} = 3-48$  Hz); Rectangular window, block size 512

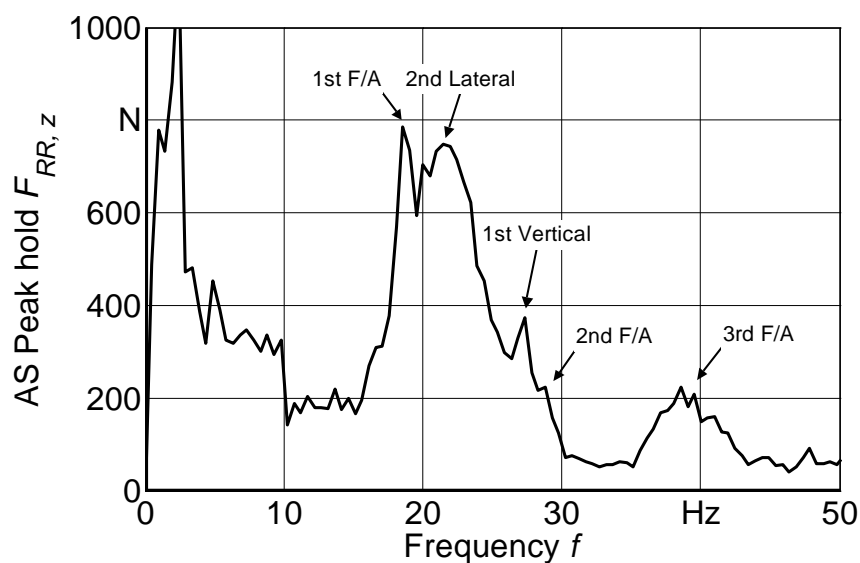
### 5.3.2 Uniformity tests

After vibration and mode behaviour of the rear tire on the tractor has been analysed by the shaker tests generating a simulated excitation, in the following the operating mode vibration behaviour is examined. As representative for real-life excitations the self-excitation by the tire over the complete speed range on a flat driveway was selected on the one hand (uniformity test). On the other hand with the cleat test a reproducible broadband excitation by the driveway can be realized ( $\rightarrow$  5.3.3).

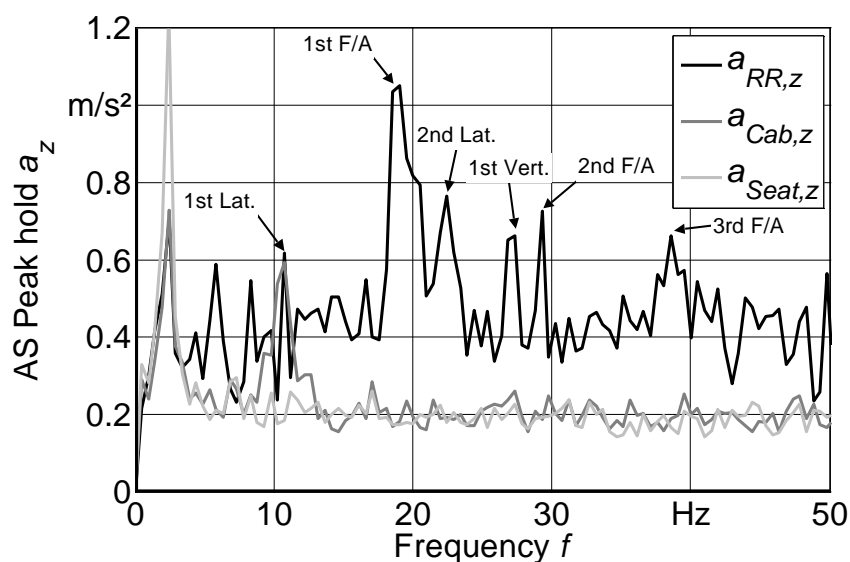
In the following for each direction the amplitude spectrum peak hold over the complete speed sweep (50 – 0 km/h) is displayed starting with the wheel force and followed by the acceleration signals. The additional accelerations of cabin and seat give an indication for the vibration stress of the driver.

Starting again with the vertical direction two dominating modes can be identified in the wheel force signal: the 1<sup>st</sup> F/A and 2<sup>nd</sup> Lateral mode (Figure 103). Compared to the vehicle bouncing mode at 2.4 Hz with an amplitude of nearly 1200 N the two tire modes show at least nearly 800 N. Whereas the tire's radial runout is relevant

for the excitation of the bouncing modes up to 1<sup>st</sup> Vertical and the 2<sup>nd</sup> and 3<sup>rd</sup> F/A mode show lower force amplitudes but can be ascertained yet.



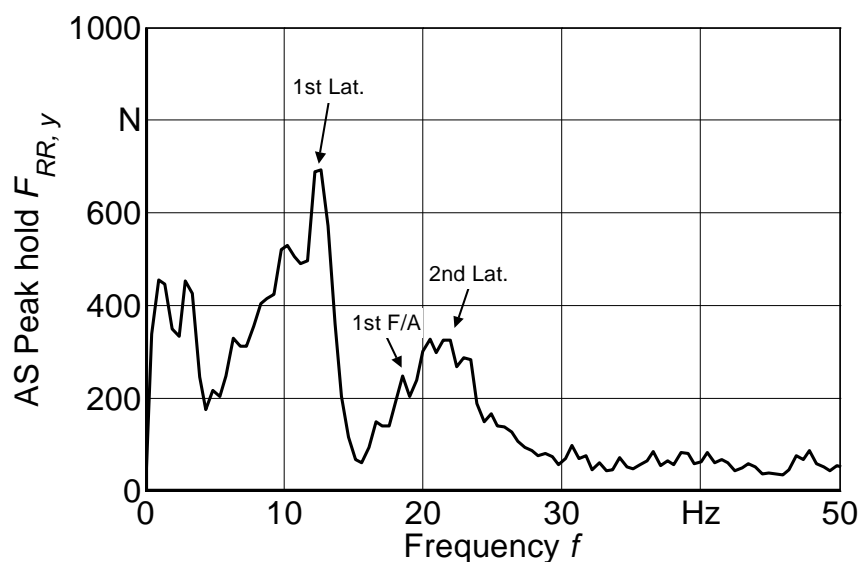
**Figure 103:** Amplitude spectrum peak hold of the right rear wheel's vertical force signal  $F_{RR,z}$  for a speed sweep (Goodyear Optitrac 520/70 R38,  $F_z = 17.6$  kN,  $p_i = 1.2$  bar,  $v = 50-0$  km/h); Rectangular window, block size 512



**Figure 104:** Amplitude spectrum peak hold of the vertical acceleration signals  $a_{RR,z}$ ,  $a_{Cab,z}$  and  $a_{Seat,z}$  for a speed sweep (Goodyear Optitrac 520/70 R38,  $F_z = 17.6$  kN,  $p_i = 1.2$  bar,  $v = 50-0$  km/h); Rectangular window, block size 512

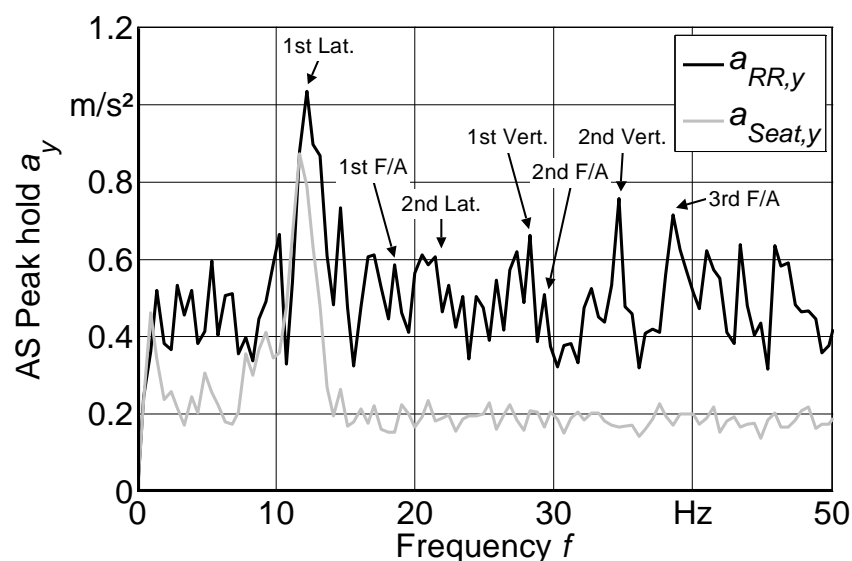
Regarding the effect on the wheel acceleration (Figure 104) the 1<sup>st</sup> F/A mode here also shows the highest amplitude (1.2 m/s<sup>2</sup>) and even exceeds that of the vehicle bouncing mode (0.7 m/s<sup>2</sup>). All further modes above 20 Hz show amplitudes around 0.7 m/s<sup>2</sup>. The base level is around 0.4 m/s<sup>2</sup>.

Two further effects need to be explained. At the 1<sup>st</sup> Lateral mode frequency the vertical cabin acceleration shows the same amplitude as the wheel suspension. So there is obviously no or only little isolation by the cabin suspension at this frequency which points to accordance with a cabin bouncing or pitching mode. At the vehicle bouncing mode frequency a strong exaggeration of the vertical seat acceleration amplitude can be determined. This also points to the seat eigenfrequency at exactly this frequency. Except these two characteristic peaks the cabin and seat suspension is obviously able to decrease the basic acceleration level down to approximately 0.2 m/s<sup>2</sup> for the complete frequency range up to 50 Hz. This is why the 1<sup>st</sup> F/A mode for the driver is imperceptible on this tractor just like also the other eigenfrequencies above 20 Hz.



**Figure 105:** Amplitude spectrum peak hold of the right rear wheel's lateral force signal  $F_{RR,y}$  for a speed sweep (Goodyear Optitrac 520/70 R38,  $F_z = 17.6$  kN,  $p_i = 1.2$  bar,  $v = 50-0$  km/h); Rectangular window, block size 512

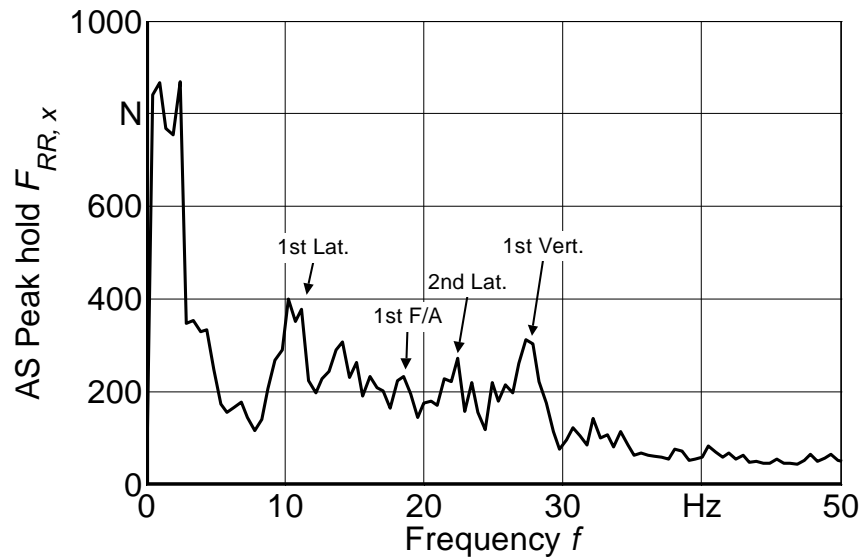
The lateral direction is strongly dominated by the 1<sup>st</sup> Lateral mode amplitude at 12.5 Hz. The force reaches 700 N at its maximum (Figure 105). The lateral acceleration even exceeds 1.0 m/s<sup>2</sup> (Figure 106) similar to the 1<sup>st</sup> F/A mode. The hardly smaller seat acceleration amplitude at this frequency reveals an even higher cabin amplitude corresponding to the results mentioned above for the z-direction. Furthermore, the 1<sup>st</sup> and 2<sup>nd</sup> Vertical and the 3<sup>rd</sup> F/A modes are showing a higher amplitude level around 0.7 m/s<sup>2</sup>, but only in the acceleration signal.



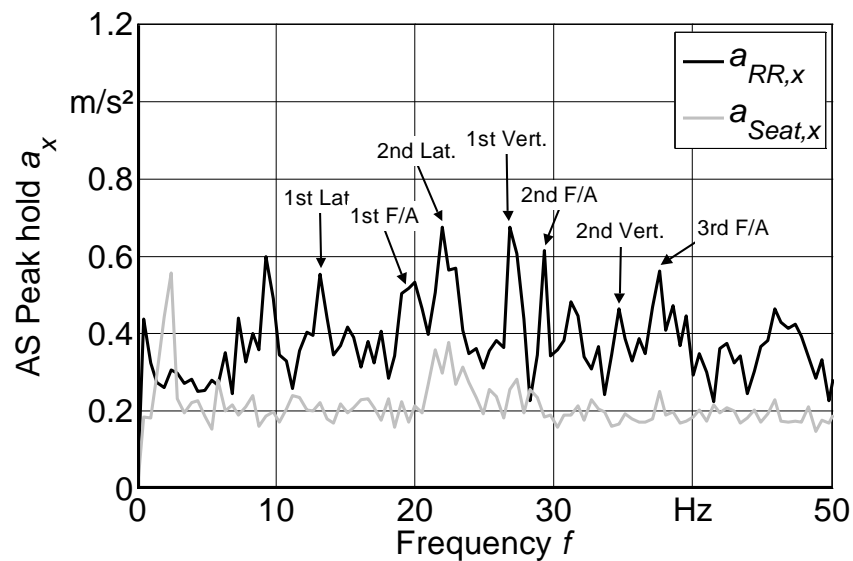
**Figure 106:** Amplitude spectrum peak hold of the lateral acceleration signals  $a_{RR,y}$  and  $a_{Seat,y}$  for a speed sweep (Goodyear Optitrac 520/70 R38,  $F_z = 17.6$  kN,  $p_i = 1.2$  bar,  $v = 50-0$  km/h); Rectangular window, block size 512

Regarding the longitudinal direction signals no really dominating frequency peaks can be determined (Figure 107). Concerning the force signal the maximum peaks stay below 400 N. The acceleration peaks are below 0.7 m/s<sup>2</sup>. 1<sup>st</sup> and 2<sup>nd</sup> Lateral and 1<sup>st</sup> Vertical mode show the most noticeable peaks (Figure 108).

Concerning the vibration transfer to the driver it can be observed that for the longitudinal direction the seat acceleration is increasing noticeable between 21 and 23 Hz which matches with the 2<sup>nd</sup> Lateral mode frequency.



**Figure 107:** Amplitude spectrum peak hold of the right rear wheel's longitudinal force signal  $F_{RR,x}$  for a speed sweep (Goodyear Optitrac 520/70 R38,  $F_z = 17.6$  kN,  $p_i = 1.2$  bar,  $v = 50-0$  km/h); Rectangular window, block size 512



**Figure 108:** Amplitude spectrum peak hold of the longitudinal acceleration signals  $a_{RR,x}$  and  $a_{Seat,x}$  for a speed sweep (Goodyear Optitrac 520/70 R38,  $F_z = 17.6$  kN,  $p_i = 1.2$  bar,  $v = 50-0$  km/h); Rectangular window, block size 512

### 5.3.3 Cleat tests

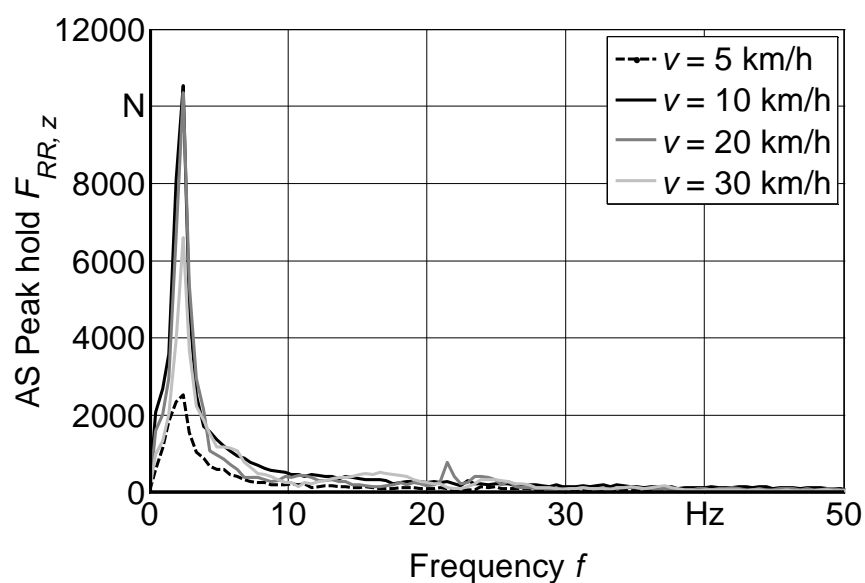
For the cleat test analysis the data files were triggered in order to analyse always the same manoeuvre. The trigger point was set at that moment when the rear wheel hits the cleat and the vertical wheel force measured by the hub starts growing very strongly. The end of the measurement is defined after the block size of 512 which corresponds to 2.048 s for the maximum possible sample rate of 250 Hz after the trigger event. This block size is the minimum size for a suitable resolution of the amplitude spectra. For high speed tests the end point is too far away from the “cleat event” which falsifies the analysis. This is the reason why 30 km/h were selected as maximum driving speed. Unfortunately, a higher sample rate was not possible with the preset measuring equipment.

Due to the coarse lug tire tread pattern the excitation by cleats is less reproducible than e.g. that of a fine passenger car tire profile. Consequently, the excitation spectrum is not that consistent over the regarded frequency range due to different speeds and cleat heights. This is why these two important parameters have been selected for the following cleat test analysis.

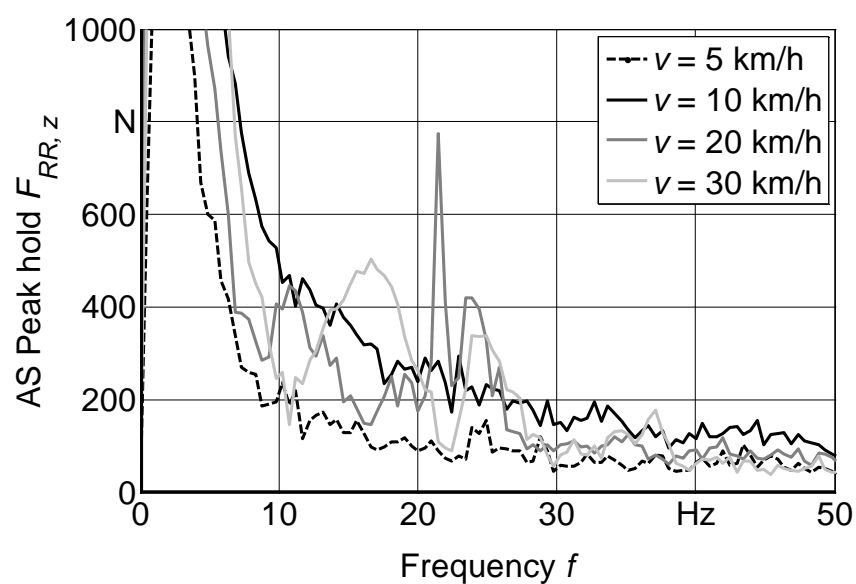
#### Speed influence

Regarding the speed influence the vertical wheel force signal exemplifies the choice which was made. The dominating peak of the vertical force amplitude spectrum is that of the vehicle bouncing mode frequency at 2.4 Hz (Figure 109). At 5 km/h it is reaching 2.5 kN, at 10 and 20 km/h 10.5 kN. At 30 km/h it is decreasing again down to 6.6 kN. Figure 110 enables a closer view on the peaks of the tire modes above 10 Hz which show much lower amplitudes. It can be observed that additional to the bouncing mode the already from the shaker and uniformity tests well-known tire modes also show their strongest occurrence also at 20 km/h. This is why 20 km/h was selected as default speed for the further investigation concerning the cleat height.





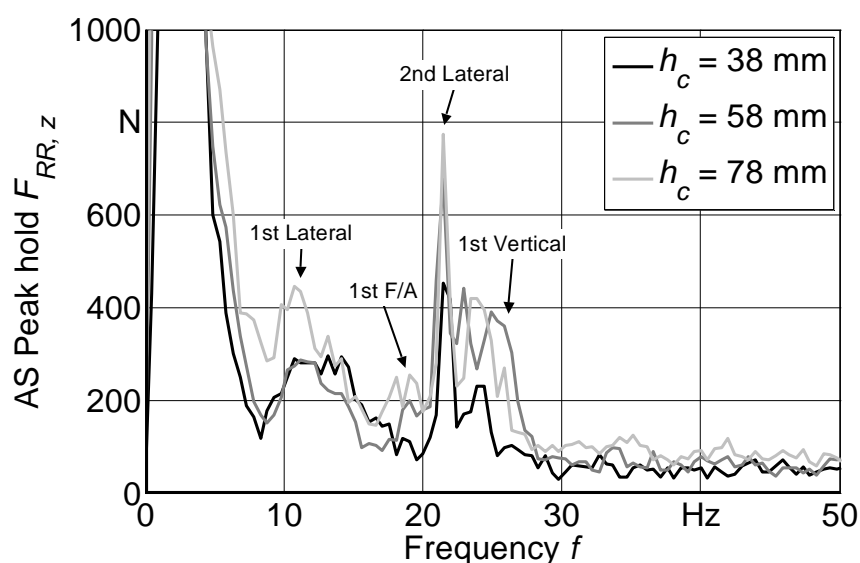
**Figure 109:** Amplitude spectrum peak hold of the right rear wheel's vertical force signal  $F_{RR,z}$  for different speeds (Goodyear Optitrac 520/70 R38,  $F_z = 17.6$  kN,  $h_c = 78$  mm,  $p_i = 1.2$  bar); Transient window, block size 512



**Figure 110:** Amplitude spectrum peak hold of the right rear wheel's vertical force signal  $F_{RR,z}$  for different speeds (Goodyear Optitrac 520/70 R38,  $F_z = 17.6$  kN,  $h_c = 78$  mm,  $p_i = 1.2$  bar); Transient window, block size 512

### Cleat height influence

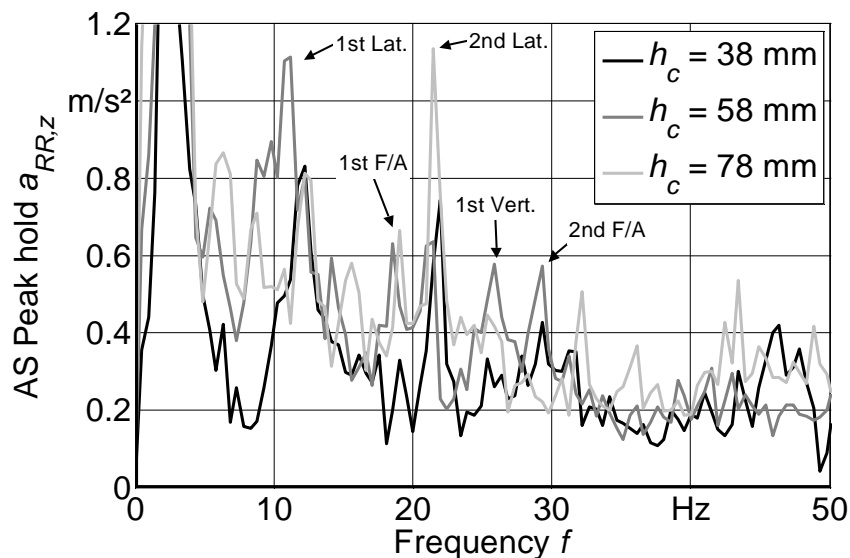
As already mentioned in 4.5.5 three different cleat heights were tested with the tractor. All cleats have a length of 58 mm. With growing cleat height the vertical force signal (Figure 111) shows nearly over the complete range increasing amplitudes especially for the tire modes. This proves the force amplitude's dependency on the cleat height. On the other hand this effect does not fully apply accordingly for the vertical acceleration (Figure 112).



**Figure 111:** Amplitude spectrum peak hold of the right rear wheel's vertical force signal  $F_{RR,z}$  for different cleat heights ( $h_c$ ) (Goodyear Optitrac 520/70 R38,  $F_z = 17.6$  kN,  $p_i = 1.2$  bar,  $v = 20$  km/h); Transient window, block size 512

Regarding the vertical direction the bouncing mode at 2.4 Hz is dominating the amplitude spectrum as mentioned above. The amplitudes show direct dependency to the cleat height. So the the 38 mm cleat leads to 3.4 kN, the 58 mm to 5.7 kN and the 78 mm to 10.5 kN. The corresponding acceleration peak values are 2.5, 4.1 and 7.3 m/s<sup>2</sup>. The 1<sup>st</sup> and 2<sup>nd</sup> Lateral modes show noticeable peaks both in the force and acceleration signal. Furthermore, the 1<sup>st</sup> F/A and 1<sup>st</sup> Vertical mode can be identified, but on a lower peak level. Compared to the uniformity tests, where the 1<sup>st</sup> F/A mode is dominant, it decreases noticeable for the cleat excitation. Remarkably is that the 58 mm high cleat leads to higher peaks especially at the 1<sup>st</sup> Lateral, 1<sup>st</sup> Vertical and 2<sup>nd</sup> F/A mode frequencies. Above 30 Hz the force signal

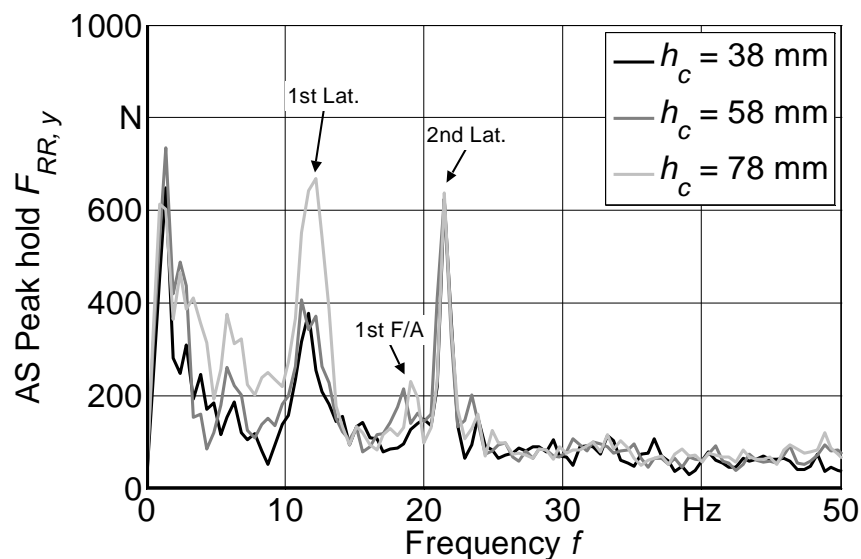
does not show any peaks anymore which leads to the assumption that this could be the limitation of the broad band excitation by the cleat. Generally, also the acceleration signal's amplitudes are decreasing in this frequency range.



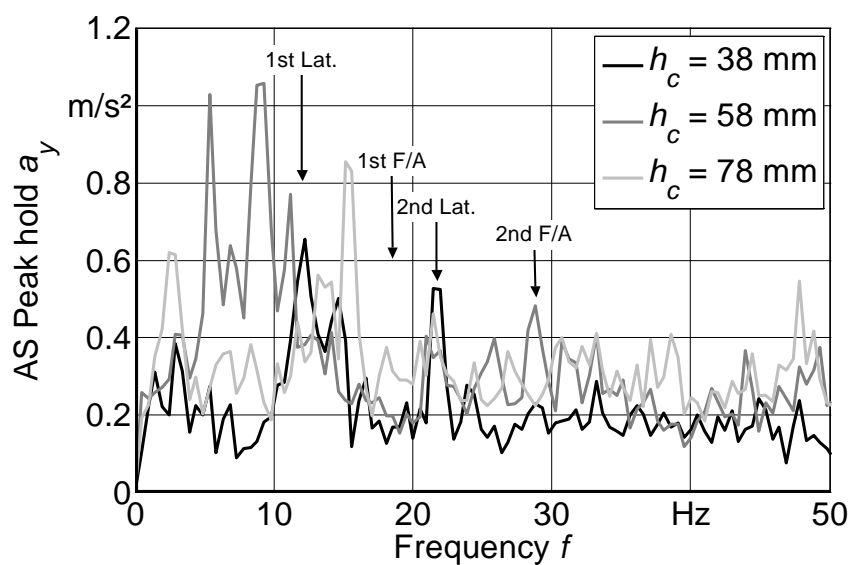
**Figure 112:** Amplitude spectrum peak hold of the right rear wheel's vertical acceleration signal  $a_{RR,z}$  for different cleat heights ( $h_c$ ) (Goodyear Optitrac 520/70 R38,  $F_z = 17.6$  kN,  $p_i = 1.2$  bar,  $v = 20$  km/h); Transient window, block size 512

As expected the lateral force signal is showing very clearly peaks at the 1<sup>st</sup> and 2<sup>nd</sup> Lateral mode frequency (Figure 113). There is no extremely exaggerated bouncing mode amplitude. Except the 1<sup>st</sup> F/A mode no other tire modes can be identified due to the comparably low and smooth amplitude spectrum at the frequency range above 25 Hz.

Similar to the vertical direction also the lateral acceleration's amplitude spectrum is not as consistent as the force signal. Especially the two peaks between 5 and 10 Hz, which obviously maximize for the 58 mm cleat, cannot be assigned clearly to any vehicle or axle vibration mode. The mentioned tire vibration modes can be found in the curves but do not show distinct peaks (Figure 114).

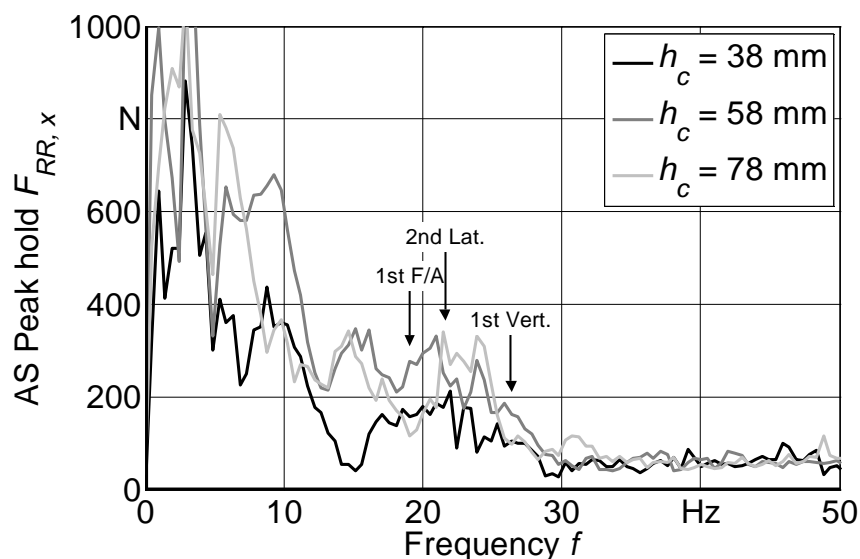


**Figure 113:** Amplitude spectrum peak hold of the right rear wheel's lateral force signal  $F_{RR,y}$  for different cleat heights ( $h_c$ ) (Goodyear Optitrac 520/70 R38,  $F_z = 17.6$  kN,  $p_i = 1.2$  bar,  $v = 20$  km/h); Transient window, block size 512



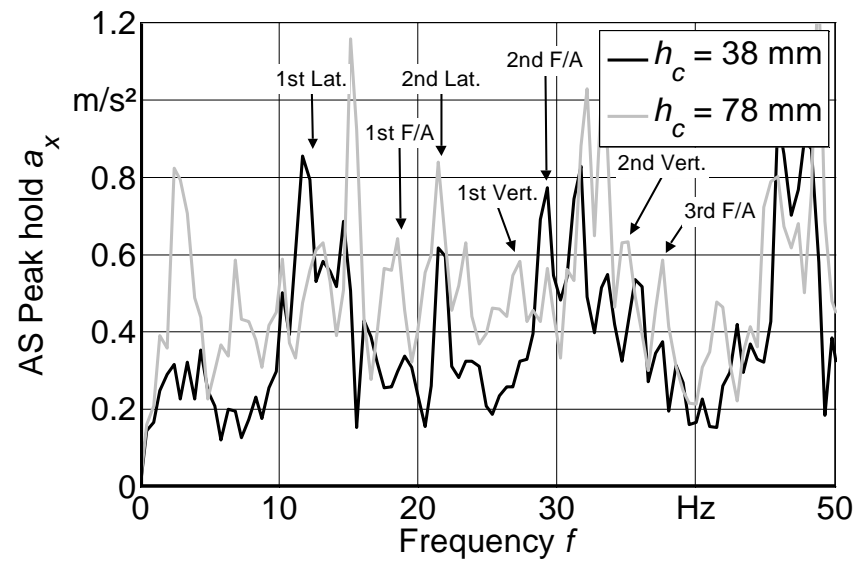
**Figure 114:** Amplitude spectrum peak hold of the right rear wheel's lateral acceleration signal  $a_{RR,y}$  for different cleat heights ( $h_c$ ) (Goodyear Optitrac 520/70 R38,  $F_z = 17.6$  kN,  $p_i = 1.2$  bar,  $v = 20$  km/h); Transient window, block size 512

Regarding the longitudinal force the amplitude spectrum above 10 Hz shows similarities with that of the uniformity tests concerning the amplitudes below 400 N and the recognizability of the mode shapes except the 1<sup>st</sup> Lateral mode (Figure 115). In the range below 10 Hz at around 3.4 Hz a peak up to 1200 N can be found which might be characteristic for a longitudinal bouncing mode.



**Figure 115:** Amplitude spectrum peak hold of the right rear wheel's longitudinal force signal  $F_{RR,x}$  for different cleat heights ( $h_c$ ) (Goodyear Optitrac 520/70 R38,  $F_z = 17.6$  kN,  $p_i = 1.2$  bar,  $v = 20$  km/h); Transient window, block size 512

Contrary to the force signal the acceleration values show higher amplitudes than those for the uniformity tests (Figure 116). However, the shape and recognisability is comparable again. All modes in the frequency range up to 50 Hz generally can be identified in this amplitude spectrum even if not that clearly. The high bouncing mode force amplitude cannot be found in the acceleration signal. One peculiar peak at around 15 Hz shows the maximum amplitude of the spectrum but cannot be assigned clearly.



**Figure 116:** Amplitude spectrum peak hold of the right rear wheel's longitudinal acceleration signal  $a_{RR,x}$  for different cleat heights ( $h_c$ ) (Goodyear Optitrac 520/70 R38,  $F_z = 17.6$  kN,  $p_i = 1.2$  bar,  $v = 20$  km/h); Transient window, block size 512

## 6 CONCLUSIONS AND OUTLOOK

The conducted experimental investigations on the modal properties of tractor tires have been realized with three different setups:

- Investigations on a single wheel
- Investigations on a test rig
- Investigations on a vehicle

On the single wheel an experimental modal analysis was conducted for the non-rolling wheel at unloaded and loaded condition. The results show first of all that for this tire size within the frequency range 0 – 80 Hz up to 15 tire modes can occur unlike passenger car or truck tires. All these tire modes can be determined precisely concerning eigenfrequency, modal damping and mode shape. The general influence of the inflation pressure on eigenfrequency and modal damping can be proven. Furthermore, the rim modes only occur above 80 Hz. From the analysis of the axle dynamics arises that the bigger the tire the better is the clear identification of its modes. Besides the rigid body modes most 2<sup>nd</sup> order modes and further the Vertical and F/A modes also show noticeable influence on the axle dynamics. The modal analysis of the single wheel shaped up as the basis for the analysis of all the following tests.

The subsequent modal analysis of the rear tire on the flat-belt test stand shows an acceptable agreement with the results for the single wheel. The determined rig modes within the regarded frequency range need to be considered though, but obviously do not cover or neutralize the tire modes. The Hohenheim shaker device is a monofrequent harmonic excitation source and can be installed on different testing facilities. Results of the shaker tests on the flat-belt test rig show that most of the modes in the mentioned frequency range can be identified. Furthermore, the effects of excitation amplitude, tire load and inflation pressure variation on frequency and amplitude can be demonstrated qualitatively. The speed influence was one of the key aspects to be examined. Results are showing a slight frequency decrease with the onset of rolling. The force amplitudes measured in the tread pattern increase at first with the onset of rolling and then decrease at

speeds above 3 km/h significantly. 1<sup>st</sup> and 2<sup>nd</sup> Lateral, 1<sup>st</sup> Vertical as well as 1<sup>st</sup> and 2<sup>nd</sup> F/A modes still show the noticeable amplitudes for the rolling tire.

On the Fendt research tractor at first compatible shaker tests were conducted for a comparison with the flat-belt test stand. The eigenfrequencies show a good agreement. Concerning the wheel force and acceleration amplitudes with the onset of rolling also the slight frequency decrease can be observed. Unlike to the tread pattern force signals on the rig with the onset of rolling the amplitudes are decreasing by 35-50% and stay nearly on this level with increasing speed. Relevant amplitudes are exhibited by the 1<sup>st</sup> and 2<sup>nd</sup> Lateral, 1<sup>st</sup> F/A and 1<sup>st</sup> Vertical modes. Uniformity and cleat tests excite the tire in a completely different way. Nevertheless, their frequency spectra show certain similarities. The above mentioned four tire modes are also for these operating conditions the most relevant and can be identified. Regarding and classifying the amplitudes of the uniformity test it can be exhibited that the 1<sup>st</sup> Lateral and 1<sup>st</sup> F/A reach maximum wheel acceleration amplitudes of more than 1 m/s<sup>2</sup> which is even more than the bouncing modes. Regarding the cleat test the bouncing mode amplitudes are strongly dominant, but 1<sup>st</sup> Lateral and 1<sup>st</sup> F/A also reach a level of more than 1 m/s<sup>2</sup>. The wheel vibrations are isolated by cabin and seat suspension. Above 12 Hz this isolation is working very well so that the driver's exposition for this frequency range is not critical. Large vibration amplitudes for the driver are especially due to the bouncing and 1<sup>st</sup> Lateral mode.

From these results it can be concluded that tractor tire modes have influence on the vibration transfer into the vehicle. These vibrations represent first of all increased stress for the vehicle components exposed to it. Secondly, especially lower frequency vibrations can be transferred to cabin and seat in large parts, if the cabin and seat suspension is not adjusted correctly.

Consequently, for an adequate precise ride comfort and load simulation the tire model needs to be able to cover and represent the mentioned driving manoeuvres and frequency range. For this reason the Hohenheim tire model is going to be upgraded [28; 29]. A promising simulation approach for an automatic optimization of the cabin suspension was conducted by Jaksch [169]. This kind of future



applications will also require corresponding tire models. Concerning a vehicle simulation model for ride comfort purposes another main requirement is that body/chassis/suspension models also need to be able to reproduce vibrations in the required frequency range up to 80 Hz or more [114].

With the experience from this project several extensions and improvements of the test rigs can be proposed. Essential for more precise measurements is a sufficient dynamic stability which requires further extensive design changes and replacements. Additionally, the test rigs can be extended to realize all possible boundary conditions of the spindle in all directions. This would provide the possibility for a much better comparison between different test rigs and also with other references.

Other important challenges are increasing driving velocity, power and dimensions of agricultural machinery. In order to cope with this evolution new tire testing facilities and up to date measuring vehicles are necessary. In this context a top of the range tractor has been equipped with new 6 component measuring wheels and further extensive measuring equipment. Schulze Zumkley examined with this tractor an alternative identification of tire parameters from road tests [26; 27]. Furthermore, a concept for a new test trailer has been developed which enables bigger tires, higher load and speed [170]. This concept is being substantiated and may also lead to a comprehensive research project.

An additional approach to overcome the deficiency of adequate testing facilities was presented by Weinhold et al. [171]. For the parameterization of MBS tire models a purely virtual process chain is introduced based on detailed FE models instead of extensive tests on complex and expensive test rigs.

## 7 REFERENCES

- [1] Directive 2002/44/EC: On the minimum health and safety requirements regarding the exposure of workers to the risks arising from physical agents (vibration). Official Journal of the European Communities L 177, S. 13-19, 25-6-2002.
- [2] Verordnung zu Umsetzung der EG-Richtlinien 2002/44/EG und 2003/10/EG zum Schutz der Beschäftigten vor Gefährdungen durch Lärm und Vibrationen. Bundesgesetzblatt Jahrgang 2007 Teil I Nr. 8, S. 261-277, 6-3-2007.
- [3] Schrottmaier, J. und M. Nadlinger: Untersuchung und Optimierung der schwingungstechnischen Eigenschaften von Traktoren mit gefederter Vorderachse und gefederter Fahrerkabine. 58. VDI-MEG-Tagung Landtechnik, 2000.
- [4] Hechenblaikner, J., S. Göhl und R. Käsler: Benchmarking als Hilfsmittel zur schwingungstechnischen Auslegung von Lagerungssystemen. VDI-MEG Tagung Landtechnik, Hannover (2005), Nr. 1895, S. 171-176.
- [5] Anthonis, J., P. Kennes und H. Ramon: Design and evaluation of a low-power mobile shaker for vibration tests on heavy wheeled vehicles. Journal of Terramechanics 37 (2000), S. 191-205.
- [6] Yilmaz, C., G.M. Hulbert und N. Kikuchi: Reducing Tire-Induced Noise and Vibration. Tire Science and Technology, TSTCA Vol. 34 (2006) No. 2, S. 135-147.
- [7] • Pacejka, H.B.: Analysis of Tire Properties, in Clark, S.K.: *Mechanics of Pneumatic Tires*, Chapter 9, S. 721-870, United States Department of Transportation Washington D.C., 1981.
- [8] VDI 2057: Einwirkung mechanischer Schwingungen auf den Menschen - Ganzkörper-Schwingungen, Blatt 1. VDI-Richtlinien, S. 1-39, 2002.
- [9] ISO 2631-1:1997: Mechanical vibration and shock - Evaluation of human exposure to whole-body vibration - Part1: General requirements., S. 1-44, 1997.
- [10] ISO 2631-1:1997/Amd.1:2010: Mechanical vibration and shock - Evaluation of human exposure to whole-body vibration - Part1: General requirements AMENDMENT, S. 1-12, 2010.
- [11] Troulis, M.: Übertragungsverhalten von Radaufhängungen für Personenwagen im komfortrelevanten Frequenzbereich - Simulationsmodell, experimentelle Untersuchungen und Konzeption einer Prüfeinrichtung. Dissertation Universität Karlsruhe 2002. Shaker Verlag Aachen, Berichte aus der Fahrzeugtechnik.

- [12] • Heißing, B. und M. Ersoy: Fahrwerkhandbuch. Vieweg Verlag Wiesbaden, 2007.
- [13] Balfanz, H.-G.: Zum Einfluß des Reifens auf die Beanspruchung der Automobilkarosserie. Dissertation Technische Universität Clausthal 1997 Clausthal-Zellerfeld.
- [14] Mousseau, C.W. und G.M. Hulbert: The Dynamic Response of Spindle Forces Produced by a Tire Impacting Large Obstacles in a Plane. Journal of Sound and Vibration 195(5) (1996), S. 775-796.
- [15] Ferhadbegović, B.: Entwicklung und Applikation eines instationären Reifenmodells zur Fahrdynamiksimulation von Ackerschleppern. Dissertation Universität Stuttgart 2009. Shaker Verlag Aachen, Forschungsbericht Agrartechnik des Arbeitskreises Forschung und Lehre der Max-Eyth-Gesellschaft Agrartechnik im VDI, 475.
- [16] Langenbeck, B.: Nichtlineares Reifenmodell. VDI/MEG Kolloquium Landtechnik, München (1989), Reifen landwirtschaftlicher Fahrzeuge, S. 86-93.
- [17] Langenbeck, B.: Reifenkennwerte. Landtechnik 46 (1991) 5, S. 221-224.
- [18] Langenbeck, B.: Untersuchungen zum Fahrverhalten von Ackerschleppern unter besonderer Berücksichtigung der Reifeneigenschaften. Dissertation Universität Stuttgart 1992. VDI-Verlag Düsseldorf, VDI Fortschritt-Berichte, Reihe 14, Nr. 55.
- [19] Plesser, J.: Dynamisches Verhalten von Ackerschlepperreifen in Vertikal- und Längsrichtung auf fester Fahrbahn. Dissertation Universität Stuttgart 1997. VDI-Verlag Düsseldorf, VDI Fortschritt-Berichte, Reihe 14, Nr. 83.
- [20] Schrogl, H.: Dynamische Eigenschaften von Ackerschlepper-Triebradreifen bei höheren Rollgeschwindigkeiten. Dissertation Universität Hohenheim 1989. Forschungsbericht Agrartechnik MEG Hohenheim, Forschungsbericht Agrartechnik des Arbeitskreises Forschung und Lehre der Max-Eyth-Gesellschaft, 159.
- [21] Armbruster, K.: Untersuchung der Kräfte an schräglaufenden angetriebenen Ackerschlepperrädern. Dissertation Universität Stuttgart 1991. VDI Verlag Düsseldorf, VDI Fortschritt-Berichte, Reihe 14, Nr. 53.
- [22] Barreilmeyer, Th.: Untersuchung der Kräfte an gelenkten und angetriebenen Ackerschlepperrädern bei Gelände- und Straßenfahrt. Dissertation Universität Stuttgart 1996. VDI Verlag Düsseldorf, VDI Fortschritt-Berichte, Reihe 14, Nr. 79.
- [23] Schlotter, V.: Einfluss dynamischer Radlastschwankungen und Schräglaufwinkeländerungen auf die horizontale Kraftübertragung von Ackerschlepperreifen. Dissertation Universität Stuttgart 2006. Shaker Verlag Aachen, Forschungsbericht Agrartechnik des Arbeitskreises

- Forschung und Lehre der Max-Eyth-Gesellschaft Agrartechnik im VDI, 437.
- [24] Schlotter, V. und H.D. Kutzbach: The lateral force generation of agricultural tyres. 8th European Conference of ISTVS, Umea, Sweden (2000), S. 95-102.
- [25] Schlotter, V. und A. Keen: The dynamic characteristics of off road tyres. Proceedings of the 9<sup>th</sup> European Conference of the ISTVS, Harper Adams (2003), S. 460-479.
- [26] Schulze Zumkley, H. und S. Böttinger: Tyre parameter identification from road tests with agricultural tractors. Proceedings of the 11th European Regional Conference of the International Society for Terrain-Vehicle Systems, Bremen, Germany (2009).
- [27] Schulze Zumkley, H. und S. Böttinger: Identification of side force-slip angle characteristic from road tests with an agricultural tractor. Landtechnik 65 (2010) H. 6, S. 426-428.
- [28] Witzel, P., H. Schulze Zumkley und S. Böttinger: Passage of obstacles with the Hohenheim Tyre Model. Landtechnik 66 (2011) H. 1, S. 64-66.
- [29] Witzel, P. und S. Böttinger: Upgrading of the Hohenheim Tyre Model to a radial approach. Landtechnik 66 (2011) H. 2, S. 144-146.
- [30] Witzel, P. und S. Böttinger: The New Hohenheim Tyre Model. 14. Internationales Stuttgarter Symposium, Stuttgart (2014), Band 1, S. 987-1001.
- [31] Sharon, I.: Untersuchungen über die Schwingungseigenschaften großvolumiger Niederdruckreifen. Dissertation Technische Universität Berlin 1975. Forschungsbericht Agrartechnik MEG Berlin, Forschungsbericht Agrartechnik des Arbeitskreises Forschung und Lehre der Max-Eyth-Gesellschaft, 3.
- [32] Owzar, A.: Ein Beitrag zur Untersuchung des Schwingungsverhaltens von ungefederten luftbereiften Fahrzeugen. Dissertation Technische Universität Berlin 1975. Forschungsbericht Agrartechnik MEG Berlin, Forschungsbericht Agrartechnik des Arbeitskreises Forschung und Lehre der Max-Eyth-Gesellschaft, 2.
- [33] Kising, A.: Dynamische Eigenschaften von Traktor-Reifen. Dissertation Technische Universität Berlin 1988. VDI-Verlag Düsseldorf, VDI Fortschritt-Berichte, Reihe 14, Nr. 40.
- [34] Göhlich, H., F. Schütz und H. Jungerberg: Untersuchungen zum vertikalen Schwingungsverhalten von Ackerschleppern. Grundlagen der Landtechnik Bd. 34 (1984) Nr. 1, S. 13-18.
- [35] Yeh, C.K.: Experimentelle Untersuchungen über Unwuchten und Unrundheiten von Ackerschlepperreifen. Dissertation Technische

- Universität Berlin 1992. Forschungsbericht Agrartechnik MEG Berlin, Forschungsbericht Agrartechnik des Arbeitskreises Forschung und Lehre der Max-Eyth-Gesellschaft, 219.
- [36] Siefkes, T.: Die Dynamik in der Kontaktfläche von Reifen und Fahrbahn und ihr Einfluß auf das Verschleißverhalten von Traktor-Triebradreifen. Dissertation Technische Universität Berlin 1994. VDI-Verlag Düsseldorf, VDI Fortschritt-Berichte, Reihe 14, Nr. 67.
- [37] Siefkes, T. und H. Göhlich: Dynamic characteristics of very large agricultural tires. AgEng, Berlin (1990), S. 1-14.
- [38] von Holst, C. und H. Göhlich: The System Tractor - Tire under the Influence of Tractor Development. Tyre Models for Vehicle Dynamic Analysis, Berlin, Deutschland (1997), Volume 27, S. 330-334.
- [39] von Holst, C.: Simulation and Verification of Complex Systems Vibration Behaviour. AgEng Oslo 98 (1998), S. 1-8.
- [40] von Holst, C.: Vergleich von Reifenmodellen zur Simulation der Fahrdynamik von Traktoren. Dissertation Technische Universität Berlin 2001. VDI Verlag Düsseldorf, VDI Fortschritt-Berichte, Reihe 14, Nr. 102.
- [41] Böhm, F.: Zur Mechanik des Luftreifens. Habilitationsschrift TH Stuttgart 1966.
- [42] Masenger, U.: Dynamisches Verhalten von Ackerschlepper-Reifen auf der Straße und auf dem Acker - Erweiterung einer instationären Rolltheorie auf großvolumige Reifen im Einsatz auf visko-elastischen Böden. Dissertation TU Berlin 1992, D83.
- [43] Wille, R., F. Böhm und A. Duda: Calculation of the rolling contact between a tyre and deformable ground. Tyre Models for Vehicle Dynamics Analysis, Wien (2005), Supplement to Vehicle System Dynamics, Volume 43, S. 483-492.
- [44] Böhm, F. und A. Duda: Off-road cars and tractors with 3D tyre models for fast rolling simulation. Tyre Models for Vehicle Dynamics Analysis, Wien (2005), Supplement to Vehicle System Dynamics, Vol. 43, S. 493-507.
- [45] Coenenberg, H.H.: Dynamische Beanspruchungen bei Ackerschleppern I. Landtechnische Forschung H.1 (1961) 12, S. 7-12.
- [46] Wendeborn, J.O.: Ein Beitrag zur Verbesserung des Fahrkomforts auf Ackerschleppern. Dissertation Forschungsanstalt für Landwirtschaft, Braunschweig-Völkenrode 1968. VDI-Verlag Düsseldorf, VDI Fortschritt-Berichte, Reihe 14, Nr. 8.
- [47] Hlawitschka, E.: Federungs- und Dämpfungsverhalten von Reifen auf gekrümmten Aufstandsflächen. Deutsche Agrartechnik 21. (1971) 2, S. 72-75.

- [48] Müller, H.: Beitrag zu rechnerischen Ermittlung von Belastungen in Tragwerken landwirtschaftlicher Fahrzeuge beim Überqueren großer Fahrbahnunebenheiten. Technische Universität Dresden 1976.
- [49] Laib, L.: A Vibration Analysis of Agricultural Tyres. Proceedings of the 6th International Conference of the ISTVS, Wien (1978), Volume III, S. 1317-1341.
- [50] Stayner, R.M., T.S. Collins und J.A. Lines: Tractor Ride Vibration Simulation as an Aid to Design. Journal of Agricultural Engineering Research (1984) 29, S. 345-355.
- [51] Crolla, D.A. und D.N.L. Horton: Factors Affecting the Dynamic Behaviour of Higher Speed Agricultural Vehicles. Journal of Agricultural Engineering Research (1984) 30, S. 277-288.
- [52] Crolla, D.A., D.N.L. Horton und R.M. Stayner: Effect of Tyre Modelling on Tractor Ride Vibration Predictions. Journal of Agricultural Engineering Research (1990) 47, S. 55-57.
- [53] Lines, J.A.: Rolling tyre characteristics and their effect on prediction of unsuspended vehicle ride. Proceedings of 5th European Conference ISTVS, 1991.
- [54] Lines, J.A.: The Suspension Characteristics of Agricultural Tractor Tyres. PhD Thesis Cranfield Institute of Technology Silsoe College 1991.
- [55] Deltenre, A. und M.-F. Detain: Numerical Simulation of Agricultural Tractors Ride Vibration. AgEng, Berlin (1990), S. 1-12.
- [56] Niskanen, M.: Ride Vibrations of an Agricultural Tractor Driving on an Asphalt Road. AgEng, Berlin (1990), S. 1-12.
- [57] Keen, A.: The Tyre and Suspension Characteristics of an off Road Vehicle Determined using a Single Wheel Tester. European Automotive Congress Bratislava, 2001.
- [58] Keen, A.: The Effect of Wheel Vibration on Traction - An Investigation using a Single Wheel Tester. Proceedings of the 6th Asian-Pacific ISTVS Conference, 2001.
- [59] Ahmed, O.B. und J.F. Goupillon: Predicting the ride vibration of an agricultural tractor. Journal of Terramechanics 1997 (1997) 34, S. 1-11.
- [60] Clijmans, L., H. Ramon, J. Langenakens und J. De Baerdemaeker: The Influence of Tyres on the Dynamic Behaviour of a Lawn Mower. Journal of Terramechanics Vol. 33 (1996) No. 4, S. 195-208.
- [61] Clijmans, L., H. Ramon und J. De Baerdemaeker: Structural Modification Effects on the Dynamic Behaviour of an Agricultural Tractor. Transactions of the ASAE Vol. 41(1) (1998), S. 5-10.

- [62] Kennes, P., J. Anthonis, L. Clijmans und H. Ramon: Construction of a Portable Test Rig to Perform Experimental Modal Analysis on Mobile Agricultural Machinery. *Journal of Sound and Vibration* 228(2) (1999), S. 421-441.
- [63] Hostens, I., J. Anthonis, P. Kennes und H. Ramon: Six-degrees-of-freedom Test Rig Design for Simulation of Mobile Agricultural Machinery Vibrations. *Journal of Agricultural Engineering Research* 77(2) (2000), S. 155-169.
- [64] Böhm, F.: Zur Statik und Dynamik des Gürtelreifens. *Automobiltechnische Zeitschrift* 69 (1967) H. 8, S. 255-261.
- [65] Böhm, F.: On the Roots of Tire Mechanics. Tyre Models for Vehicle Dynamic Analysis, Berlin (1997), Supplement to Vehicle System Dynamics, Volume 27, S. 303-317.
- [66] Böhm, F.: Theorie schnell veränderlicher Rollzustände für Gürtelreifen. *Ingenieur-Archiv* (1985) 55, S. 30-44.
- [67] Oertel, Ch.: Untersuchung von Stick-Slip-Effekten am Gürtelreifen. Dissertation TU Berlin 1990. VDI-Verlag Düsseldorf, VDI Fortschritt-Berichte, Reihe 12, Nr. 147.
- [68] Böhm, F., M. Swierczek und G. Csaki: Hochfrequente Rolldynamik des Gürtelreifens - das Kreisringmodell und seine Erweiterung. TU Berlin 1989. VDI-Verlag Düsseldorf, VDI Fortschritt-Berichte, Reihe 12, Nr. 135.
- [69] Böhm, F.: Reifenmodell für hochfrequente Rollvorgänge auf kurzwelligen Fahrbahnen. VDI-Verlag Düsseldorf, VDI Berichte Nr. 1088, 1993.
- [70] Zhang, T.: Höherfrequente Übertragungseigenschaften der Kraftfahrzeug-Fahrwerksysteme. Dissertation Technische Universität Berlin 1991. Selbstverlag Berlin, D 83.
- [71] Kmoch, K.: Meßtechnische Methoden zur Bewertung dynamischer Reifeneigenschaften. Dissertation Technische Universität Berlin 1992. Selbstverlag Berlin, D 83.
- [72] Zachow, D.: 3D Membrane Shell Model in Application of a Tractor and PKW Tyre. Tyre Models for Vehicle Dynamic Analysis, Berlin, Deutschland (1997), Volume 27, S. 163-172.
- [73] • Böhm, F.H. und K.H. Knothe: Hochfrequenter Rollkontakt der Fahrzeugräder. WILEY-VCH Weinheim, 1998.
- [74] Zegelaar, P.: The Dynamic Response of Tyres to Brake Torque Variations and Road Unevenness. PhD Thesis Delft University of Technology 1998 Delft.
- [75] Zegelaar, P.: Modal Analysis of Tire In-Plane Vibrations. SAE International: SAE International Congress and Exposition, SAE Paper 971101, 1997.

- [76] Maurice, J.P.: Short Wavelength and Dynamic Tyre Behaviour under Lateral and Combined Slip Conditions. PhD Thesis Delft University of Technology 1999 Delft.
- [77] Schmeitz, A.J.C.: A Semi-Empirical Three-Dimensional Model of the Pneumatic Tyre Rolling over Arbitrarily Uneven Road Surfaces. PhD Thesis Delft University of Technology 2004 Delft.
- [78] Kindt, P., F. De Coninck, P. Sas und W. Desmet: Experimental modal analysis of radial tires and the influence of the tire modes on vehicle structure borne noise. FISITA 2006 World Automotive Congress F2006D210, 2006.
- [79] Kindt, P., F. De Coninck, P. Sas und W. Desmet: Test setup for tire/road noise caused by road impact excitations: first outlines. Proceedings of ISMA 2006 International Conference on Noise & Vibration Engineering, Leuven, Belgium (2006), Vehicle Noise and Vibration (NVH), S. 4327-4336.
- [80] Kindt, P., P. Sas und W. Desmet: Three-dimensional Ring Model for the Prediction of the Tyre Structural Dynamic Behaviour. Proceedings of ISMA 2008 International Conference on Noise & Vibration Engineering, Leuven, Belgium (2008), S. 4155-4170.
- [81] Kindt, P., F. De Coninck, P. Sas und W. Desmet: Measurement of the Tire Dynamic Transfer Stiffness at Operational Excitation Levels. Proceedings of ISMA 2010 International Conference on Noise & Vibration Engineering, Leuven, Belgium (2010), S. 3991-4002.
- [82] Yu, H.J. und H. Aboutorabi: Dynamics of Tire, Wheel, and Suspension Assembly. Tire Science and Technology, TSTCA Vol. 29 (2001) No. 2, S. 66-78.
- [83] Bruni, S., F. Cheli und F. Resta: On the Identification in Time Domain of the Parameters of a Tyre Model for the Study of In-Plane Dynamics. Tyre Models for Vehicle Dynamic Analysis, Berlin, Deutschland (1997), Volume 27, S. 136-150.
- [84] Belluzzo, D., F. Mancosu, R. Sangalli, F. Cheli und S. Bruni: New Predictive Model for the Study of Vertical Forces (up to 250 Hz) Induced on the Tire Hub by Road Irregularities. Tire Science and Technology, TSTCA Vol. 30 (2002) No. 1, S. 2-18.
- [85] Soedel, W. und M.G. Prasad: Calculation of Natural Frequencies and Modes of Tires in Road Contact by Utilizing Eigenvalues of the Axisymmetric Non-Contacting Tire. Journal of Sound and Vibration 70(4) (1980), S. 573-584.
- [86] Kung, L.E., W. Soedel und T.Y. Yang: On the Dynamic Response at the Wheel Axle of a Pneumatic Tire. Journal of Sound and Vibration 107(2) (1986), S. 195-213.



- [87] Kung, L.E., W. Soedel und T.Y. Yang: On the Vibration Transmission of a Rolling Tire on a Suspension System Due to Periodic Tread Excitation. *Journal of Sound and Vibration* 115(1) (1987), S. 37-63.
- [88] Ushijima, T. und M. Takayama: Modal analysis of tire and system simulation. SAE International: SAE International Congress and Exposition, SAE Paper 880585, 1988.
- [89] Kao, B.G.: A Three-Dimensional Dynamic Tire Model for Vehicle Dynamic Simulations. *Tire Science and Technology, TSTCA Vol. 28 (2000) No. 2*, S. 72-95.
- [90] Kao, B.G.: Tire Vibration Modes and Tire Stiffness. *Tire Science and Technology, TSTCA Vol. 30 (2002) No. 3*, S. 136-155.
- [91] Scavuzzo, R.W., T.R. Richards und L.T. Charek: Tire Vibration Modes and Effects on Vehicle Ride Quality. *Tire Science and Technology, TSTCA Vol. 21 (1993) No. 1*, S. 23-39.
- [92] Richards, T.R., L.T. Charek und R.W. Scavuzzo: The Effects of Spindle and Patch Boundary Conditions on Tire Vibration Modes. SAE International: SAE International Congress and Exposition, SAE Paper 860243, 1986.
- [93] Liu, H.: Tread Discontinuities as Source of Vibration/Noise - Transient Dynamics of Rolling Tires. *Tire Science and Technology, TSTCA Vol. 31 (2003) No. 4*, S. 204-224.
- [94] Dorfi, H.R.: A Study of the In-Plane Force Transmission of Tires. *Tire Science and Technology, TSTCA Vol. 32 (2004) No. 4*, S. 188-213.
- [95] Dorfi, H.R.: Tyre non-uniformities: comparison of analytical and numerical tyre models and correlation to experimentally measured data. *Tyre Models for Vehicle Dynamics Analysis, Wien, Österreich (2005), Volume 43*, S. 223-240.
- [96] Wheeler, R.L., H.R. Dorfi und B.B. Keum: Vibration Modes of Radial Tires: Measurement, Prediction, and Categorization Under Different Boundary and Operating Conditions. SAE International: SAE Noise & Vibration Conference, SAE Technical Paper Series 2005-01-2523, 2005.
- [97] Dorfi, H.R., R.L. Wheeler und B.B. Keum: Vibration Modes of Radial Tires: Application to Non-rolling and Rolling Events. SAE International: SAE Noise & Vibration Conference, SAE Technical Paper Series 2005-01-2526, 2005.
- [98] Barz, D. und E. Donges: Neue Erkenntnisse zur Ungleichförmigkeit von Reifen. VDI-Gesellschaft Fahrzeug- und Verkehrstechnik: Reifen - Fahrwerk - Fahrbahn, VDI-Verlag Düsseldorf, VDI Berichte Nr. 650, 1987.
- [99] Lion, A.: Dynamische Modellierung von elastomeren Bauteilen. Haus der Technik: Geräusch- und Schwingungskomfort von Kraftfahrzeugen, 2006.

- [100] Said, M.: Prüfstand zur Messung der dynamischen Radlast von Kraftfahrzeugen. Dissertation Universität Stuttgart 1991. Selbstverlag Stuttgart.
- [101] Allison, D.J. und R.S. Sharp: On the low-frequency in-plane forced vibrations of pneumatic tyre / wheel / suspension assemblies. Tyre Models for Vehicle Dynamic Analysis, Berlin, Deutschland (1997), Volume 27, S. 151-162.
- [102] Leyssens, J. und W. Gnoerich: Vehicle Interior Noise - a Result of Road / Tire / Vehicle Interaction. Stuttgarter Symposium 2001, Stuttgart (2001), S. 298-304.
- [103] Dihua, G. und F. Chengjian: Tire Modeling for Vertical Properties Including Enveloping Properties Using Experimental Modal Parameters. Vehicle System Dynamics Vol. 40 (2004) No. 6, S. 419-433.
- [104] Duvernier, M., P. Fraysse, V. Bomblain und E. Dormegnien: Tyre Modelling for NVH Engineering in ADAMS. Michelin Tyre Company: 2002.
- [105] Tsihlias, D., T. Lacroix und B. Clayton: A Comparison of Two Substructuring Techniques for Representing the Modal Properties of Tires. Tire Science and Technology, TSTCA Vol. 29 (2001) No. 1, S. 23-43.
- [106] Ropers, C.: Untersuchung der Reifenschwingung bei Überfahrt von Einzelhindernissen. VDI Verlag: VDI-Berichte Nr. 1912, 2005.
- [107] -, -: Ermüdungsprüfstand mit neuartigen Flachbahnen ist realitätsnäher. Instron Structural Testing Systems GmbH, 2002.
- [108] Braess, H.-H.: Der Reifen - Schlüsselkomponente für Fahrdynamik und Lenkverhalten von Fahrzeugen. (2000), 3. Darmstädter Reifenkolloquium, VDI-Fortschrittberichte, Reihe 12, Nr. 437, S. 1-28.
- [109] Schieschke, R. und R. Gnadler: Modellbildung und Simulation von Reifeneigenschaften. VDI Berichte (1987) 650, S. 95-114.
- [110] Schieschke, R.: Zur Relevanz der Reifendynamik in der Fahrzeugsimulation. VDI-Verlag Düsseldorf, VDI Berichte Nr. 778, (1989), S. 249-264.
- [111] Bösch, P., D. Ammon und F. Klempau: Reifenmodelle - Wunsch und Wirklichkeit aus der Sicht der Fahrzeugentwicklung. 4. Darmstädter Reifenkolloquium, Darmstadt (2002), S. 87-101.
- [112] Einsle, S.: Analyse und Modellierung des Reifenübertragungsverhaltens bei transienten und extremen Fahrmanövern. Dissertation Technische Universität Dresden 2011. TUDpress Dresden.
- [113] Lugner, P. und M. Plöchl: Tyre model performance test: first experiences and results. Tyre Models for Vehicle Dynamics Analysis, Wien, Österreich (2004), Volume 43, S. 48-62.

- [114] • Böhm, F.: Zusammenwirken von Kontaktmechanik, Reifen und Achsdynamik beim instationären Rollkontakt, in Böhm, F.H. und K.H. Knothe: *Hochfrequenter Rollkontakt der Fahrzeugräder*, 6, S. 116-136, WILEY-VCH Weinheim, 1998.
- [115] • Gipser, M.: Pneumatic Tire Models: the Detailed Mechanical Approach, in Mastinu, G. und M. Plöchl: *Road and Off-Road Vehicle System Dynamics Handbook*, Taylor and Francis London, 2007.
- [116] Fodor, E., S. Kriston, F. Nandori, L. Sarközi und T. Szabo: A Finite Element System for the Hierarchical Design of Agricultural Tires. *Tire Science and Technology*, TSTCA Vol. 26 (1998) No. 4, S. 222-240.
- [117] Gipser, M.: DNS-Tire 3.0: die Weiterentwicklung eines bewährten strukturmechanischen Reifenmodells. Darmstädter Reifenkolloquium, Darmstadt (1996), S. 52-62.
- [118] Gipser, M.: FTire, a New Fast Tire Model for Ride Comfort Simulations. International ADAMS User's Conference, Berlin (1999), S. 1-11.
- [119] Gipser, M.: ADAMS/FTire - A Tire Model for Ride & Durability Simulations. International ADAMS User's Conference, Tokio (2000), S. 1-13.
- [120] Gipser, M.: FTire: Ein physikalisch basiertes, anwendungsorientiertes Reifenmodell für alle wichtigen fahrzeugdynamischen Fragestellungen. 4. Darmstädter Reifenkolloquium, Darmstadt (2002), S. 42-68.
- [121] Gipser, M.: Reifenmodelle in der Fahrzeugdynamik: eine einfache Formel genügt nicht mehr, auch wenn sie magisch ist (2005), URL: [http://www.ftire.com/download/ftire\\_germ.pdf](http://www.ftire.com/download/ftire_germ.pdf).
- [122] Gipser, M.: Reifensimulation mit FTire: Stand und Ausblick. 15. Aachener Kolloquium Fahrzeug- und Motorentechnik, Aachen (2006), S. 1-23.
- [123] Riepl, A., W. Reinalter und G. Fruhmann: Rough road simulation with tire model RMOD-K and FTire. *Tyre Models for Vehicle Dynamics Analysis*, Wien, Österreich (2004), Volume 43, S. 734-743.
- [124] Oertel, Ch. und Fandre A.: Das Reifenmodellsystem RMOD-K. *Automobiltechnische Zeitschrift* 103 (2001) H. 11, S. 1074-1079.
- [125] Oertel, Ch. und A. Fandre: Ride Comfort Simulations and Steps Towards Life Time Calculations: RMOD-K and ADAMS. International ADAMS Users' Conference, 1999.
- [126] Oertel, Ch.: Eigensystem of Tangential Contact in Tyre Models. *Vehicle System Dynamics* Vol. 38 (2002) No. 4, S. 245-260.
- [127] Einsle, S.: Reifenmodelle - Simulation und Messung der Reaktionsgrößen am Reifen bei Schlagleistenüberfahrt. Diplomarbeit Technische Universität Dresden 2004, dKA 2004-23, unveröffentlicht.

- [128] Bremer, G. und H. Mauch: Virtuelle Lastannahme. DVM-Arbeitskreis Betriebsfestigkeit: Von der Betriebsmessung zur Lastannahme (3. Runde - Teil 2), 2006.
- [129] Riener, H., D. Peiskammer, W. Witteveen und A. Lion: Modal Durability Analysis of a Passenger Cars Front Supporting Frame due to Full Vehicle Simulation Loads. ADAMS User Conference 2001 - North America, 2001.
- [130] Mancosu, F., R. Sangalli, F. Cheli, G. Ciarlariello und F. Braghin: A Mathematical-physical 3D Tire Model for Handling/comfort Optimization on a Vehicle: Comparison with Experimental Results. Tire Science and Technology, TSTCA Vol. 28 (2000) No. 4, S. 210-232.
- [131] Pacejka, H.B. und I.J.M. Besselink: Magic Formula Tyre Model with Transient Properties. Tyre Models for Vehicle Dynamic Analysis, Berlin (1997), Supplement to Vehicle System Dynamics 27, S. 234-249.
- [132] • Pacejka, H.B.: Tyre and Vehicle Dynamics. Butterworth-Heinemann Oxford, 2002.
- [133] Brinkmann, C., S. Böttinger und H.D. Kutzbach: Investigations on high-frequency vibration behaviour of agricultural tyres. Proceedings of the 16th CIGR World Congress, Bonn (2006).
- [134] Dossing, O.: Structural Testing, Part 2: Modal Analysis and Simulation. Brüel & Kjaer, 1988.
- [135] • Mitschke, M. und H. Wallentowitz: Dynamik der Kraftfahrzeuge. Springer Verlag Berlin Heidelberg, 2003.
- [136] • Wallentowitz, H.: Vertikal-/Querdynamik von Kraftfahrzeugen. Institut für Kraftfahrwesen Aachen, RWTH Aachen (Hrsg.) Aachen, 1997.
- [137] -, -: Tire Modal Behaviour., Goodyear S.A. Powerpoint presentation, 2007.
- [138] Wallentowitz, H. und T. Hüsemann: Reifentechnologie - Simulation und Versuch. Institut für Kraftfahrwesen, RWTH Aachen: Kraftfahrzeuglabor II, 2007.
- [139] Beckers, M.: Tractor vibrations - Theoretical and practical considerations. Farm Tire Development in the Goodyear Technical Center Luxembourg, 1997.
- [140] Potts, G.R.: The Tire as a Vehicle Component. The University of Akron, Department of Mechanical Engineering: 32nd Tire Mechanics Short Course in Conjunction with Tire Technology Expo & Conference, 2007.
- [141] Potts, G.R. und T.T. Csora: Tire vibration studies: the state of the art. Tire Science and Technology, TSTCA Vol. 3 (1975) No. 3, S. 196-210.
- [142] Potts, G.R.: Application of holography to the study of tire vibration. Tire Science and Technology, TSTCA Vol. 1 (1973) No. 3, S. 255-266.

- [143] Brinkmann, C., J. Haberland, S. Böttinger, O. Erne und G. Sanow: Optisches 3D-Messsystem zur Untersuchung von Reifenverformungen. Landtechnik 62 (2007) H. 5, S. 326-327.
- [144] Zamow, J.: Messung des Reifenverhaltens auf unterschiedlichen Prüfständen. VDI Berichte Nr. 1224, (1995), S. 43-60.
- [145] Böhler, H.: Traktormodell zur Simulation der dynamischen Belastungen bei Transportfahrten. Dissertation Technische Universität München 2001. VDI-Verlag Düsseldorf, VDI Fortschritt-Berichte, Reihe 14, Nr. 104.
- [146] Ferhadbegović, B., C. Brinkmann, H.D. Kutzbach und S. Böttinger: Hohenheimer Reifenmodell - ein dynamisches dreidimensionales Modell für Fahrdynamiksimulation. Agrartechnische Forschung 13 (2007) 1, S. 1-14.
- [147] -, -: Goodyear: Farm und Industrie/Baumaschinenreifen. Goodyear GmbH & Co. KG, 2006.
- [148] -, -: Measuring Vibration. Brüel & Kjaer, 1982.
- [149] Dossing, O.: Structural Testing, Part 1: Mechanical Mobility Measurements. Brüel & Kjaer, 1988.
- [150] • Kuitsch, W.: Umweltsimulation von Schwingungs- und Stoßbelastungen - Shakerkursus, Nr. 31918/41.849. Technische Akademie Esslingen, 2006.
- [152] • de Silva, C.W.: Vibration: fundamentals and practice. CRC Press LLC Boca Raton, Florida, 2000.
- [153] Baumann, M.: Konstruktion eines Aktuators zur Schwingungsanregung von Ackerschlepperreifen. Diplomarbeit Universität Hohenheim 2002. Institut für Agrartechnik Stuttgart-Hohenheim, unveröffentlicht.
- [154] Brinkmann, C. und V. Schlotter: High Frequent Excitation of Agricultural Tyres and the Effect on Driving Comfort. Proceedings of the 7th Asia-Pacific Conference of the International Society for Terrain-Vehicle Systems, Changchun, China (2004), S. 20-34.
- [155] Brinkmann, C. und H.D. Kutzbach: Höherfrequente Anregung von Traktorreifen. Landtechnik 59 (2004) 4, S. 208-209.
- [156] Brinkmann, C. und H.D. Kutzbach: Vibration Characteristics of Agricultural Tyres in the Comfort Relevant Frequency Range. Proceedings of the 33. International Symposium on Agricultural Engineering, Opatija (2005), S. 111-121.
- [157] -, -: Model EGCS-DO/D1S Accelerometer. Measurement Specialties, Inc., 2007.
- [158] -, -: Non-Contacting Angel Sensors - Novotechnik RSC2200 Series. Novotechnik Stiftung & Co., 2004.

- [159] Ehmann, S.: Erweiterung eines Reifenprüfstands für AS-Reifen zur Messung komfortrelevanter Schwingungen. Studienarbeit Universität Stuttgart 2005. Lehr- und Forschungsgebiet Landmaschinen Stuttgart-Hohenheim, HS 618 S, unveröffentlicht.
- [160] Späth, R.: Dynamische Kräfte an Standardtraktoren und ihre Wirkungen auf den Rumpf. Dissertation Technische Universität München 2003. VDI Verlag Düsseldorf, VDI Fortschritt-Berichte, Reihe 14, Nr. 115.
- [161] Späth, R.: Messrad für die Erfassung der Radkräfte an der Traktorhinterachse. Agrartechnische Forschung 7 (2001) Heft 5, S. 86-91.
- [162] Schulz, C.: Konstruktive Erweiterung eines Messfahrzeugs für Ackerschlepperreifen. Studienarbeit Universität Stuttgart 2007. Lehr- und Forschungsgebiet Landmaschinen Stuttgart-Hohenheim, HS 628 S, unveröffentlicht.
- [163] • Böhm, F.: Reifenmodelle und ihre experimentelle Überprüfung, in Böhm, F.H. und K.H. Knothe: *Hochfrequenter Rollkontakt der Fahrzeugräder*, 5, S. 80-114, WILEY-VCH Weinheim, 1998.
- [164] • Gough, V.E.: Structure of the Pneumatic Tire, in Clark, S.K.: *Mechanics of Pneumatic Tires*, Chap. 4, S. 203-248, U.S. Dept. of Transportation Washington D.C., 1981.
- [165] Reibert, J.-P.: Automatisierung der Messdatenauswertung von Schwingungsversuchen an AS-Reifen. Studienarbeit Universität Stuttgart 2005. Lehr- und Forschungsgebiet Landmaschinen Stuttgart-Hohenheim, HS 619 S, unveröffentlicht.
- [166] Böttinger, S., J. Haberland, C. Brinkmann und S. Jantzen: Driving Comfort with Agricultural Tractors - State of the Art and Objectification of the Evaluation. Proceedings of the 10th European Conference of ISTVS, Budapest (2006).
- [167] Haberland, J., C. Brinkmann und S. Böttinger: Ride Comfort of Agricultural Tractors - Objective Measurements and Subjective Evaluation. Asia-Pacific ISTVS Conference and Annual Meeting of Japanese Society for Terramechanics, Fairbanks, USA (2007).
- [168] Haberland, J., C. Brinkmann und S. Böttinger: Fahrkomfort bei Ackerschleppern - Stand der Technik und Objektivierung der Beurteilung. 7. Internationales Stuttgarter Symposium, Stuttgart (2007), Band 1, S. 233-249.
- [169] Jaksch, J.: Multiple Setpoint Parameter Optimization of Tractors Using Multibody System Simulation. Diploma Thesis University of Heidelberg 2008. Interdisciplinary Center for Scientific Computing (IWR) Heidelberg, unveröffentlicht.

- 
- [170] Wolfer, A.: Konzeption eines Reifenmessanhängers zur Untersuchung des Schwingungsverhaltens von AS-Reifen. Diplomarbeit Universität Hohenheim 2004. Institut für Agrartechnik Stuttgart-Hohenheim, unveröffentlicht.
- [171] Weinhold, O., S. Baumann, M. Obermayr und C. von Holst: Prozesskette zur Parametrierung von Reifenmodellen in der Landtechnik. 13. Internationale VDI-Tagung Reifen - Fahrwerk - Fahrbahn, Hannover, Germany (2011), VDI-Berichte 2137, S. 323-332.

## 8 APPENDIX

### Sensor setup of the research tractor

**Table 39:** Installed sensors at 32 channel measuring box

Channel No.	Sensor	Abbrev.	range	max. deviation	Measured quantity
1	Accelerometer	Acc_RF_X	±5 g	±1% non-linearity	Acceleration of RF wheel in longitud. direction
2	Accelerometer	Acc_RF_Y	±5 g	±1% non-linearity	Acceleration of RF wheel in lateral direction
3	Accelerometer	Acc_RF_Z	±5 g	±1% non-linearity	Acceleration of RF wheel in vertical direction
4	Strain gage wheels	F_VR_S1	0 - 100 kN	100 N	Force in spokes pair No. 1
5	Strain gage wheels	F_VR_S2	0 - 100 kN	100 N	Force in spokes pair No. 2
6	Accelerometer	Acc_Cab_Z	±5 g	±1% non-linearity	Acceleration of cabin floor in vertical direction
7	Angular sensor	VA_lenk	0 - 360°		Steering angle of front axle
8	empty				
9	Accelerometer	Acc_RR_X	±5 g	±1% non-linearity	Acceleration of RR wheel in longitud. direction
10	Accelerometer	Acc_RR_Y	±5 g	±1% non-linearity	Acceleration of RR wheel in lateral direction
11	Accelerometer	Acc_RR_Z	±5 g	±1% non-linearity	Acceleration of RR wheel in vertical direction
12	empty				
13	empty				
14	empty				
15	Corrsys-Datron Correvit S-400	Vx	0 - 250 km/h	±0,1 %	Driving velocity in x-direction
16	Corrsys-Datron Correvit S-400	Vy	0 - 250 km/h	±0,1 %	Driving velocity in y-direction
17	Strain gage wheels	VR_RE_S	0 - 60 kN	100 N	Lateral force of right front wheel



Channel No.	Sensor	Abbrev.	range	max. deviation	Measured quantity
18	Strain gage wheels	VR_RE_Mom			Driving torque of right front wheel
19	Strain gage wheels	HR_LI_13	0 - 100 kN	100 N	Force in spokes No. 1+3
20	Strain gage wheels	HR_LI_24	0 - 100 kN	100 N	Force in spokes No. 2+4
21	Strain gage wheels	HR_LI_S	0 - 60 kN	100 N	Lateral force of left rear wheel
22	Strain gage wheels	HR_RE_57	0 - 100 kN	100 N	Force in spokes No. 5+7
23	Strain gage wheels	HR_RE_68	0 - 100 kN	100 N	Force in spokes No. 6+8
24	Strain gage wheels	HR_RE_S	0 - 60 kN	100 N	Lateral force of right rear wheel
25	Angular sensor wheel	Winkel_L	0 - 360°		Turning angle of left rear wheel
26	Angular sensor wheel	Winkel_R	0 - 360°		Turning angle of right rear wheel
27	Angular sensor wheel	Winkel_VA	0 - 360°		Turning angle of right front wheel
28	Angular sensor shaker	Winkel_Sh	0 - 360°	±0,1 %	Angle of shaker shafts
29	empty				
30	Accelerometer	Acc_Seat_X	±5 g	±1% non-linearity	Acceleration of seat in longitud. direction
31	Accelerometer	Acc_Seat_Y	±5 g	±1% non-linearity	Acceleration of seat in lateral direction
32	Accelerometer	Acc_Seat_Z	±5 g	±1% non-linearity	Acceleration of seat in vertical direction

**Table 40:** Sensor setup for the cleat tests

Channel No.	Sensor	Abbrev.	range	max. deviation	Measured quantity
1	Accelerometer	Acc_RF_X	±5 g	±1% non-linearity	Acceleration of RF wheel in longitud. direction
2	Accelerometer	Acc_RF_Y	±5 g	±1% non-linearity	Acceleration of RF wheel in lateral direction
3	Accelerometer	Acc_RF_Z	±5 g	±1% non-linearity	Acceleration of RF wheel in vertical direction
4	Strain gage wheels	F_VR_S1	0 - 100 kN	100 N	Force in spokes pair No. 1
5	Strain gage wheels	F_VR_S2	0 - 100 kN	100 N	Force in spokes pair No. 2
6	Accelerometer	Acc_Seat_X	±5 g	±1% non-linearity	Acceleration of seat in longitudinal direction
7	Angular sensor	VA_lenk	0 - 360°		Steering angle of front axle
8	Accelerometer	Acc_RR_X	±5 g	±1% non-linearity	Acceleration of RR wheel in longitudinal direction
9	Accelerometer	Acc_RR_Y	±5 g	±1% non-linearity	Acceleration of RR wheel in lateral direction
10	Accelerometer	Acc_RR_Z	±5 g	±1% non-linearity	Acceleration of RR wheel in vertical direction
11	Accelerometer	Acc_Cab_X	±5 g	±1% non-linearity	Acceleration of cabin floor in longitudinal direction
12	Accelerometer	Acc_Cab_Y	±5 g	±1% non-linearity	Acceleration of cabin floor in lateral direction
13	Accelerometer	Acc_Cab_Z	±5 g	±1% non-linearity	Acceleration of cabin floor in vertical direction
14	Systron Donner MotionPak Multi Axis Inertial Sensing System	Roll	±20°/s	±2% bias factory set	Angular rate around x-axis (rolling)

Chan- nel No.	Sensor	Abbrev.	range	max. deviation	Measured quantity
15	Systron Donner MotionPak Multi Axis Inertial Sensing Sytem	Pitch	$\pm 20^\circ/s$	$\pm 2\%$ bias factory set	Angular rate around y-axis (pitching)
16	Systron Donner MotionPak Multi Axis Inertial Sensing Sytem	Yaw	$\pm 50^\circ/s$	$\pm 2\%$ bias factory set	Angular rate around z-axis (yawing)
17	Strain gage wheels	VR_RE_S	0 - 60 kN	100 N	Lateral force of right front wheel
18	Strain gage wheels	VR_RE_Mom			Driving torque of right front wheel
19	Strain gage wheels	HR_LI_13	0 - 100 kN	100 N	Force in spokes No. 1+3
20	Strain gage wheels	HR_LI_24	0 - 100 kN	100 N	Force in spokes No. 2+4
21	Strain gage wheels	HR_LI_S	0 - 60 kN	100 N	Lateral force of left rear wheel
22	Strain gage wheels	HR_RE_57	0 - 100 kN	100 N	Force in spokes No. 5+7
23	Strain gage wheels	HR_RE_68	0 - 100 kN	100 N	Force in spokes No. 6+8
24	Strain gage wheels	HR_RE_S	0 - 60 kN	100 N	Lateral force of right rear wheel
25	Angular sensor wheel	Winkel_L	0 - 360°		Turning angle of left rear wheel
26	Angular sensor wheel	Winkel_R	0 - 360°		Turning angle of right rear wheel
27	Angular sensor wheel	Winkel_VA	0 - 360°		Turning angle of right front wheel
28	Accelerometer	Acc_Seat_Z	$\pm 5$ g	$\pm 1\%$ non-linearity	Acceleration of seat in vertical direction
29	Corrsys-Datron Correvit S-400	Vx	0 - 250 km/h	$\pm 0,1 \%$	Driving velocity in x-direction
30	Accelerometer	Acc_FA_X	$\pm 5$ g	$\pm 1\%$ non-linearity	Acceleration of front axle in longitud. direction
31	Accelerometer	Acc_FA_Y	$\pm 5$ g	$\pm 1\%$ non-linearity	Acceleration of front axle in lateral direction
32	Accelerometer	Acc_FA_Z	$\pm 5$ g	$\pm 1\%$ non-linearity	Acceleration of front axle in vertical direction

## Modal characteristics of the tires

**Table 41:** Frequency and damping values of the unloaded front tire's modes

Mode shape	Front 0.8 bar		Front 1.2 bar		Front 1.6 bar		Front 2.0 bar	
	Freq. [Hz]	Damp. [%]	Freq. [Hz]	Damp. [%]	Freq. [Hz]	Damp. [%]	Freq. [Hz]	Damp. [%]
Radial 0	56.456	4.998	57.924	4.852	59.062	4.672	60.106	4.454
Radial 1	31.548	4.407	36.335	4.804	37.913	4.224	39.208	4.150
Radial 2	39.262	4.490	41.828	4.032	43.867	3.749	45.877	3.490
Radial 3	50.027	4.347	53.285	3.855	55.979	3.535	58.599	3.279
Radial 4	61.772	4.307	65.965	3.473	69.145	3.521	72.386	3.258
Radial 5	74.174	4.690	78.974	3.968	82.545	3.820	87.140	3.061
Radial 6	85.946	5.103	92.385	3.797	97.657	3.474	102.070	3.227
Lateral 0	13.869	5.734	15.171	5.386	16.672	3.606	17.671	5.088
Lateral 1	14.441	7.085	15.171		15.484	3.795	15.897	4.079
Lateral 2	36.500	4.798	38.237	4.460	39.351	4.178	42.114	1.913
Lateral 3	60.177	4.514	62.689	4.188	65.074	4.162	67.112	3.939
Lateral 4							85.650	4.859
Breathing	114.200	3.655	121.140	2.939	127.730	3.160	131.790	3.460

**Table 42:** Frequency and damping values of the unloaded rear tire's modes

Mode shape	Rear 0.8 bar		Rear 1.2 bar		Rear 1.6 bar		Rear 2.0 bar	
	Freq. [Hz]	Damp. [%]	Freq. [Hz]	Damp. [%]	Freq. [Hz]	Damp. [%]	Freq. [Hz]	Damp. [%]
Radial 0	45.385	3.227	45.752	2.621	47.172	3.012	48.001	2.631
Radial 1			34.009	2.194	35.407	1.933	36.871	1.799
Radial 2	32.246	2.395	35.026	2.074	37.564	1.430	39.154	1.768
Radial 3	38.813	2.396	42.232	2.060	45.058	1.711	47.608	1.661
Radial 4	46.211	2.390	50.040	2.048	53.593	1.891	56.710	1.709
Radial 5	54.124	2.438	58.939	2.219	62.965	1.997	66.614	1.845
Radial 6	62.687	2.620	68.230	2.276	72.950	2.130	77.083	1.942
Lateral 0	12.906	1.304	14.711	1.109	16.168	1.056	17.384	1.044
Lateral 1	14.213	1.282	14.711		15.062	0.987	15.288	0.950
Lateral 2	27.789	2.397	29.025	2.346	29.984	2.141	30.887	2.003
Lateral 3	49.627	0.254	50.040	2.048	51.564	2.658	53.319	2.471
Lateral 4	60.293	3.263	63.639	2.906	67.065	2.954	69.157	2.626
Rim radial 1	74.518	1.143	77.473	1.086	79.502	0.955	81.456	0.859
Breathing	81.873	3.125	87.825	2.524			98.898	2.134

**Table 43:** Frequency and damping values of the loaded front tire's modes

Mode shape	Front 0.8 bar		Front 1.2 bar		Front 1.6 bar		Front 2.0 bar	
	Freq. [Hz]	Damp. [%]	Freq. [Hz]	Damp. [%]	Freq. [Hz]	Damp. [%]	Freq. [Hz]	Damp. [%]
vert. Bouncing	3.331	17.856			4.012	11.146	6.267	10.717
lat. Bouncing	5.503	10.463	5.272	14.706	6.806	10.505	7.984	8.369
1st Lateral	15.426	5.811	16.761	5.284	17.900	4.689	18.719	4.615
1st F/A	18.048	6.637	18.806	6.216	19.303	5.893	19.759	5.759
1st Steering	19.687	5.798	20.860	5.223	21.832	4.912	22.606	4.541
1st Vertical	33.659	4.896	34.753	4.760	36.882	4.249	38.362	4.043
2nd Lateral	30.268	6.265			33.613	4.962	34.765	4.391
2nd F/A	37.792	4.065	39.278	3.121	41.595	3.174	44.106	5.105
2nd Steering			36.275	4.804	39.237	2.717	42.112	3.996
2nd Vertical	39.441	3.481	41.497	1.293	46.527	4.782	50.188	3.545
3rd Lateral	67.454	2.644	70.196	3.856	72.953	3.936	75.882	3.627
3rd F/A			53.942	4.147	55.096	4.079	57.505	3.821
3rd Vertical	56.600	4.328	60.112	4.179	62.969	3.458	65.141	3.200
4th F/A	62.124	3.436	65.507	3.666	66.974	4.129	68.610	3.928
4th Vertical	76.892	4.162	81.528	3.818	85.469	4.280	88.932	3.969
5th F/A	71.400	4.798	74.119	5.011	77.131	3.843	80.131	3.572
6th F/A	89.168	4.424	95.299	4.038	100.520	1.867	104.590	3.488
Rim Radial	101.180	1.474	102.920	3.091	103.230	2.551	109.970	2.393
Breathing	116.890	3.980	122.250	3.417	126.540	2.982	126.940	1.107

**Table 44:** Frequency and damping values of the loaded rear tire's modes

Mode shape	Rear 0.8 bar		Rear 1.2 bar		Rear 1.6 bar		Rear 2.0 bar	
	Freq. [Hz]	Damp. [%]	Freq. [Hz]	Damp. [%]	Freq. [Hz]	Damp. [%]	Freq. [Hz]	Damp. [%]
vert. Bouncing	4.800	3.804	5.118	2.853	5.537	2.730	5.680	2.520
lat. Bouncing	7.562	1.832	8.443	2.542	9.142	1.969	9.638	1.804
1st Lateral	15.437	1.813	17.019	1.585	18.193	1.483	19.158	1.362
1st F/A	16.925	3.664	17.621	3.671	17.944	3.386	18.305	3.622
1st Steering	18.891	1.832	20.342	1.581	21.399	1.388	22.244	1.294
1st Vertical	30.303	2.885	32.284	2.783	33.669	2.412	35.136	2.089
2nd Lateral	24.505	2.688	25.482	2.338	25.958	2.637	26.748	2.073
2nd F/A	31.931	2.395	34.115	2.321	35.919	2.579	37.684	2.305
2nd Steering	29.221	2.966	30.428	2.537	31.404	2.386	32.106	2.259
2nd Vertical	34.703	2.941	39.021	2.136	39.672	2.359		
3rd Lateral	48.084	2.957	51.604	2.623	53.005	2.602	54.503	2.483
3rd F/A	38.240	2.885	40.902	2.742	42.249	2.550	43.219	1.870
3rd Vertical	43.188	2.586	46.821	2.307	49.935	1.230	52.549	1.837
4th F/A	51.769	2.050	55.850	2.333	59.419	2.048	63.169	1.962
4th Vertical	60.397	2.472	65.484	2.532	69.795	2.236	73.548	2.033
5th F/A	55.940	3.598	61.648	2.493	65.255	2.119	68.748	1.908
6th F/A	65.658	2.760	70.867	2.659	75.055	2.495	79.191	1.199
Rim Radial	74.064	1.844	75.856	2.268	78.031	1.005	81.692	0.986
Breathing	79.254	2.543	84.673	3.182	90.844	2.375	95.402	2.304

**Table 45:** Frequency and damping values of the rear rim modes

Mode shape	Frequency, Hz	Damping, %
Suspension	18.771	2.150
	21.409	1.484
Lateral 1	82.463	0.502
Radial 2	83.381	0.244
Lateral 0	125.870	0.749
Radial 3	189.040	0.098
Radial 3	189.930	0.146
Radial 0 (Axle/Rim)	323.120	0.824
Radial 4	342.500	0.061

**Table 46:** Frequency values of the loaded rear tire's modes from modal analysis ( $F_z = 20$  kN,  $p_i = 1.5$  bar,  $v = 0$  km/h) and shaker test ( $e_{Sh} = 1.44$  mm,  $F_z = 20$  kN,  $p_i = 1.5$  bar,  $v = 0$  km/h,  $f_{Sh} = 5-80$  Hz)

Mode shape	Frequency, Hz	
	Modal analysis	Shaker test
1st Lateral	14.09	14.65
1st F/A	18.52	18.07
1st Steering	17.64	---
1st Vertical	31.75	31.25
2nd Lateral	27.02	26.86
2nd F/A	36.00	35.64
2nd Steering	33.44	---
2nd Vertical	41.00	42.48
3rd Lateral	54.66	53.22
3rd F/A	---	46.88
3rd Vertical	50.20	49.80
4th F/A	---	56.64
4th Vertical	---	69.82
5th F/A	---	64.94
6th F/A	---	---